

Abstract

The behaviour of waste biomass materials, specifically bagasse* and sawdust, in deep fluidized beds was investigated. The bagasse used was dry. (less than 1% moisture by mass) Sawdust was from mixed eucalyptus hardwoods with moisture contents up to 25% by mass.

A series of cold flow visualisation tests were completed in a bed of 190mm diameter using graded river sand of surface mean particle diameters of 180 and 490 microns. Bagasse was added to the bed in various quantities and the ingestion and mixing phenomena observed. The influence of distributor design, cones, and draft tubes on mixing rates were investigated for use in the combustor design.

Combustion Tests using Sawdust and Bagasse were completed in a Combustor of 489mm diameter with graded river sands of surface mean particle diameters of 300, 490 and 530 microns. Various configurations were tested including a shallow bed of depth 130mm, deep beds of depths up to 460mm, a Reverse Circulation Bed, and Modified Spouted Beds of depths up to 740mm. Fuel feeding systems included above bed chutes, an ingestor tube, a direct bed wall screw feeder, and a pressurised screw feeder fitted to the air supply of a Modified Spouted Bed. Bagasse was not successfully fed through the screw feeder systems used. Sawdust, which has similar fluidized bed combustion characteristics to bagasse, was used in screw feeders to indicate the possible results that could be obtained from bagasse using below bed feed systems. Configurations utilising direct below bed surface screw feed, Ingestor tube feed, and pressurised screw feed to the fluidizing air were all successful in increasing the percentage of combustion occurring below the bed surface. The best results were obtained from pre-mixed air and fuel particles entering the modified spouted bed giving combustion efficiencies of up to 60% comparable to coal. Higher efficiencies would be possible with further optimisation of the design.

The results of the investigation open several avenues of development including partial gasification/combustion systems and further development of the ingestor tube, reverse circulation bed and modified spouted bed concepts. The problems encountered with the combustion of lightweight, particulate biomass fuels are now reduced to finding practical methods of fuel feeding and rate control.

*Bagasse is the cellulose residue from sugar cane stalks which remains after crushing. It is particulate, fibrous, tangled and irregular in size, length and aspect ratio.

Fluidized Bed Combustion of Waste Material

Volume 1 of 2

by

Colin Robert Cole

Submitted in fulfilment of the requirements for the
degree of

Master of Engineering (Mechanical)

at the

University of Central Queensland.
Rockhampton.

Department of Mechanical Engineering

James Goldston Faculty of Engineering

Submitted : January, 1994

CENTRAL QUEENSLAND
UNIVERSITY - LIBRARY

Table of Contents

Abstract	i
Title Page	ii
Table of Contents	iii
List of Tables	v
List of Figures and Illustrations	vii
Acknowledgements	x
Declaration	xi
Volume 1 : Main Text	
1.0 INTRODUCTION	1
2.0 LITERATURE REVIEW: FLUIDIZED BED COMBUSTION OF BIOMASS	8
3.0 THEORY	
3.1 Nomenclature	16
3.2 Gross Fluid-Particle Behaviour	27
3.3 Thermodynamic Behaviour	33
3.4 Combustion Heat Release Below Bed Surface	40
3.41 Determination of Equivalent Specific Heat of Bed structure and solids.	46
3.42 Estimation of Fuel and Moisture Heat Fractions for Above Bed Fuel Feed Systems	47
3.43 Estimation of Fuel Particle Fall and Bed Residence Times	51
3.44 Heat of Combustion	58
4.0 EQUIPMENT DETAILS	
4.1 Flow Visualisation Equipment	60
4.2 Fluidized Bed Combustor	62
5.0 RESULTS	
5.1 Introduction	64
5.2 Phase 1: Flow Visualisation	66
5.21 Fluidization Behaviour of Deep Beds	66
5.22 Fluidization Behaviour of Sand Bagasse Mixtures	69
5.23 Enhanced Bed Circulation	75
5.24 Reversed Bed Circulation	79
5.3 Phase 2: Combustion Results	83
5.31 Combustion of Bagasse Bricks, Deep Bed, Above Bed Feed	83
5.32 Combustion of Particulate Bagasse, Deep Bed, Above Bed Feed	89

Table of Contents (Cont.)

5.33	Combustion of Particulate Bagasse, Deep Bed, Ingestor Feed	95
5.34	Combustion of Particulate Bagasse, Sawdust and Coal, Shallow Bed, Above Bed Feed	97
5.35	Combustion of Sawdust, Deep bed, Direct Screw Feed	105
5.36	Combustion of Particulate Bagasse, Sawdust, Deep Bed, Ingestor Feed	110
5.37	Combustion of Sawdust, Modified Spouted Bed, Pre-mixed Fuel and Air	115
6.0	DISCUSSION OF RESULTS	124
7.0	CONCLUSIONS	137
8.0	RECOMMENDATIONS FOR FURTHER WORK	140
9.0	REFERENCES	144
10.0	BIBLIOGRAPHY	146
11.0	RESULTS TABLES	147
12.0	FIGURES AND ILLUSTRATIONS	173

Volume 2 : Appendices

A.	Sample Calculations	1
B.	Experimental Data and U_f/U_{mf} Charts	28
C.	Equipment Drawings and Photographs	69
D.	Equipment Data	108
E.	Fuel Properties	116
F.	Sand Properties	128
G.	Combustor Operation Instructions and Charts	138
H.	Equipment Design Calculations	145
I.	Commissioning Notes	152

List of Tables

Volume 1 : Main Text

Table 2.1	Comparative Operational Data For Alternative Bed Solids.	13
Table 3.1	Comparative Predictions of Minimum Fluidization Velocity.	30
Table 4.1	Flow Visualisation Equipment Modifications	61
Table 4.2	Fluidized Bed Combustion Test Equipment Modifications	63
Table 11.1	Flow Visualisation Results Summary	148
Table 11.2	Deep Bed Flow Visualisation	149
Table 11.3	Bagasse - Sand Mixing 180 micron Sand	150
Table 11.4	Bagasse - Sand Mixing 490 micron Sand	151
Table 11.5	Minimum Operational Velocities For Bagasse Sand Mixtures.	152
Table 11.6	Enhanced Sand Circulation Results	153
Table 11.7	Reversed Sand Circulation Results	154
Table 11.8	Combustion Test Results Summary	155
Table 11.9a	Combustion and Heat Release Efficiencies, Deep Bed, Chute Feed.	156
Table 11.9b	Combustion Heat Balance, Deep Bed, Chute Feed	157
Table 11.9c	Combustion Heat Balance-Details, Deep Bed, Chute Feed	158
Table 11.9d	Fluidization Behaviour, Deep Bed, Chute Feed	159
Table 11.10a	Combustion and Heat Release Efficiencies, Shallow Bed, Chute Feed.	160
Table 11.10b	Combustion Heat Balance, Shallow Bed, Chute Feed	161
Table 11.10c	Combustion Heat Balance-Details, Shallow Bed, Chute Feed	162

List of Tables(Cont.)

Table 11.10d	Fluidization Behaviour, Shallow Bed, Chute Feed	163
Table 11.11a	Combustion and Heat Release Efficiencies, Deep Bed, Screw and Ingestor Feed.	164
Table 11.11b	Combustion Heat Balance, Deep Bed, Screw and Ingestor Feed.	165
Table 11.11c	Combustion Heat Balance-Details, Deep Bed, Screw and Ingestor Feed.	166
Table 11.11d	Fluidization Behaviour, Deep Bed, Screw and Ingestor Feed.	167
Table 11.12a	Combustion and Heat Release Efficiencies, Modified Spouted Bed, Screw Feed	168
Table 11.12b	Combustion Heat Balance, Modified Spouted Bed, Screw Feed	169
Table 11.12c	Combustion Heat Balance-Details, Modified Spouted Bed, Screw Feed	170
Table 11.12d	Fluidization Behaviour, Modified Spouted Bed, Screw Feed	171
Table 11.13	Uncertainty Estimates of Data and Calculated Results	172

Volume 2 : Appendices

Table A1-A2	Iterative Calculations	25
Table B1-B33	Experimental Data	28
Table D1	Combustor Specific Heat and Wall Losses	109
Table E1-13	Fuel Properties and Calculations	116
Table F1-F14	Sand Properties and Calculations	128
Table H1	Materials Costs	151

List Figures and Illustrations

Volume 1 : Main Text

Fig.12.1	Pressure Drop Charateristic , Deep Beds	174
Fig.12.2	Pressure Drop Charateristic ,Bagasse-Sand Mixtures, 180 micron Sand	175
Fig.12.3	Pressure Drop Charateristic ,Bagasse-Sand Mixtures, 490 micron Sand	176
Fig.12.4	Bagasse-Sand Mixing Velocities	177
Fig.12.5	Bagasse-Sand Mixing Velocity Charateristic	178
Fig.12.6	Pressure Drop Characteristic,Enhanced Circulation Devices	179
Fig.12.7	Pressure Drop, Peak Velocity Characteristic, Enhanced Circulation Devices	180
Fig.12.8	Pressure Drop Characteristic,Reversed Circulation Devices	181
Fig.12.9	Pressure Drop, Peak Velocity Characteristic, Reversed Circulation Devices	182
Fig.12.10	Temperatures: Deep Bed, Chute Feed, 50mm Bagasse Bricks	183
Fig.12.11	Temperatures: Deep Bed, Chute Feed, Bagasse Fibres	184
Fig.12.12	Temperatures: Shallow Bed, Chute Feed, Sawdust, Bagasse Fibres	185
Fig.12.13	Temperatures: Shallow Bed, Chute Feed, Coal, Sawdust, Bagasse Fibres	186
Fig.12.14	Temperatures: Deep Bed, Screw Feed,Sawdust	187
Fig.12.15	Temperatures: Deep Bed, Ingestor Feed, Sawdust, Bagasse Fibres	188
Fig.12.16	Temperatures: Modified Spouted Bed, Screw Feed, Sawdust	189
Fig.12.17	Temperatures: Modified Spouted Bed , Screw Feed, Sawdust	190
Fig.12.18	Combustion Efficencies: Above Bed Feed	191

List of Figures and Illustrations(Cont.)

Fig.12.19	Fluidized Bed Efficiencies:Above Bed Feed	192
Fig.12.20	Overall Bed Efficiencies: Above Bed Feed	193
Fig.12.21	Combustion Efficiencies:Ingestor Feed	194
Fig.12.22	Fluidized Bed Efficiencies:Ingestor Feed	195
Fig.12.23	Overall Bed Efficiencies:Ingestor Feed	196
Fig.12.24	Combustion Efficiencies: Below Bed Feed	197
Fig.12.25	Fluidised Bed Efficiencies:Below Bed Feed	198
Fig.12.26	Overall Bed Efficiencies:Below Bed Feed	199
Fig.12.27	Combustion Efficiency,Depth Characteristic	200
Fig.12.28	Overall Bed Efficiency, Depth Characteristic	201
Fig.12.29	Heat Flux : Above Bed Feed Systems	202
Fig.12.30	Heat Flux : Below Bed Feed Systems	203
Fig.12.31	Proposed Devolatilizer/Partial Gasifier with Pressurised Fuel Feed	204
Fig.12.32	Proposed Devolatilizer/Partial Gasifier with Mechanical Fuel Feed	205
Fig.12.33	Proposed Pre- Gasification Combustor with Secondary Air	206
Fig.12.34	Proposed Pre- Gasification Combustor without Secondary Air	207
Fig.12.35	Proposed Modified Spouted Bed with Fuel/Air Pre-heated	208
Fig.12.36	Proposed Modified Dual Chamber Spouted Bed	209
Fig.12.37	Proposed Modified Spouted Bed with Bubble Controls	210
Fig.12.38	Proposed Spouted Bed with Multi-Point Fuel Feed	211
Fig.12.39	Proposed Improved Ingestor with Above Tube Feed	212
Fig.12.40	Proposed Improved Ingestor with Pneumatic Fuel-Air Jet Injection.	213

List of Figures and Illustrations(Cont.)**Volume 2 : Appendices**

Fig. B1-B17	Temperature and U_f/U_{mf} Charts	52
Fig. C1-C13	Flow Visualisation Equipment Drawings	69
Fig. C14-C31	Combustor Equipment Drawings	82
Fig. C32-C46	Photographs	100
Fig. D1-D8	Equipment Data Graphs	110
Fig. E1-E7	Fuel Properties and Calculations	123
Fig. G1-G9	Combustor Operation Charts	140

Acknowledgements

Acknowledgement and thanks is extended for the supervision of Senior Lecturer Mr.J.Czekanski of the University of Central Queensland and the helpful suggestions of co-supervisor Dr.T. Dixon of Sugar Research Institute, Mackay. Helpful suggestions and ideas were also contributed by Senior Lecturer D. Roach and Mr R Boyle regarding bulk materials handling methods for bagasse.

The University of Central Queensland is acknowledged for it's contribution of the opportunity, funding, Research Scholarship and the facilities which enabled the research to be completed.

The advice, work and support of the technician staff of the University of Central Queensland is acknowledged with special thanks to Mr.C. Friend and Mr.R.Kearney for assistance in manufacture of equipment and Mr.K.Morrison for the plumbing of the LPG system.

The assistance of Gas Examiner Mr.J.Jones of the Department of Minerals and Energy, Queensland is acknowledged in the design and commissioning of the LPG system.

The bagasse fuel used was supplied by Sugar Research Institute, Mackay. The Sawdust used was supplied free of charge by Hyne & Son Pty. Ltd., North Rockhampton. The coal was supplied by Stanwell Power Station by favour of Mr. R. Knight.

Finally, I acknowledge the unfailing support, encouragement and sacrifice of my wife Ruth and daughters Elizabeth and Hannah.

Declaration

I declare that the data, calculations, results, some theoretical development and conclusions are original work in every respect and are derived only from experiments performed by myself at the University of Central Queensland during 1992 and 1993.

I acknowledge the use of theory and information from previous authors in the Introduction, Literature Review, Theory and Appendices and declare that such usage is appropriately referenced.

Signed: Signature
Redacted _____

Dated: _____

18/1/94

1.0 INTRODUCTION

(a) History

Fluidization was first used commercially in mining and metallurgical applications such as liquid settling, sedimentation and density classifications. Such applications, according to Botterill, can be identified as early as 1556, (1). Squires notes an early commercial fluidized bed gasification process which began operation in 1926, (2). Gas-fluidization began with a catalytic cracking process required by the demand for more efficient methods of producing high octane aviation fuel, during World War II, as noted by Botterill, (1) and Kunii and Levenspiel, (3). The development appears to have taken place independent of the earlier developments noted by Squires, (2). Since that time applications have expanded to include gasifiers, catalytic cracking plants, mixers, coolers, dryers and combustors.

Fluidized bed combustors find applications as incinerators, gasifiers and boilers. The development of fluidized bed boilers has been mainly focused on the combustion of coal. Coal burning Fluidized Bed Boilers can be purchased in various configurations and quite large capacities as the following list shows;

150 MW	Reducing atmosphere type	Fives-Cail Babcock
250 MW	Bubbling Fluidized Bed Boilers	Deutsche Babcock
110 MW	Circulating Fluidized Bed Boilers	Babcock&Wilcox.Co, (4)
100 MW	Bubbling Fluidized Bed	Pope, Evans&Roberts, (5)

Fluidized bed combustors can also be used with liquid or

gaseous fuels with relative ease as such fuels can be easily controlled and introduced at the bottom of the bed. Liquid or gaseous fuels are often used as pre-heat fuels for combustors which operate on fuels such as coal which are difficult to initially ignite. Liquid and gaseous fuels are also used for the heating of fluidized particles when the fluidized bed is used for heat treatments, as in the case of metallurgical furnaces, dryers or solids processors, as noted by Broughton, (6).

(b) The Phenomena of Fluidization

For combustion applications a bed of loose solid particles are fluidized with air. Fluidization refers to the state where the upward flow of air through the bed particles produces sufficient drag to balance the weight of the particles. The minimum air velocity for which the weight of the entire bed is balanced is called the minimum fluidization velocity. The bed is said to be at the point of incipient fluidization at minimum fluidization velocity. As velocity is increased the particles will rearrange themselves to maintain the pressure balance causing bed expansion or bubbling. Air flow can be increased until the fraction of particles with the smallest diameter begin to be pneumatically transported. The approximate ratio of maximum to minimum operational velocities in beds of single size solids range from 90 to 10 corresponding to small (e.g. $100\mu\text{m}$) and large (e.g. $1000\mu\text{m}$) particle sizes respectively. In beds having a mixture of different particle sizes, minimum fluidization velocity corresponds to that predicted for the surface mean diameter of particles provided there are no discontinuities of particle size fractions. (ie the Mass

Fraction vs diameter curve is basically a bell curve.) By contrast, the upper velocity limit of such beds corresponds to the terminal velocity of the smallest diameter particles. The operational range of velocities is therefore reduced by having a broad size range of solids in a bed.

It would be incorrect, however, to view a fluidized bed as an ordered suspension of solids. At gas velocities above minimum fluidization mixing patterns are established. As there is always a velocity profile in a tube due to wall friction there are slightly higher velocities at the centre of the bed. The higher velocities result in a net upward flow of solids in the centre of the bed with solids returning in stick-slip flow down the bed walls. In a bubbling bed, the behaviour can be thought of in two zones or phases, bubbles and emulsion. Upward solids transport is in the bubble wake. This view or model of bed behaviour is called the two-phase theory and is the most utilised due to it's simplicity.

The response of a fluidized bed to increasing temperature, when fluidized with air, is a reduction in the required minimum fluidization velocities, due to increases in air viscosity. Air density is also reduced in the bed due to the temperature increase, compounding with lower velocity requirements to give significant reductions in air mass flow. The air mass flow can be reduced to between 1/5th and 1/10th of cold bed requirements, during warm up, if the same operation point is being maintained in the bed. (See Appendix G)

The principle interest in fluidized beds for combustion stems from improvements in heat transfer obtained by the [hot gas(flame)]-to-[bed solids]-to-[hot gas]-to-[surfaces]

mechanism. High heat transfer rates from flame or hot gas to bed particles are achieved by the large surface area available on bed particles. The surface area of typical $300\mu\text{m}$ sand is approximately 12600 square metres per cubic metre of sand. The gas-to-particle heat transfer coefficients are quite low, typically in the range of 6 to $23 \text{ W/m}^2\text{K}$, as noted by Kunii and Levenspiel, (3). The large particle surface area easily compensates for any limitation imposed by the low gas-to-particle heat transfer coefficients. Conversely, high heat transfer coefficients are achieved in fluidized beds between bed particles and surfaces. Botterill reports heat transfer coefficients in the range of 200 to $700 \text{ W/m}^2\text{K}$, (1).

Of interest to the combustion of particulate fuels is the rapid normalisation of bed solids to a single bed temperature and the high internal particle-to-particle heat transfer coefficients. For $300\mu\text{m}$ sand and large fuel lumps $\sim 50\text{mm}$, heat transfer coefficients of at least $925 \text{ W/m}^2\text{K}$ can be expected and higher values for smaller fuel particles, as calculated using the equation given by Broughton and Howard, (7), (See also Appendix E and Eq.3.41, Section 3.3).

The large storage of heat afforded by the mass of the bed solids make fluidized beds ideal for fuels which are irregular sized, difficult to ignite and have varying moisture contents. Above bed fuel feed systems can exploit flue gas heat to dry and pre-heat the fuel. A combination of heat storage and high internal particle-to-particle heat transfer make fluidized beds ideal for the combustion of irregular and poor quality coals.

(c) Biomass Fuels

The combustion of biomass fuels of light particle densities such as bagasse, sawdust and rice husks present unique problems for fluidized bed combustion. These fuels are basically variations of cellulose and decompose to volatiles and char at temperatures of approximately 300°C, as noted by Luo et al., (8). Ignition takes place at approximately the same temperature. The volatile content of such fuels is usually of the order of 80 - 85% by mass. In the dry state these fuels are highly reactive due to the relatively small particle size. Past experiments with combustion of biomass fuels have resulted in insufficient heat release to the bed solids, with subsequent bed cooling and shutdown as detailed by Peel et al., (9). While there are examples of commercial and pilot scaled fluidized bed combustors operating on biomass fuels, these are limited to fuels of larger particle sizes, eg. wood chips, prunings etc, which are not so reactive and would allow longer bed surface residence times. To the knowledge of the author, commercial fluidized bed combustors for lightweight fuels such as bagasse, sawdust and rice husks are yet to be developed. There is however current research as detailed in the Literature Review.

(d) Research Project Definition

From the above understanding of the problem the following Definition for Research was formed:

"To investigate the feasibility of sustained fluidized bed combustion of lightweight biomass waste materials, specifically particulate fibrous bagasse and similar materials. Research is to be restricted to bubbling, atmospheric beds

without cyclone particle re-circulation systems and the burning of bagasse as received after sugar mill crushing without further processing".

(e) Approach to Research.

It was understood at the beginning of the project that the failure of attempts to burn lightweight biomass fuels in fluidized bed combustors was related to insufficient fuel residence times. It was reasoned that residence time could be improved by deep beds and the introduction of fuel to the base of the bed. The methodology of observing the behaviour of deep beds and bagasse mixing in a flow visualisation bed and then using the experience and data gained for the design of a combustor was adopted. Due to the problems envisaged with feeding materials such as bagasse against a fluid pressure, various methods of above bed feed, rapid ingestion and mixing were investigated in the flow visualisation test equipment.

Bagasse, which had been chosen as the fuel for investigation due to its relevance to the local Sugar Industry, proved extremely difficult feed except by crude batch methods. These problems led to the use of sawdust in later tests to confine research to combustion behaviour and prevent the inclusion of a full scale investigation of bagasse feeders.

(f) Thesis Presentation

A literature review including recent research is presented in the next chapter.

A theory chapter is included which details the equations used in calculations. The problem of quantifying the percentage of fuel heat energy that is released within the bed is critical to the investigation of sustainable combustion. The criteria

are presented in Section 3.4. Little developed theory was located in standard texts. A further problem of comparing the performance of beds at different operating conditions was noted, hence the development of the concepts of Fluidized Bed Efficiency, Overall Bed Efficiency and Operating Ratio. (See Section 3.4)

As the research project was completed in two parts, Results are presented in two sections; Phase 1: Flow Visualisation, (Section 5.2), and Phase 2: Combustion Results, (Section 5.3). As there were many variations in equipment and experimental method in the testing program, each results section presents relevant equipment details, experimental method and a discussion specific to that test. An overall Discussion of Results follows the Results section which compares and discusses results of the research project as a whole. Finally, useful conclusions are made and several options for future research immerge in the recommendations for further work.

Sample calculations with Uncertainty Analysis for each calculation is presented in Appendix A. Appendix B includes raw data tables, temperature vs time reproduced from Chart Recorder Data and Bar charts for the U_f/U_{mf} ratio during each test. Equipment Drawings and Photographs are located in Appendix C and Equipment Data in Appendix D. Detailed Properties and theoretical calculations relevant to sand and fuels are included in Appendices E & F. Useful information for any who would either use the facility or upgrade it is located in the operational details, design calculations and commissioning notes located in Appendices G ,H,&I.

2.0 LITERATURE REVIEW: FLUIDIZED BED COMBUSTION OF BIOMASS

The Literature search carried out by the University of Central Queensland Library yielded few direct references to Fluidized Bed Combustion of Biomass and no responses to Combustion of Bagasse. Abstracts received included a biomass pilot scale Fluidized Bed Combustor, operating on wood fuel, by Vafaei.M. et al.,(10). A multi-fuel Re-Circulating Fluidized Bed Combustor, operating on orchard prunings,secondary wood, almond shells, and cotton stalks, by Hanson.J., (11) and Fir Wood Pyrolysis in a Fluidized Bed reactor, by Samolada.M.C. and Vasalos. I.A., (12). None of the biomass fuels noted in the abstracts matched the unique lightweight and fibrous properties of bagasse so copies of the full articles were not obtained. Wood fuels such as prunings and wood chips have particle sizes much larger than bagasse and hence higher terminal velocities and would be more readily ingested into a bed for combustion below the bed surface. The following papers were found in the University library and sourced from conferences which occurred during period of the project.

(a) "Fluidized Bed Combustion of Vegetable Fuels"

The above paper was the earliest cited, published 1980 by Peel R & Santos. F., (9). The paper examined the combustion of several biomass fuels including rice husks, bagasse and sawdust. Peel and Santos were unsuccessful in burning these fuels due to low residence times and fuel feeding problems. Researchers reported that sawdust and bagasse could be mixed in a cold bed indicating that combustion may be possible. When gravity fed both fuels ignited before reaching the bed surface

and most combustion occurred in the freeboard region above the bed. Only small amounts of heat were transferred to the bed solids and the bed subsequently cooled. Satisfactory combustion was reported for larger particle fuels such as +2mm wood chips. The bed solids were -830 micron sand and operation was at velocities of 1.0-1.3m/s.

Evaluation : No attempt was made to quantify the combustion processes and the authors readily admitted the qualitative nature of their findings. The qualitative results were useful as a starting point for experimental research.

(b) "Bagasse Combustion in a Fluidised Bed"

The above paper by Chong .Y.O. et al., (13) produced at Queensland University in 1992 takes the approach common to two research groups of selecting a fluidizable material with particle density as close as possible to that of bagasse. The paper does not report any combustion tests and is only concerned with the mixing behaviour in cold test observation equipment. The Bed material used is porous alumina of particle density of 1450 kg/m^3 , bulk density of 950 kg/m^3 and a surface mean particle diameter of 90 microns. Fluidization velocities are very small beginning with $U_{mf}=0.0038\text{m/s}$ and terminal velocities of the order of 0.38m/s . The paper documented bagasse-sand mixing behaviour and reported it's metastable nature and the increase of the minimum fluidization velocity with increased bagasse content.

Evaluation: The paper only documented cold mixing tests. The low operational velocities would ensure little or no loss of bagasse. Predicting the combustion operation from the

reported data will depend on the combustor design chosen. Based on the successful mixing in the cold bed, it can probably be assumed that the bagasse will ingest and mix quickly in a combustor. Scaling the cold behaviour of the bed to an operational temperature of 600°C and assuming a minimum particle size of 40 microns the operational velocities fall in the range of 0.0018 to 0.033 m/sec, (see Table 2.1). Higher velocities could be achieved by either removing the fines fractions or adding a particle recirculation system to the design. Assuming a simple atmospheric bed for the sake of comparison and operational velocities at mid range, ie $U_f/U_{mf}=9.5$; $U_f=0.017$ m/s, a 100kW combustor would need a bed diameter of 2170mm, (Assuming stoichiometric mixture). Even at maximum operating velocities a bed diameter of 1586mm would be required. Approximately 30% can be added to these bed size estimations for excess air requirements. A bed utilising 300 micron sand would achieve the same fuel combustion capacities with bed diameters of 685mm and 504 mm respectively. The relatively low operational velocities extract a similar penalty in heat flux values which are, assuming 60% below bed combustion for comparison, limited to 304 kW/m³, compared to that of sand at 3006 kW/m³, (Table 2.1) [Maximum packed bed heat flux as defined by Eq.3.45, (Section 3.3)]. The usefulness of the porous alumina particles would therefore seem to depend on how the practical problems of combustor size and/or particle control were solved. Combustion tests would be required to fully evaluate these practical considerations and investigate feasible methods of heat transfer.

(c) "Bloated Clay Aggregate as Inert Bed Material for Fluidized Combustion of Bagasse"

A similar approach was taken by researchers Singh et al., (4) in trying to select a suitable bed material that would allow successful combustion of bagasse. Bloated clay of particle density of 835kg/m^3 was crushed to an average size of 2mm and size range 1.5 to 2.5mm. Bagasse particles were of average length of 25mm. The other dimensions of bagasse fibres were not given. Researchers reported the successful combustion of bagasse with temperatures of 800°C reached. The bed was reported to have a superficial velocity of 1.35m/sec.

Evaluation: The technique of using a very light solid of relatively large particle size allows both material density compatibility with bagasse and relatively high superficial velocities and therefore good heat flux values. There was no attempt to quantify the combustion process so it is not clear what percentage of the combustion heat release actually occurred below the bed surface. There was therefore no way to determine if the heat up of the bed was achieved efficiently or wastefully using excess fuel. Conceivably, bed heat up could be achieved using excess fuel as a sufficient fraction of larger particles would probably reach the bed and mix and release heat within the bed. The smaller particles above the bed would then remain unburnt and be lost in flue gases. The high operational velocity would suggest some loss of bagasse fuel by pneumatic transport. No comment was made regarding such losses suggesting that the bagasse used may have a much smaller percentage of

fine dust than is typical of Australian Sugar Mill bagasse.

Comparison of Porous Alumina, Bloated Clay and Sand.

In comparing the two alternate materials offered by the previous two research groups with ordinary sand, clear overall advantages do not emerge, (See Table 2.1, following page). Using the criteria for mixing given by Singh et al., (4), of requiring the mass to surface ratio of bed solids and fuel to be of the same order, sand would still be a suitable bed material. Bagasse is quoted to have a mass to surface ratio of 0.02 to 0.04 g/cm² which in S.I units is 0.2 to 0.4kg/m². Further, the criteria does not seem to explain the favourable mixing of Bagasse in porous Alumina particles reported by Chong.Y.O. et al., (13).

The favourable results obtained from tests using bloated clay at velocities of 1.35 m/s seem to conflict with those of Peel and Santos using similar velocities and -830 micron sand. There is insufficient data presented in these two papers to determine the dependence of the results on mixing and fuel losses.

The results from porous alumina would indicate that there are definite advantages for fuel mixing to be gained by the correct choice of bed material. There is, however, the need for more research and quantified combustion results before a true understanding of bagasse mixing and combustion in different bed materials will be gained.

Table 2.1 Comparative Operational Data for Alternative Bed Solids (Bed Operating Temperature of 600°C.)

Operational Parameter	Porous Alumina	Bloated Clay	Sand
Mean Diameter(μm)	90	2000	300
Particle Density(kg/m^3)	1450	835	2300
Bulk Density($\text{kg}/\text{cu.m}^3$)	950	500	1450
U _{mf} (m/sec)	0.0018	0.52	0.032
Minimum Diameter(μm)	40	1500	100
U _t (m/sec)	0.033	6.38	0.33
Specific Surface a' m^{-1}	70200	3200	21100
Specific Surface a m^{-1}	42100	1900	12600
Mass/Surface Ratio kg/m^2	0.02	0.26	0.11
Typical Operating Vel. m/sec	0.017*	1.35	0.18*
Maximum Operating Vel. m/sec	0.033	6.38**	0.33
Typical U_f/U_{mf}	9.5	2.6	5.5
Maximum U_f/U_{mf}	18.3	12.3**	10.2
Typical Fuel Heat Value Per Unit Bed Area, kW ***	27	2070	271
Maximum Fuel Heat Value Per Unit Bed Area, kW ***	51	N/A**	501
Typical Packed Bed Heat Flux $\text{kW}/\text{m}^2, \eta_c = 0.60, L_m = 100\text{mm}$	162	12420	1626
Maximum Packed Bed Heat Flux $\text{kW}/\text{m}^2, \eta_c = 0.60, L_m = 100\text{mm}$	304	N/A**	3006

* Taken at Mid Operating Range for comparison.

**It is not expected that lightweight particulate biomass fuels can be burnt with superficial velocities of this order due to pneumatic transport losses

***Calculations based on stoichiometric Air/Fuel ratio and fuel calorific value of dry bagasse, 19500 kJ/kg.

(d)"Peat Fired Fluidised Bed Combustor Indicates Potential for the Sugar Mill Bagasse/Coal Fired Boilers"

The experience of researchers Pontifex.K.R. et al., (14) with fluidized combustion of peat is of interest. Peat which is an irregular, fibrous waste fuel was burnt successfully in a fluidized bed combustor. Combustion was proven for fuel moisture levels from 45 to 65% by mass with gross calorific values of 8.4-11.2 MJ/kg. The peat used consisted of wood-like twigs, long fibrous strands and compact nuggets like small pieces of brown coal. Combustion was autothermic at temperatures of 800-900°C. Combustion was quantified as 55% in-bed (primary) and 45% above bed (secondary). Fuel was added by a drop chute feeder. Researchers noted that some of the very fine particles of fuel ignited before reaching the bed and that secondary stage combustion was mainly burning particles suspended in the air stream. Complete combustion of suspended particles is ensured prior to reaching the superheater tubes by a 14m column giving a 4 second residence time for rising gases.

Evaluation: The fluidized bed is essentially used as a partial gasifier/partial combustor of the poor quality fuel. There are no heat transfer surfaces in the bed itself. The heat release in the bed only needs to be sufficient to balance the sum of its losses. No advantage can be taken, therefore, of the superior bed-to-surface heat transfer coefficients available in the fluidized bed. It should also be noted that peat has a lower percentage of volatiles (65-70%) than bagasse (80-85%). The compact nuggets of peat which are similar to coal would contribute significant levels of below bed combustion.

Conversely, bagasse is light fibrous particles, short fibres and dust and even the largest particles would not provide comparable energy or the long burn out time which would be expected from peat nuggets. The method of evaluating above and below bed surface combustion was not given so it is not known whether this is an estimate or a calculated result. Overall the paper provides a useful contribution toward a practical bagasse burner and its ideas are taken up in the Gasifier options in the Recommendations for Further Work.

3.0 THEORY

3.1 Nomenclature

Symbol	Definition
A	Area, m^2
A_p	Particle surface area, m^2
A_r	Archimedes Number, $\rho_g (\rho_p - \rho_g) g d_p^3 / \mu_g^2$
A_t	Plan or tube area, m^2
a'	Specific surface, particle basis, m^2/m^3
a	Specific surface, bed volume basis, m^2/m^3
a_p	Particle acceleration, m/sec
C_d	Drag Coefficient
C_{pp}	Specific heat of bed Solids, $kJ/kg K$
\bar{C}_{pa}	Average Specific heat of air, $kJ/kg K$
\bar{C}_{pf}	Average Specific heat of fuel, $kJ/kg K$
\bar{C}_{pw}	Average Specific heat of water, $kJ/kg K$
C_{pBe}	Equivalent specific heat of bed structure and solids, $kJ/kg K$

CV	Lower Calorific Value, kJ/kg
$CV_{T_{1,2}}$	Lower Calorific Value corrected for operating conditions, kJ/kg
D_c	Diameter of Bed Column, Spouted Bed, m
D_i	Diameter of Air Inlet, Spouted Bed, m
D_s	Diameter of Spout, Spouted Bed, m
d_c	Diameter of cylindrical particle, m
d_B	Diameter of Bubble, m
d_p	Equivalent particle diameter, m
\bar{d}_p	Mean surface particle diameter, m
d_{pf}	Equivalent fuel particle diameter, m
d_t	Tube diameter of bed, m
F	Force, N
F_b	Buoyancy Force, N
F_d	Drag Force, N

Fr_{mf}	Froude number based on U_{mf} and d_p .
f	Pipe friction factor
GCV	Gross or Higher Calorific Value, kJ/kg
g	Gravitational acceleration, m/s^2
H_{P_0}	Enthalpy of products at calorimeter test temperature, kJ/kg
$H_{P_{T_2}}$	Enthalpy of products at actual final temperature, kJ/kg.
H_{R_0}	Enthalpy of reactants at calorimeter test temperature, kJ/kg
$H_{R_{T_1}}$	Enthalpy of Reactants at actual initial temperature, kJ/kg
ΔH_w	Latent heat of water at operating pressure, kJ/kg
h_o	Enthalpy of water at initial temperature, kJ/kg
h_{pi}	Enthalpy of moisture at bed impact temperature, kJ/kg
h_{300}	Enthalpy of steam at $300^\circ C$, kJ/kg

h_B	Enthalpy of steam at bed temperature, kJ/kg
h_{conv}	Heat transfer coefficient for natural convection cooling of bed, kW/m ² K
h_{gp}	Gas to particle heat transfer coefficient, W/m ² K
h_{pp}	Particle to particle heat transfer coefficient, W/m ² K
L_f	Height of fluidized bed, m
L_m	Height of packed bed, m
$L_{m_{max}}$	Maximum Height of Spouted Bed that will Spout, m.
L_{mf}	Height of bed at minimum fluidization, m
J	Turnover rate of solids, kg/m ² s
m_B	Mass of bed solids, kg
m_p	Mass of particle, kg
\dot{m}_a	Mass flow of air, kg/s
\dot{m}_f	Mass flow of fuel, kg/s

\dot{m}_{fn}	Net mass flow of fuel to the bed, kg/s
\dot{m}_{ft}	Mass flow of fuel pneumatically transported and lost from above the bed, kg/s
\dot{m}_{fd}	Mass flow of fuel decomposed to char and volatiles above bed before bed entry. kg/s
\dot{m}_{mf}	Mass flow of air for U_{mf} , kg/s
\dot{m}_w	Mass flow of moisture with fuel, kg/s
MC	Moisture content of fuel
MC_o	Moisture content of fuel at initial conditions
Nu_D	Nusselt Number based on cylinder diameter
Nu_p	Nusselt Number based on equivalent particle diameter
n	Drying index, s^{-1}
O_r	Operating Ratio: Ratio of Maximum possible Useful Heat release at operation condition to that at ideal fuel /air conditions.
P	Pressure, Pa
P_a	Atmosphere Pressure, Pa

P_b	Pressure at Base of the Bed, Pa
P_{drop}	Bed Pressure drop, Pa
P_{max}	Maximum pressure drop across the bed, ie Bed weight per unit area for gas fluidization, Pa
P_o	Static Pressure Measured Using Pitot-Static Tube, Pa
Pr	Prandtl Number
P_s	Stagnation Pressure Measured Using Pitot-Static Tube, Pa
P_t	Pressure at Top of the Bed, Pa
Q_a	Heat supplied to the air, kW
Q_B	Heat supplied to bed solids ,kW
$Q_{B_{max}}$	Maximum possible heat supplied to bed solids at the given operating and fuel conditions, kW
$Q_{B_{th_{max}}}$	Maximum possible heat supplied to bed solids with dry fuel,stoichiometric mixture and zero wall losses(ie ideal conditions), kW
Q_c	Heat supplied to heat transfer cooling surfaces, kW
Q_f	Heat supplied to the fuel, kW

Q_1	Total wall and convective Heat lost during cooldown, kW
Q_{lw}	Heat lost through combustor walls, kW
Q_{Total}	Total Heat Release Below Bed Surface, kW
Q_w	Heat supplied to fuel moisture, kW
Re_p	Reynold's number based on equivalent surface mean particle diameter and superficial velocity.
Re_{pt}	Reynold's number based on equivalent particle diameter and terminal particle velocity.
s	Particle fall displacement, m
st	Subscript indicating stoichiometric air-fuel ratio
T	Temperature in C or K as specified
T_s	Temperature at Stagnation Point on a Pitot-Static Tube, K
T_B	Temperature of bed solids, C
T_{gi}	Input or Initial gas temperature, C
T_{ge}	Exit or final gas temperature, C

T_o	Ambient temperature, C
T_p	Particle temperature, C
Δt_{fall}	Particle fall time in flue gases, s
t	Time, s
U_{mf}	Minimum Superficial Fluidizing Velocity (gas velocity in an empty tube), m/s
U_f	Superficial Velocity, m/s
U_t	Terminal Velocity of Particle, m/s
U_{rel}	Velocity of particle relative to flue gas, m/s
u_B	Absolute bubble rise velocity, m/s
u_{br}	Relative bubble rise velocity, m/s
u_p	Absolute particle velocity, m/s
\dot{V}	Volumetric Flow, m ³ /s
V_B	Bubble volume, m ³
V_w	Bubble wake volume, m ³

V_p Particle volume, m^3

Greek Symbols

α Ratio of bubble wake volume to bubble volume

α_f Fraction of heat supplied to the fuel by the bed solids

α_w Fraction of heat supplied to fuel moisture by the bed solids

ϵ_f Voidage of fluidized bed

ϵ_m Voidage of packed (unfluidized) bed

ϵ_{mf} Voidage at minimum fluidization velocity

η_c Combustion efficiency of the fluidized bed: proportion of fuel combustion heat release below bed surface, Eqs. 3.47, 3.48, 3.49

$\eta_{c_{min}}$ Minimum combustion efficiency required for sustained operation (ie constant bed temperature) with the production of no useful heat in the bed, Eq. 3.54

η_B Fluidized bed efficiency or Heat transfer efficiency: ratio of actual useful heat to maximum useful heat possible at a given operation condition, Eq 3.59

η_{BC}	Overall bed efficiency: ratio of useful heat transfer to the total fuel heat supplied, Eq.3.60
$\eta_{BC_{max}}$	Maximum overall bed efficiency at given operating and fuel conditions, Eq.3.61
$\eta_{BC_{thmax}}$	Theoretical maximum or limiting overall bed efficiency for dry fuel, stoichiometric mixtures and no heat losses through combustor walls (ie ideal conditions), Eq. 3.62
γ	Angle of internal friction of a particulate solid
δ	Bubble fraction
ϕ	Sphericity
μ_g	Gas dynamic viscosity, Pa.s
ρ_f	Effective density of fluidised bed, kg/m^3
ρ_g	Gas density, kg/m^3
ρ_m	Packed bed density or bulk density of a particulate solid, kg/m^3
ρ_{mf}	Effective density of bed at minimum fluidization conditions, kg/m^3
ρ_p	Particle density, kg/m^3

ρ_{pf}	Fuel particle density, kg/m^3
ρ_{pf_0}	Initial fuel particle density including moisture, kg/m^3
ψ_m	Packed Bed Heat Flux, kW/m^3 , Eq. 3.45
ψ_f	Operating Heat Flux, kW/m^3 , Eq. 3.46
ζ	Behaviour Index, Eqs. 3.30, 3.31

3.2 Gross Fluid-Particle Behaviour

(a) Definitions

Particle Diameter

$$d_p = \left[\frac{6 (\text{Particle Volume})}{\pi} \right]^{(1/3)} = \left[\frac{6 V_p}{\pi} \right]^{(1/3)} \quad (3.1)$$

Ref. (3)

Sphericity

$$\phi = \left[\frac{\text{Surface Area of Sphere}}{\text{Surface Area of Particle}} \right]_{\text{same volume}} \quad (3.2)$$

Ref. (3)

Voidage

$$\epsilon = \frac{\text{Volume} - \text{Volume}_{\text{solids}}}{\text{Volume}} = 1 - \frac{\rho_f}{\rho_p} \quad (3.3)$$

Ref. (15)

Specific Surface

$$a' = \frac{\text{Surface of Particle}}{\text{Volume of Particle}} = \frac{6}{\phi d_p} \quad (3.4)$$

$$a = \frac{\text{Surface of Particles}}{\text{Volume of bed}} = \frac{6 (1 - \epsilon_m)}{\phi d_p} \quad (3.5)$$

Ref. (3)

Surface Mean Particle Size

$$\bar{d}_p = \frac{1}{\sum \left[\frac{x}{d_p} \right]_i} \quad (3.6)$$

Ref. (3)

(b) Bed Pressure Drop

For conventional beds, uniform flow distributor plate, vertical walls, the pressure drop is given by Ergun's equation.

$$\frac{\Delta P}{L} = 150 \frac{(1-\epsilon)^2}{\epsilon^3} \frac{\mu_g U_f}{(\phi \bar{d}_p)^2} + 1.75 \frac{(1-\epsilon)}{\epsilon^3} \frac{\rho_g U_f^2}{\phi \bar{d}_p} \quad (3.7)$$

Ref. (15)

For U_f greater than minimum fluidization velocity

$$\frac{\Delta P}{L_f} = (1 - \epsilon_f) (\rho_p - \rho_g) g \quad (3.8)$$

Ref. (3)

If voidage is expressed in terms of bed solids bulk and particle densities the equation becomes:

$$\Delta P A_t = \frac{m}{\rho_p} (\rho_p - \rho_g) g \quad (3.9)$$

Ref. (16)

and for systems fluidized with gases such as air and dense bed solids:

$$\Delta P = \frac{mg}{A_t} \quad \text{where} \quad \rho_p \gg \rho_g \quad (3.10)$$

or simply, when the bed is fluidized the weight per unit area is equal to the pressure drop across it. As superficial velocities increase, voidage and the expanded bed depth increase keeping pressure drop constant until pneumatic transport velocities are reached.

(c) Minimum Fluidization Velocity

Various correlations for minimum fluidization are offered by different authors.

$$U_{mf} = \frac{d_p^2 (\rho_p - \rho_g) g}{877 \mu_g} \quad (3.11)$$

Ref. (17)

$$U_{mf} = \frac{d_p^2 (\rho_p - \rho_g) g}{1235 \mu_g} \quad (3.12)$$

Ref. (17)

$$U_{mf} = \frac{d_p^2 (\rho_p - \rho_g) g}{1650 \mu_g} \quad Re_p < 20 \quad (3.13)$$

Ref. (3)

Equation 3.13 assumes

$$\frac{1}{\phi \epsilon_{mf}^3} = 14 \quad \text{and} \quad \frac{1 - \epsilon_{mf}}{\phi^2 \epsilon_{mf}^3} = 11 \quad (3.14, 3.15)$$

Ref. (3)

Other Correlations include:

$$U_{mf} = 0.00044 \rho_g^{-0.067} (g(\rho_p - \rho_g))^{1.063} d_p^{2.059} \mu_g^{-0.996} \quad (3.16)$$

Ref. (17)

$$U_{mf} = 0.00094 \rho_g^{-0.066} (g(\rho_p - \rho_g))^{0.934} d_p^{1.8} \mu_g^{-0.87} \quad (3.17)$$

Ref. (15)

Equation 3.17 is for small particles <100 microns.

Alternative solutions are given as solutions of re-arranged Ergun's Equation.

$$Ar = 150 \frac{(1-\epsilon_{mf})}{\epsilon_{mf}^3} \frac{Re_{pmf}}{\phi^2} + 1.75 \frac{Re_{pmf}}{\epsilon_{mf}^3 \phi} \quad (3.18)$$

Ref. (15)

$$Ar = 1823 Re_{pmf}^{1.07} + 21.7 Re_{pmf}^2 \quad (3.19)$$

Ref. (15)

Comparison of the various correlations show little significant variation in the more recent authors as shown by the following table for 490 micron sand.

Table 3.1 Comparative Predictions of Minimum Fluidization Velocity, m/s

Equation Source & No.	T =27C	T =600C
Davidson, Eq.3.11	0.339	0.142
Rowe, Eq.3.12	0.241	0.101
Leva, Eq.3.16	0.149	0.068
Baeyens, Geldart, Eq.3.19	0.140	0.075
Ergun, Eq.3.18	0.167	0.075
Kunii, Eq. 3.13	0.180	0.076

For reasons of ease of use and acceptable accuracy, the equation proposed by Kunii was used in calculations. It was also noted that the consistency of predictions was greater at elevated temperatures with good agreement between Leva, Baeyens, Ergun and Kunii.

(d) Spouted Beds.

Since a modified Spouted Bed was utilised in the final stages of the project the simple theory used for calculations is included.

(i) Peak Pressure Drop

The required pressure to rupture the bed and begin spouting will fall between the two equations:

$$\Delta P = \frac{mg}{A_t} = \rho_m g L_m \quad (3.20)$$

Ref. (18)

which is the same as the pressure drop for a conventional gas fluidized bed, and the equation:

$$\Delta P = \rho_m g L_m \left[\left[\frac{6.8}{\tan \gamma} \frac{D_i}{D_c} + 0.8 \right] - 34.4 \frac{d_p}{L_m} \right] \quad (3.21)$$

Ref. (18)

(ii) Operating Pressure Drop

Operating pressure drop is typically 70-80% of the pressure required to support the whole weight of the bed. (18)

(iii) Maximum Spoutable Depth

Various Correlations are given, eg:

$$L_{m_{\max}} = 0.72 D_c^2 / D_s \quad (3.22)$$

$$L_{m_{\max}} = 0.67 D_c^{4/3} / d_p^{1/3} \quad (3.23)$$

$$L_{m_{\max}} = 0.192 \, d_p \, D_c^4 / (D_i^2 D_s^2) \quad (3.24)$$

$$L_{m_{\max}} = 0.168 \, d_p^{1/3} \, D_c^{8/3} / D_i^2 \quad (3.25)$$

Ref. (18)

3.3 Thermodynamic Behaviour

(a) Operational Velocities.

As in Section 3.2, Minimum Fluidization conditions for sand particle sizes in the ranges considered in this research are predicted by the equation

$$U_{mf} = \frac{\bar{d}_p^2 (\rho_p - \rho_g) g}{1650 \mu_g} \quad Re_p < 20 \quad (3.26)$$

Ref. (3)

The upper limit of fluidized bed operation is given by the terminal velocity of the particles of smallest diameter in the bed being either:

$$U_t = \frac{d_p^2 (\rho_p - \rho_g) g}{18 \mu_g} \quad Re_p < 0.4 \quad (3.27)$$

or:

$$U_t = \left[\frac{4}{225} \frac{(\rho_p - \rho_g)^2 g^2}{\rho_g \mu_g} \right]^{(1/3)} d_p \quad 0.4 < Re_p < 500 \quad (3.28)$$

Ref. (3)

Minimum fluidization velocity is clearly inversely proportional to gas viscosity. For particles of higher density in gas flow, the density difference term is almost constant. Since air viscosity increases with temperature U_{mf} must decrease. The reduced gas density is however significant in reducing the mass flow for U_{mf} as :

$$\dot{m}_{mf} = \rho_g A_t U_{mf} \quad (3.29)$$

where both ρ_g and U_{mf} are reduced with temperature. The result is that for a given operational condition, for example $4U_{mf}$, the Free Air Delivery has to be continually reduced in proportion to bed temperature increase, (Figs.G1 to G8, Appendix G).

Conversely, the upper limit of operation will increase if the Reynolds number calculated on smallest particle diameter and terminal velocity is in the range $0.4 < Re_p < 500$, but decrease if $Re_p < 0.4$ due to the significance of either changes in gas viscosity or a combination of changes in gas viscosity and density as predicted by Equations 3.27 & 3.28.

(b) Operational Regime

The regime of fluidization may change in some cases from bubbling/aggregative to smooth/particulate during warm up as the criteria are:

$$\zeta = Fr_{mf} Re_{p_{mf}} \left(\frac{\rho_p - \rho_g}{\rho_g} \right) \left(\frac{L_{mf}}{d_t} \right) < 100 \quad \text{smooth} \quad (3.30)$$

$$\zeta = Fr_{mf} Re_{p_{mf}} \left(\frac{\rho_p - \rho_g}{\rho_g} \right) \left(\frac{L_{mf}}{d_t} \right) > 100 \quad \text{bubbling} \quad (3.31)$$

Ref. (3)

For the purposes of reporting the above criteria will be referred to as the Behaviour Index. A distinction must be made between these criteria and the flow regimes in the bed voids which are:

which are:	$Re_p < 10$	Laminar
	$10 < Re_p < 1000$	Transitional
	$Re_p > 1000$	Turbulent , (15)

(c) Bubbling Behaviour and Solids Turnover Rate

Bubble rise velocity relative to emulsion phase is given by:

$$u_{br} = 0.711 \sqrt{g d_B} \quad (3.32)$$

Ref. (3)

and absolute bubble rise velocity is given by:

$$u_B = U_f - U_{mf} + u_{br} \quad (3.33)$$

Ref. (3)

According to the two-phase theory for bubbling beds:

$$\Sigma A_B u_B = (U_f - U_{mf}) A_t \quad (3.34)$$

Ref. (7)

The increase of temperature at constant free air delivery will result in a larger percentage of flow in the bubble phase. The superficial velocity will increase due to reduced density and the minimum fluidization velocity will decrease due to increased air viscosity. As Kunii and Levenspiel, (3), report the virtual independence of bubble frequency from gas flow rates at distances greater than 150mm above the distributor, the consequence of increased temperature whilst keeping Free Air Delivery constant is bubbles of larger volume. This conclusion is supported by Broughton and Howard, (7).

The turnover rate of solids can be determined by:

$$J = \alpha \delta u_B \rho_p (1 - \epsilon_{mf}) \quad \text{kg/m}^2 \text{s} \quad (3.35)$$

Ref. (3)

where :

$$\alpha = \frac{V_w}{V_B} = 0.25 \quad \text{for sand} \quad (3.36)$$

Ref. (3)

and :

$$\delta = 1 - \frac{L_{mf}}{L_f} = 1 - \frac{\rho_f}{\rho_{mf}} = \frac{\epsilon_f - \epsilon_{mf}}{1 - \epsilon_{mf}} \quad (3.37)$$

Ref. (3)

Theoretical values of ϵ_f can be determined by substituting the voidage - bed depth relationship from the above equation, (Eq.3.37) into Ergun's equation (Eq.3.7) and solving the resulting quadratic equation for various voidage values. Theoretical values relating ϵ_f to the ratio U_f/U_{mf} , δ , J , u_B , u_f , u_e and u_s for the sand sizes used in this project are generated and presented in Tables F7 to F14, (Appendix F). Alternatively, the bubble size can be measured or estimated and δ can be obtained by re-arranging one of the following equations:

$$U_f = (1 - \delta) U_{mf} + \delta (u_B + 3 U_{mf}) \quad \text{where} \quad \frac{u_B}{(U_{mf}/\epsilon_{mf})} < 1 \quad (3.38)$$

$$U_f = (1-\delta) U_{mf} + \delta U_B \quad \text{where} \quad \frac{U_B}{(U_{mf}/\epsilon_{mf})} > 5 \quad (3.39)$$

Ref. (3)

(d) Heat Transfer Coefficients within the Bed

(i) Gas-to-Particle

$$Nu_p = \frac{h_{gp} d_p}{k_g} = 0.03 Re_p^{1.3} \quad (3.40)$$

Ref. (16)

(ii) Bed Particle-to-Fuel Particle

The following equation is given for coal with k_g modified for radiation.

$$h_{pp} = \frac{2k_g}{d_{pf}} + \frac{0.016}{\sqrt{d_p}} \quad \text{kW/m}^2 \cdot \text{K} \quad (3.41)$$

Ref. (7)

As the equation does not refer to properties specific to coal it is useful for calculating the orders of magnitude of h_{pp} for bagasse and sawdust. Some modification would be expected for the lower sphericity but a more detailed empirical formula was not found. For the purposes of calculation the values obtained for h_{pp} would be conservative, as appropriate increases in k_g for radiation, were not known, and could not be added.

(iii) Bed Particles-to-Surface Heat Transfer Coefficients

These are not detailed as the thesis is only concerned with achieving sustainable operations, that is, adequate heat

transfer to the bed solids. Bed to Surface Heat Transfer theory is well developed, except for the annulus flow area of spouted beds, and can be found in texts by Botterill, (1), Howard, (15) and Kunii, (3).

(e) Thermal Equilibrium of Gas and Solids

The relationship between air entry and exit temperatures is given by:

$$\frac{T_{g_e} - T_B}{T_{g_i} - T_B} = \exp \left[- \frac{h_{gp}}{\rho_g U_f \bar{C}_{pa}} \frac{6 (1 - \epsilon_f) L_f}{\phi \bar{d}_p} \right] \quad (3.42)$$

which can be written as :

$$\frac{T_{g_e} - T_B}{T_{g_i} - T_B} = \exp \left[- \frac{Nu_p}{Pr Re_p} \frac{6 (1 - \epsilon_m) L_m}{\phi \bar{d}_p} \right] \quad (3.43)$$

Ref. (3)

(f) Changing Bed Temperature with Time

Similar expressions are derived for the change of bed temperature with time.

$$\frac{T_{g_i} - T_B}{T_{g_i} - T_{Bo}} = \exp \left[\frac{-\rho_g \bar{C}_{pg} U_f t}{\rho_p \bar{C}_{pp} (1 - \epsilon_m) L_m} \right] \quad (3.44)$$

Ref. (3)

If the Fluidized Bed Combustor is small the heat stored in the steel structure and insulation becomes significant, therefore the specific heat of the bed solids must be replaced by an equivalent specific heat for the bed as a whole, C_{pBe} .

(g) Heat Flux**(i) Packed Bed Heat Flux**

$$\psi_m = \frac{\dot{m}_f CV \eta_c}{A_t L_m} \quad (3.45)$$

(ii) Operating Bed Heat Flux

$$\psi_f = \frac{\dot{m}_f CV \eta_c}{A_t L_f} \quad (3.46)$$

The most useful criteria for quantifying heat flux in a combustor without water heating tubes is the packed bed heat flux, (Eq.3.45), because it can be related directly to sand volume and sand surface area. Operating heat flux will always be a lower value than packed bed heat flux due to expansion of the bed.

3.4 Combustion Heat Release Below Bed Surface.

In analysing the burning of a lightweight fuel, with a high volatiles content (eg cellulose 80% by mass), in a Fluidized Bed Combustor, the most important quantity to measure is the heat release which occurs below the bed surface. Three modes of Combustor operation are possible:

- (i) Sufficient heat release below bed surface for heat transfer to heat extraction surfaces , eg steam pipes
- (ii) Sufficient heat release to balance flue gas losses but no useable heat extracted. In this case the Fluidized Bed Combustor output is limited to the production of hot gases.
- (iii) Insufficient heat release to maintain bed temperature.

Energy balance within the bed for steady conditions is given by:

(Heat Release in Bed) = (Air Enthalpy Increase)+(Solids Heat Removal)+(Heat Removed by Cooling Surfaces)

That is ,

$$\dot{m}_f CV \eta_c = \dot{m}_a \bar{C}_{pa} (T_B - T_0) + \dot{m}_f \bar{C}_{pf} (T_B - T_0) + Q_c \quad (3.47)$$

Ref. (7)

For the experimental Combustor used, no heat transfer surfaces were added, so it is necessary to consider the rate of change of heat stored in the bed structure and solids. The above equation also assumes dry fuel. Cellulose fuels can be moist. The amount of heat required to heat the fuel solids and evaporate and superheat water also depends on the fuel feed

point. With a light fuel such as bagasse, a proportion of smaller particles will be immediately lost to the flue stream if the fuel is fed from the top. Modifying the equation for these parameters gives:

$$\begin{aligned} \dot{m}_f C V \eta_c = & \dot{m}_a \bar{C}_{pa} (T_B - T_O) + \alpha_f \dot{m}_f \bar{C}_{pf} (T_B - T_O) \\ & + m_B C_{pBe} \frac{(T_{B2} - T_{B1})}{(t_2 - t_1)} + \alpha_w \dot{m}_w (h_B - h_O) + Q_{lw} \end{aligned} \quad (3.48)$$

The equation must be evaluated at average conditions between time t_1 and t_2 . The equation still assumes steady air and fuel mass flows.

The below surface combustion efficiency η_c approaches 100% for a deep bed and/or dense fuels of low volatile contents.

The factors α_f and α_w are the fraction of the total possible heat supplied by the bed solids and absorbed by fuel and fuel moisture respectively. In a deep bed with fuel introduced at the bottom it can be assumed that α_f and α_w equal unity. For top feed systems α_f and α_w will be less than unity. Methods of estimating α_f and α_w are given in Section 3.42.

The product $m_B C_{pBe}$ must be determined experimentally as the heat stored in the steel bed walls and insulation contribute to the thermal response of the Combustor. The experimental method used and forms of the energy balance equation used are given in Section 3.41.

The heat loss term Q_{lw} must be estimated theoretically for the wall area which is in contact with the bed solids.

Replacing the heat transfer terms with single symbols, the energy balance equation 3.48 can be rewritten more neatly as follows:

$$\dot{m}_f CV \eta_c = Q_a + \alpha_f Q_f + Q_B + \alpha_w Q_w + Q_{lw} \quad (3.49)$$

Refer to Section 3.1 for nomenclature. The useful heat that could be extracted by heat transfer surfaces in the bed is then just Q_B , which can be written as:

$$Q_B = \dot{m}_f CV \eta_c - (Q_a + \alpha_f Q_f + \alpha_w Q_w + Q_{lw}) \quad (3.50)$$

The three modes of Fluidized Bed Combustor operation, as detailed in the first paragraph of this section, can now be quantified as:

$$(i) \quad Q_B > 0, \quad \dot{m}_f CV \eta_c > (Q_a + \alpha_f Q_f + \alpha_w Q_w + Q_{lw}) \quad (3.51)$$

$$(ii) \quad Q_B = 0, \quad \dot{m}_f CV \eta_c = (Q_a + \alpha_f Q_f + \alpha_w Q_w + Q_{lw}) \quad (3.52)$$

$$(iii) \quad Q_B < 0, \quad \dot{m}_f CV \eta_c < (Q_a + \alpha_f Q_f + \alpha_w Q_w + Q_{lw}) \quad (3.53)$$

Hence useful heat is dependent on a minimum η_c value and can be reduced to zero or become negative (ie bed cooling) if there is too much excess air, fuel moisture and wall heat loss.

Taking Eq.3.52 and re-writing, assuming minimum air (stoichiometric mixture), the minimum η_c values, for sustainable operation without yielding useful heat, (i.e. $Q_g=0$), for various fuel moisture contents can be calculated. eg.

$$\eta_{c_{\min}} = \frac{[5.09 \bar{C}_{pa} + \alpha_f \bar{C}_{pf} + \alpha_w \bar{C}_{pw} MC / (1-MC)] (T_B - T_o)}{CV} \quad (3.54)$$

The requirement imposed by moisture is demonstrated in theoretical curves generated from the above equation in Fig.E8. The equation also illustrates the dependence on air/fuel ratio (5.09 for cellulose), calorific value and bed temperature for sustained operation.

(a) The Maximum Useful FBC Heat Transfer

The Maximum Useful Heat which could be extracted at a given operating condition is then:

$$Q_{B_{\max}} = \dot{m}_f CV - (Q_a + \alpha_f Q_f + \alpha_w Q_w + Q_{lw}) \quad (3.55)$$

The theoretical maximum useful heat would occur when Q_a is a minimum and Q_w and Q_{lw} are zero hence:

$$Q_{B_{th_{\max}}} = \dot{m}_f CV - (Q_{a_{\min}} + \alpha_f Q_f) \quad (3.56)$$

Which is :

$$Q_{B_{th_{\max}}} = \dot{m}_f [CV - (T_B - T_o) ((\dot{m}_a / \dot{m}_f)_{st} \bar{C}_{pa} + \alpha_f \bar{C}_{pf})] \quad (3.57)$$

(b) Fluidized Bed Operating Ratio

An operating ratio of a fluidized bed at given bed temperature can therefore be found in terms of the ratio of the maximum useful heat possible at the given operating condition to the theoretical maximum. The operating ratio for the fluidized bed will be defined as:

$$\text{Operating ratio} = O_r = \frac{Q_{Bmax}}{Q_{B_{th_{max}}}} \quad (3.58)$$

The ratio O_r will always be less than 100% for excess air or stoichiometric operations as $Q_{lw} > 0$. The operating ratio should not be used for comparison where air/fuel ratios fall below stoichiometric which could give ratios greater than 100% or mask the effect of fuel moisture.

(c) Fluidized Bed Efficiency or Heat Transfer Efficiency

A convenient measure of the efficiency of useful heat transfer is the Fluidized Bed Efficiency. It will be defined as the percentage of maximum useful heat which is available in the bed for a given air flow, fuel flow and fuel moisture flow. eg.

$$\eta_B = \frac{Q_B}{Q_{Bmax}} \quad (3.59)$$

Fluidized bed efficiency η_B will generally be lower than η_c , and will approach 100% as η_c approaches 100%

(d) Overall Bed Efficiency

The Overall Bed Efficiency will be defined as the ratio of useful heat release in the bed to the total heat release of the fuel:

$$\eta_{BC} = \frac{Q_B}{\dot{m}_f CV} \quad (3.60)$$

The maximum value of Overall Bed Efficiency at a given operating condition is given by:

$$\eta_{BC_{\max}} = \frac{Q_{B_{\max}}}{\dot{m}_f CV} \quad (3.61)$$

and the maximum theoretical overall bed efficiency is:

$$\eta_{BC_{th_{\max}}} = \frac{Q_{B_{th_{\max}}}}{\dot{m}_f CV} = 1 - \frac{(T_B - T_O) ((\dot{m}_a / \dot{m}_f)_{st} \bar{C}_{pa} + \alpha_f \bar{C}_{pf})}{CV} \quad (3.62)$$

The above equation relates bed temperature, air/fuel ratio, specific heats of air and fuel and fuel calorific value to a maximum limiting value. The maximum theoretical overall bed efficiency for cellulose fuels is typically 70% to 80% for a bed temperature of 600°C.

3.41 Determination of Equivalent Specific Heat of Fluidized Bed Combustor Structure and Solids.

During Combustor cooldown the energy balance Eq.3.48 simplifies to:

$$0 = \dot{m}_a \bar{C}_{pa} (T_B - T_O) + m_B C_{pBe} (T_{B2} - T_{B1}) / (t_2 - t_1) + Q_1 \quad (3.63)$$

The heat loss through the Combustor walls Q_{lw} becomes Q_l , and includes cooling to the top of the bed by natural convection. It is assumed that natural convection heat loss through the top bed surface is small during combustion, due to heat release being partially above the bed. The heat loss Q_l must be obtained experimentally and is given by :

$$Q_l = h_{conv} A (T_B - T_O) \quad (3.64)$$

During cooling without air flow the energy balance Eq.3.48 becomes:

$$0 = m_B C_{pBe} (T_{B2} - T_{B1}) / (t_2 - t_1) + Q_l \quad (3.65)$$

Which is:

$$0 = m_B C_{pBe} (T_{B2} - T_{B1}) / (t_2 - t_1) + h_{conv} A (T_B - T_O) \quad (3.66)$$

Equations 3.63 and 3.66 are then solved iteratively using Combustor cooldown data obtained with air flow for Eq.3.63, and without air flow for Eq.3.66. The value of Q_l in Eq. 3.65 is approximately equal to Q_l in equation Eq.3.63 as heat losses by both natural convection and conduction in the plenum chamber, during periods of no air flow, are small and can be neglected.

Having solved the energy balance equation for $m_B C_{pBe}$, the value obtained can then be used to determine η_c and other useful operational parameters as detailed in Section 3.4.

3.42 Estimation of Fuel and Moisture Heat Fractions for Above Bed Fuel Feed Systems (Evaluating Parameters α_f and α_w)

To determine α_f , two modes of fuel losses must be considered for above bed feeders, namely;

- (i) Pneumatic transport
- (ii) Decomposition.

The mass flow rate of fuel actually reaching the bed will be:

(Net mass flow into FBC) = (Total fuel mass flow) - (Fuel pneumatically transported) - (Fuel decomposed at $T > 300^\circ\text{C}$)

which is :

$$\dot{m}_{fn} = \dot{m}_f - \dot{m}_{ft} - \dot{m}_{fd} \quad (3.67)$$

Similarly the mass flow of moisture in the fuel must be modified for drying in the flue stream:

(Net Moisture into FBC) = (Total Moisture Flow) - (Moisture evaporated during feeding)

Which is:

$$\dot{m}_{wn} = \dot{m}_{fr} MC \quad (3.68)$$

The pneumatically conveyed mass fraction is obtained by analysing the particle size distribution and densities of the fuel. The mass fractions that dry and/or decompose must then be calculated for the remaining sample. If sawdust and bagasse particles are modelled as cylinders in an airstream then the drying period and heating period can be modelled by the following equations. (beginning on the next page)

The remaining moisture in a particle of given size is:

$$MC = MC_o(1 - nt) \quad (3.69)$$

Where n is given by :

$$n = \frac{2h_{gp}(T_g - T_o)}{\Delta H_w d_c \rho_{pf_o} (MC_o / (1 + MC_o))} \quad (3.70)$$

Ref. (8)

Similarly particle temperature is given by:

$$m_p \bar{C}_{pf} \frac{dT_p}{dt} = h_{gp} A_p (T_g - T_p) \quad (3.71)$$

Ref. (7)

Relationships given in Eqs. 3.69 & 3.71 are equally valid for heat transfer taking place within the bed. The gas-to-particle heat transfer coefficient is simply replaced by a particle-to-particle heat transfer coefficient. The relevant relationships after integration are then:

(i) Fuel particle temperature in a flue stream;

$$\frac{T_g - T_{p2}}{T_g - T_{p1}} = \exp \left(\frac{-6h_{gp}(t_2 - t_1)}{\phi d_{pf} \rho_{pf} \bar{C}_{pf}} \right) \quad (3.72)$$

(ii) Fuel particle temperature in a bed;

$$\frac{T_B - T_{p2}}{T_B - T_{p1}} = \exp \left(\frac{-6h_{pp}(t_2 - t_1)}{\phi d_{pf} \rho_{pf} \bar{C}_{pf}} \right) \quad (3.73)$$

For heat transfer above the bed times t_2 and t_1 must be

estimated from the terminal velocities of particles and flue gas velocity. A value for heat transfer coefficient h_{gp} can be estimated from empirical heat transfer equations applicable to a cylinder in a fluid stream. The percentage of moisture, fuel mass and fuel temperature entering the bed can then be obtained from the above equations.

Similarly particle residence times in the bed can be estimated using the equations relevant to in-bed heat transfer. As cellulose particles decompose at approximately 300°C particle residence as such ceases at this point. What is critical is the bed depth the particle has attained as both heat transfer from the burning fuel particle and heat transfer from the following fuel gas combustion depends on bed depth. The relationship between bed depth and equilibrium gas temperature is given by Eqs.3.42 & 3.43 in Section 3.3. Due to the very small bed residence times calculated it was estimated that the heat supplied by the bed and absorbed by the fuel would be only that required to bring the fuel to a temperature of 300°C. Some heat would be supplied to fuel particles above the bed surface before bed entry. The bed would supply heat to bring the particle from the temperature attained before entry to just above 300°C allowing for some heating of the exiting fuel gases. The combustion products would then be supplied with further heat by heat release above the bed surface. While it is realised that the true bed exit temperature of fuel reactants or products will be above 300°C there is no other logical estimate to take. Equilibrium bed depth is usually of the order of 10mm, (Table F2). There was no way to estimate or

measure particle penetration depth with the equipment available. The relationships for heat release from the bed combustion to incoming fuel then become:

$$\alpha_f \dot{m}_f \bar{C}_{pf} (T_B - T_o) = \dot{m}_{fn} \bar{C}_{pf} (300 - T_{pi}) \quad (3.74)$$

Similarly for fuel moisture

$$\alpha_w \dot{m}_w (h_B - h_o) = MC_1 \dot{m}_{fn} (h_{300} - h_{pi}) \quad (3.75)$$

Taking this approach values for α_f and α_w were typically 0.37 to 0.4 for above bed chute feeders.

3.43 Estimation of Fuel Particle Fall and Bed Residence Times.

(a) Continuous Fuel Feed Above the Bed Surface.

For continuous fuel feed, fuel can be considered on a particle by particle basis. The flue gas stream will provide the required heat energy for heat transfer proportional to the h_{gp} , particle surface area and temperature difference. If good particle - flue stream mixing is assumed the analysis will involve:

- (i) Estimation of Fuel Particle Transport Fraction.
- (ii) Estimation of Fuel Particle Fall Durations and Velocities.
- (iii) Calculation of Reynolds Number.
- (iv) Calculation of Nusselt Number.
- (v) Prediction of Moisture Content and Particle temperature at Ingestion.
- (vi) Particle Residence Time in the Bed

Typical values of fuel particle fall times and bed residence times are calculated and tabulated in Tables.E2 to E5.

(i) Estimation of the Pneumatic Transport Fraction

For a useful estimation of the terminal velocity of irregular shaped particles the relationship between the sphericity of the particle and the drag coefficient must be considered. True drag coefficients for non-spherical particles can be up to ten times the corresponding coefficient for a spherical particle predicted by the usual correlations of Reynolds number. Values of $C_d Re_p^2$ verses Re_p have been plotted

for various ϕ have been plotted by Kunii and Levenspiel, (3), (Fig.E5). The procedure is firstly to calculate the velocity independent group $C_d Re_p^2$ as follows:

$$C_d Re_p^2 = \frac{4gd_p^3 \rho_g (\rho_p - \rho_g)}{3\mu_g^2} \quad (3.76)$$

Ref. (3)

and then the Reynolds number corresponding to the sphericity is obtained from the chart, Fig.E5, allowing U_t to be calculated from

$$Re_{p_t} = \frac{\rho_g d_p U_t}{\mu_g} \quad (3.77)$$

Ref. (3)

The proportion of the fuel for which $U_t < U_f$ is the pneumatic transport fraction.

(ii) Estimation of Fuel Particle Fall Durations and Velocities.

The net force on a particle falling in an upward stream of gas is given by:

$$F = m_p a = m_p g - F_d - F_b \quad (3.78)$$

which gives an acceleration of:

$$a_p = \frac{m_p g - \frac{1}{2} A C_d U_{rel}^2 - V_p \rho_g g}{m_p} \quad (3.79)$$

The drag coefficients for spherical particles are given by:

$$(3.80)$$

$$C_d = \frac{24}{Re_p} \quad Re_p < 0.4$$

$$C_d = \frac{10}{Re_p^{0.5}} \quad 0.4 < Re_p < 500 \quad (3.81)$$

$$C_d = 0.43 \quad 500 < Re_p < 200,000 \quad (3.82)$$

Ref. (3)

For non-spherical particles C_d must be corrected from Fig.E5. Since the velocity of the falling particle is not constant the ratio of the actual C_d to that for a spherical particle must be related to Re_p by regression analysis for the range of Reynolds number expected. With an approximate relationship between C_d and Re_p , Eq.3.79 can be solved numerically by writing:

$$\Delta u_p = \left[\frac{m_p g - \frac{1}{2} A f(Re_p) U_{rel}^2 - V_p \rho_g g}{m_p} \right] \Delta t \quad (3.84)$$

Which gives the displacement and absolute velocity of the particle at any time t . eg

$$u_p(t) = \sum \Delta u_p \quad ; \quad s(t) = \sum u_p \Delta t \quad (3.85, 3.86)$$

(iii) Calculation of Reynolds Number

Having obtained u_p and Re_p at various times t , sufficient

information is available to estimate an average value of Re_p and hence calculate average Nusselt number. Some Nusselt number relationships require Re_D based on cylinder diameter which can also be obtained from the iterative data generated for u_p .

(iv) Calculation of Nusselt Number.

(i) For Cylinders.

$$Nu_D = \frac{hd_D}{k} = C Re_D^m Pr^{1/3} \quad (3.87)$$

Where Constants C and m are given by :

Re_D	C	m
0.4-4	0.989	0.33
4-40	0.911	0.385
40-4000	0.683	0.466

Ref. (19)

(ii) For Spheres.

$$Nu_d = \frac{hd}{k} = 2 + 0.6 Re_d^{0.5} Pr^{1/3} \quad (3.88)$$

Ref. (19)

From Nusselt number it is a simple matter to calculate average h_{gp} during the particle fall period.

(v) Prediction of Moisture Content and Particle Temperature at Ingestion.

Moisture content and particle temperature at bed surface entry are calculated using Eqs 3.69 and 3.72. The particle-by-particle analysis assumes sufficient heat energy is available in flue gases.

Fuel pre-heat during falling may be limited by the heat available since:

(Heat Lost by Flue Gases) = (Heat gained by fuel & fuel moisture)

Which is:

$$\dot{m}_a \bar{C}_{pa} (T_g - T_{pi}) = (\dot{m}_f - \dot{m}_{ft}) \bar{C}_{pf} (T_{pi} - T_o) + \dot{m}_w \bar{C}_{pw} (T_{pi} - T_o) \quad (3.89)$$

If T_{pi} obtained from the above equation is less than T_{pi} obtained from particle-by-particle analysis then the fuel pre-heat is energy limited rather than heat transfer rate limited. The best estimate of T_{pi} is the lowest temperature of the values calculated. If T_{pi} exceeds 300°C for any fuel particle size fraction, then that fraction will decompose and must be subtracted from the total fuel mass flow when calculating the heat supplied from the bed to heat the fuel.

(vi) Particle Residence Time in the Bed

For the case where particles do not decompose before impacting the bed surface (ie where $T_{pi} < 300^\circ\text{C}$), residence time for the particle will be limited to the period from $T_p = T_{pi}$ to $T_p = 300^\circ\text{C}$. The particle-to-particle heat transfer coefficient can be taken as:

$$h_{pp} = \frac{2k_g}{d_{pf}} + \frac{0.016}{\sqrt{d_p}} \quad \text{kW/m}^2\text{K} \quad (\text{from 3.41})$$

Residence time can then be calculated using Eq 3.73 and evaluating for $T_p = 300^\circ\text{C}$. At 300°C the cellulose particles

decompose to volatiles and char and the volatiles if unburnt will move out of the bed at either emulsion or bubble velocity.

Particle-to-particle heat transfer coefficient values, even without increasing k_g for radiation effects, are quite large for small particles of sawdust and bagasse. Values for h_{pp} are typically of the order of $1000 \text{ W/m}^2\text{K}$ giving extremely short bed residence times. Even if d_{pf} is taken as a constant and at it's initial value residence times are of the order of 0.1 to 0.7 seconds. Rearranging Eq.3.73 as :

$$\Delta t = \frac{\phi d_{pf} \rho_{pf} \bar{C}_{pf}}{6 h_{pp}} \ln \left[\frac{T_B - T_{p1}}{T_B - T_{p2}} \right] \quad (3.90)$$

it can be seen that residence times can be lengthened by increases in ϕ , d_{pf} , ρ_{pf} and C_{pf} of the fuel and decreased by increases in h_{pp} and bed temperature. The parameters which would appear to offer potential for improving residence time are particle size and bed temperatures as both have the possibility of modification. The effect of varying fuel particle size is further demonstrated by examining the heat transfer per unit fuel particle mass which is given by :

$$\frac{Q}{m} = \frac{h_{pp} A_p \Delta T}{\rho_{pf} V_p} = \frac{6 h_{pp} \Delta T}{\rho_{pf} d_{pf}} \quad (3.91)$$

Which when considered with the Eq.3.41 gives:

$$\frac{Q}{m} \propto d_{pf}^{-2} \quad (3.92)$$

The significance of fuel particle size on heat transfer

The significance of fuel particle size on heat transfer per unit mass and therefore fuel particle heat up time is dramatically demonstrated in Figs E6 & E7.

The volatiles and moisture coming out of the particle will have extremely short bed residence time due to the particle having insufficient time to sink and mix into the bed. The best estimate therefore for the fuel bed residence time is taken as the time required to raise the particle from its entry temperature to 300°C. Note this approximation was used in Eqs.3.74 & 3.75.

(b) Batch Fuel Feed.

For batch fuel feed operation, as used in the combustor tests using the top feed chutes, much lower T_{pi} temperatures are obtained if average fuel batch temperatures are considered. There will be very hot particles on the edge of the batch and cold particles at it's centre, but taking an average the energy balance for the fuel pre-heat energy becomes:

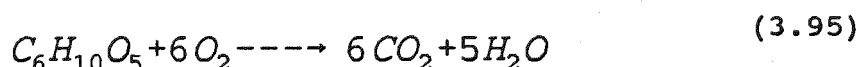
$$\begin{aligned} \dot{m}_a \bar{C}_{pa} (T_g - T_{pi}) &= \frac{(m_f - m_{ft})}{\Delta t_{fall}} \bar{C}_{pf} (T_{pi} - T_o) \\ &+ \frac{m_{wn}}{\Delta t_{fall}} \bar{C}_{pw} (T_{pi} - T_o) \end{aligned} \quad (3.93)$$

3.44 Heat of Combustion

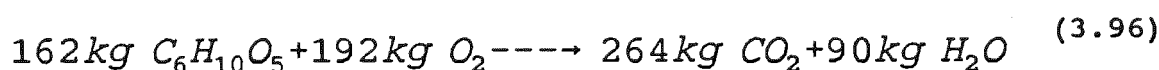
The Heat of Combustion required for use in Equation 3.48, (Section 3.4) is the Net or Lower Calorific Value which is given by :

$$CV = GCV - H_{fg_{H_2O}} \quad (3.94)$$

For Cellulose the Combustion Reaction is given by:



Which in terms of molecular mass is:



Hence Stoichiometric Air/Fuel Ratio is:

$$\frac{Air}{fuel} = \frac{192/0.233}{162} = 5.09 \quad (3.97)$$

And the correction to obtain CV will be:

$$H_{fg_{H_2O}} = \frac{90}{162} h_{fg_{H_2O}} \quad (3.98)$$

Where h_{fg} is taken at the jacket temperature of the bomb calorimeter test for the fuel.

Normally a fuel calorific value must also be adjusted for the enthalpy differences between products and reactants and the enthalpies of the components for which the Calorific Value was determined.

The relationship can be stated as follows:

$$CV_{T_{1,2}} = CV_o + (H_{R_{T_1}} - H_{R_o}) - (H_{P_{T_2}} - H_{P_o}) \quad (3.99)$$

Ref. (2 0)

(where R-Reactants, P - products ,1-start, 2 -finish)

Which can be re-written the combustion reactions for this project as:

$$CV_{T_{1,2}} = CV_o + (T_B - T_o) (mC_p)_{O_2} - (T_B - T_o) ((mC_p)_{CO_2} + (mC_p)_{H_2O}) \quad (3.100)$$

Which is simply:

(Heat of combustion) = (Calorific Value) + (Oxygen Pre-heat in the Air Supplied) - (Heat of products).

The oxygen pre-heat is supplied by the bed which is heated by combustion and is part of the increase in air enthalpy term in Eq.3.48, it therefore cannot be added to the CV. The heat of the products approximates to the heat required to heat the fuel solids (included in Eq.3.48). The Specific Heat of Cellulose which was taken as 2.4 KJ/kg in Eq.3.48. The $((mC_p)_{CO_2} + (mC_p)_{H_2O})$ term equates to 2.87, (evaluating Specific Heats at an average temperature of 600K), and therefore suggests the need to use a slightly higher value for the average specific heat of cellulose in Eq.3.48. The values for combustion efficiency calculated will therefore be slightly conservative.

4.0 EQUIPMENT DETAILS SUMMARY

4.1 Flow Visualisation Equipment

(a) Flow Visualisation Bed

(i) Fluidized Bed Details

Designed and constructed at UCQ. Relevant drawings are included in Appendix C. Specifications are as follows:

Bed Diameter :	190mm
Operating Depth:	1000mm max
Column Height:	1500/2500mm
Distributor Plate:	Bubble cap type, removable Mesh Plate with packed Bed
Air Supply:	Roots blower, variable 0-120 l/s
Electricity Supply:	3-phase Inverter Frequency Control
Three Phase Supply	Hitachi HFC-VWS Inverter. Serial No. SE11HF3H 80A

(ii) Blower Details

Godfrey Precision Products Ltd. Model X420/237, Serial no.75536. Operational limits, 15 psi, 165C.
Blower Delivery Characteristic Fig D1 , Appendix D

(iii) Motor Details

Crompton Greaves. No R1943n35/DA2960, 7.5kW, 1440 rpm.
Belt Drive Ratio : Step up 1 : 1.26

(b) Instrumentation

(i) Air Flow Measurement

British Standard Nozzle	Dia 74.95mm, Plint Partners Ltd. Serial No. TE84/3302
Digital Pressure Gauge	0 to 1.0 kPa TSE.EMA84 Serial No.48860035
Pitot-Static Tube	Fitted to 21mm diameter pipe 2m long. Constructed UCQ.

(ii) Temperature Measurement

Type K thermocouple	
Digital Thermometer	Dobbie Instruments. Model B. Serial No.2709 Code J83

(iii) Pressure Measurement

Digital Pressure Gauge	0-10.0 kPa TSE EMA84 Serial No.50870047
Mercury Manometer	400mm tubes, constructed at UCQ.

(c) Equipment Modifications.

Various modifications for different tests were made as summarised in the table below. Full details of each modification are given in drawings in Appendix C.

Table 4.1 Flow Visualisation Test Equipment Modifications

Test No.	Sand dia (micron)	Bed depth (mm)	Plate Type	Comments
1 Deep Beds	180	330	Mesh	Deep Bed Observation Fig.C3
		440	Mesh	
		590	Mesh	
2 Mixing	180	185	Mesh	Bagasse-Sand Mixing Observation Fig.C4
	490	215	Mesh	
3 Enhanced Circulation	490	180	5 caps	Centre bubble caps. Fig.C5,C6
		365	5 caps	Centre bubble caps Fig.C5,C6
		245	Mesh	Small Cone Fig.C9
		260	Mesh	Large Cone Fig.C10
		515	5 caps	Draft Tube Fig.C7,C8
4 Reversed Circulation	490	110	6 caps	Annulus Flow Fig.C11,C12
		195	6 caps	Annulus Flow Fig.C11,C12
		265	6 caps	Ingestor Tube Fig.C13

4.2 Fluidized Bed Combustor

(a) Combustor Equipment

(i) Fluidized Bed Combustor

Designed and constructed at UCQ. Relevant details are included in Appendix C. Specifications are as follows:

Bed Diameter :	489mm
Operating Depth:	500mm max
Column Height:	1200mm
Chimney Diameter:	150mm
Distributor Plate:	Bubble cap type, removable
Spout Cone	400/50 mm, 300mm deep, removable
Insulation:	160 kg/cu.m Ceramic Fibre,
Fuel Feeder:	Various: Chutes, Screw
Air Supply:	Roots blower, variable 0-120 l/s
Electricity Supply:	3-phase Inverter Frequency Control
Warm Up System:	LPG supplied at bed depth 75mm with pilot flame above bed.
Three Phase Supply	Hitachi HFC-VWS Inverter. Serial No. SE11HF3H 80A

(ii) Blower & Motor Details

As for Flow Visualisation equipment

(b) Instrumentation

(i) Air Flow Measurement

British Standard Nozzle	Dia 74.95mm, Plint Partners Ltd. Serial No. TE84/3302
Digital Pressure Gauge	0 to 1.0 kPa TSE EMA84 Serial No.48860035
Rotameter	Rotameter Manufacturing Co. Serial No. R394601

(ii) Temperature Measurement

Type K thermocouples	
Digital Thermometer	Dobbie Instruments. Model B. Serial No.2709 Code J83
Chart Recorder	Four Channel, Rikadenki Kogyo Co.Ltd. Model R-14, Serial No. 7170511

(iii) Pressure Measurement

Digital Pressure Gauge	0-10.0 kPa TSE EMA84 Serial No.50870047
Mercury Manometer	400mm tubes, constructed at UCQ.

(iv) Fuel Mass Measurement

Electric Scales

0-30 kg Sartorius. Type 3862, MP8-1, Serial No. 36100018

(c) Equipment Modifications

The various modifications are summarised below. Full details are given in drawings in Appendix C.

Table 4.2 Fluidized Bed Combustion Test Equipment Modifications

Combustor Run No.	Sand dia (μm)	Bed Depth (mm)	Plate Type	Feeder	Fuels
1 Fig.C16, C23	490	325	Bubble caps Pat.No.2	Top Chute	Bagasse Bricks
2 Fig.C16, C23	490	305	Bubble caps Pat.No.2	Top Chute	Bagasse Fibres
3 Fig.C17, C24	300	360	Bubble caps Pat.No.3	Ingester	Nil Failed Test
4 Fig.C18, C25	300	130	Bubble caps Pat.No.4	Top Chute	Sawdust Bagasse
5 Fig.C18, C25	300	125	Bubble caps Pat.No.4	Top Chute	Coal Sawdust Bagasse
6 Fig.C19, C25	300	325	Bubble caps Pat.No.4	Direct Screw Feeder	Sawdust
7 Fig.C19, C25	300	460	Bubble caps Pat.No.4	Direct Screw Feeder	Sawdust
8 Fig.C20, C26	300	355	Bubble caps Pat.No.5	Ingester	Sawdust Bagasse
9 Fig.C21, C27, C28	530	515	Modified Spouted Pat.No.6	Spout Screw Feeder	Sawdust
10 Fig.C21, C27, C28	530	583 to 740	Modified Spouted Pat.No.6	Spout Screw Feeder	Sawdust

5.0 RESULTS

5.1 Introduction

Flow visualisation results, (Research Phase 1), are presented as plots and tables of Bed Pressure Drop versus Superficial Velocity. As experimental measurement of bubbles and turnover rates are difficult, descriptive comments are included in the tables. Wherever possible, data is presented in dimensionless form for easy comparison. A summary table of flow visualisation results is presented in Table 11.1. The flow visualisation results are presented in four test groups namely Deep Beds, Bagasse-Sand Mixing, Enhanced Circulation and Reversed Circulation. Tables 11.2 to 11.7 and Figs.12.1 to 12.9 refer.

Combustion results, (Research Phase 2), for each group of combustor test runs are presented as a plots of average bed and flue gas temperatures Figs 12.10 to 12.17 and four consecutive Tables giving Combustion and Heat Release Efficiencies (suffix (a)), Combustion Heat Balance (suffix(b)), Heat Balance Details (suffix(c)) and Fluidization Behaviour (suffix(d)). Tables 11.9(a-d) to 11.12(a-d). Each group of four tables relate to similar combustor configurations and data is keyed to period numbers in each table. The Period No., (on the extreme left of these tables), relates to the operation period over which data was collected, temperatures averaged and the energy balance and Fluidized Bed Combustor behaviour calculated.

A Summary table of all combustion results is given in Table.11.8. Scatter diagrams comparing significant combustion

results from different test runs are presented in the Figs 12.18 to 12.30.

The following Results Sections 5.2 and 5.3, (Phase 1 and Phase 2 respectively), include Equipment Details, Experimental Method and a detailed Discussion relevant to each test or test group. Observations which are significant but not easily quantified are presented before each discussion section. A discussion of the entire research project is presented in the following chapter, (Chapter 6.0), which summarises detailed findings and makes overall comparisons of results obtained.

5.2 Phase 1: Flow Visualisation

5.21 Fluidization Behaviour of Deep Beds

(a) Introduction

As it was believed that improvement in fuel residence times would be achieved in deep beds, investigations began at this point. These tests would also allow the verification of existing theory, equipment operation and instrument accuracy.

(b) Equipment

The 190mm perspex tube bed was fitted with a mesh distributor with a packed bed below the mesh. (Fig.C1,C2,Appendix C). Sand with surface mean diameter of 180 microns was used. Bed depths of 330mm, 440mm and 590mm were tested, (Fig.C3).

(c) Experimental Method

Air flow was gradually increased and pressure drops across the bed were measured.

(d) Results

(i) Observations

Fluidization was characterised by bubbling just before or at minimum fluidization velocity in agreement with Botterill, (1), as sand of this size is a group B material. Group B materials are characterised by bubbling fluidization and have particle sizes and densities in the ranges 40-500 μ m and 1400-

4000 kg/m³ respectively. Bubbles breaking the surface tended to be larger in deeper beds and the tendency to slug increased with depth. (Slugging occurs when the bubble size reaches the tube diameter and solids are transported up the tube before the gas escapes and solids return.)

(ii) Quantitative Results

Results are tabulated in Table 11.2 and plotted in Fig.12.1

(e) Discussion

The results for minimum fluidization velocity measured were within 5% of predictions using Equation 3.13 and the usual approximations for sphericity and voidage from Kunii and Levenspiel, (Eq.3.14, 3.15), (3). The difference between experimental results and the predicted value is less than the 6% calculated experimental uncertainty given in Table 11.13. The distinction between minimum fluidization velocity and the state of observable fluidic movement and mixing must be made. The equations offered by Kunii define minimum fluidization as the point where the weight of the bed is first balanced. At such a point bed particles may be almost static which explains the disagreement with earlier correlations offered by Davidson, (17), which predict minimum fluidization velocities of almost double that of Kunii and Levenspiel, (17), (see also Section 3.2).

The results confirm the independence of minimum fluidization velocity from bed depth as reported by Kunii and Levenspiel, (3), (Fig.12.1). The only variation was that deeper

beds gave greater pressure drop fluctuations when slugging or bubbling violently.

The pressure drops measured typically reached 90% of the maximum possible pressure drop which is bed weight divided by bed area. The failure of bed pressure drop to reach the weight per unit area is reported in both Kunii and Levenspiel, (3) and Botterill, (1) and is attributed to inter-particle, wall forces and experimental difficulties with pressure tappings. Lower than expected bed pressure drop can also indicate partial or poor fluidization. In these tests the whole bed was observed to be fluidized and mixing so it was concluded that for the experimental equipment used a pressure drop reading of approximately 90% of bed weight per unit area did represent complete fluidization.

The mixing behaviour of deep beds is quite different from shallow beds. Shallow beds permit quite rapid and random motion of particles. In deep beds circulation currents are established. There is downward flow of solids at the bed wall which appears to be incipiently fluidized. The particle motion at the wall is ordered, whilst at the centre of the bed it is aggregative. With the objective of increasing residence time it was thought that the downward flow of solids at the wall could prove useful in taking fuel to the base of the bed.

Higher velocities and deeper beds increased the tendency of the bed to slug. The result was more localised mixing of bed solids at various bed levels. It was observed that slugging would generally be detrimental to any particle residence time improvement due to the reduction of top to bottom mixing.

5.22 Fluidization Behaviour of Sand-Bagasse Mixtures

(a) Introduction

Bagasse being a lightweight fibrous material with significant inter-particle adhesiveness is very difficult to fluidize alone. It was envisaged that the bagasse would be burnt in a sand bed so it was necessary to investigate it's mixing characteristics.

(b) Equipment

The 190mm perspex tube bed was fitted with a mesh distributor with a packed bed below the mesh, (Fig.C1,C2,Appendix C). Sands with surface mean diameter of 180 and 490 microns were used. Bed depths of 185mm and 215mm were tested respectively, (Fig.C4).

(c) Experimental Method

Air flow was gradually increased and pressure drops across the bed were measured. Samples of Bagasse were progressively added, the first sample to the base of the bed and subsequent samples to the top of the bed. Initial mixing times and minimum operational velocities for good mixing noted.

(d) Results

(i) Observations

The bagasse introduced at the base of the bed was very difficult to mix. The fibres compressed during feeding and the bagasse remained at the bottom of the bed at normal

fluidization velocities. The presence of the bagasse lump caused bed channelling via the easier air path through the bagasse lump and reduced mass of sand above it. After this difficulty, high air flow rates were used to mix the bagasse before further testing. Samples were then added to the top of the bed.

With higher contents of mixed bagasse there was a tendency of the bed fluidization to be meta-stable. If the velocity was reduced sufficiently, the bed shifted randomly from a fluidized to unfluidized state. In the unfluidized state air flow was channelled through paths opened by structures of tangled bagasse fibres. Instability resulted because, after a period of time, a few bagasse fibres would dislodge and the bed would slowly re-fluidize. The period required was variable. Further variation of phenomena was observed with the coarse sand which would alternate between meta-stable states of channelling, fluidization, and fluidization with bagasse floating on the top of the bed. The fine sand mixtures showed a greater tendency toward channelling while the bagasse in the coarse sand mixtures was more likely to separate and float.

Ingestion times for a bagasse sample of approximately 40 grams dropped on the top of the bed was of the order of 20 seconds at $6 U_{mf}$ in 180 micron sand. The time could be shortened by increasing the U_f/U_{mf} ratio and was lengthened by increased resident bagasse content.

(ii) Quantitative Results

Results are tabulated in Tables 11.3 to 11.5 and plotted in Figs.12.2 to 12.5.

(e) Discussion

The increase content of bagasse in the 180 micron sand was characterised by the progressive loss of a definite corner on the Pressure drop verses Superficial Velocity graph which characterises incipient fluidization, (Fig.12.2). At higher bagasse contents, channelling preceded fluidization, so that bed pressure drop gradually increased with velocity until fluidization was achieved at quite high U_f/U_{mf} ratios, (Fig.12.2). The effect was not as significant using coarser sand, (Fig.12.3). The different behaviour is probably due to the interstitial air velocities in the coarse sand being much higher, and therefore the paths of least resistance produced by bagasse fibres for channelling provided comparatively less air by-pass. It is also clear that testing was not as extensive for the coarse sand but a similar trend was observed. (Fig 12.4,12.5) It is not expected that U_f/U_{mf} ratios for satisfactory mixing for the coarse sand will exceed those for fine sand for any higher bagasse content, (Fig.12.4,12.5). Satisfactory mixing was taken as the operation point where the entire bed was fluidized and bagasse was evenly distributed through the bed sand.

Of further interest is the tendency of bagasse to float on a fluidized bed, which was notably stronger in the bagasse - 490 micron sand mixtures. The relationship between pressure

drop and superficial velocity shows minimal modification from channelling. (Fig.12.3) Flotation of bagasse with bed concentration of 1.6% by mass, (6.4% by particle volume) occurred at $U_f/U_{mf}=1.65$, or 0.294 m/s Good mixing in the same bed was observed at $U_f/U_{mf}=2.33$ or 0.414 m/s. Using theoretical calculations as tabulated in Appendix F, voidage, effective density and emulsion velocities of the two states are : 0.484, 0.538; 1187kg/m³, 1063kg/m³ and 0.605 m/s, 0.769m/s respectively. Identifying exactly what triggers the change in the fluidization state from stable mixing to meta-stable behaviour is not revealed by these bed parameters. Both beds have effective densities greater than the bagasse particle density. From the terminal velocity analysis of bagasse particles in Appendix E (Fig.E2), a significant proportion of bagasse would be expected to be lifted out of the bed by average emulsion velocities of the order 0.6-0.77 m/s. The observed results were precisely the reverse, the bagasse was lifted out of the bed and separated at lower superficial and emulsion velocities.

The reporting of mixing phenomena verses bagasse mass content is deceptive when the vast difference in bulk densities of sand and bagasse is considered. Table 11.5 gives comparative bagasse by both mass particle volume and bulk volume. When sand and bagasse are mixed the sand occupies the large volumes of voids between the bagasse fibres. A relatively small mass of bagasse will occupy a large bed volume with only small distances between the individual fibres. The need for high operational velocities, for the mixture having 3.22% bagasse by

mass (12.1% bagasse by particle volume), is better understood when it is realised that this corresponds to 60% by volume based on bulk density. That is, if the bagasse were placed in the bed enclosure, without the sand, in it's loose state, it would occupy 60% of the bed volume. The sand occupies the voids which must be of the order of 85% of the bagasse bulk volume. (taking particle density as 540 kg/m^3). The meta-stable behaviour observed is therefore understandable in view of the adhesive and tangled nature of bagasse fibres.

The dependency of fluidization/mixing behaviour on the content of bagasse tends to suggest a complex relationship relating to the modification of bed structure. Bagasse within the bed appears at least in the case of the finer sand to modify the voidage so that it no longer reflects either that for bagasse or sand. The required $8U_{mf}$ to achieve good mixing and complete fluidization with a bagasse content of 3.22% by mass, (Table.11.3, Fig.12.2) corresponds to the minimum fluidization velocity of 500 micron sand. Standard fluidization theory which requires the determination of surface mean particle size does not treat mixtures of different particle densities and has limitations in applicability to non-spherical shapes. Equivalent particle sizes of the bagasse -sand mixtures were calculated for interest on both mass and particle volume bases and are included in Appendix.E. (Table E12) The standard theory predicts a 75% by mass bagasse content to give surface mean particle diameters of the correct order for fluidization at $8U_{mf}$.

The meta-stable behaviour of bagasse-sand mixtures remains

complex and poorly understood. The presence of bagasse does not significantly modify the calculated surface mean diameter of the bed material to explain the increase in minimum fluidization velocity. In the case of coarser sand the average emulsion velocity is high enough to lift most of a bagasse sample out of the bed but flotation only occurs when velocities are too low for adequate mixing. The effective bed density for both good mixing and meta-sable behaviour is approximately twice the particle density of bagasse. It can only be deduced that the mixing behaviour is dependent on a complex interrelationship of bagasse size, sphericity, content and bed particle size and U_t/U_{mf} ratio. While no theory adequately explains the behaviour, the results do concur with those of Chong et al(13), which also reported the meta-sable nature of mixtures of porous alumina and bagasse. It is also reasoned that the problem can be solved in a number of ways, exploiting the findings that small concentrations of bagasse have little or no effect on fluidization behaviour and that mixing of higher concentrations can be achieved at higher superficial velocities. It is also probable that in combustion the residence time of bagasse particles will be quite short, resulting in low resident contents of bagasse and possibly minimal mixing problems.

5.23 Enhanced Bed Circulation

(a) Introduction

While mixing of bagasse in the bed did not appear to present a problem, it was envisaged that the fuel would have to be buried quickly or most combustion would occur on the top of the bed. As bagasse is a bulky fuel, 80 kg/m^3 , the downward solids transport at the bed walls would have to be of quite large volume to contain the fuel. To achieve this type of bed solids circulation, three different bed modifications were trialled : Central flow distributor, cones and a draft tube. It was believed that the optimum bed dynamics would be extremely rapid fuel burial and slow downward transport to maximise residence time.

(b) Equipment

The mesh distributor was retained in the 190mm perspex tube bed and two tests completed with cones of different sizes in the bed positioned in the bed. (Figs. C1,C2,C9,C10, Appendix C)

The mesh distributor was then replaced with a bubble cap type for tests with five centrally placed bubble caps for bed depths of 180 and 365 mm. A bed of depth of 515mm was also tested with a draft tube added. (Figs.C5,C6,C7,C8)

Sand of surface mean diameter of 490 micron was used.

(c) Experimental Method

Airflow was gradually increased and bed pressure drops measured. The Bed behaviour was observed and noted. Match

sticks were used as solids flow tracers.

(d) Results

(i) Observations

Large volume flow rates of solids at the bed wall were established using the centrally placed bubble caps and a bed depth of 180mm. Making the bed deeper resulted in more conventional fluidization behaviour due to the dispersion of the central air flow over a larger percentage of bed area.

The small cone gave little observable difference in mixing behaviour to that of a conventional bed. The large cone resulted in definite regimes within the bed. The sand inside the cone was turbulent and slugging, whilst the sand outside the cone was flowing downward being either incipiently fluidised or moving as a bulk solid. There was a tendency for the downward flow to be uneven and it was found that central placement of the cone in the bed tube was essential to get solids flow on all sides of the cone.

The draft tube gave typical spouted bed behaviour and it was difficult to get uniform external downward flow. There was a strong tendency for only one region of the sand outside the tube to be flowing at any one time.

(ii) Quantitative Results

Measured velocities and pressure drops are tabulated in Table.11.6. The results are plotted together for comparison in Fig.12.6. It was considered a useful parameter to also plot

data against the maximum air velocity ratio, (superficial basis), to give a measure of the range of fluidization regimes co-existent in the bed. (Fig.12.7)

(e) Discussion

Estimates of the percentage of the bed fluidized can be made by comparing the pressure drops of the various configurations with a normal bed with mesh plate, depth 215mm plotted in Figs.12.6.& 12.7.

The shallow bed, 180mm, with central flow delivery, gives similar pressure drop behaviour to the spouted bed with a pre-fluidization pressure peak, (Fig.12.6). The pressure drop of the deeper bed, with central flow delivery, gives behaviour closer to a normal bed reaching 80% of the bed weight per unit area. Clearly any deep spouted bed would require a draft tube to limit flow dispersion. The spouting type beds, 180mm, 365mm deep, with central air flow and the 515mm bed with spouted tube all exhibit the typically larger pressure peak which begins fluidization.

The small cone, which had little observable effect on bed behaviour, also gave no measurable difference in the results. The pressure drop data follows that for a normal bed and reaches the same maximum value, (Fig.12.6). The larger cone which did result in ordered fast circulation showed a slightly lower pressure drop due to bulk mass solids flow instead of fluidized flow. The increased particle-wall interaction, facilitated by the cone walls and the cone angle would provide supporting weight reactions for sand particles outside the

cone. The pressure drop is still of the same order as a normal bed as the total bed is suspended below the cone. The cone of this configuration offers the advantage of no stagnant zones in the bed while still enhancing wall flow volume.

Presentation of maximum superficial velocities in Fig.12.7 highlights the velocities possible in the cone configurations. These are estimated on minimum cone or tube diameters. Since the small cone did not establish enhanced circulation, its U_{\max} would not be significantly higher than average superficial velocity and is not plotted. The trade-off involved when enhancing solids volume circulation is a reduction of the fluidized volume in favour of increasing the size of a zone that can be used for fuel ingestion and retention. By necessity the remaining fluidized zone is operated at a much higher U_f/U_{mf} ratio. The possible residence time in the fluidized zone for a fuel particle is therefore reduced. It is probable that no net gain in bed residence time for fuel particles is achieved. The fuel will spend a longer time in the wall flow and a shorter time in the central bed area. The higher velocities in the central area of the bed increase the likelihood of the fuel being in the bed for only one downward and one upward pass. Clearly the usefulness of enhanced circulation devices, as tested, will be restricted to enhancing fuel ingestion. Better fluidization behaviour and mixing can be achieved with uniform velocity profiles.

5.24 Reversed Bed Circulation

(a) Introduction

It was reasoned that downward solids flow in the centre of a bed would have practical benefits for the feeding of particulate fuels. A region of downward solids flow in the centre of the bed would allow single point feeding and even fuel distribution to the bed. As for the previous experiments the intention was to optimise the downward flow of solids to ensure that fuel was rapidly buried and carried to the bottom of the bed to maximise it's residence time.

(b) Equipment

The 190 mm perspex tube was fitted with a bubble cap type distributor. The bubble caps were placed near the bed wall to provide air flow to an annulus area of the bed, (Figs.C11,C12, Appendix C). Bed depths were 110mm and 195mm.

The mesh distributor was used for the test using a central downward flow tube or ingestor, (Fig.C13). The air flow through the mesh area beneath the tube was blocked off by a baffle plate. The bed depth was 265mm.

Sand of surface mean diameter of 490 micron was used.

(c) Experimental Method

Airflow was gradually increased and bed pressure drops measured. The bed behaviour was observed and noted. Match sticks were used as solids flow tracers.

(d) Results

(i) Observations

The annulus air flow delivery allowed rapid ingestion of match sticks for shallow beds. Based on entry angles of match sticks there was a large unfluidized cone shaped volume in the centre of the bed. Observation was difficult, as unlike circulation in the normal direction, sand mass flow is in the centre of the bed. For deeper beds the centre is completely covered by fluidized sand moving from side to side as the result of bubble bursts and solids transport coming in from the outside perimeter of the bed. Like the earlier observations using central flow distributors, the deeper beds supplied with air to the annulus behaved more like normal beds due to the dispersion of flow across the entire bed area.

The central down flow tube gave only slow downward flow of solids. The vertical walls of the tube seem to restrict the solids velocity and very turbulent fluidization was required in the annulus region before significant downward flow was observed.

(ii) Quantitative Results

Results are tabulated in Table.11.7 and plotted in Figs.12.8 and 12.9.

(e) Discussion

Pressure drops for annulus flow air supply tests were 70 to 80% of weight per unit area. The slighter higher percentages

than similar central flow spouting configurations is simply explained by the much larger areas being fluidized with annulus flow.

As noted in the observations, the region of downward solids flow was difficult to observe in deeper beds. It is probable, in deeper beds, that the downward solids flow is commencing at a point below the bed surface. The region above this point, where the annulus flow has dispersed sufficiently, would be fluidized across the whole bed area. Increased flow dispersion in the bed would also result from increased air flow due to the design of the bubble caps. (ie the air streams emerging from the bubble caps are initially horizontal) Clearly, to combine deep beds with central downward flow of solids, the annulus air flow would have to be confined to the annulus area. The concept of the ingestor tube, being the reverse of a draft tube in a spouted bed, was therefore developed.

The principle difficulties with the ingestor tube are the slow downward flow characteristic of solids in the tube and it's limited capacity to collect solids that are transported to the top of the bed. Since bubbles burst at random positions in the annulus area, only some of the solids return through the tube with the balance returning in the emulsion phase outside. Conversely, with a spouting type bed, solids transported upward are naturally thrown to the perimeter of the bed.

The conflicting requirements for using a central ingestor tube for fuel feeding are noted in that it is desirable to:

(a) Maximise inward flow of solids

(b) Minimise outflow of fuel by the use of an extended tube and solids return slots or windows.

(c) Maximise upward solids transport in annulus

(d) Establish Incipient Fluidization in the Ingestor Tube.

A complex compromise emerges. The downward flow in the tube is maximised if the tube is at the point of incipient fluidization and the tube is filled to it's maximum level with bed solids. Fuel burial, in the bed solids, in the tube, is best served by a lower level of solids in the tube and solids pouring in the return slots and covering the fuel. The first requirement is improved by larger return slots, while the second is improved by smaller ones. Both requirements are improved by higher airflows in the annulus which increase solids transport but higher flows can lead to particle control problems and sufficient airflow may disperse into the tube to reduce downward solids flow. Incipient fluidization in the ingestor tube is desirable but not essential. If the solids in the tube are not fluidized, they will still flow as a bulk material at a slower rate due to wall friction.

Some rough experimentation was done with a fuel feed tube submerged in the sand within the ingestor tube but successful ingestion and mixing was not achieved. The sand and bagasse in the feed tube did not feed downward because no bed solids were deposited on top to provide an ingesting force. A pneumatic feed tube would, however, probably operate satisfactorily.

The ingestor tube concept would appear to have the potential to provide a practical feed system. Further theoretical and experimental research is warranted.

5.3 Phase 2: Combustion Results

5.31 Combustion of Bagasse Bricks, Deep Bed, Above Bed Feed (Combustor Run No.1)

(a) Introduction

Bagasse bricks were cut from compressed sheets of bagasse fibres. The resulting bricks were 50mm cubes. The test was completed during the commissioning phase of the combustor installation and was not intended for the research program as such. Research was intended to focus on particulate, fibrous bagasse. In retrospect it was decided to include the results as they show the highest combustion efficiencies achieved while burning bagasse and using above bed feed systems. The burning of bagasse in brick form may be a viable solution to the problem of poor below bed combustion efficiencies encountered with above bed feed systems and particulate bagasse.

(b) Equipment

The 489mm combustor was fitted with a bubble cap type distributor, (Figs.C14 to C16,C36, Appendix C). A total of 19 caps were arranged in Plate Pattern No. 2, (Fig.C23). Pattern No.2 was designed to give enhanced mixing and circulation with 66% of the airflow being directed through the central bed half area. Fluidization throughout the bed was verified visually before the test. Wall downflow of solids was verified using a matchstick on a string which was ingested into the wall solids downflow. The surface mean particle diameter of the sand used was 490 microns and the bed was 325mm deep. Bagasse bricks were

added manually via a horizontal feed chute located 565mm above the packed bed surface, (Fig.C16).

Bagasse bricks were of nominal size of 50mm cubes and density 240 kg/m^3 .

Thermocouples were located as follows:

Wall probes (12mm from wall)	Heights :	40mm
		190mm
		290mm

(c) Experimental Method

The fluidized bed was heated using the LPG warm up system incorporated in the design, (Fig C15,C30 & C31). The bed was heated to 650°C and the LPG was switched off. Bagasse bricks were added until combustion was established and bed temperature began to rise. Bagasse was then added to maintain combustion. Air flow rates were kept constant at 42.5 l/s FAD. The U_f/U_{mf} ratio was 8.3. Fuel was fed manually via a feed chute until combustion was established. The feed rate was then reduced to that required to maintain combustion.

(d) Results

(i) Observations

In addition to the quantitative data, the test was characterised by large above bed flames up to one metre high. There was a tendency for the larger bricks to float on the bed surface for long durations, ie 30-90 seconds. During such periods the bricks were not burning as such but smouldering and

releasing volatiles which burnt near the brick surfaces.

(ii) Quantitative Results

The average bed temperature for the duration of the operation on Bagasse Bricks is plotted in Fig. 12.10. The initial drop in temperature is due to the time lapse between shutoff of LPG supply and the beginning of Bagasse combustion. Temperature first stabilised, then increased, then due to inadequate feed rate, fell. For purposes of analysis the test was considered over two periods, Period No.1 during the rise in temperature and Period No.2 during the fall in temperature. Results of calculations are found in Tables 11.9a, 11.9b, 11.9c and 11.9d.

(e) Discussion

As the test was part of the commissioning program, many experimental problems were evident. The operation point was chosen at $U_f/U_{mf} = 8.3$ to ensure good mixing. The corresponding air flow was 42.5 litres/s requiring 36kg/hr of bagasse. It was found that manual feeding, requiring weighing of each batch of fuel, was not feasible at feed rates of this order. The result was air/fuel ratios much higher than stoichiometric, with feed rates of only 16kg/hr being achieved to give a fuel Heat Energy feed rate of 88kW, (Table 11.9a).

Examination of the raw data in Appendix B will reveal a temperature profile in the bed. The profile only exists due to the placement of thermocouples in stationary or poorly fluidized sections in the lower areas adjacent to combustor walls. The poor fluidization in these areas resulted from the

bubble cap pattern used. Deeper thermocouple probes were later added. For the purposes of the analysis, the bed temperature reading of the uppermost probe is, therefore, the best approximation of bed solids temperature.

Despite these problems, combustion efficiencies of up to 59% (Table.11.9a) were achieved, making the results of the test of reporting interest. The combustion efficiency result assumes the proportion of heat provided from the bed solids to heat the fuel is 100%. (Table.11.9c) While heat transfer during free fall would be minimal, the tendency of bricks to float would indicate a value less than 100% to be correct. There is, however, no way to produce a more accurate estimate from the data. The possible error introduced to combustion efficiencies calculated above normal uncertainties is no greater than 4% of the figure presented. As experimental techniques were still being developed the $m_b C_{pbe}$ was not determined from the data but taken from a later test of similar bed depth.

From the Observations, (Section 5.31,(d),(i)), it is predicted that higher combustion efficiencies could be achieved at higher U_f/U_{mf} ratios which would reduce the effective density of the bed, allow better ingestion of bricks and hence allow more combustion of volatiles below bed surface. Similarly bed solids of lower particle density, such as porous alumina, would improve below bed surface combustion.

The poor heat transfer performance as measured by η_b and η_{bc} , (Table 11.9a), including negative values in Period No.2 was the direct result of too much excess air. Another indicator is the operating ratio, which compares the operation point to

ideal conditions in terms of the maximum possible useful heat, which was 70% in the first period falling to 48% in the second period. It is noted, in Table 11.9c, that the heat loss to the airflow is 39% and 57% of input fuel energy for Period Nos. 1 & 2 respectively. In both periods, the heat loss to the airflow could have been reduced to approximately 18% corresponding to the stoichiometric air/fuel ratio. Operating at or near stoichiometric mixtures the overall bed efficiency could be expected to reach approximately 26%.

Packed Bed heat flux values of 773 and 583 kW/m³ were achieved for Period Nos 1 & 2, (Table 11.9b). These values compare favourably with typical values for coal fluidized bed boilers of 300-750 kW/m³ based on water tube volume given by Highley & Kaye, (5).

The bed behaviour index, (Table.11.9d), is clearly indicative of bubbling, aggregative fluidization and particle Reynolds number is less than ten indicating laminar gas flow in the voids, as defined by Howard, (15). The gas-to-particle heat transfer rates of the order of 19 W/m².K, combined with specific surface of approximately 7730m²/m³ and bed depth of 325mm, gives a possible 8.9 kW/K. (Gas-to-particle heat transfer per degree temperature difference.) Clearly gas-to-particle heat transfer is not limited by either sand surface area or temperature differences at operations of a nominal 100 kW.

Although Bagasse Bricks were not pursued further, an optimal bed for combustion would incorporate a finer or less dense bed solid particle to ensure a high U_f/U_{mf} value and feed rates to allow no more than 30% excess air. Larger and denser

bricks would also improve performance. Optimisation would allow similar behaviour to coal combustion to be achieved with bricks falling to the bottom of the bed maximising the burning of volatiles below the bed surface.

5.32 Combustion of Particulate Bagasse, Deep Bed, Above Bed Feed (Combustor Run No.2)

(a) Introduction

Bagasse, in particulate fibrous form, is the waste material from sugarcane crushing. It would be ideal to be able to burn such material without further processing and obtain useful heat transfer from the combustion in a fluidized bed. Various feeder systems were examined but a simple batch feed system using an above bed chute was selected to gain experience with bagasse combustion and feeding before an expensive feeder was designed and added.

(b) Equipment

The combustor and distributor were as per Combustor Run No.1. The distributor plate with 19 caps arranged in Plate Pattern No.2, (Fig.C23, Appendix C), was retained. Sand was retained with a surface mean diameter of 490 microns and the bed depth was 305mm.

Bagasse particles were of broad nominal size range including dust -100 microns and fibres up to 50mm long and with width and depth dimensions of up to 5 and 1mm respectively, (Table E2 & E3, Fig.E1, Appendix E). Bagasse was added manually via a horizontal chute located 585mm above the packed bed surface.

Thermocouples were located as follows:

Wall probes (12mm from wall)	Heights:	40mm
		190mm
		290mm
Deep probes (75mm from wall)	Height:	290mm
Flue Gas Probe	Height	650mm

(c) Experimental Method

The fluidized bed was heated using the LPG warm up system. The bed was heated to 700°C and the LPG was switched off. Bagasse was added in batches and combustion established. Fuel was fed manually via a feed chute and stoker. Air flow rates were progressively reduced in an attempt to get bed temperature to increase. The U_f/U_{mf} ratio ranged from 3.9 to 1.6. Air/fuel ratios were achieved ranging from small amounts of excess air to almost 400% excess fuel. At each stage temperatures were observed for indications of increase and hence useful heat transfer.

(d) Results

(i) Observations

At least part of each batch of bagasse fuel ignited before impacting the bed. The remaining portion of the batch, not ignited during the fall, would ignite instantaneously on contact with the bed surface. Large above bed flames were again observed. The proportion of the batch which ignited above the bed was dependent on the existence and size of above bed

flames.

At low air flow rates during the last test period, hot spots were observed in the bed via the use of a stainless steel reflector, (Fig C15). After bed shutdown, several samples of fused sand were found in the bed sand.

(ii) Quantitative Results

As the Combustor details were similar to that of Combustor Run No.1, the results are tabulated in Table 11.9a, 11.9b, 11.9c & 11.9d. Results are keyed to Period Nos. 3 to 9. A plot of average bed temperature for the time operating on bagasse is given in Fig. 12.11.

(e) Discussion

In-bed combustion efficiencies of the order of 20% were achieved for air fuel ratios near stoichiometric, (Table 11.9a, Period Nos 3 to 5). The heat release beneath the bed surface was just sufficient to balance heat losses from the bed, hence no useful heat was available. Decreasing the air/fuel ratio to compensate for losses of fuel in flue gases did not result in the expected significant increases in bed temperature and logically gave lower combustion efficiencies, (Period Nos 6 to 9). Excess fuel did appear to result in the release of some useable heat with positive values for η_g , (Table 11.9a, Period Nos 6 to 8). The improvement was possibly due to the longer residence time of larger numbers of large particles in the bed, (Period Nos. 7 & 8). The reliability, however, of the bed temperatures for the final two test periods is doubted due to the observation of hot spots and fused sand. The mixing rate

during these tests would have been quite low corresponding to U_f/U_{mf} ratios of 1.8 and 1.6 respectively, (ie $J = 28 \text{ kg/m}^2\text{s}$, Table F13, Appendix F). There is, therefore, no guarantee that the temperatures measured represent average bed solid temperatures. Analysis of the raw data tables in Appendix B will reveal a large discrepancy between deep and wall probe temperatures first noted at $t = 100$ minutes. It is suggested the low mixing rates, combined with the excess levels of fuel, allowed stagnant regions in the bed to develop. It is probable that the meta-stable bagasse sand mixing behaviour observed in cold mixing tests, (Section 5.22), occurred due to excess fuel and the low superficial velocities. The unfluidized stagnant areas would still be supplied with air flow resulting in localised temperatures of burning bagasse to rise high enough to fuse quartz.

The question also is raised as to how the excess fuel was burnt, as there was no significant observable continuation of combustion after fuel feeding had ceased or combustion above the flue gas exit. It was concluded that secondary air was being obtained from above bed chutes and portholes allowing combustion of any unburnt fuel in the free board region. The rapid decomposition of cellulose fuels was not observed or understood at this stage and was revealed by later tests which attempted secondary air control.

Only two calculations of operating ratio, (Period Nos.3 & 4), are presented as these are the only periods with excess air. Ratios were 98% and 94% respectively giving possible maximum η_{bc} values of 76% and 74% respectively, (Table.11.9a).

These results highlight the minimal heat release below the bed surface, which was negative or zero in these two periods. All of the possible 74-76% useful heat available in the fuel was released above the bed.

Packed bed heat flux values reflect the poorer combustion efficiencies with most results less than 300 kW/m^3 , (Table.11.9.b). The above bed heat release is consistently 80% independent of air/fuel ratio. While the individual calorific values of the char and volatiles are not known, the volatiles content of the fuel (ie 80-85%) and the above bed heat release results would indicate that almost all volatiles combustion occurs above the bed. The estimation of zero bed residence time for released volatiles appears to be valid. Hence the values for α_f and α_w of the order of 0.36 are also valid. (Table 11.9c)

The bed behaviour index is of the same order as Combustor Run. No.1, reducing with elevated temperatures but still clearly aggregative, (Table 11.9d). Particle Reynolds and Nusselt Number are much smaller due to lower operational velocities. Taking the lowest gas-to-particle heat coefficient of $1.6 \text{ W/m}^2\text{K}$, gas to particle heat transfer per unit temperature for this bed depth and sand size is still 0.7 kW/K . Flame to bed heat transfer of a nominal 100 kW is still possible with a flame to bed temperature difference of only 171°C . The major proportion of combustion and heat release obviously occurred in the freeboard region, as suggested by Peel.R.B. et al, (9). The fact that bed solids temperature could be maintained, but not increased, indicates the potential of fluidized beds to gasify cellulose fuels. The in-bed

combustion results are much poorer than those for bagasse bricks, due to the large proportion of above bed combustion.

The burning of bagasse in a fluidized bed, using above bed batch feed does not appear to be feasible for useful heat transfer. Batch feed is wasteful, as upon introduction, excess fuel exists in the bed and some volatiles are lost before combustion due localised lack of air. The problem could be reduced by having smaller batches but loss would still occur. Batch feeding does have the advantages of longer fuel bed residence times and a higher proportion of the fuel reaches the bed. Calculations indicate that even more fuel would be burnt in the flue gas stream and fuel particle bed residence times shorter for continuous feed systems, (Table E2 & E3, Appendix E). Continuous feed would therefore probably allow more complete combustion, but yield less useful heat transfer.

5.33 Combustion of Particulate Bagasse, Deep Bed, Ingestor Feed (Combustor Run No.3)

(a) Introduction

The failure of Combustor Run No.2 to produce significant useful heat transfer led to the attempt at using a central ingestor tube to increase the below bed surface combustion. The experience and results gained from flow visualisation tests, (Section 5.24), were used to design a suitable ingestor tube.

(b) Equipment

The 489mm diameter Combustor was fitted with a modified distributor plate with bubble caps arranged in Plate Pattern No.3, (Figs.C17,C24, Appendix C). Pattern No.3 located 16 bubble caps at a PCD of 400mm and three caps at PCD 200mm. The bubble caps were fitted with a 4mm bush to increase plate pressure drop and therefore provide even flow distribution in the annulus area of the bed. An ingestor tube of 200mm diameter with sand entry windows and a feed chute at the top was fitted, (Fig.C17). The intention was to fluidize and expand the outer annulus area of the bed while the sand in the central tube was in downward flow, either just fluidized or bulk solids downward flow. The downward mass flow in the centre tube was verified visually in the cold condition before testing. The surface mean diameter of the sand was reduced to 300 microns to reduce the air and fuel flow requirements at suitable bed operating points. The bed depth was 360mm. Bagasse was fibrous and particulate as for previous tests.

(c) Experimental Method

The fluidized bed was pre-heated to a temperature of 670°C using LPG. Bagasse was then added via the feed chute system directly into the ingestor tube.

(d) Results

(i) Observations

Bagasse failed to ingest and burnt above the sand in the ingestor tube. The operating point of the bed was increased until sand was being lost with no improvement in ingestion. The operating U_f/U_{mf} ratio was approximately 6.0.

(ii) Quantitative Results

Since no bagasse was ingested there were no useful results to report.

(e) Discussion

What was learned from the test was that a much higher U_f/U_{mf} ratio and attention to particle deflection and control systems would be required if such a system were to be successful. There were also feed problems with the tube and chute even though the tube diameter was 200mm. The bagasse tended to hang up between chute and tube. Sufficient understanding of the problems was gained to allow re-design and a more successful test to be carried out later, (see Combustor Run No.8, Section 5.36).

5.34 Combustion of Particulate Bagasse, Sawdust and Coal, Shallow Bed, Above Bed Feed. (Combustor Run Nos. 4 & 5)

(a) Introduction

As combustion tests using deep beds had not yielded useable heat transfer it was decided to complete some tests using a shallow bed for comparison. Having gained some experience with the feed problems of bagasse it was thought that comparative tests using sawdust and coal could prove useful. Peel and Santos had reported the similar behaviour of bagasse and sawdust in a Fluidized Bed Combustor.(9) Sawdust was viewed as a similar fuel with less feed problems, hence useful in preventing the project from being diverted to bagasse feeder research and development. Coal was included to provide a datum as the combustion of coal is well documented and developed. The inclusion of coal would allow both quantitative and qualitative comparisons with a 'well behaved' fuel.

(b) Equipment

The 489mm combustor was fitted with the bubble cap distributor modified to take 42 bubble caps and arranged in Plate Pattern No.4, (Fig.C18,C24, Appendix C). To ensure sufficient plate pressure drop, the 9mm ID inlet tubes of the bubble caps were fitted with bushes to give an ID of 2.5mm. The bubble caps were arranged to give the most uniform flow distribution possible within the constraints of the design. The sand of surface mean diameter of 300 micron was retained and the bed depths were 130 and 125mm for Combustor Run Nos 4 & 5 respectively.

The feed chute was lowered to 410mm above the packed bed of 130mm, (Figs.C18,C37). Feed was still manual by batch. Bagasse fuel was broad range fibrous particulate, as in previous tests. The Sawdust was more regular ranging from dust -100 microns to chips 1mm in diameter up to 12mm long, (Tables. E4 & E5, Fig.E2). The coal was mixed, -60mm sieve size, so included powder and large lumps.

The top of the combustor was fitted with a chimney of 150mm diameter and removable covers were made to cover chutes to cut off secondary air. A chimney choke was fitted for Combustor Run No.5 to try to create a positive pressure in the combustor above the bed and prevent secondary air entry via the LPG pilot flame tube.

Thermocouples were fitted as follows:

Wall Probes (12mm from wall)	Heights	40mm
		190mm
Deep Probes (75mm from wall)	Heights	40mm
		90mm
Flue Probe	Height	1500mm

(c) Experimental Method

The bed was heated to a temperature of 600-700°C using LPG. During Run No.4 Sawdust was added, followed by bagasse. During Run No.5 the sequence was Coal, Sawdust, Wet Bagasse, Dry Bagasse. The air flow rate (FAD) was varied during Run No.4 but held constant for Run No.5. Operational velocities were kept in the range of $U_f/U_{mf} = 3$ to 5 to ensure good mixing.

Fuel feed rate was estimated and an attempt was made to

keep batch sizes even and as small as practically possible.

(d) Results

(i) Observations

Observable coal combustion characteristics were vastly different from those of cellulose fuels. Coal was added with no immediate temperature rise or observable flame at the feed chute. When sufficient coal had been added and time for devolatilisation passed the bed steadily increased in temperature. The flue gases appeared to be clean.

Large above bed flames were observed for both sawdust and bagasse. The addition of a large sample of sawdust or bagasse could result in flames outside the feed chute. Combustion of both sawdust and bagasse yielded large amounts of smoke, (see photographs Fig.C40 & C41). Sawdust flue gases were visibly more dense than bagasse flue gases. The combustion of both sawdust and bagasse appeared to be incomplete.

The wet bagasse sample burnt in the bed but the bed cooled.

(ii) Quantitative Results

The average temperature and flue gas temperatures are plotted in Figs.12.12 & 12.13. The flue gas temperatures obviously still include secondary air and are included because they are a useful indicator of above bed flames and combustion. The thermodynamic performance of the fuels in the shallow beds are tabulated in Tables.11.10a,11.10b,11.10c & 11.10d. The results of Combustion Run No.5 are of most interest and are

presented first in the tables keyed to period Nos 1 to 4.

(e) Discussion

In view of the observed combustion characteristics of coal, it is not surprising that combustion efficiencies of up to 66% were achieved, (Table.11.10a). Clearly the absence of large above bed flames indicates a much reduced percentage of above bed combustion and heat release. The conclusion is supported by the larger difference between flue gas temperature and bed temperature during coal combustion, (Fig.12.13). The fluidized bed and overall fluidized bed efficiencies of 47% and 30% respectively are considerably better than any earlier test using cellulose fuels. Due to the manageable characteristic of coal, there is a pause in the temperature rise at the beginning of the feed period which is followed by rapid heat release as volatiles burn and then slower burn of remaining char. When the slow burn characteristic of coal is considered, it can also be concluded that the efficiency values for the first period are conservative, as the calculations assume all the fed fuel is burnt within the analysis period.

The second period efficiency values were computed over a longer period giving a higher effective air/fuel ratio and lower average useful heat transfer values. The coal test fuel feed was firstly rapid, until temperature gain was achieved, then a slower feed rate was used, to maintain temperature. The coal feed rate had to be limited and further reduced to allow temperature to reduce for further tests. The poor useful heat values reflected in the low η_b and η_{bc} values in Period No 2 are

simply the result of too much excess air.

Sawdust tests were characterised by excess smoke, probably due to incomplete combustion and the high moisture content of 25%. Sawdust combustion with excess air did result in combustion efficiencies of 35% in period No.3, (Table 11.10a). Significantly, no useful heat was available, (Table 11.10b). Confirming the similarity of sawdust combustion behaviour to bagasse, useful heat transfer was only achieved in Period No.5 with excess fuel, (Table 11.10a). The rapid decomposition of sawdust to volatiles and combustion in the gas phase similar to bagasse, was confirmed by flames appearing outside the feed chute, (see Photograph Fig.C41). In such cases the base of the flame was outside the combustor, indicating the use of outside air as secondary air.

Bagasse results were similar with combustion efficiencies in the order of 30% approaching stoichiometric mixture, (Period No.7), but nil or small percentages of useful heat transfer. For excess fuel and small amounts of useful heat, the typical combustion efficiencies were 20%, (Period Nos. 4, 6 to 10, Table.11.10a).

A sample of wet bagasse had been prepared by soaking bagasse in water. The sample was approximately 80% moisture by mass and resulted in the bed temperature drop in Fig.12.13. The result is not surprising when it is considered that the dry bagasse combustion only releases sufficient heat in the bed to balance wall and flue losses. An energy balance calculation confirmed the energy loss in the bed to be approximately equal to the energy required to evaporate and superheat the fuel

moisture. The consistently higher combustion efficiencies of the sawdust and lower amounts of heat release above the bed, (Table 11.10a,11.10b), is probably due to a combination of better mixing, higher particle densities and moisture content. The smaller more regular sawdust particles would be expected to ingest more rapidly than fibrous tangled bagasse. The sawdust was hardwood and would probably have higher particle densities and hence longer bed residence times. Particle density measurements were attempted, but the uncertainties were so large with the equipment used, that the results were considered meaningless. The masses are small and particle shapes are irregular and difficult to measure. As the fuel particles are porous, the particle volumes cannot be deduced by liquid displacement. Another consideration is that the higher moisture content in the sawdust may allow greater bed depths to be obtained increasing below bed combustion time of volatiles. (Note : Moisture does not reduce the combustion efficiency but it does reduce the useful heat available. see Section 3.4)

Operating ratio and maximum η_{gc} are not presented for Period Nos 4 to 10 as these parameters are misleading for excess fuel mixtures, (Table 11.10a).

Packed bed heat flux values for coal compared well with typical values being 726 and 408 kW/m³ for the two periods analysed, (Table 11.10b). High packed bed heat flux rates were also achieved with bagasse 844 kW/m³, (Period No.6), and sawdust 737 kW/m³, (Period No.5). Both results were in excess fuel condition, (Table 11.10b). As the air flow rates are of similar order to Combustor Run No.2 and the bed is shallower,

these heat flux results do not indicate a significant improvement in below bed surface combustion.

The fluidization behaviour of 300 micron sand goes through a transition during the warm up phase to give behaviour index values less than 100 at operating temperatures, (Table 11.10d). The sand mixing rate at $U_f/U_{mf} = 4$ is comparatively less than that for 490 micron sand; ie 300 micron, $J = 37 \text{ kg/m}^2\text{s}$; 490 micron $J = 100 \text{ kg/m}^2\text{s}$, (Table F12, F13 Appendix F). There was however no evidence of hot spots in the thermocouple data so adequate mixing was obviously maintained.

Gas-to-particle heat transfer coefficients are again quite low $0.9\text{--}1.9 \text{ W/m}^2\text{K}$ due to the low Reynolds number, (Table 11.10d). Considering the specific surface of 300 micron sand of $12630 \text{ m}^2/\text{m}^3$ and a nominal bed depth of 130mm the gas-to-particle heat transfer per degree temperature difference is in the range 0.3 to 0.6 kW/K . Despite the smaller values, no limitation due to gas-to-particle heat transfer can be considered as a typical fuel heat release of 43 kW , (based on typical air flow rates), would require a flame to bed temperature difference of only 130°C .

The comparative tests confirmed the similar nature of sawdust and bagasse combustion and would allow the use of sawdust to further investigation with different feed methods. The comparison revealed the very different characteristics of coal and cellulose fuel combustion using above bed feeders. Coal is slow to ignite and burns mainly below the bed surface, while the particulate cellulose fuels are highly reactive and release most of their heat above the bed. It was concluded

that, to improve cellulose combustion, the fuel must be added below the bed surface and the bed depth increased until the combustion efficiencies were acceptable for sustained operation.

5.35 Combustion of Sawdust, Deep Bed, Direct Screw Feed(Combustor Run No. 6, & 7)

(a) Introduction

As results of all above bed feed system tests indicated low percentages of below bed combustion, a Screw feeder was fitted directly to the side of the combustor. Fuel feed below bed surface would allow decomposition and release of volatiles and at least some of the combustion of gas phase fuel to occur below bed surface. It was hoped that the major proportion of fuel particles would be caught in the wall downward flow of solids and provide for both good mixing and a longer bed path for volatile gases.

(b) Equipment

The 489mm diameter combustor was fitted with a screw feeder positioned 140mm above the distributor plate. The distributor Plate Pattern No.4 was retained, as was the sand of size 300 microns, (Figs. C19, C25, Appendix C). The Screw feeder was 50mm in diameter and had a hopper capable of holding 3kg of sawdust. A lid was fitted for Combustion run No.7 with air fittings to provide back pressure in the hopper, (Fig.C42).

Sawdust of the same size distribution as previous tests was used. Bed depths were 325 and 460mm for Run Nos. 6 & 7 respectively.

Thermocouples were positioned as follows:

Wall probes (12mm from wall)	Height:	40mm
		290mm
Deep probes (75mm from wall)	Height:	40mm
		290mm
Flue Gas	Height:	1500mm

(c) Experimental Method

The bed solids were heated using LPG to a temperature of 550°C (Run No.6) and 710°C (Run No.7). The LPG was then switched off and screw feed of sawdust commenced. The fuel feed rate was calculated and the rotation speed of the feeder estimated from bench delivery test data. The feeder was rotated manually. The U_f/U_{mf} ratios were the order of 3.9 to 4.3. Air flow rates of 10.4 l/sec and 8.1 l/s FAD were used during Period Nos 1 & 2 respectively and 8.1 l/s for the cooldown period. The temperatures were recorded on a chart recorder for the warm up, sawdust combustion and cooldown periods. Temperature data from the cooldown period was used to estimate the equivalent specific heat of the bed structure and solids.

(d) Results

(i) Observations

The extremely rapid decomposition of the fuel upon contact with hot sand was again underscored by the release of volatiles in the screw feeder. During the sixth combustor run, the open hopper became impossible to operate due to the continual stream

of smoke, volatiles and incomplete combustion products escaping back through the screw feeder. Large amounts of eucalyptus oil were also released which in turn made the feeder sticky and eventually jammed the feeder. Removal of the sand from the combustor after the test revealed flame stains emanating from the screw feed entry point indicating that the fuel had released all or most of its volatiles whilst in the screw feeder. The seventh combustor run which utilised a feeder hopper with back pressure was plagued with the same problem of oil release and also had to be shutdown.

The residence time of the fuel in the bed was observed to be extremely short. A sample of fed fuel was almost instantly followed by a bed flame and smoke. The flue gases, as distinct from the gases escaping in the feed hopper, appeared quite clean indicating more complete combustion than in previous tests.

(ii) Quantitative Results

The plot of average bed temperature and flue gas temperatures are plotted for Combustor Run No.6 and is shown in Fig.12.14. The test period for Combustion Run No.7 was aborted so quickly that no useful temperature data was plotted. Results are tabulated in Tables 11.11a,11.11b,11.11c & 11.11d keyed to Period Nos.1 to 3.

(e) Discussion

Despite the experimental problems observed, combustion efficiencies higher than those obtained using above bed feed systems were calculated. Significantly, combustion efficiencies

in the range of 32%-39% were associated with fluidised bed and overall efficiencies of the range of 11%-14% and 8%-10% respectively, (Table 11.11a, Period Nos 1 & 2). The air/fuel ratios were close to stoichiometric. The results were, therefore, the first to yield useful heat transfer from a particulate cellulose fuel at stoichiometric or excess air mixtures. Even higher combustion efficiencies resulted from the deeper bed test Period No.3 reaching 47%, but the possibility of improved useful heat transfer was lost due to feeder problems which resulted in too much excess air.

The earlier failure of the screw feeder due to oil release and jamming during Run No.7 was probably due the higher initial bed temperature of 710°C. The decomposition would have been more complete and rapid and probably occurred further back in the feeder.

The efficiency values calculated would be conservative due to fuel volatile and oil losses in the screw feeder. It also should be remembered that the desired initial downward flow of fuel particles at the bed wall in the bed solids did not occur due to rapid decomposition. The fuel volatile products therefore entered the bed at 185mm and 320mm below the packed bed surface for Run Nos.6 & 7 respectively. The rapid decomposition of the fuel in the screw feeder is not surprising in view of the particle-to-particle heat transfer coefficient which is inversely proportional to particle size, (Section 3.3, Eq.3.41). Further the heat transfer per unit mass is inversely proportional to the square of particle size, (Section 3.43, Eq.3.92). Sawdust particles are relatively small and would

reduce in size rapidly, decomposing at 300°C.

The reduced heat flux values reflect the deeper beds being used with 300 micron sand, (Tables 11.10b, 11.11b). The extremely low value for Period No.3 is due to the very deep bed of 460mm.

The bed behaviour index was aggregative for 300 micron sand due to increased bed depth, (Table. No.11.11c). The heat transfer coefficients are in the range 1.9 to 2.5 W/m²K, which with deeper beds than the previous shallow bed tests, ensure good gas-to-particle heat transfer. Mixing appears to be adequate at $U_f/U_{mf}=3.9$ to 4.3. Even though the fuel flame clearly emanated from the screw feeder and directly contacted approximately half the bed, there was no evidence of hot or cool spots in the bed in temperature data.

The improvement in the useful heat transfer is clearly due to below bed surface combustion of volatiles allowed by feeding the fuel directly into the bed solids. Much better results would be possible if fuel feed and fuel loss problems could be eliminated.

5.36 Combustion of Particulate Bagasse, Sawdust, Deep Bed, Ingestor Feed (Combustor Run No. 8)

(a) Introduction

As previous results clearly point to below bed fuel feed systems as a viable approach to combustion of light cellulose fuels, the next logical step is to solve the screw feed problems. There was, however, one option remaining which may prove viable for above bed feed systems, that being a re-designed ingestor tube based on the experience from the failed Combustion Run No.3. The practical usefulness of such an approach was believed to justify the investigation. If successful a commercial ingestor tube system could be pneumatically supplied without requiring high back pressures and not requiring direct screw feeding which will prove problematic for fibrous fuels such as bagasse.

(b) Equipment

The 489mm combustor was fitted with a modified ingestor tube, (Figs.C20,C44. Appendix C). The new design incorporated particle splash controls, so that the trajectories of particles, as they emerge from exploding surface bubbles, are deflected back into the bed. The distributor plate was changed to incorporate 34 bubble caps. A total of 28 caps without bushes, (ie tube diameter 9mm), were fitted outside the 200mm ingestor tube. A further six caps fitted with bushes of ID 2.5mm were fitted on the 200mm PCD below the ingestor tube, (Plate Pattern No.5 Fig.C26). Despite the fluidization profile, shown in the photograph in Fig.C43, problems were

experienced with significant air flow from the annulus zone entering the bottom of the central tube. The problem was finally solved by adding a 40mm high ring of diameter 300 mm to the distributor plate to limit inward flow from bubble caps, (Fig C20). Rapid solids downward flow was verified in the central tube in the cold condition. The sand of surface mean diameter of 300 microns was retained and the bed depth was 355mm. The fuel feed chute was modified to attach directly to the ingestor tube above the sand return windows. The feed chute was located 195mm above the packed bed surface.

Sawdust and bagasse were of the same size distributions as in previous tests.

Thermocouples were positioned as follows:

Wall probes (12mm from wall)	Height:	40mm
		290mm
Deep probes (75mm from wall)	Height:	40mm
		290mm
Flue Gas	Height:	1500mm

(c) Experimental Method

The bed solids were heated using LPG to a temperature of 690°C and then fuel feed via the feed chute commenced. The required fuel feed rate was estimated and batch sizes were kept as even and small as practically possible. Based on the experience of the earlier tests the U_f/U_{mf} ratio of 10 was chosen for sawdust and in the range of 14 to 21 for bagasse. Corresponding air flow rates were 19.8 l/s, 35.3 l/s and 42.6 l/s FAD.

The temperatures were recorded on a chart recorder for the warm up, sawdust and bagasse combustion and cooldown periods. Temperature data from the cooldown period was used to estimate the equivalent specific heat of the bed structure and solids.

(d) Results

(i) Observations

Problems with the LPG system were experienced with frequent loss of ignition. The problem was identified as being due to shock waves from bubble bursts blowing out the flame. The centre section of the top particle control cone had to be removed before successful gas burn was achieved. Shock waves and shutdowns were still a problem but the bed solids were successfully heated by limiting operational airflows to a minimum.

The combustion of each batch of sawdust was characterised by two definite periods of combustion. Upon entry, the sawdust fell to the sand in the central tube and was instantly ignited. Approximately twenty seconds elapsed between the instant of the fuel batch introduction and a second burst of ignition. The second ignition was from a portion of the fuel batch which had been ingested to the bottom of the bed and ignited in excess air in the bed annulus area. Surprisingly, a similar two stage ignition and combustion of bagasse was not observed.

(ii) Quantitative Results

The average bed temperature and flue gas temperatures were

plotted and are found in Fig.12.15. Results of calculations are found in Tables 11.11a,11.11b,11.11c & 11.11d keyed to Period Nos. 4 to 8.

(e) Discussion

The most obvious problem encountered was similar to Combustion Run No.1 in that maintaining sufficient fuel feed using manual feeding was difficult. High operational velocities were required to ensure sufficient annulus solids upward flow and therefore sufficiently rapid central downward flow. The potential favourable results for useful heat transfer, were not achieved due to too much excess air. Sawdust combustion efficiencies were higher than for screw fed fuel, in a bed of the same depth, reaching 45%, (Table.11.11a).

Much higher operational velocities were used with bagasse based on the earlier test problems of ingestion. The velocity ratios of the annulus and tube are plotted and presented in Fig.B13,(Appendix B). The approach seems to be justified by the surprising result of zero below bed surface combustion in Period No.7. In this test period, heat lost in flue gases plus wall losses equalled the loss in energy stored. It is possible, that on contact with the bed solids in the central tube, the bagasse ignited and released nearly all it's energy before being buried. Alternatively, the bagasse may have hung in the tube above the sand and ignited in the flue gases. In either case, the difficulty of handling bagasse as a fuel is again emphasised.

The combustion efficiencies of the bagasse were of the

order of 30% with excess air, which is comparable with efficiencies achieved with other above bed feed systems. (see Table.11.10a, Period No 7 & Table.11.11a, Period No.6 to 8)

Useful heat transfer was either small or negative due to too much excess air, (Tables.11.11a,11.11b). Of note is the very low values and negative values of O_r and η_{bc} . The negative values in Period No.8 resulted from 690% excess air.

Packed bed heat flux for the sawdust are quite acceptable resulting from the improvement in combustion efficiency, (Table.11.11b). By contrast, the values for the bagasse combustion are quite low, reflecting the combination of a deep bed and lower combustion efficiencies.

All α_f and α_w parameters are set at unity but clearly the residence time of the fuel ignited on first bed contact is extremely short, (Table.11.11c). There is, however, no way to provide better estimates. The true figures are probably in the range 0.7 to 0.9 and would depend on the fuel ingestion characteristic and the downward solids flow velocity in the tube. There is still very little understanding of what is actually happening in the ingestor tube during operation.

The bed behaviour index was again aggregative due to bed depth. Heat transfer coefficients were improved due to the higher Reynold numbers, (Table.11.11d).

The trial of the ingestor system proved that such an approach is worthy of further investigation and may allow the design of a viable commercial system. A complete re-design of the experimental equipment used would be required to solve the problems of bubble burst induced shock waves which frequently caused LPG flame failure and shutdown.

5.37 Combustion of Sawdust, Modified Spouted Bed, Pre-mixed Fuel and Air (Combustor Run Nos 9 & 10)

(a) Introduction

The tests using direct screw feed highlighted the need to place the fuel at the base of the bed, to adequately mix the fuel in the bed and to prevent fuel decomposition and loss prior to bed entry. Direct screw feed through the combustor wall had two problems namely, poor fuel distribution and early fuel decomposition due to sand - fuel mixing in the screw. It was therefore reasoned that the best solution to both problems was to pre-mix the fuel with the fluidizing air. A conventional distributor plate design could not be used as fuel would not pass through the bubble caps. A conventional spouted bed would not be expected to yield useful heat transfer as fuel would be conveyed quickly through the bed in the spout and burn either in the freeboard or on the bed surface. The options were to either make the spouted bed very deep, (ie exceeding the maximum spoutable depth to ensure conventional fluidization), or use baffles to redistribute the spouted air flow and refluidize the major proportion of the bed. The sond option was chosen as calculations using empirical formulae predicted a spouted bed depth of in excess of 3m for conventional fluidization to be established.

(b) Equipment

The 489mm diameter combustor was modified by removing the bubble cap distributor plate and replacing it with a conical hopper, (Figs.C21,C27,C28 & C46. Appendix C). Fluidizing air was

supplied via a 50mm diameter pipe connected to the base of the hopper. To ensure no pre-combustion of fuel, a screw feeder was fitted to the 50mm diameter fluidizing air supply pipe 300 mm below the apex of the hopper, (Figs.C28,C46). The hopper was pressurised to prevent air leakage back through the feed screw.

Since lightweight fuel retention in a conventional spouted bed would be small, a 300mm diameter baffle plate was fitted at the top of the conical hopper to break the spout flow and redistribute the airflow to create a conventional fluidized bed above the conical hopper, (Fig.C27). Full fluidization was verified in the cold condition and an absence of semi-fluidized regions was confirmed at U_f/U_{mf} ratios of 2 or greater, (Fig.D8, Appendix D).

The standpipe, of 300mm in length, connected to the hopper and filled with bed sand, combined with the required rupture pressure for starting a spouted bed, generated starting pressures beyond the capabilities of the roots blower. It was therefore necessary to add a controllable bubble cap plate to the bottom of the hopper, (Fig.C28). The operational start up problems were solved by establishing fluidization with the bubble cap plate closed. A minimum air flow corresponding to terminal velocity in the 50mm diameter pipe for the largest sand particle diameter was required whilst the bubble cap plate was open.

Sawdust was passed through a 4.75mm sieve to remove any large particles which may be difficult to pneumatically convey.

As the intention was to increase fuel residence time, the

sand was replaced with sand of surface mean diameter of 530 microns to reduce the U_f/U_{mf} ratio and hence the proportion of air and fuel passing rapidly through the bed as bubbles. The 530 micron sand was also chosen to reduce particle elutriation. The bed was expected to be aggregative with excessive surface bubble bursts resulting from the poor flow distribution. Bed depths of 515mm (Combustor Run No.9) and 583mm, 654mm and 740mm (Combustor Run No.10) were used. The cone at the base of the bed had a depth of 300mm and is inclusive in the bed depths quoted.

Thermocouple positions were as follows.

Wall probes (12mm from wall) Height: 40mm

290mm

Deep probes (75mm from wall) Height: 40mm

190mm

Flue Gas **Height:** 1500mm

(Thermocouple positions measured from the top of the base cone)

(c) Experimental Method

The fluidized bed was heated in the usual way using LPG with the bubble cap plate closed. When the bed had been raised to a sufficient temperature (500-600°C), the bubble cap plate at the hopper base was confirmed closed and then the air supply shut down. The screw feed hopper was then loaded and air tight lid re-fitted and the air back pressure for the hopper switched on. The screw feeder would not feed satisfactorily without back pressure. Air supply was then re-started and fluidization established. Air flow was confirmed at 24 l/s FAD and then the

bubble cap plate was opened and fuel feed started. The screw feeder was rotated manually at the approximate rate required for stoichiometric air/fuel ratio. Air flow and temperature measurements were made.

When feed hopper had emptied, the air shutdown procedure was repeated and the feed hopper reloaded for further testing. Two boiler test runs were completed with starting bed depths, including the conical hopper, of 515mm and 583mm. Two tests on deeper bed depths of 654 and 740 mm were included in the sand boiler test run by adding sand through a feed chute. The technique of adding sand during testing to achieve a deeper bed was developed due to problems with the LPG pilot burner when a warm up of a 740mm bed was attempted. The bubbles breaking the surface provided sufficient shock waves to extinguish the pilot flame. The only solution available was to reduce the bed depth so that bubble bursts were well below the pilot burner.

The temperatures were recorded on a chart recorder for the warm up, sawdust combustion and cooldown periods. Temperature data from the cooldown period was used to estimate the equivalent specific heat of the bed structure and solids.

(d) Results

(i) Observations

Combustion behaviour was similar to that observed for coal, with minimal smoke and no flames visible at the observation port. It was necessary to verify the feeder operation by feeding excess fuel to observe flame and above bed

combustion which can occur in sondary air drawn in by the exhaust draft through the observation port.

(ii) Quantitative Results

The average bed temperatures and flue gas temperatures are plotted in Figs.12.16 & 12.17. Results of calculations are presented in Tables 11.12a,11.12b,11.12c & 11.12d.

(e) Discussion

All tests were performed at a FAD of 24l/s, (air mass flow 0.028kg/s). The flow rate of 24l/s (FAD) is slightly excess to requirements for maintaining the 50mm pipe free of particles and ensures good pneumatic conveying of the fuel. As the flow rate could not be reduced, the bed behaviour became more violent as higher temperatures were reached. The U_f/U_{mf} ratios were typically of the range 3-5, (see Table 11.12d).

In both Combustor Run Nos.9 & 10 feed problems were experienced early in tests resulting in higher than desirable air/fuel ratios in Periods Nos 1 & 6 and poor useful heat transfer results. Bed temperature was observed to rise at fuel feed rates of stoichiometric and with some excess air. Heat released beneath the bed surface was of the order of 40-60% and the useable heat in the bed was in the range of 15-30% of fuel calorific value, (Tables 11.12a,11.12b,11.12c). The heat available for use in the bed is strongly dependent on limiting excess air to an optimum level which maximises combustion and heat release and minimises heat losses in flue gases. Although the air/fuel ratio was difficult to control, the results showed a vague peak in overall bed efficiencies with 20 - 40 % excess

air, (Fig.12.26). Significantly useful heat was available at air/fuel ratios which would allow complete combustion. The variation in the percentage heat release calculated for successive test runs is due to the uncertainty of the mass of fuel left in the feed hopper which could only be estimated. Since the overall fuel feed mass is known it is certain that correct heat release percentages vary only between the values calculated for successive tests.

Slight improvement was evident in the deeper beds but not as much as would be expected or desired, (Table 11.12a). It is reasoned that the major proportion of volatiles must be burning and travelling in the bubble phase. At 600°C , operating at $4.5U_{mf}$, the theoretical bubble speed is 1.184 m/s and superficial velocity is 0.45m/s, (Table F14, Appendix F). Following the two phase theory 77% of air will pass in the bubble phase with a residence time of just 0.43 ss in a conventional bed of 515mm depth. It should be noted that the bubble sizes, and hence velocities, would be larger than the sizes predicted by theory due to type of flow distribution used. Theoretical predictions assume a even flow distribution from a conventional distributor plate. The bubbles would probably be of the order of 50mm starting at the baffle plate. The velocities of air in the region below the spout plate are variable as follows:

- (i) 37 m/s (atfer entrance, after gas temperature equilibrium),
 - (ii) 0.57 m/s (at maximum hopper diameter)
- and (iii) 1.3 m/s. (at exit to the bed column above)

The gas residence time in the spout hopper of 300mm depth will be much shorter than in the main bed column. These factors all combine to give lower than calculated residence time. More significant improvement would therefore be expected if the bubble fraction and bubble velocity were reduced by the use of a larger bed solid, bubble control baffles or two chamber systems to maximise burning gas to particle contact time. An alternative approach could be investigated using bed solids of smaller size, opening the possibility of using a group A material which would allow operation up to $3U_{mf}$ without bubbling. The lower velocities would require a much larger (bed column diameter)/(spout inlet diameter) ratio as the velocities in the air supply tube must still be sufficient to convey the fuel.

Since excess air was present in all tests except Period No.7, Parameters O_p and maximum η_{bc} can be used for useful operating point comparisons, (Table.11.12a).

Packed bed heat flux values, ignoring Periods 1 & 6 which had too much excess air, were all above 500 kW/m^3 , (Table.11.12b). The result is a reflection of higher operational velocities and in-bed heat release. It is also a significant result when it is realised that these results are calculated on larger bed volumes than all previous tests.

Parameters α_f and α_w were all taken as unity and considering the combustion efficiencies achieved these are good approximations, (Table 11.12c).

The bed behaviour was quite aggregative with a behaviour index of order 4000 - 8000 due to the large particle size and

deep beds, (Table 11.12d). The U_f/U_{mf} ratio shows a progressive increase due to increased temperature, noting that the mass flow rate of air cannot be reduced due to feed standpipe velocity requirements, (Table 11.12d).

Gas-to-particle heat transfer coefficients were of order of $9 \text{ W/m}^2\text{K}$, (Table 11.12d), giving a Heat Transfer per unit temperature difference for a bed depth of 515mm of 2.6 kW/K . Excellent gas-to-particle heat transfer potential is therefore available.

The combustion of sawdust using the modified spouted bed gave the best results for combustion of particulate cellulose fuels in the entire research project. The key factors to the good results are :

- (i) All fuel reached the bed.
- (ii) All fuel was introduced into the bottom of the bed
- (iii) Fuel feed was relatively even
- (iv) The bed was deep enough to achieve heat transfer from the burning volatiles
- (v) Fuel particles were small enough to decompose and begin burning at a point very low in the bed

The combustion process can therefore be simply optimised by:

- (i) Even Continuous feed
- (ii) Smaller fuel particles
- (iii) Pre-heat the fuel and/or air using flue gases
- (iv) Deeper Beds

Further to the above obvious optimisations there is also the potential gains achievable by bubble control. These would be expected to be quite significant due to the relatively poor,

large bubble, fluidization achieved for these tests using a very crude baffle plate. Reductions in the rate of air flow bypass in spouts or large bubbles could result in acceptable combustion efficiencies at shallower bed depths.

6.0 DISCUSSION OF RESULTS

6.1 Phase 1: Flow Visualisation

The flow visualisation experiments demonstrated that bagasse would mix with sand in the cold state confirming the results of Peel and Santos, 1980, (9), (Tables.11.3 to 11.5; Figs.12.2 to 12.5). The mixing phenomena appears to be a complex function of bed particle diameter, superficial velocity and the modification to bed voidage by the presence of bagasse particles. The mass fraction, particle size distribution and particle aspect ratios of bagasse appear to be significant. Results showed that adequate mixing can be achieved by increasing either operating velocities or bed mass. As the only concern for combustion applications is maintaining adequate mixing, no attempt was made to develop a suitable relationship which would describe the behaviour of sand-bagasse mixtures. Operational velocity or bed mass could simply be increased if problems were encountered. It was also expected that actual fuel residence time for bagasse in combustion would be small, resulting in small mass percentages of bagasse particles resident in the bed. It was therefore probable that the meta-stable mixing, channelling, floating phenomena observed would not occur.

The experiments with deep beds allowed the research of modifications which it was believed would have application in rapid burial of fuels added to the top of the bed, (Tables.11.6,11.7; Figs.12.7,12.9). The enlargement of solids mass flow areas in the bed by either enhancement of solids

circulation in the natural direction or in the reverse direction, always resulted in some loss of fluidized volume. Fuel introduced to, and buried in, the mass flow regions would therefore not be exposed to adequate levels of air. It was reasoned, that if fuel buried in mass flows could reach the bottom of the bed, it would then be released and burn completely in a single upward pass of a sufficiently deep bed. Configurations utilising cones, draft tubes and increased central flow would require multiple fuel entry points at the bed walls, preferably below bed surface level. Such requirements present problems for a fibrous fuel, such as bagasse, which is difficult to feed mechanically. The possibility of reverse circulation of solids has the obvious benefit of a single central feed point and even distribution emanating from a point in the centre of the bed.

The combustion experiments in fact only utilised two concepts from these experiments; the use of a distributor with increased air flow in the centre and the Ingestor Tube. There is no evidence to suggest that any fuel ingestion advantage was gained using increased central flow, (Combustion Run Nos 1&2). The ingestor tube was successful during it's second test after extensive modification. The reason for the limited application of the flow visualisation results is the extremely short particle bed residence times of cellulose fuels. Based on observations from Combustor Run No.2, no significant change in fluidization phenomena in a combustor will result unless excessive amounts of particulate fuel are added at low superficial velocities, (eg $U_f/U_{mf} < 2$). The results of the

investigation of fuel particle mixing in a cold bed are therefore almost irrelevant to combustion problems. The problem of below bed surface combustion quickly changes from a particle-fuel problem to a gas-fuel problem. The ingestor application was successful because bed solid downward velocities in the tube were large enough to allow downward transport of fuel volatiles in the ingestor tube in addition to fuel particles and char.

6.2 Phase 2: Combustion Results

The experimental and combustion problems experienced in the combustion tests resulted from difficulties in handling and controlling fuel feed. Bagasse, in its irregular form, cannot be screw fed and requires negative hopper angles. The introduction of sawdust at later stages allowed research to proceed to conclusion without development of a specialised feeder. The difficulty of developing a satisfactory feeder before the combustion characteristics are researched, is one of economics. A suitable continuous feeder for bagasse would involve at least one chain conveyor, hoppers etc, assuming that above bed introduction of fuel was successful. If below bed feed was required, a whole new feeder would be required. It was therefore decided, at an early stage of the project, to use the simplest feeding systems possible, obtain combustion results and deduce the correct approach to Fluidized Bed Combustor design and consequently feeder design. The approach is now justified when the number of different configurations trialled in the combustion tests are considered. The result for research

was relatively crude apparatus and manually controlled batch and screw feed systems.

Fuel feeding methods represent the most significant area for uncertainty in the results obtained. Uncertainty is not just limited to the measurements and calculations, (Table 11.13), but also includes the feeding methods. In the case of batch feed using an above bed chute, the speed of fuel being pushed into the combustor is significant. If the fuel is introduced very slowly it will fall onto the bed lump by lump and be mixed after impact. A small percentage of the fuel will ignite as it falls. The remaining fuel will release volatiles before reaching much bed depth or lateral displacement due to the extremely rapid rise of particle temperature in the bed and decomposition of cellulose at 300°C. It is likely that air will not be available to burn all the volatiles released. These volatiles will move out of the bed with flue gases. Conversely, if the fuel enters the bed with considerable horizontal velocity, a larger proportion of the fuel will be lost via pneumatic transport and ignition before bed contact. In either case, the localised actual air/fuel ratio is to begin with, rich, reducing quickly to lean as fuel is burnt. A large proportion of the fuel volatiles are lost during the fuel rich period, moving out of the bed with flue gases. These unburnt volatiles either burn in secondary air above the bed or chimney or are just lost. Screw feeding using a closed hopper to prevent volatiles loss allows more regular fuel feed but problems still exist due to the fuel failing to drop from the hopper into the feeder auger. Further variation is introduced

by the fuel itself. Each sample, due to irregular sizes and moisture contents, will have slightly different levels of above bed ignition and fuel transport losses.

Quantifying the combustion efficiency and other parameters in a fluidized bed combustor, without water heating tubes, presents further problems as the yield of useful heat can only be measured in the heat up of bed solids. An estimation of wall losses must also be made. With a small installation like the combustor used, significant levels of heat energy are stored in the steel bed enclosure and plate and must be included in calculations. As heat transfer is proportional to temperature difference, the heat transfer rate to the bed structure and solids will reduce as the bed temperature increases. Combustion efficiency and other performance parameters will therefore be conservative if compared with a steady state condition giving constant useful heat transfer to water tubes. The advantage of using a combustor without heating tubes, was that unsustainable conditions are clearly identified. While the estimates of the specific heat of bed structure and solids, fuel specific heat and fuel moisture content are all sources of uncertainty the increase or decrease of bed temperatures clearly prove or disprove combustion sustainability. Since efficiency of operation can be deduced from examination of air/fuel ratio the most basic requirements for investigation are achieved.

The uncertainties, as presented in Table 11.13, are satisfactory in view of the equipment used. Distinct from the problems of measurement uncertainty, are the problems of measurement and result accuracies. Calculations of combustion

efficiencies and related parameters require accurate measurement of air flow rates, temperatures, fuel flow rates and calculations of wall losses. Air and fuel property data is also required. The air flow instruments were checked against each other and gave agreement within the expected uncertainties of the measuring process, (Fig. D2, Appendix D.). Temperature thermocouples were within 2% of a commercially produced probe. Wall loss estimates could only be calculated using the usual theory, but as they represent quite a small percentage of the calculated results, the inaccuracies of these estimates are not considered significant. The calculations of the heat transfer required to heat the fuel depend on an estimate of fuel specific heat. An accurate figure for the actual fuel used was impossible to obtain but the figure used is thought to be conservative as discussed in Section 3.44.

With the above considerations in mind, the various parameters η_c (Combustion Efficiency), η_B (Fluidized Bed Efficiency), η_{BC} (Overall Bed Efficiency) are plotted against air/fuel ratio in Figs. 12.18 to 12.26. Data is collected and plotted in three groups for comparison, above bed feed systems, ingestor feed systems and below bed feed systems.

(i) Above Bed Fuel Feed Systems.

Acceptable combustion efficiencies were only achieved with bagasse bricks and coal, both having relatively large fuel particle size. The problems identified using fuels of small particle size were :

- (a) Batches of particulate bagasse and sawdust fuels partially ignited before reaching the fluidized bed surface.

- (b) Immediate loss of small particles pneumatically transported in the flue gas stream. The problem is unavoidable due to the fine fibrous nature of the fuel and its broad size range. There will always be a significant level of dust in such fuels.
- (c) Extremely short residence times of all fuel particles of typical sizes for sawdust and bagasse. The rapid decomposition to char and volatiles is due to high particle-particle heat transfer rates. Fuel volatiles move quickly out of the bed with flue gases resulting in a high proportion of combustion occurring above the bed in secondary air, if available. If secondary air was shut-off, unburnt fuel was either lost from the combustor, or if temperatures permitted, ignited in the atmosphere in the flue gases. As a result of these problems, excess fuel was required to achieve even marginal temperature increases of the bed solids. The use of continuous fuel feed systems, (eg pneumatic conveyors), would not be expected to improve bed performance. Calculations indicate that even poorer below bed surface combustion efficiencies could be expected, as a higher proportion of the fuel would decompose in the flue gas stream and each particle will be subject to bed solid heat transfer immediately upon bed contact.
- (d) The difficulty of obtaining useful heat transfer from the heat release of 80-85% of the fuel by mass which burns as volatiles after the fuel particles have decomposed at 300°C. Enhanced Circulation systems, while in cold operations, appear to improve fuel ingestion, did not ingest fuel and

fuel volatiles in the short time frames required to improve combustion efficiency. Deep Beds offer no significant improvement in combustion efficiency confirming that fuel particles and fuel volatiles do not attain significant bed depth.

The significance of particle size to particle heat up time, and hence to particle bed residence time, is demonstrated by h_{pp} and Q/m values tabulated in Appendix E. Heat transfer to the fuel per unit mass per K is inversely proportional to the square of equivalent fuel particle diameter.

$$\frac{Q}{m} \propto d_{pf}^{-2}$$

The heat transfer per kg to a bagasse fuel brick of size 50mm and density 240 kg/m^3 is significantly reduced, approximately 1/50 of the heat transfer rate calculated for particulate bagasse at bed entry. The fuel heat up is therefore more gradual giving gradual release of volatiles and long bed residence times. It is anticipated that results similar to coal combustion could be obtained by optimising brick size, brick density and ensuring the fluidized bed voidage is sufficiently large to allow the ingesting of bricks to the bottom of the bed.

The difference between the results of coal and bagasse bricks compared to fibrous bagasse particles is dramatically shown in Fig.12.18. The seemingly peak combustion efficiency

result for particulate bagasse of 35% in Fig 12.18 did not result in any production of useful heat, (Figs.12.19,12.20). Useful heat transfer was only achieved under excess fuel conditions while using particulate fuels, (Figs 12.19,12.20). Poor useful heat transfer results were also obtained with the larger particle fuels, due to the experimental problem of insufficient fuel feed, resulting in too much excess air, (Fig.12.20). Coal yielded better results for useful heat transfer than bagasse bricks, as would be expected, due to it's higher density, higher de-volatilisation temperature and lower percentage of volatiles.

The combustion efficiencies for particulate bagasse, presented in Fig.12.18, do not offer much potential for within bed heat transfer, when it is considered that the minimum combustion efficiency for sustained combustion without yielding useful heat with dry fuel at 600°C is 23%. At a more realistic practical operation of 30% excess air with 50% fuel moisture would require a combustion efficiency of 44% just to maintain bed temperature, (See Table.E13; Fig.E8, Appendix. E). The possibility still exists for the use of the bed as a partial fuel gasifier using excess fuel.

An alternate solution may be low temperature operation. Lower bed temperatures (eg 400°C), just above ignition temperature of cellulose fuels, would significantly increase bed particle residence time resulting in increased ingestion depth and fuel gas residence time. All heat losses, particularly those in flue gases are also reduced at lower temperatures while the fuel energy remains the same. (It also

follows that operation at higher temperatures will give even poorer results.) Further research would be required to establish what improvements in combustion efficiency and useful heat transfer are possible.

(ii) The Ingestor Fuel Feed System

The ingestor feed system obviously offers possibilities with combustion efficiencies of 45% with 100% excess air, (Fig.12.21). Useful heat transfer was not realised due to fuel feed problems, (Figs.12.22,12.23). Useable heat yield could be achieved with higher fuel flow rates or by reducing the bed particle size and air flow. Further research and modification of the tube design and bed solids size and the incorporation of a pneumatic feeder could result in a successful above bed feed combustion system. Further testing was not done due to the need to re-design the LPG warm up system and solve the flame surge problems, (See Section 5.36).

(iii) Below Bed Fuel Feed Systems

A significant improvement is noted in combustor performance with below bed feed systems in Figs.12.24 to 12.26. Combustion efficiencies of similar order to that of coal were achieved when fuel was pre-mixed with fluidizing air and introduced to a modified spouted bed. Almost all tests were carried out with excess air, as calculated fuel feed rates did not have to be increased to maintain bed temperatures. The poorer results from the direct screw feeders need to be considered in view of the volatiles losses in the feeder and the relatively shallow bed depths. (NB. The screw feeder was located 140mm from the base of the bed). It is questionable as

to whether successful direct screw feeding of cellulose fuel particles can be achieved. The hot bed solids will always backmix with the fuel in the feeder at some point causing rapid fuel decomposition and possibly jamming.

A vague peak in efficiency values can be identified, (Figs.12.24 to 12.26), at air fuel ratios of approximately 6/1 to 7/1 which is to be expected for the combustion of cellulose, (eg 20 - 40% excess air). The order of magnitude of combustion efficiencies is significantly higher than with above bed feed systems and particulate fuels; eg Above bed feed 10-35%, below bed feed 30-65%. Operation yielding significant levels of useful heat or at quite high fuel moisture contents is possible, (Table.E13 Fig.E8 Appendix E). Even higher combustion efficiencies in the modified spouted bed would be expected with a reduction of bubble size and hence bubble speed resulting in longer residence time of volatiles. Similarly fuel pre-heating and drying become important considerations as it is optimal for the fuel, after introduction to the bottom of the bed, to be decomposed to volatiles and char as rapidly as possible. The burning fuel gas would then have maximum bed residence time for flame-to-bed heat transfer.

(iv) Improvements using Deeper Beds

The comparison of combustion efficiency and overall efficiency verses bed depth in Figs.12.27 & 12.28 clearly show that deeper beds result in no improvement when using above bed feed systems. Conversely, there is a definite upward trend in these results with increased bed depth when using below bed fuel feeders. The only exceptions are the test results from the

coal and bagasse bricks which were discussed earlier. These fuels would give similar results at various entry points as the large lumps sink to the bottom of the bed or mix in the bed remaining mostly below the bed surface. Residence time is relatively high and the volatiles release rate is reduced by the large particle size. The large fuel particles therefore release volatiles for combustion below bed surface giving adequate in-bed combustion and heat release.

(v) Packed Bed Heat Flux

Packed bed heat fluxes are presented for comparison, (Fig.12.29,12.30). The presentation and use of these heat flux values is somewhat problematic as it is usual to base calculations on water heating volume as done by Highley and Kaye, (5). Since this could not be done, the concept of Packed Bed Heat Flux was developed based on packed bed volume. The value so calculated can be converted to kW/m^2 based on sand area using the specific surface. Alternatively, an estimate of water heating volume per unit sand volume can be used and the normal comparisons made. It is emphasised that direct comparison of heat flux values from this thesis, with data from other boilers, must not be made without comparison of definitions used. The values presented are therefore readily useable but much lower numerically than calculations based on water heating volume. High heat fluxes can be achieved with above bed feed systems, shallow beds and excess fuel, (Fig.12.29), but generally results just reflect those of combustion efficiency and bed depth and are higher for higher operational air flow rates,(eg larger bed solids sizes).

Significant changes in orders of magnitude relating to feeder systems are noted. Packed bed heat fluxes with above bed feed systems are typically less than 500 kW/m^3 , whilst for below bed feed systems are usually above 500 kW/m^3 .

7.0 CONCLUSIONS

The investigation of the fluidized bed combustion of waste biomass materials, was completed by obtaining data from flow visualisation tests and ten combustion runs using various fuels. Fibrous, particulate bagasse, hardwood sawdust, coal and bagasse bricks were burnt in the combustor using various fuel feed systems. In the course of research the following problems were identified :

(a) Ignition of particulate fuels above the bed if added via above bed feed systems.

(b) Immediate loss of small fuel particles pneumatically transported in the flue gas stream.

(c) Extremely short residence times of all fuel particles of typical sizes for sawdust and bagasse due to the high particle-particle heat transfer within the bed.

(d) The difficulty of obtaining useful heat transfer from the heat release of 80-85% by mass, of the cellulose fuels, which burns as volatiles after the fuel particles have decomposed at 300°C.

The results of the investigation of fuel particle mixing in a cold bed are therefore almost irrelevant to combustion problems due to points (c) and (d). Enhanced circulation techniques for fuel and bed solids are only useful if they add to the residence time of, not only fuel particles, but the decomposition products of volatiles and char. The ingestor tube system appears to be the only configuration tested that offers such potential.

Fluidized bed combustion, using above bed feed systems and small particulate cellulose fuels, is clearly not feasible for the production of useful heat within the bed at the temperatures tested. The use of the bed for partial fuel gasification would appear to be an option operating with excess fuel. There is also the possibility of the yield of useful heat at lower bed temperatures due to longer fuel particle residence times and reduced heat losses.

The use of relatively large fuel particle sizes with above bed feed systems appears to offer a feasible option for the burning of cellulose fuels. The heat transfer per kg to the fuel brick is significantly reduced by increased size. For 50mm bagasse bricks, the heat transfer rate from bed solids to fuel is approximately $1/50$ of that calculated for particulate bagasse. The fuel heat up is therefore more gradual giving gradual release of volatiles and longer bed residence times.

Fluidized bed combustion, using below bed surface feed systems and small particulate cellulose fuels, is considered feasible for both partial gasification and the production of useful heat within the bed. The main problem becomes one of providing more elaborate feed systems.

Deep Beds offer no significant improvement in combustion efficiency when combined with above bed feed systems due to the extremely short particle bed residence time. Conversely, combustion efficiency improves with bed depth, if the fuel is introduced at the bottom of the bed as gas flame-to-bed-particle contact time is increased.

Continuous fuel feed systems will improve the results

obtained for combustion using below bed feeders, as improved fuel control will ensure a small amount of excess air at all times. Conversely, continuous feeders are not expected to improve combustion efficiency of particulate fuels using above bed feed systems. Calculations predict a higher proportion of above bed ignition and even further reduced particle bed residence times.

Two options for successful Fluidized Bed Combustor design are evident:

(i) Above Bed Feed Systems: Increase the fuel particle and fuel volatiles residence times by increasing fuel particle size. This would require fuel pre-processing to produce fuel briquettes.

(ii) Below Bed Feed Systems: Increase of the fuel volatiles residence time and decrease fuel particle residence time by reducing particle size, pre-heating the air-fuel mixture and using deeper or multiple beds.

Sustained fluidized bed combustion and the production of useful heat within the bed using lightweight cellulose biomass fuels is clearly feasible. The problem of fluidized bed combustion of bagasse and other similar fuels, (eg sawdust, rice husks etc), is now reduced to the problem of fuel feed method and rate control. Further optimisation and research is still required and recommendations are detailed in the next chapter.

8.0 RECOMMENDATIONS FOR FURTHER WORK

Due to the different Fluidized Bed Combustor configurations investigated, several options for further research can be suggested.

8.1 Investigation of Fuel Brick and Bed Particle Size

The favourable results from the single test utilising bagasse bricks of approximate density of 240 kg/m^3 indicates the need for further research. The direction of research should be:

(a) The relationship between combustion efficiency and fuel brick size.

(b) The relationship between combustion efficiency and the U_f/U_{mf} operating point. (ie effective bed density)

A series of combustion tests would be required using various brick sizes and bed particle sizes. The investigation may also include alternate bed materials such as porous alumina and bloated clay.

8.2 Fuel Gasification with Above Bed Feeder

Fluidized bed combustors clearly can provide effective gasification of cellulose fuels. Results from this research would indicate that bed temperature is only increased in excess fuel conditions, allowing for the combination of sustainable combustion and gasification of the excess fuel. A useful bagasse combustor could be built using similar principles to the successful peat combustor detailed by Pontifex.K.R. et.al,

(14). The fluidized bed would be used for primary combustion and to gasify the excess fuel. The unburnt gasified fuel would be burnt in secondary air above the bed. The approach opens the possibility of operating the bed at lower temperatures which would increase bagasse bed residence time and combustion efficiency and may allow some heat transfer from the bed. Most heat transfer would have to occur above the bed and above the secondary air combustion zone. Possible configurations are given in Figs.12.31,12.32.

8.3 Pre-Gasification of Fuel

Following the principles of the previous proposal, there is the option of using two fluidised beds in series to achieve optimum operation. Two options exist, these being the use of secondary air, (Fig.12.33), and the use of bed solids recirculation, (Fig.12.34). In either case, the first bed would begin combustion and gasify all fuel and the second bed will ensure the completion of combustion and sufficient gas-to-particle heat transfer.

The use of secondary air as proposed in Fig.12.33 would allow the first or lower bed to be sustained by excess fuel. The unburnt fuel would be burnt above the bed and heat release transferred to the solids in the second bed.

The use of solids recirculation, (Fig.12.34), depends on being able to feed the fuel against a back pressure, either mechanically or by using an air lock feeder. No excess fuel would be used, instead the gasifier bed would be maintained at temperature by recirculating bed solids from the second bed.

8.4 Pre-Mixed Fuel Air using Modified Spouted beds

Further work is recommended based on the good results from modified spouted beds in this research. The following modifications should be investigated.

(a) Fuel Pre-Heating, (Fig.12.35).

It is envisaged that heat transfer to the bed solids could be improved by advancing the point of ignition by pre-heating the fuel. It would even be desirable if sufficient heat transfer could be achieved to pre-ignite the fuel.

(b) Dual Chamber, (Fig.12.36).

A dual chamber bed would improve heat transfer by breaking bubble flow. The lower chamber would be self sustaining. The upper chamber would be designed to meet heat transfer requirements.

(c) Single Chamber with Bubble Controls, (Fig.12.37).

The single chamber as shown is the next logical step following Combustor Run No.10. The proposed design exploits the property of conical hoppers to provide backflow but require high pressures to rupture and allow upward flow. The large bubbles, which were not controlled in the final two Combustor Runs, would be controlled by the baffle plate design concept presented. Flow visualisation could be used to obtain the initial design details. Alternatively, the design would be a possible application for computational fluid mechanics.

8.5 Conventional Spouted Bed with Multi-Point Fuel Feed

An interesting possibility is offered by the idea of feeding fuel into the bulk mass flow of bed solids at the walls of a spouted bed. The difficulties of direct fuel feed at the fluidized bed wall should be noted from Section 5.35. Ideally, fuel should be fed below the bed surface but useful results may be possible with above bed feeders. The spouted bed would have to be wide enough to ensure the fuel stays in the Annulus downflow. The heat stored in the bed solids would decompose the cellulose fuel and allow volatiles to diffuse to the spout region to burn in adequate air, (Fig.12.38).

8.6 Ingestor Feed Systems

Further research is recommended using the ingestor system reported upon as a starting point. A complete re-design of the LPG warm up system would be required in conjunction with ingestor design. There would be advantages in narrowing the range of bed particle sizes to reduce particle control requirements. The ingestor tube could be replaced by a cone shape to increase bulk solid flow. A pneumatic feeder could be used to inject fuel particles into ingestion flow, (Figs.12.39,12.40).

9.0 RERERENCES

- (1) Botterill.J.S.M. Fluid-Bed Heat Transfer. Academic Press, London 1975.
- (2) Squires.A.M. Three Bold Exploiters of Coal Gasification: Winkler, Godel and Porta in Howard.J.R. Fluidized Beds : Combustion and Applications. Applied Science Publishers . London and New York.1983.
- (3) Kunii.D and Levenspiel.O Fluidization Engineering. R.E.Kruger Publishing.Co. New York.1977.
- (4) Singh.H, Sharma.S.M., Prasad.C.R.K. Bloated Clay Aggregate as Inert Bed Material for Fluidized Combustion of Bagasse. International Sugar Journal. Vol 95, No.1130. 1993.
- (5) Highley.J. and Kaye.W.G. Fluidized Bed Industrial Furnaces and Boilers in Howard.J.R. Fluidized Beds : Combustion and Applications. Applied Science Publishers . London and New York.1983.
- (6) Broughton.J. Combustion of Gases in Fluidized Beds in Howard.J.R. Fluidized Beds : Combustion and Applications. Applied Science Publishers . London and New York.1983.
- (7) Broughton.J.and Howard.J.R. Combustion of Coal in Fluidized Beds in Howard.J.R. Fluidized Beds : Combustion and Applications. Applied Science Publishers . London and New York.1983.
- (8) Luo.M, Stanmore.B.& Dixon.T Computer Modelling of a Sugar Mill Boiler. Dept. Chemical Eng. University of Qld & Sugar Research Institute Mackay. 1992.
- (9) Peel.R.B. & Santos.F.J. Fluidized Bed Combustion of Vegetable Fuels in Fluidized Combustion: Systems and Application. The Institute of energy , London. 1980
- (10) Vafaei.M. Jenkins.B.M. Salour.D. Reardon.F. Heat Transfer to Horizontal Tubes measured in the Bed and Convective Zones of a Biomass Fueled Pilot Scale Fluidized Bed Combustor. 11th International Conference on Fluidized Bed Combustion. 1991. Montreal.
- (11) Hanson.J. Agricultural Waste Fired Fluid Bed Combustor Delano. California. 11th International Conference on Fluidized Bed Combustion. 1991. Montreal.
- (12) Samolada.M.C. Vasalos. I.A. Kinetic Approach to the Flash Pyrolysis of Biomass in a Fluidized Bed Reactor. Fuel. Jul.1991.

- (13) Chong.Y.O., White.E.T. Rudolph.V. Judd.M.R. Bagasse Combustion in a Fluidized Bed. Proceedings Australian Society of Sugar Cane Technologists. 1992.
- (14) Pontifex.K.R. ,Newman.R, Williams.E.G. Peat Fired Fluidised Bed Combustor Indicates Potential for the Sugar Mill Bagasse/Coal Fired Boilers Proceedings Australian Society of Sugar Cane Technologists. Cairns 1993
- (15) Howard.J.R. Fluidized Bed Technology. Principles and Applications. Adam Hilger. Bristol, New York. 1989.
- (16) Botterill.J.S.M Fluidized Bed Behaviour in Howard.J.R. Fluidized Beds : Combustion and Applications. Applied Science Publishers . London and New York.1983.
- (17) Davidson.J.F and Harrison.D. Fluidised Particles Cambridge University Press. Cambridge.1963.
- (18) Mathur.K.B. & Epstein.N. Spouted Beds. Academic Press Inc. New York. 1974.
- (19) Incropera.F.P & De Witt D.P. Introduction to Heat Transfer 2nd Ed. J Wiley & Sons. NY. 1990
- (20) Eastop.T.D & McKonkey.A. Applied Thermodynamics. Longman. London.1978

10.0 BIBLIOGRAPHY

The Bibliography includes secondary source material which was consulted during research to provide background information, fluid property data and useful experimental data for test equipment design and thesis calculations.

Basu.P, Horio.M, Hasatani.M **Circulating Fluidized Bed Technology III** . Pergamon Press. New York. 1990.

Becker.M. **Heat Transfer: A Modern Approach**. Plenum Press. New York.1986

Black.W.Z & Hartley.J.G. **Thermodynamics**. 2nd Ed. Harper Collins Publishing. New York. 1991

Craig.R. **Investigation of Convective Heat Transfer to Free Falling Bodies**. Dept. Of Mechanical Engineering. C.I.A.E.1988

Czekanski.J. **An Introduction To High Velocity Fast Fluidised Bed Combustion Technology**. GEC Power Engineering. Leicester.1981.

Goodger.E.M. **Combustion Calculations**. Gresham Press. London 1977.

Grace.J.R. and Matsen.J.M. **Fluidization**. International Fluidization Conference.Henniker Plenum Press. New York 1980

Fluidised Combustion: Systems and Applications. Proceedings Institute of Energy's International Conference London. 1980

Hanley.D.P. **Introduction to the Selection of Engineering Materials**. Van Nostrand Reinhold. New York. 1980

Howard.J.R. **Fluidized Beds : Combustion and Applications**. Applied Science Publishers . London and New York.1983.

Mayhew.Y.R & Rogers.G.F.C. **Thermodynamic and Transport Properties of Fluids**. 2nd Ed. Oxford.1972

Mujumdar.A.S **Drying 84** Hemisphere Publishing Co. New York 1984.

Potter. O.E. and Nicklin.D.J. **Fluidization IV**. Engineering Foundation. New York. 1992.

Thring.M.W. **The Science of Flames and Furnaces**. 2nd Ed. Chapman and Hall. London.1962.

11.0 RESULTS TABLES**Phase 1: Flow Visualisation**

Table 11.1	Flow Visualisation Results Summary
Table 11.2-11.5	Deep Bed and Bagasse-Sand Mixing Characteristics
Table 11.6-11.7	Enhanced and Reversed Sand Circulation Characteristics.

Phase 2: Combustion Results

Table 11.8	Combustion Test Results Summary
Table 11.9a-d	Combustion Results: Deep Bed, Chute Feed.
Table 11.10a-d	Combustion Results: Shallow Bed, Chute Feed.
Table 11.11a-d	Combustion Results: Deep Bed, Screw and Ingestor Feed.
Table 11.12a-d	Combustion Results: Modified Spouted Bed, Screw Feed
Table 11.13	Uncertainty Estimates of Data and Calculated Results

Phase 1: Flow Visualisation

Table. 11.1 Flow Visualisation Results Summary

Test No.	Sand Size microns	Bed Depth mm	Bed Detail	Observations
1 Deep Beds	180	330 440 590	Mesh Distributor	Mixing by bubbling induced solids transport Convective solids flow patterns established. Tendency for deeper beds to slug and have areas of localised mixing
2a Bagasse-Sand mix	180	185	Mesh Distributor	Bagasse mixed easily with sand. Umf and required Uf for adequate mixing increases with bagasse content. If Uf is too low, the bed is meta-stable alternating from channelling to fluidization.
2b Bagasse-Sand mix	490	215	Mesh Distributor	Comments as for Test No. 2b Increased tendency for bagasse to 'float' at low Uf instead of channelling
3 Enhanced Circulation	490	180 365 245 260 515	Centre Flow Centre Flow Small Cone Large Cone Draft Tube	Larger volume of wall solids downflow. Similar behaviour to an ordinary bed Similar behaviour to an ordinary bed Larger volume of wall solids downflow. Larger volume of wall solids downflow.
4 Reversed Circulation	490	110 195 265	Annulus flow Annulus flow Ingester tube	Observable central solids downflow Un-observabale central solids downflow Observable solids downflow in tube

Table. 11.2 Deep Bed Flow Visualisation

Bed Conditions		Type	190 mm Diameter, Deep Bed, Mesh Plate		
		Depth	330 mm	Pmax = 4.69 kPa	
			440 mm	Pmax = 6.26 kPa	
			590 mm	Pmax = 8.39 kPa	
		Sand	180 mm	Umf = 0.024 m/sec	
Bed Depth mm	U f m/sec	Uf Umf	Bed Pressure Drop kPa	P drop P max	Comments
330	0.020	0.84	3.90	0.83	
	0.023	0.96	3.97	0.85	A few 20mm bubbles
	0.038	1.59	4.01	0.85	50% mixing
	0.047	1.97	4.09	0.87	50mm bubbles
	0.057	2.38	4.14	0.88	
	0.059	2.47	4.30	0.92	
	0.063	2.64	4.18	0.89	20-100mm bubbles
440	0.016	0.69	4.42	0.71	
	0.020	0.84	4.87	0.78	Fines seperation
	0.023	0.96	5.26	0.84	
	0.030	1.27	5.56	0.89	50mm bubbles
	0.049	2.03	5.61	0.90	
	0.051	2.13	5.55	0.89	Full mixing
	0.059	2.46	5.62	0.90	20-100mm bubbles
	0.064	2.67	5.68	0.91	
590	0.020	0.83	6.30	0.75	
	0.020	0.83	7.01	0.84	Small bubbles
	0.034	1.43	7.40	0.88	Fines Separation
	0.038	1.57	7.77	0.93	
	0.045	1.89	7.65	0.91	
	0.053	2.20	7.67	0.91	Full mixing
	0.066	2.75	7.68	0.92	

Table. 11.3

Bagasse - Sand Mixing ,180 micron Sand

Bed Conditions		Type	190mm Diameter,Deep Bed, Mesh plate		
		Depth	185 mm	Pmax=	2.632 kPa
		Sand	180 micron	Umf=	0.024 m/s
Bagasse by Mass %	U f m/sec	Uf Umf	Bed Pressure Drop kPa	P drop Pmax	Comments
0	0.012	0.49	1.49	0.57	Normal behaviour
	0.020	0.85	1.70	0.65	
	0.020	0.85	1.93	0.73	
	0.026	1.10	2.08	0.79	
	0.041	1.70	2.09	0.79	
	0.057	2.36	2.11	0.80	Good mixing
	0.068	2.82	2.16	0.82	
	0.073	3.02	2.17	0.82	
	0.095	3.95	2.22	0.84	
0.65	0.020	0.85	1.46	0.55	
	0.024	0.98	1.67	0.63	
	0.024	0.98	1.89	0.72	Bubbling
	0.055	2.30	2.04	0.78	
	0.053	2.19	2.00	0.76	
	0.074	3.10	2.03	0.77	Channelling
	0.090	3.73	2.17	0.82	Good Mixing
1.29	0.026	1.10	1.57	0.60	
	0.031	1.30	1.65	0.63	
	0.037	1.55	1.69	0.64	40mm bubbles
	0.046	1.90	1.74	0.66	'Channelling',bubbling
	0.065	2.69	1.80	0.68	'Sticky mixing'
	0.082	3.40	1.87	0.71	Good mixing
1.88	0.034	1.40	1.36	0.52	
	0.039	1.64	1.46	0.55	
	0.044	1.84	1.55	0.59	
	0.057	2.36	1.62	0.62	
	0.066	2.74	1.73	0.66	
	0.089	3.71	1.70	0.65	70% mixing
	0.103	4.28	1.76	0.67	
	0.128	5.32	1.91	0.73	Good mixing
3.22	0.093	3.87	1.64	0.62	
	0.116	4.83	1.42	0.54	Channelling
	0.127	5.28	1.60	0.61	Channelling
	0.150	6.24	1.80	0.68	Channelling
	0.165	6.86	1.92	0.73	50% mixing
	0.183	7.63	1.93	0.73	80-100mm bubbles
	0.206	8.57	2.01	0.76	Good turbulent mixing

Table. 11.4

Bagasse - Sand Mixing, 490 micron Sand

Bed Conditions		Type	190mm Diameter, Deep Bed, Mesh plate		
		Depth	215 mm	P _{max} =	3.058 kPa
		Sand	490 micron	U _{mf} =	0.178 m/s
Bagasse by Mass %	U f m/sec	U _f U _{mf}	Bed Pressure Drop kPa	P drop P _{max}	Comments
0	0.071	0.40	1.34	0.44	
	0.087	0.49	1.65	0.54	
	0.100	0.56	1.90	0.62	
	0.117	0.66	2.32	0.76	
	0.134	0.75	2.58	0.84	First bubbles
	0.163	0.92	2.63	0.86	80mm bubbles
	0.183	1.03	2.77	0.91	
	0.209	1.18	2.80	0.92	Partial mixing
	0.228	1.28	2.78	0.91	Good mixing
	0.247	1.39	2.81	0.92	
	0.274	1.54	2.80	0.92	
	0.293	1.65	2.83	0.93	Almost slugging
0.5	0.083	0.46	1.74	0.57	
	0.095	0.53	2.04	0.67	
	0.133	0.75	2.25	0.74	
	0.147	0.83	2.50	0.82	
	0.169	0.95	2.79	0.91	
	0.197	1.11	2.73	0.89	
	0.215	1.21	2.80	0.92	
	0.235	1.32	2.95	0.96	
	0.256	1.44	2.87	0.94	90% mixing
	0.275	1.55	2.93	0.96	
	0.300	1.69	2.94	0.96	
	0.313	1.76	2.95	0.96	140mm bubbles
0.5	0.095	0.54	1.74	0.57	Bagasse pre-mixed
	0.133	0.75	2.36	0.77	
	0.179	1.01	2.65	0.87	
	0.222	1.25	2.80	0.92	
	0.259	1.46	2.82	0.92	Good mixing
	0.297	1.67	2.89	0.94	
1.13	0.095	0.53	1.76	0.58	
	0.123	0.69	2.51	0.82	
	0.146	0.82	2.74	0.90	First bubbles
	0.174	0.98	2.76	0.90	Slow ingestion
	0.173	0.97	2.77	0.91	
	0.203	1.14	2.79	0.91	Complete ingestion
	0.220	1.24	2.75	0.90	
	0.244	1.37	2.74	0.90	Still dead zones
	0.262	1.47	2.70	0.88	
	0.298	1.68	2.89	0.94	Mixing
	0.338	1.90	2.89	0.94	Good mixing
1.6	0.165	0.93	2.31	0.76	Channelling
	0.199	1.12	2.76	0.90	
	0.262	1.48	2.86	0.94	
	0.304	1.71	2.83	0.93	50% mixing
	0.343	1.93	2.79	0.91	
	0.378	2.13	2.43	0.79	80% mixing
	0.414	2.33	2.95	0.96	Good mixing
	0.294	1.65	2.91	0.95	Separation, floating

**Table. 11.5 Minimum Operational Velocities for
Bagasse-Sand Mixtures**

Mean Sand Diameter microns	Bagasse by Mass %	Bagasse by Particle Volume %	Bagasse by Bulk Volume %	Observed Minimum Operational Uf/Umf
180	0.00	0.0	0	2.30
	0.65	2.7	12	3.64
	1.29	5.2	24	3.96
	1.88	7.4	35	5.20
	3.22	12.1	60	8.37
490	0.00	0.0	0	1.28
	0.50	2.1	9	1.69
	1.13	4.6	21	1.69
	1.60	6.4	29	2.35

Table. 11.6 Enhanced Sand Circulation Results

Bed Conditions		Type	190mm Diameter, Deep Bed, Mesh plate				
		Depth	215 mm	Pmax=		3.058 kPa	
			180 mm			2.560 kPa	
			365 mm			5.192 kPa	
			245 mm			3.485 kPa	
			260 mm			3.698 kPa	
			515 mm			7.326 kPa	
		Sand	490 micron	Umf=		0.178 m/s	
Bed Config. & Depth mm	U f m/sec	Uf Umf	Bed Pressure Drop kPa	P drop Pmax	Umax m/sec	Umax Umf	Comments
215 Mesh Plate	0.071	0.40	1.34	0.44	N/A	N/A	
	0.087	0.49	1.65	0.54			
	0.100	0.56	1.90	0.62			
	0.117	0.66	2.32	0.76			
	0.134	0.75	2.58	0.84			
	0.163	0.92	2.63	0.86			
	0.183	1.03	2.77	0.91			
	0.210	1.18	2.80	0.92			
	0.228	1.28	2.78	0.91			
	0.247	1.39	2.81	0.92			
180 5 caps in centre	0.135	0.76	1.51	0.59	0.49	2.75	Umax estimated on dia 100mm
	0.155	0.87	1.66	0.65	0.56	3.15	Central Bubbles
	0.189	1.06	1.56	0.61	0.68	3.84	
	0.214	1.20	1.57	0.61	0.77	4.35	External downflow
	0.237	1.33	1.58	0.62	0.85	4.80	Faster downflow
	0.258	1.45	1.57	0.61	0.93	5.24	Faster downflow
	0.280	1.58	1.57	0.61	1.01	5.70	Faster downflow
	0.304	1.71	1.59	0.62	1.10	6.18	Spout fountain 250mm
	0.322	1.81	1.59	0.62	1.16	6.54	
	0.339	1.91	1.59	0.62	1.22	6.89	
	0.360	2.03	1.60	0.63	1.30	7.32	
365 5 caps in centre	0.083	0.47	2.11	0.41	0.30	1.69	Umax estimated on dia 100mm
	0.096	0.54	2.53	0.49	0.35	1.95	
	0.128	0.72	3.54	0.68	0.46	2.60	
	0.150	0.85	4.27	0.82	0.54	3.06	Top 50% fluidized
	0.201	1.13	4.22	0.81	0.73	4.09	Slow wall downflow
	0.248	1.40	4.18	0.81	0.90	5.05	Almost slugging
	0.280	1.57	4.13	0.80	1.01	5.68	
	0.307	1.73	4.23	0.82	1.11	6.24	
	0.336	1.89	4.28	0.82	1.21	6.84	
245 Small Cone	0.086	0.48	1.64	0.47	0.54	3.02	Umax estimated on dia 76mm
	0.109	0.61	2.10	0.60	0.68	3.82	
	0.128	0.72	2.42	0.69	0.80	4.50	Bubbles inner, dead outer
	0.162	0.91	2.96	0.85	1.01	5.70	25mm bubbles outer
	0.192	1.08	3.10	0.89	1.20	6.76	
	0.217	1.22	3.17	0.91	1.35	7.62	
	0.247	1.39	3.25	0.93	1.54	8.68	
	0.268	1.51	3.26	0.94	1.67	9.42	Slow circulation
	0.298	1.68	3.26	0.94	1.86	10.48	Good circulation
	0.318	1.79	3.26	0.94	1.99	11.17	Fast circulation
260 Large Cone	0.083	0.47	1.90	0.51	0.52	2.92	Umax estimated on dia 76mm
	0.106	0.59	2.40	0.65	0.66	3.72	
	0.154	0.87	3.23	0.87	0.96	5.41	
	0.225	1.26	3.26	0.88	1.40	7.90	First circulation, one side
	0.255	1.43	3.14	0.85	1.59	8.95	
	0.270	1.52	3.18	0.86	1.69	9.49	75% circulation
	0.294	1.66	3.15	0.85	1.84	10.35	
	0.316	1.78	3.17	0.86	1.98	11.12	Good circulation
515 Draft Tube	0.104	0.59	4.19	0.57	0.38	2.12	Umax in tube dia 100mm
	0.124	0.70	5.19	0.71	0.45	2.52	
	0.162	0.91	5.32	0.73	0.58	3.29	Bubbles/slugs in tube
	0.194	1.09	5.05	0.69	0.70	3.95	First downflow
	0.224	1.26	5.10	0.70	0.81	4.56	
	0.353	1.98	5.15	0.70	1.27	7.16	80% external downflow

Table. 11.7 Reversed Sand Circulation Results

Bed Conditions Type 190mm Diameter, Deep Bed, Mesh plate Depth 110 mm Pmax= 1.565 kPa 195 mm 2.774 kPa 265 mm 3.769 kPa Sand 490 micron Umf= 0.178 m/s							
Bed Config. Depth mm	U f m/sec	Uf Umf	Bed Pressure Drop kPa	P drop Pmax	Umax m/sec	Umax Umf	Comments
110 Annulus flow	0.105	0.59	0.83	0.53	0.17	0.98	
	0.129	0.73	1.11	0.71	0.22	1.21	
	0.164	0.92	1.20	0.77	0.27	1.53	First bubbles
	0.197	1.11	1.15	0.73	0.33	1.85	
	0.221	1.25	1.16	0.74	0.37	2.07	
	0.246	1.38	1.17	0.75	0.41	2.30	
	0.267	1.50	1.15	0.73	0.44	2.50	Ingestion of Matchsticks
	0.289	1.63	1.15	0.73	0.48	2.70	
	0.309	1.74	1.16	0.74	0.51	2.89	Rapid ingestion
	0.330	1.86	1.18	0.75	0.55	3.09	
195 Annulus flow 5 caps in centre	0.113	0.64	1.74	0.63	0.19	1.06	
	0.137	0.77	2.26	0.81	0.23	1.28	
	0.163	0.92	2.36	0.85	0.27	1.53	First bubbles
	0.195	1.10	2.36	0.85	0.33	1.83	
	0.221	1.24	2.35	0.85	0.37	2.07	
	0.243	1.37	2.35	0.85	0.40	2.28	Rapid ingestion
	0.267	1.50	2.37	0.85	0.44	2.50	
	0.290	1.63	2.40	0.87	0.48	2.72	
	0.314	1.77	2.40	0.87	0.52	2.94	Good visible circulation
	0.332	1.87	2.39	0.86	0.55	3.11	
265 Ingestor tube	0.165	0.93	3.42	0.91	0.21	1.20	Surface bubbles, annulus
	0.188	1.06	3.59	0.95	0.24	1.37	
	0.222	1.25	3.49	0.93	0.29	1.61	Large bubbles,annulus
	0.244	1.37	3.44	0.91	0.31	1.77	
	0.262	1.48	3.48	0.92	0.34	1.90	
	0.290	1.63	3.58	0.95	0.37	2.10	Slow tube downflow
	0.331	1.86	3.69	0.98	0.43	2.40	
	0.390	2.19	3.69	0.98	0.50	2.83	Annulus almost slugging Good tube downflow

Phase 2: Combustion Results

Table. 11.8 **Combustion Test Results Summary**

Bed Depth mm	Bed Type	Feed System	Fuel	Maximum Fuel Size mm	η_c %
125-130	Shallow	Top Chute	Bagasse Sawdust Coal	50 x 5 10 x 2 60	30 35 66
300-325	Deep	Top Chute	Bagasse Bagasse	50 x 5 50 bricks	25 59
325 460	Deep	Direct Screw	Sawdust Sawdust	10 x 2 10 x 2	39 47
355	Reverse Circulating	Ingestor Tube	Sawdust Bagasse	10 x 2 50 x 5	45 35
515 583 654 740	Deep, Re-Fluidized	Screw Pre-mixed with air	Sawdust Sawdust Sawdust Sawdust	10 x 2 10 x 2 10 x 2 10 x 2	55 55 54 61

Table. 11.9a Combustion and Heat Release Efficiencies
Deep Bed, Chute Feed.
 Combustor Run Nos 1 & 2

Bed Conditions		Type	Deep Bed, Pattern No. 2 Bubble Caps						
		Depth	325 mm Run no.1, Period No.1&2						
			305 mm Run No.2, Period Nos.3 to 9						
		Sand	490 micron						
		Fuel	Bagasse bricks,50mm Period No.1&2						
			Particulate Bagasse Period Nos.3 to 9						
Period No.	Average Temp C	Fuel Heat kW	Air/Fuel Ratio	η_c %	O _r %	η_B %	η_{Bc} Actual %	η_{Bc} Maximum %	η_{Bc} Theoretical %
Bagasse Bricks									
1	666	88	11.2	54	70	11	5	52	74
2	649	60	16.4	59	48	-18	-6	36	75
Bagasse Fibres									
3	713	81	5.2	20	98	-5	-4	76	78
4	710	63	6.7	26	94	0	0	74	78
5	710	65	4.8	23	N/A	0	0	N/A	78
6	717	109	2.9	17	N/A	5	4	N/A	78
7	727	110	1.9	15	N/A	4	4	N/A	77
8	747	96	2.2	24	N/A	14	12	N/A	77
9	757	123	1.3	5	N/A	-4	-4	N/A	76

η_c Combustion Efficiency, % (in-bed combustion)
 ie % Total Fuel Heat released below bed surface

O_r Operating Ratio: % of ideal dry fuel/stoich. condition in terms of Useful Heat

η_B Fluidized Bed Efficiency or Heat Transfer Efficiency of the Bed

η_{Bc} Actual Overall Bed Efficiency , (Useful Heat)/(Total Fuel Heat)

η_{Bc} Maximum Maximum Overall Bed Efficiency
 at given operating conditions

η_{Bc} Theoretical Theoretical Overall Bed Combustion Efficiency
 at ideal dry fuel/stoichiometric conditions

Table. 11.9b Combustion Heat Balance, Deep Bed, Chute Feed
Combustor Run No.1 & 2

Bed Conditions		Type	Deep Bed, Pattern No. 2 Bubble Caps					
		Depth	325 mm	Run no.1, Period No.1&2				
			305 mm	Run No.2, Period Nos.3 to 9				
		Sand	490 micron					
		Fuel	50 mm	Bagasse bricks.		Period No.1&2		
				Bagasse Fibres		Period Nos.3 to 9		
Period No.	Air/Fuel Ratio	Fuel Heat Release kW	Flue Gas Heat Loss %	Wall Heat Loss %	Useable Bed Heat %	Above Bed Heat %	η_c %	Packed Bed Heat Flux kW/cu.m
Bagasse Bricks								
1	11.2	88	47	1	5	46	54	773
2	16.4	60	64	1	-6	41	59	583
Bagasse Fibres								
3	5.2	81	23	1	-4	80	20	282
4	6.7	63	25	1	0	74	26	289
5	4.8	65	21	1	0	77	23	256
6	2.9	109	12	1	4	83	17	330
7	1.9	110	11	1	4	85	15	286
8	2.2	96	10	1	12	77	24	403
9	1.3	123	10	1	-5	94	5	111

Table. 11.9c Combustion Heat Balance - Details, Deep Bed, Chute Feed
Combustor Run No.1 & 2

Bed Conditions		Type	Deep Bed, Pattern No. 2 Bubble Caps							
		Depth	325 mm				Run no.1, Period No.1&2			
			305 mm				Run No.2, Period Nos.3 to 9			
		Sand	490 micron							
		Fuel	50 mm				Bagasse bricks.	Period No.1&2		
							Bagasse Fibres	Period Nos.3 to 9		
Period No.	Air/Fuel Ratio	Fuel Heat Release kW	Air Flow Heat Loss %	Fuel Flow Heat Loss %	Moisture Heat Loss %	Wall Heat Loss %	Moisture Content %	α_f	α_w	
Bagasse Bricks										
1	11.2	87.9	39.4	7.9	0.0	0.9	0	1	1	1
2	16.4	60.1	56.6	7.8	0.0	1.3	0	1	1	1
Bagasse Fibres										
3	5.2	81.1	19.6	3.1	0.0	0.9	0	0.36	0.36	0.36
4	6.7	63.0	22.0	3.1	0.0	1.2	0	0.37	0.37	0.37
5	4.8	64.9	18.3	3.1	0.0	1.2	0	0.37	0.37	0.37
6	2.9	109.2	9.1	3.1	0.0	0.7	0	0.37	0.37	0.37
7	1.9	110.3	7.4	3.2	0.0	0.7	0	0.37	0.37	0.37
8	2.2	96.4	7.3	3.1	0.0	0.8	0	0.36	0.36	0.36
9	1.3	123.2	6.4	4.0	0.0	0.8	0	0.36	0.36	0.36

Table.11.9d Fluidization Behaviour, Deep Bed, Chute Feed
Combustor Run No.1 & 2

Bed Conditions		Type	Deep Bed, Pattern No. 2 Bubble Caps				
		Depth	325 mm	Run no.1, Period No.1&2			
			305 mm	Run No.2, Period Nos.3 to 9			
		Sand	490 micron				
		Fuel	Bagasse. bricks., 50mm	Period No.1&2			
			Bagasse Fibres	Period Nos.3 to 9			
Period No.	Temp	U f	Uf Umf	Behaviour Index ζ	Particle Reynolds Number	Particle Nusselt Number	Heat.Coeff h gp W/sq.m
	C	m/s					
Bagasse Bricks							
1	666	0.70	8.3	2200	3.29	0.141	18.7
2	649	0.69	8.2	2200	3.31	0.142	18.6
Bagasse Fibres							
3	713	0.31	3.9	1750	1.34	0.044	6.0
4	710	0.27	3.4	1780	1.17	0.037	5.0
5	710	0.23	2.9	1780	1.00	0.030	4.1
6	717	0.20	2.5	1780	0.83	0.024	3.2
7	727	0.16	2.0	1710	0.66	0.018	2.4
8	747	0.14	1.8	1680	0.57	0.015	2.0
9	757	0.12	1.6	1520	0.49	0.012	1.6

Table. 11.10a**Combustion and Heat Release Efficiencies
Shallow Bed, Chute Feed**

Combustor Run No.4 & 5

Bed Conditions		Type	Shallow Bed, Pattern No. 4 Bubble Caps							
		Depth	125 mm Run no.5, Period No.1 to 4							
			130 mm Run No.4, Period Nos.5 to 10							
		Sand	300 micron							
		Fuel	-60mm Coal, Sawdust, Bagasse Fibres							
Period No.	Average Temp	Fuel Heat	Air/Fuel Ratio	η_c	O r	η_B	η_{Bc}	η_{Bc}	η_{Bc}	
	C	kW		%	%	%	Actual	Maximum	Theoretical	
							%	%	%	
Coal										
1	758	26	9.0	66	98	47	30	65	66	
2	778	18	12.7	54	75	8	4	51	68	
Sawdust										
3	708	26	7.4	35	82	-0	-0	64	78	
Bagasse										
4	658	49	3.8	24	N/A	9	7	N/A	79	
Sawdust										
5	701	70	2.4	26	N/A	10	9	N/A	79	
Bagasse										
6	763	92	1.8	22	N/A	13	11	N/A	76	
7	794	34	4.8	31	N/A	8	6	N/A	76	
8	810	74	2.2	18	N/A	5	4	N/A	74	
9	816	111	1.5	8	N/A	-1	-1	N/A	74	
10	812	44	1.9	21	N/A	7	6	N/A	75	

η_c Combustion Efficiency, % (in-bed combustion)
ie % Total Fuel Heat released below bed surface

O_r Operating Ratio: % of ideal dry fuel/stoich. condition in terms of Useful Heat

η_B Fluidized Bed Efficiency or Heat Transfer Efficiency of the Bed

η_{Bc} Actual Overall Bed Efficiency , (Useful Heat)/(Total Fuel Heat)

η_{Bc} Maximum Maximum Overall Bed Efficiency
at given operating conditions

η_{Bc} Theoretical Theoretical Overall Bed Combustion Efficiency
at ideal dry fuel/stoichiometric conditions

Table.11.10b Combustion Heat Balance, Shallow Bed, Chute Feed
Combustor Run No.4 & 5

Bed Conditions		Type	Shallow Bed, Pattern No. 4 Bubble Caps					
		Depth	125 mm	Run no.5, Period No.1 to 4				
			130 mm	Run No.4, Period Nos.5 to 10				
		Sand	300 micron					
		Fuel	-60mm Coal, Sawdust, Bagasse Fibres					
Period No.	Air/Fuel Ratio	Fuel Heat Release kW	Flue Gas Heat Loss %	Wall Heat Loss %	Useable Bed Heat %	Above Bed Heat %	η_c %	Packed Bed Heat Flux kW/cu.m
Coal								
1	9.0	26	34	1	30	34	66	726
2	12.7	18	48	2	4	46	54	408
Sawdust								
3	7.4	26	34	1	-0	65	35	394
Bagasse								
4	3.8	49	17	1	7	76	24	515
Sawdust								
5	2.4	70	16	0	9	74	26	737
Bagasse								
6	1.8	92	11	0	11	78	22	844
7	4.8	34	24	1	6	69	31	434
8	2.2	74	13	0	4	82	18	540
9	1.5	111	8	0	-1	92	8	371
10	1.9	44	14	1	6	79	21	374

Table. 11.10c Combustion Heat Balance - Details, Shallow Bed, Chute Feed
Combustor Run No.4 & 5

Bed Conditions		Type	Shallow Bed, Pattern No. 4 Bubble Caps							
		Depth	125 mm		Run no.5, Period No.1 to 4					
			130 mm		Run No.4, Period Nos.5 to 10					
		Sand	300 micron							
		Fuel	-60mm Coal, Sawdust, Bagasse Fibres							
Period No.	Air/Fuel Ratio	Fuel Heat Release kW	Air Flow Heat Loss %	Fuel Flow Heat Loss %	Moisture Heat Loss %	Wall Heat Loss %	Moisture Content %	α_f	α_w	
Coal										
1	9.0	26.0	29.8	4.0	0.5	1.2	3	1.00	1.00	
2	12.7	17.9	43.4	3.7	0.4	1.7	3	1.00	1.00	
Sawdust										
3	7.4	26.2	26.7	3.1	4.6	1.2	25	0.38	0.38	
Bagasse										
4	3.8	49.4	13.1	3.4	0.2	0.6	1	0.44	0.44	
Sawdust										
5	2.4	70.5	8.6	3.2	4.6	0.4	25	0.40	0.40	
Bagasse										
6	1.8	92.2	7.2	3.4	0.2	0.3	1	0.37	0.37	
7	4.8	34.0	20.4	3.4	0.1	0.9	1	0.36	0.36	
8	2.2	73.6	9.6	3.4	0.1	0.4	1	0.35	0.35	
9	1.5	111.0	4.9	3.4	0.2	0.3	1	0.35	0.35	
10	1.9	43.7	10.8	3.4	0.2	0.7	1	0.35	0.35	

Table. 11.10d Fluidization Behaviour, Shallow Bed, Chute Feed
Combustor Run No.4&5

Bed Conditions		Type	Shallow Bed, Pattern No. 4 Bubble Caps					
		Depth	125 mm	Run no.5, Period No.1 to 4				
			130 mm	Run No.4, Period Nos.5 to 10				
		Sand	300 micron					
		Fuel	-60mm Coal, Sawdust, Bagasse Fibres					
Period No.	Temp	U f	$\frac{U_f}{U_{mf}}$	Behaviour Index ζ	Particle Reynolds Number	Particle Nusselt Number	Heat.Coeff h gp W/sq.m	
	C	m/s						
Coal								
1	758	0.15	5.0	36	0.37	0.0082	1.9	
2	778	0.15	5.1	37	0.36	0.0081	1.9	
Sawdust								
3	708	0.14	4.5	40	0.37	0.0082	1.8	
Bagasse								
4	658	0.13	4.2	47	0.38	0.0086	1.8	
Sawdust								
5	701	0.12	3.9	49	0.33	0.0070	1.5	
Bagasse								
6	763	0.13	4.3	40	0.31	0.0066	1.5	
7	794	0.13	4.5	37	0.31	0.0065	1.5	
8	810	0.13	4.6	35	0.31	0.0064	1.5	
9	816	0.10	3.6	34	0.23	0.0045	1.1	
10	812	0.09	3.1	34	0.20	0.0037	0.9	

**Table.11.11a Combustion and Heat Release Efficiencies, Deep Bed,
Screw and Ingestor Feed**
Combustor Run No.6,7 & 8

Bed Conditions			Type	Deep Bed, Pattern No. 4, Screw feed, Periods 1 to 3 Deep Bed, Pattern No. 5, Ingestor Periods 4 to 8						
			Depth	325 mm Run no.6, Period No.1 to 2 460 mm Run No.7, Period Nos.3 355 mm Run No.8, Period Nos. 4 to 8						
			Sand Fuel	300 micron Sawdust, Bagasse Fibres						
Period No.	Average Temp	Fuel Heat	Air/Fuel Ratio	η_c	O r	η_B	η_{Bc} Actual	η_{Bc} Maximum	η_{Bc} Theoretical	
	C	kW		%	%	%	%	%	%	
Sawdust										
1	556	53	4.8	32	N/A	11	8	N/A	80	
2	605	37	5.4	39	93	14	10	72	78	
Sawdust										
3	676	20	9.3	47	70	-2	-1	52	75	
Sawdust										
4	692	63	7.7	41	81	1	1	60	74	
5	693	51	9.6	45	72	-4	-2	53	74	
Bagasse										
6	684	33	13.9	35	52	-70	-27	38	74	
7	664	57	14.6	0	48	-159	-61	38	79	
8	631	28	35.0	31	-41		-101	-31	75	

η_c Combustion Efficiency, % (in-bed combustion)
ie % Total Fuel Heat released below bed surface

O
r Operating Ratio: % of ideal dry fuel/stoich. condition in terms of Useful Heat

η_B Fluidized Bed Efficiency or Heat Transfer Efficiency of the Bed

η_{Bc} Actual Overall Bed Efficiency , (Useful Heat)/(Total Fuel Heat)

η_{Bc} Maximum Maximum Overall Bed Efficiency
at given operating conditions

η_{Bc} Theoretical Theoretical Overall Bed Combustion Efficiency
at ideal dry fuel/stoichiometric conditions

Table.11.11b Combustion Heat Balance, Deep Bed,
Screw and Ingestor Feed
 Combustor Run No.6,7 &8

Bed Conditions		Type	Deep Bed, Pattern No. 4, Screw feed, Periods 1 to 3 Deep Bed, Pattern No. 5, Ingestor Periods 4 to 8					
		Depth	325 mm	Run no.6, Period No.1 to 2				
			460 mm	Run No.7, Period Nos.3				
			355 mm	Run No.8, Period Nos. 4 to 8				
		Sand	300 micron					
		Fuel	Sawdust, Bagasse Fibres					
Period No.	Air/Fuel Ratio	Fuel Heat Release kW	Flue Gas Heat Loss %	Wall Heat Loss %	Useable Bed Heat %	Above Bed Heat %	η_c %	Packed Bed Heat Flux kW/cu.m
Sawdust								
1	4.8	53	22	1	8	68	32	275
2	5.4	37	26	2	10	61	39	232
Sawdust								
3	9.3	20	43	4	-1	53	47	111
Sawdust								
4	7.7	63	39	1	1	59	41	382
5	9.6	51	45	2	-2	55	45	339
Bagasse								
6	13.9	33	59	2	-27	65	35	174
7	14.6	57	60	1	-61	100	0	4
8	35.0	28	128	3	-101	69	31	130

**Table 11.11c Combustion Heat Balance - Details, Deep Bed,
Screw and Ingestor Feed**
Combustor Run No.6,7,& 8

Bed Conditions		Type	Deep Bed, Pattern No. 4, Screw feed, Periods 1 to 3 Deep Bed, Pattern No. 5, Ingestor Periods 4 to 8							
		Depth	325 mm		Run no.6, Period No.1 to 2					
			460 mm		Run No.7, Period Nos.3					
			355 mm		Run No.8, Period Nos. 4 to 8					
		Sand	300 micron							
		Fuel	Sawdust, Bagasse Fibres							
Period No.	Air/Fuel Ratio	Fuel Heat Release kW	Air Flow Heat Loss %	Fuel Flow Heat Loss %	Moisture Heat Loss %	Wall Heat Loss %	Moisture Content %	α_f	α_w	
Sawdust										
1	4.8	53.1	13.3	6.4	2.4	1.5	13.5	1.00	1.00	
2	5.4	36.7	16.5	7.1	2.5	2.1	13.5	1.00	1.00	
Sawdust										
3	9.3	20.4	33.5	8.1	1.6	4.5	13.5	1.00	1.00	
Sawdust										
4	7.7	62.8	27.2	7.9	3.5	1.3	17.5	1.00	1.00	
5	9.6	50.6	33.8	7.9	3.6	1.6	17.5	1.00	1.00	
Bagasse										
6	13.9	33.4	51.1	8.1	0.0	2.4	0	1.00	1.00	
7	14.6	56.8	52.3	7.9	0.0	1.4	0	1.00	1.00	
8	35.0	28.4	120.8	7.5	0.0	2.8	0	1.00	1.00	

Table.11.11d**Fluidization Behaviour, Deep Bed, Screw
and Ingestor Feed**

Combustor Run No.6,7 & 8

Bed Conditions	Type	Deep Bed, Pattern No. 4, Screw feed, Periods 1 to 3					
	Depth	Deep Bed, Pattern No. 5, Ingestor Periods 4 to 8					
		325 mm		Run no.6, Period No.1 to 2			
		460 mm		Run No.7, Period Nos.3			
	Sand	355 mm		Run No.8, Period Nos. 4 to 8			
Fuel		300 micron Sawdust, Bagasse Fibres					
Period No.	Temp	U f	Uf Umf	Behaviour Index ζ	Particle Reynolds Number	Particle Nusselt Number	Heat.Coeff h gp W/sq.m
	C	m/s					
Sawdust							
1	556	0.15	4.3	159	0.52	0.0127	2.5
2	605	0.13	3.9	141	0.40	0.0093	1.9
Sawdust							
3	676	0.13	4.3	165	0.39	0.0088	1.9
Sawdust	0						
4	692	0.34	10.9	123	0.94	0.0275	6.1
5	693	0.34	10.9	122	0.94	0.0275	6.1
Bagasse							
6	684	0.46	14.9	123	1.31	0.0426	9.3
7	664	0.64	20.4	127	1.87	0.0677	14.6
8	631	0.68	21.1	135	2.09	0.0780	16.5

Table.11.12a Combustion and Heat Release Efficiencies
Modified Spouted Bed, Screw Feed
 Combustor Run No.9 & 10

Bed Conditions				Type	Modified Spouted Bed with Baffle				
				Depth	515 mm	Run. 9	Period Nos 1 to 5		
					583 mm	Run.10	Period Nos 6 to 9		
					654 mm	Run.10	Period No 10		
					740 mm	Run.10	Period No.11		
				Sand	530 micron				
				Fuel	-4.75 mm Sawdust				
Period No.	Average Temp	Fuel Heat	Air/Fuel Ratio	η_c	O r	η_B	η_{Bc}	η_{Bc}	η_{Bc}
	C	kW		%	%	%	Actual %	Maximum %	Theoretical %
1	595	43	13.5	52	63	3	1	50	78
2	640	90	6.5	51	90	30	20	69	77
3	705	83	7	56	87	31	20	64	74
4	758	106	5.5	46	93	20	13	67	72
5	773	75	7.8	55	82	22	13	58	72
6	571	32	18	67	47	12	4	37	79
7	594	141	4	36	N/A	18	14	N/A	78
8	636	61	9.5	60	76	31	18	58	77
9	685	87	6.6	55	87	31	20	65	75
10	645	88	6.6	54	88	31	21	67	76
11	632	80	7.2	61	86	41	27	67	77

η_c Combustion Efficiency, % (in-bed combustion)
 ie % Total Fuel Heat released below bed surface

O Operating Ratio: % of ideal dry fuel/stoich. condition in terms of Useful Heat
 r

η_B Fluidized Bed Efficiency or Heat Transfer Efficiency of the Bed

η_{Bc} Actual Overall Bed Efficiency , (Useful Heat)/(Total Fuel Heat)

η_{Bc} Maximum Maximum Overall Bed Efficiency
 at given operating conditions

η_{Bc} Theoretical Theoretical Overall Bed Combustion Efficiency
 at ideal dry fuel/stoichiometric conditions

**Table.11.12b Combustion Heat Balance, Modified Spouted Bed,
Screw Feed**
Combustor Run No.9,&10

<div> <div>Bed Conditions</div> <div> <div>Type</div> <div>Modified Spouted Bed with Baffle Plate</div> </div> </div>								
		Depth	515 mm	Run no.9, Period No.1 to 5				
			583 mm	Run No.10, Period Nos.6 to 9				
			654 mm	Run No.10, Period Nos. 10				
			740 mm	Run No.10, Period Nos. 11				
		Sand	530 micron					
		Fuel	-4.75mm Sawdust,					
Period No.	Air/Fuel Ratio	Fuel Heat Release kW	Flue Gas Heat Loss %	Wall Heat Loss %	Useable Bed Heat %	Above Bed Heat %	η_c %	Packed Bed Heat Flux kW/cu.m
Sawdust								
1	13.5	43	49	2	1	48	52	421
2	6.5	90	30	1	20	49	51	868
3	7.0	83	35	1	20	44	56	875
4	5.5	106	32	1	13	54	46	922
5	7.8	75	41	1	13	45	55	774
6	18.0	32	61	3	4	33	67	330
7	4.0	141	22	1	14	64	36	778
8	9.5	61	41	1	18	40	60	558
9	6.6	87	34	1	20	45	55	729
10	6.6	88	32	1	21	46	54	603
11	7.2	80	32	1	27	39	61	510

Table.11.12c Combustion Heat Balance - Details, Modified
Spouted Bed, Screw Feed
 Combustor Run No.9,&10

Bed Conditions Type Modified Spouted Bed with Baffle Plate Depth 515 mm Run no.9, Period No.1 to 5 583 mm Run No.10, Period Nos.6 to 9 654 mm Run No.10, Period Nos. 10 740 mm Run No.10, Period Nos. 11 Sand 530 micron Fuel -4.75mm Sawdust,									
Period No.	Air/Fuel Ratio	Fuel Heat Release kW	Air Flow Heat Loss %	Fuel Flow Heat Loss %	Moisture Heat Loss %	Wall Heat Loss %	Moisture Content %	α_f	α_w
1	13.5	43.2	39.9	6.8	2.1	1.5	12.0	1.00	1.00
2	6.5	89.7	21.0	6.8	2.2	0.7	12.0	1.00	1.00
3	7.0	82.9	25.1	7.6	2.3	0.8	12.0	1.00	1.00
4	5.5	105.6	21.5	8.4	2.3	0.6	12.0	1.00	1.00
5	7.8	74.8	30.2	8.4	2.4	0.9	12.0	1.00	1.00
6	18.0	32.2	50.9	6.4	3.2	2.5	17.0	1.00	1.00
7	4.0	141.4	12.1	6.7	3.2	0.6	17.0	1.00	1.00
8	9.5	61.1	30.2	7.2	3.3	1.3	17.0	1.00	1.00
9	6.6	87.0	23.0	7.8	3.4	0.9	17.0	1.00	1.00
10	6.6	88.2	21.3	7.3	3.3	1.0	17.0	1.00	1.00
11	7.2	80.2	22.0	6.9	3.2	1.3	17.0	1.00	1.00

Table.11.12d **Fluidization Behaviour, Modified Spouted Bed,
Screw Feed**
Combustor Run No.9,&10

Bed Conditions		Type	Modified Spouted Bed with Baffle Plate				
		Depth	515 mm	Run no.9, Period No.1 to 5			
			583 mm	Run No.10, Period Nos.6 to 9			
			654 mm	Run No.10, Period Nos. 10			
			740 mm	Run No.10, Period Nos. 11			
		Sand	530 micron				
		Fuel	-4.75mm Sawdust,				
Period No.	Temp C	U f m/s	Uf Umf	Behaviour Index ζ	Particle Reynolds Number	Particle Nusselt Number	Heat.Coeff h gp W/sq.m
1	595	0.36	3.6	6062	2.08	0.0779	9.1
2	640	0.38	4.0	5500	2.02	0.0747	9.0
3	705	0.40	4.4	4600	1.94	0.0712	8.9
4	758	0.43	4.8	4200	1.88	0.0683	8.9
5	773	0.43	4.8	4200	1.89	0.0685	9.0
6	571	0.35	3.4	7500	2.09	0.0783	9.0
7	594	0.35	3.6	7000	2.05	0.0764	8.9
8	636	0.37	3.9	6200	2.00	0.0736	8.8
9	685	0.39	4.2	5500	1.94	0.0710	8.8
10	645	0.38	3.9	6800	1.98	0.0731	8.8
11	632	0.36	3.7	8000	2.03	0.0753	9.0

Table. 11.13 Uncertainty Estimates of Data and Calculated Results

Quantity	Uncertainty absolute	Typical Value	Uncertainty %
Atmospheric Temperature	1 C	25 C	0.3
Atmospheric Pressure	50 Pa	101300 Pa	0.0
B.S. Nozzle Pressure	1 Pa	50 Pa	2.0
B.S. Flowrate.	2 l/s	40l/s	4.0
Rotameter Flowrate	0.5 l/s	2 to 25	2 to 10
Pitot-Static Tube Pressures	1 Pa	200 Pa	0.5
Pitot-Static Tube Flowrate	0.2l/s	4 l/s	6.0
Digital Thermometer (Visualisation)	1 C	25 C	4.0
Digital Thermometer (Combustion)	1 C	600 C	0.2
Chart Recorder	15 C	600 C	2.5
Fuel Mass Measurement (batch)	10 g	300 g	3.3
Fuel Mass Measurement (hopper batch)	200 g	3000 g	6.7
Time measurements (Combustion)	0.5 mins	10 mins	5.0
Fluidization Velocity (Visualisation)	0.01m/sec	0.14m/sec	6
Fluidization Velocity (Combustion)	1 l/sec	20l/sec	2 to 10
Bed Pressure Drop (Visualisation)			
Air Mass Flow	0.002kg/s	0.024kg/s	2 to 10
Fuel Mass Flow (batch feed)	0.1 g/s	0.002kg/s	5
Fuel Mass Flow (screw feed)	0.4 g/s	0.004 kg/s	10
Air/fuel Ratio	0.8	7	12
Air Flue Gas Heat Loss Qa	1 kW	20 kW	5
Fuel Flue Gas Heat Loss Qf	0.3-0.6 kW	6 kW	5 or 10
Moisture Flue Gas Heat Loss Qw	0.2-0.4 kW	4 kw	5 or 10
Wall Heat Loss Qlw	0.1 kW	1 kW	10
Useful Heat Qb	1.5 kW	10 kW	15
Combustion Efficiency	4%	40 %	
Fluidized Bed Efficiency	3%	13%	
Operating Ratio	17%	90%	
Overall Combustion Efficiency	2%	10%	

12.0 FIGURES AND ILLUSTRATIONS

Phase 1: Flow Visualisation

Fig.12.1-12.5 Deep Bed and Bagasse-Sand Mixing Characteristics

Fig.12.6-12.9 Enhanced and Reversed Sand Circulation
Characteristics

Phase 2: Combustion Results

Fig.12.10-12.17 Combustor Temperature Graphs

Fig.12.18-12.26 Combustor Efficiency Parameters verses
Air/Fuel Ratio

Fig.12.27-12.28 Combustor Efficiency Parameters verses Bed
Depth

Fig.12.29-12.30 Packed Bed Heat Flux Results

Fig.12.31-12.40 Proposals For Future Designs and Research

Fig.12.1 Pressure Drop Characteristic, Deep Beds
180 micron sand, Bed Depths 330mm, 440mm, 590mm

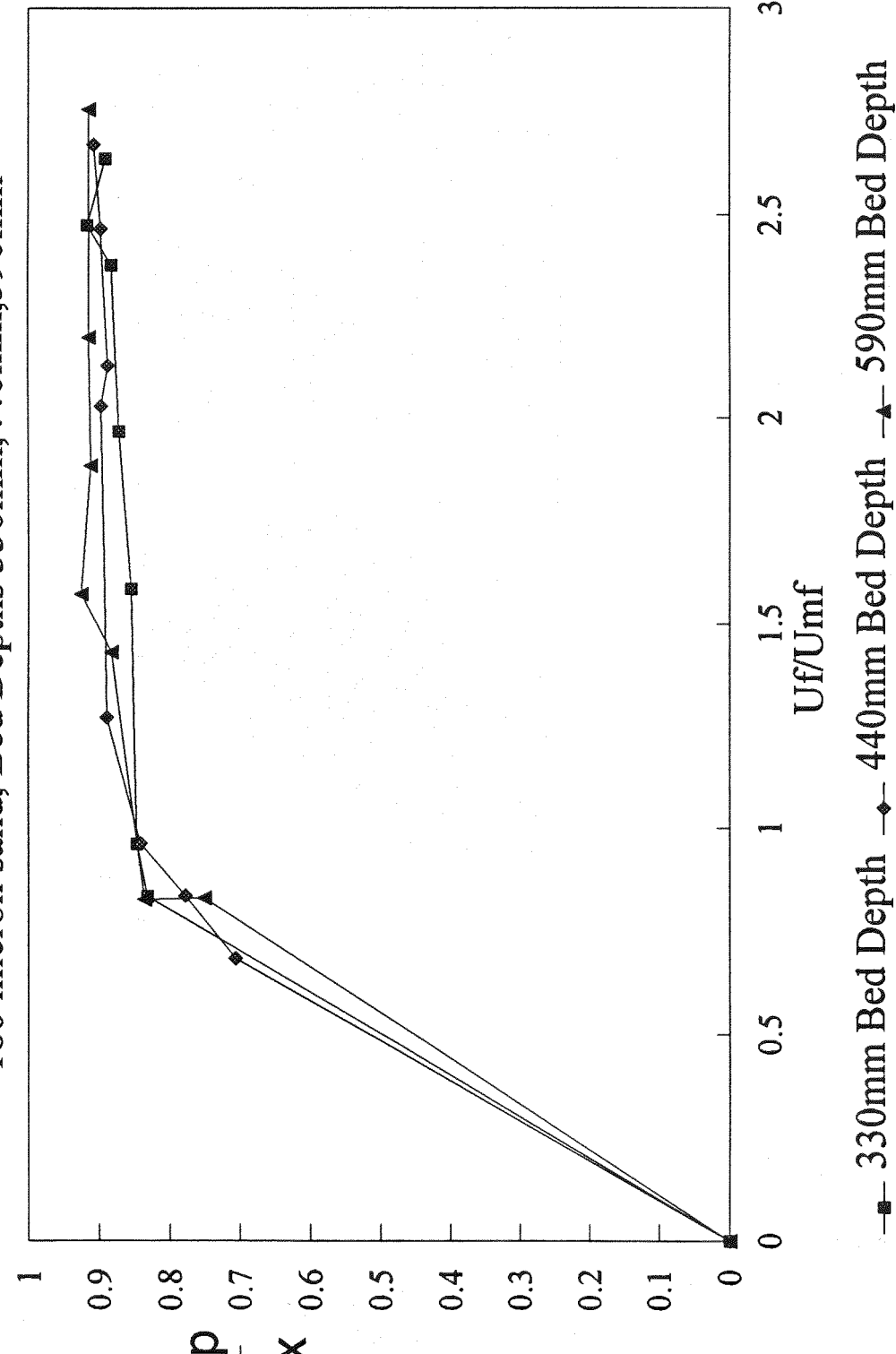


Fig.12.2 Pressure Drop Characteristic
Bagasse-Sand Mixtures, 180 micron sand.

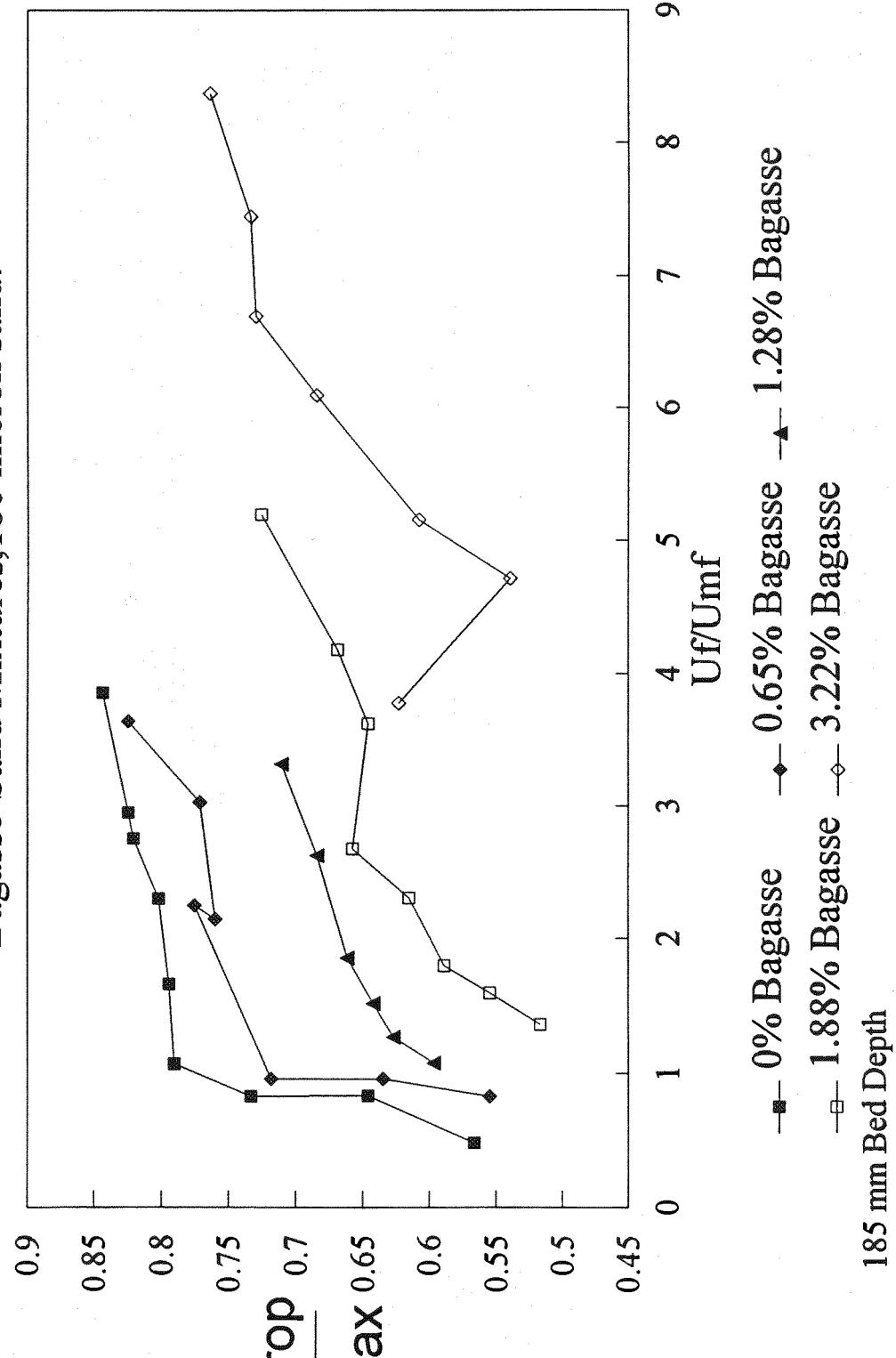


Fig. 12.3 Pressure Drop Characteristic,
Bagasse-Sand Mixtures, 490 micron Sand

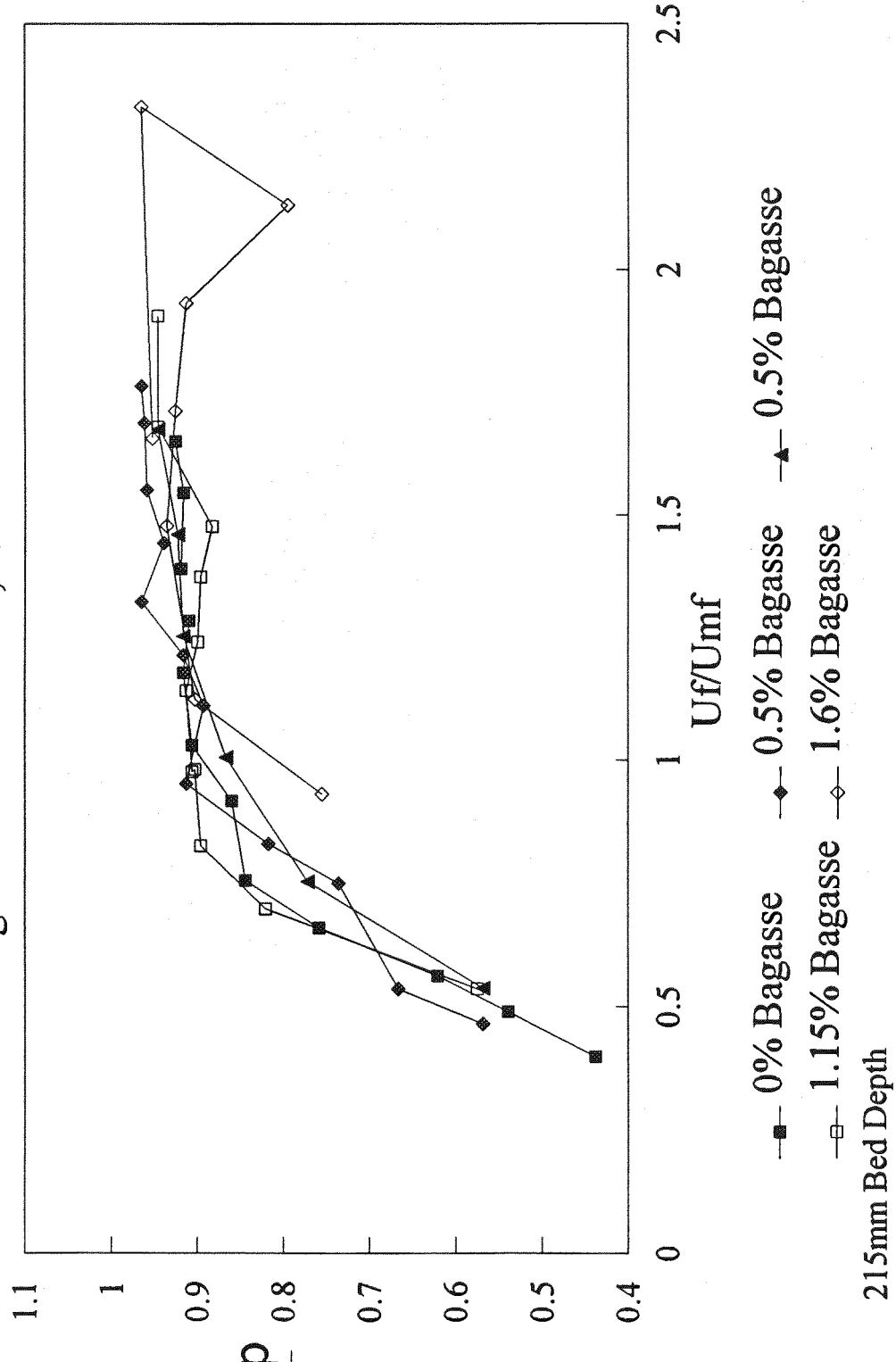


Fig. 12.4 Bagasse-Sand Mixing Velocities

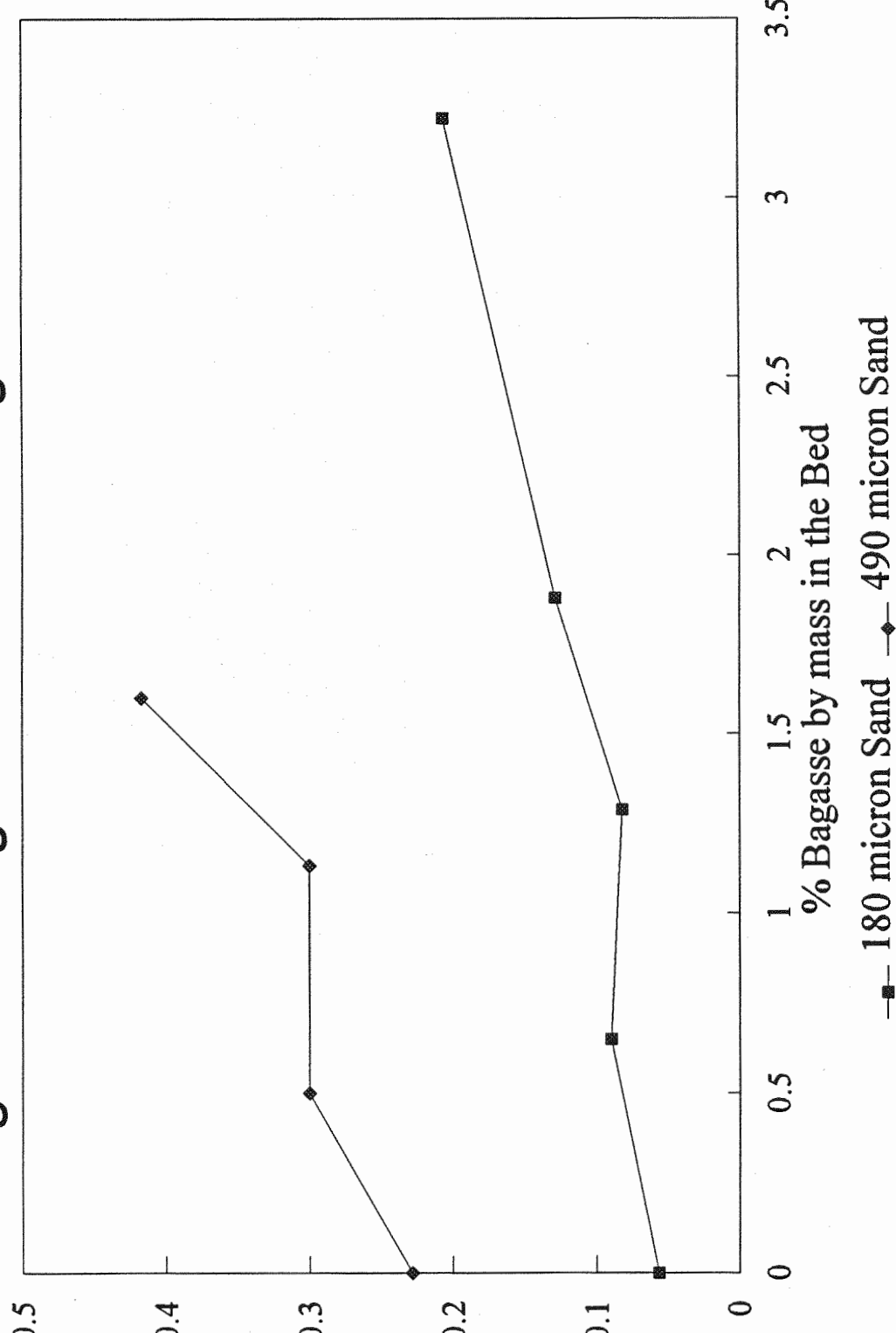


Fig. 12.5 Bagasse-Sand Mixing Velocity Characterist

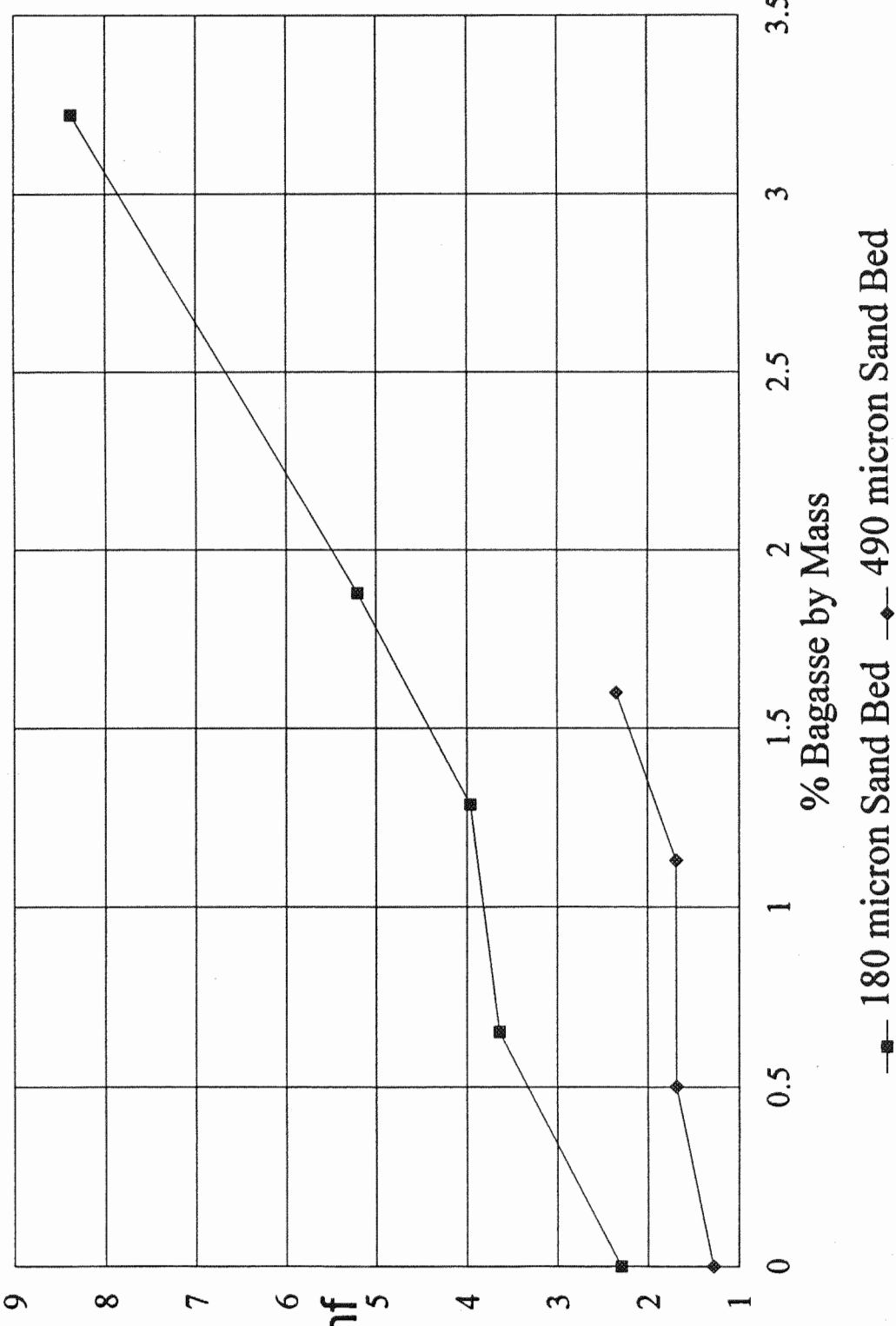


Fig.12.6 Pressure Drop Characteristic,
Enhanced Circulation Devices

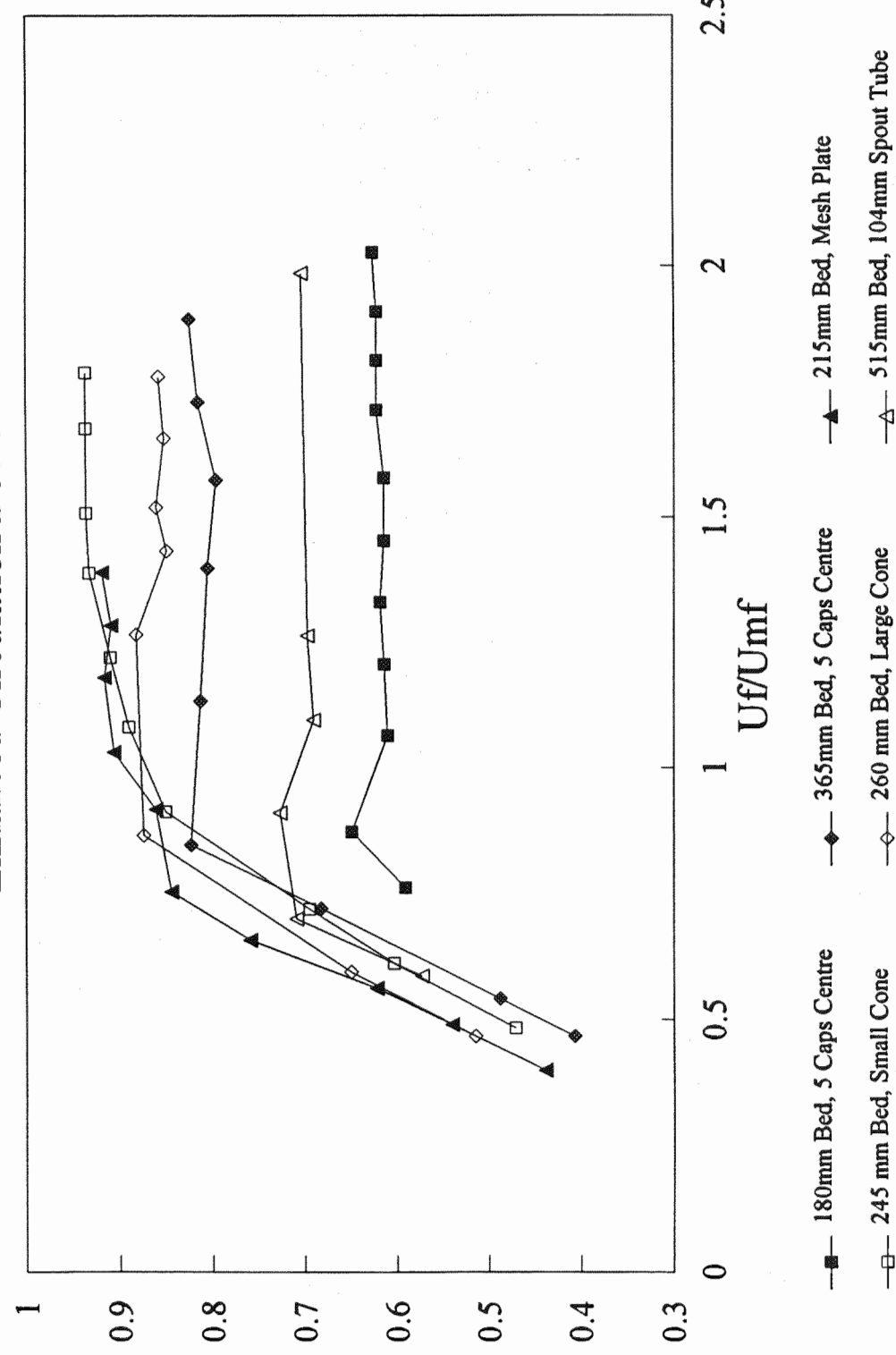


Fig.12.7 Pressure Drop, Peak Velocity Characteristic
Enhanced Circulation Devices

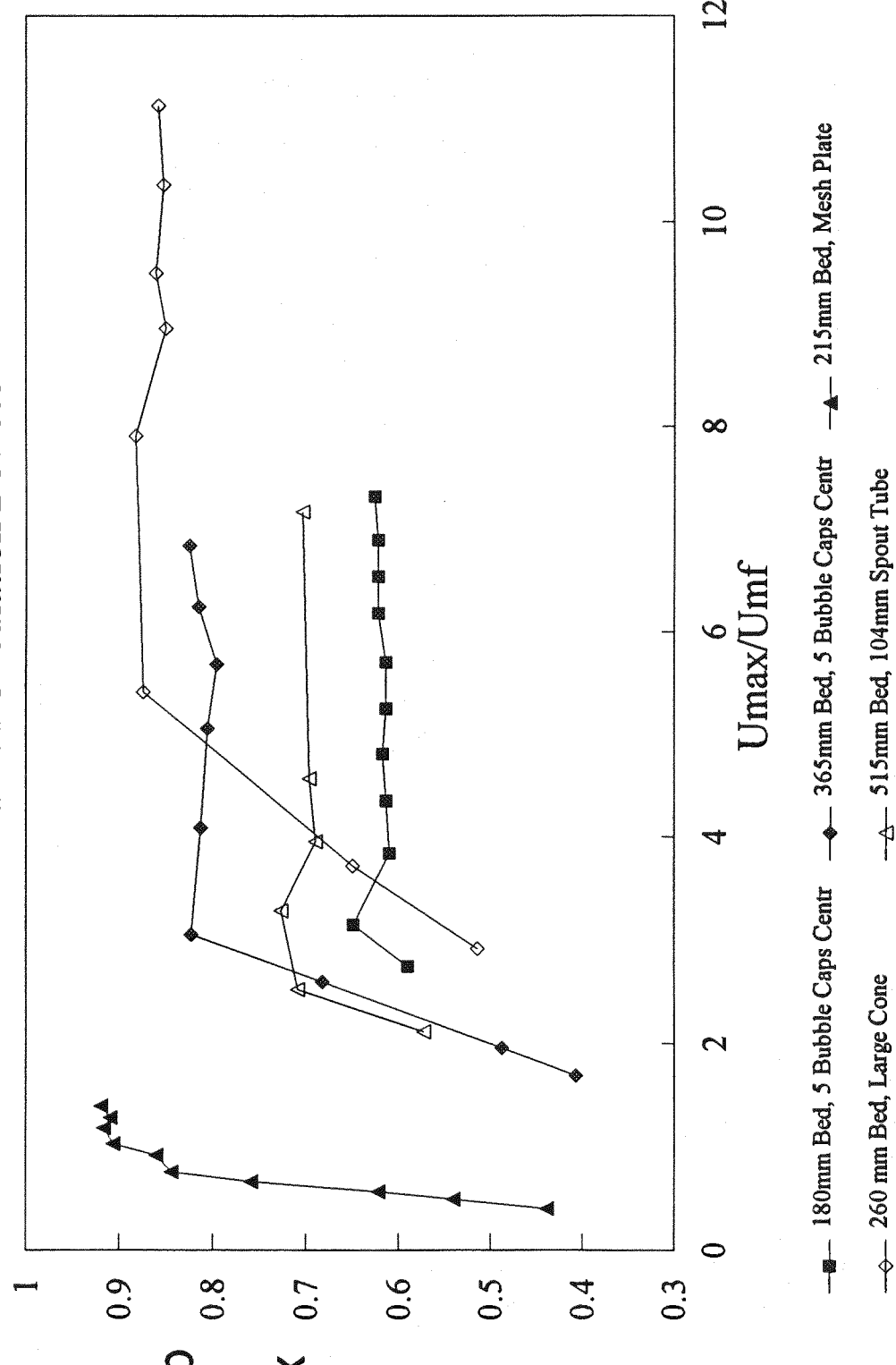


Fig.12.8 Pressure Drop Characteristic
Reversed Circulation Devices

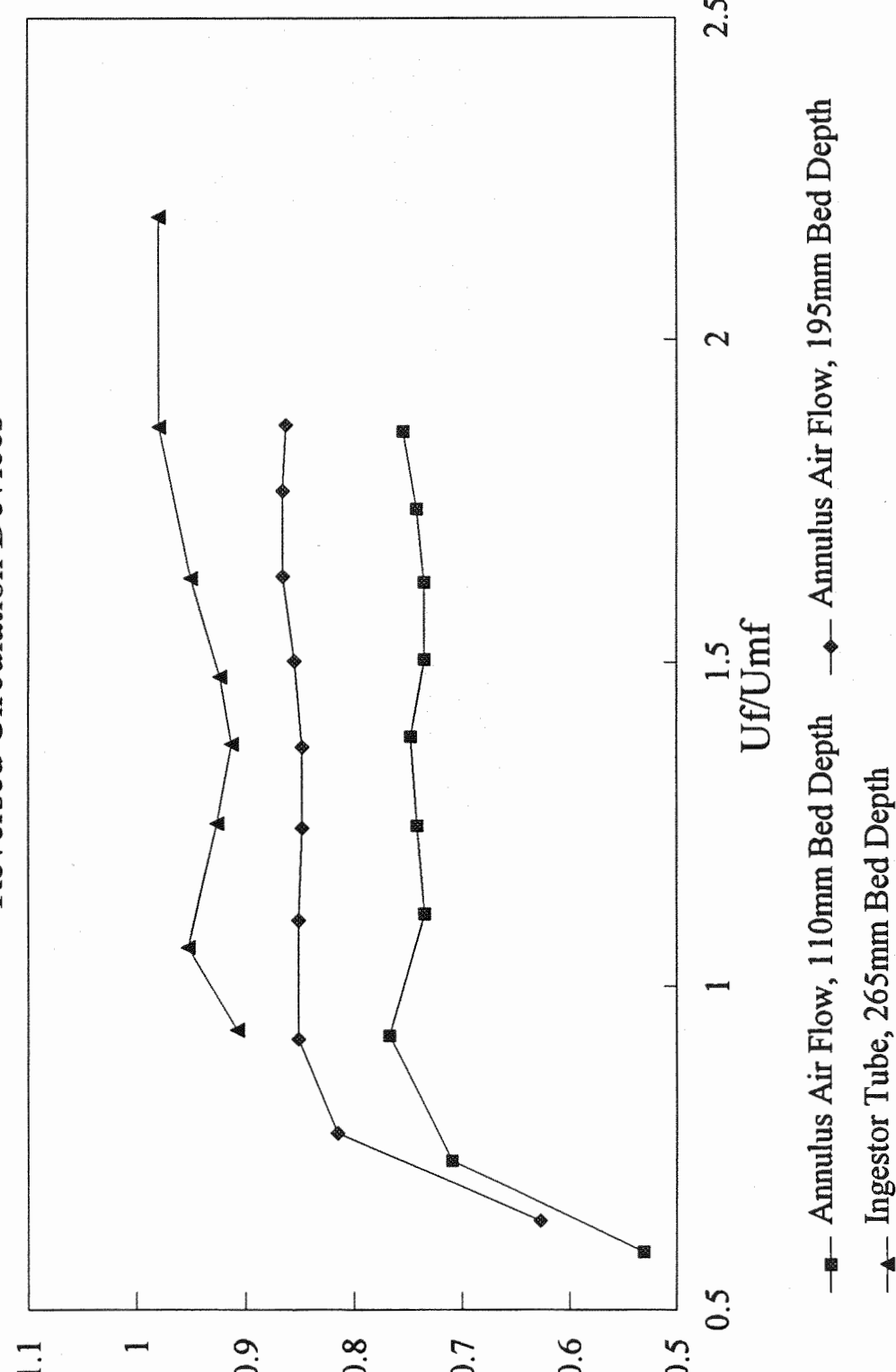


Fig.12.9 Pressure Drop, Peak Velocity Characteristics
Reversed Circulation Devices

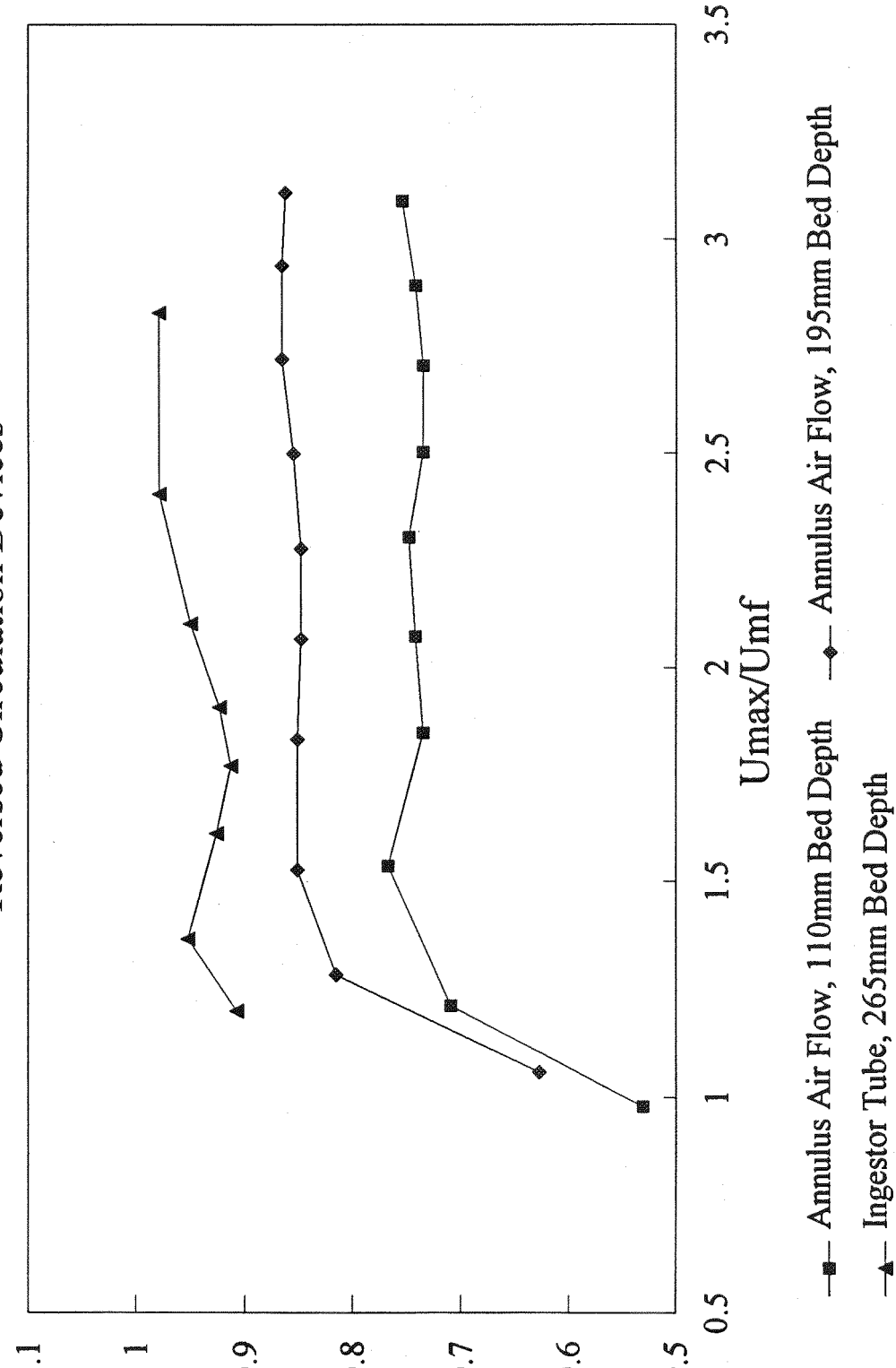


Fig.12.10 Temperatures: Deep Bed, Chute Feed
50mm Bagasse Bricks,490 micron Sand

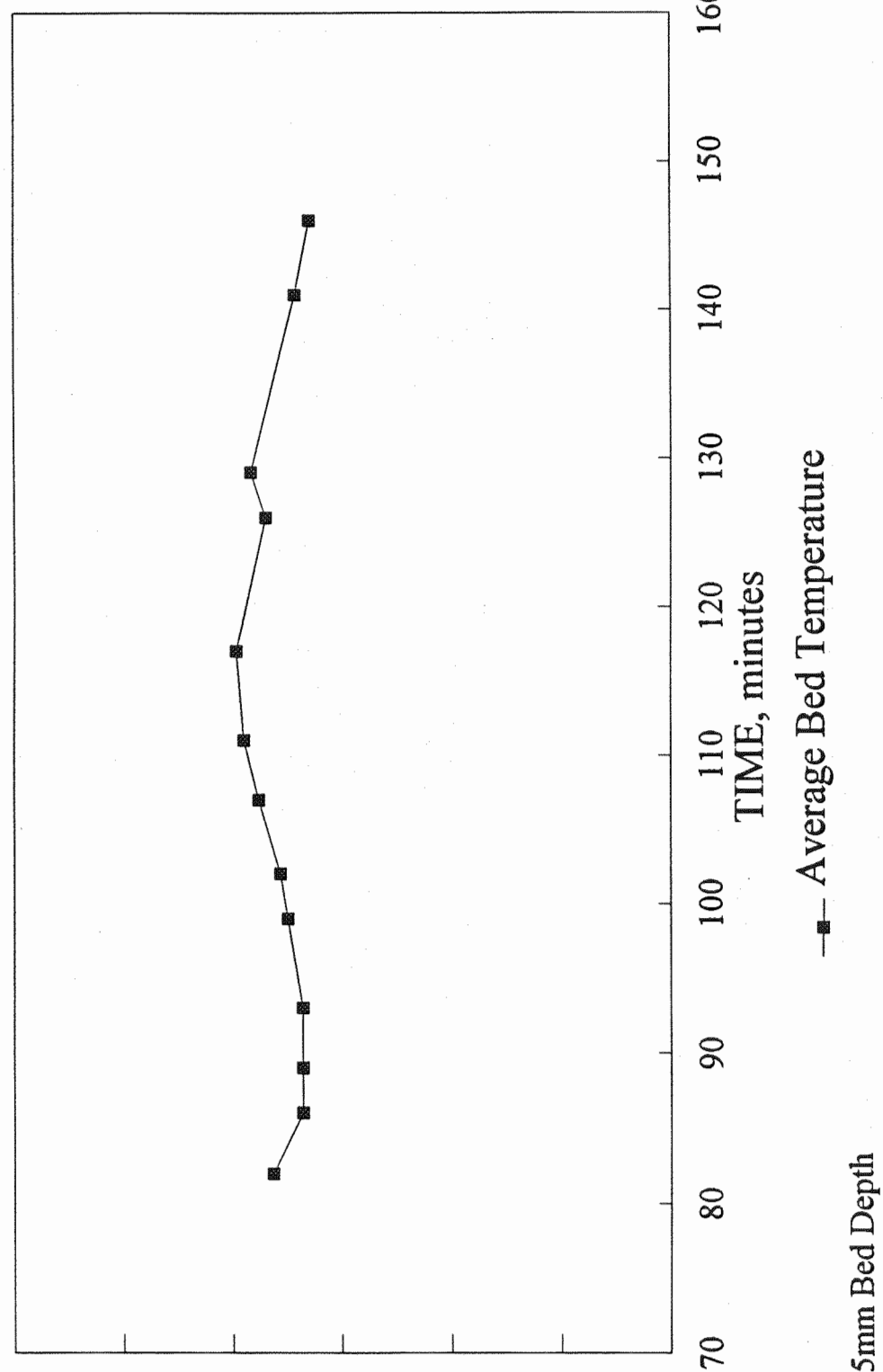


Fig.12.11 Temperatures: Deep Bed, Chute Feed
Bagasse Fibres, 490 micron Sand

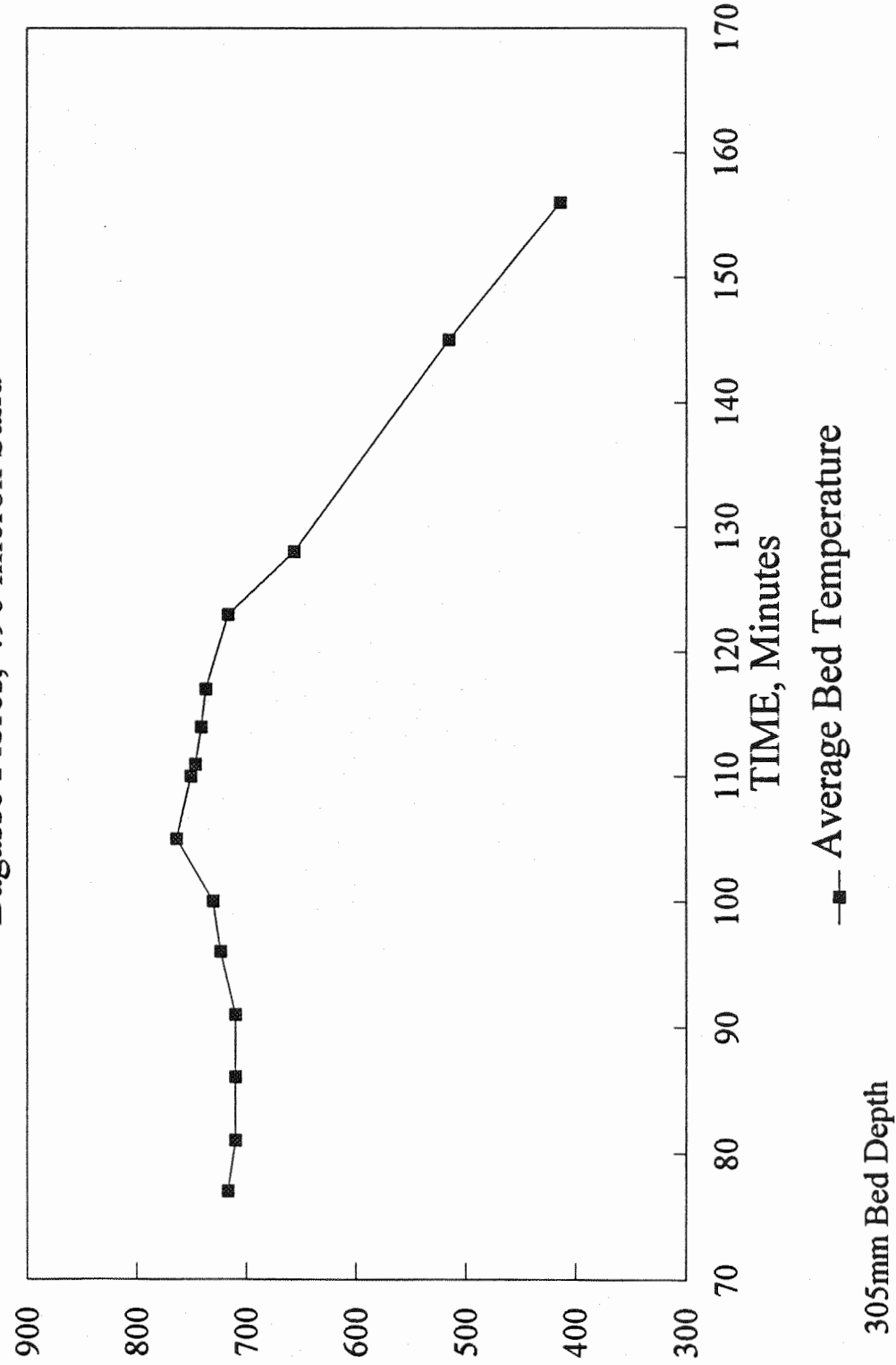


Fig.12.12 Temperatures: Shallow Bed, Chute Feed
 Sawdust, Bagasse Fibres, 300 micron Sand

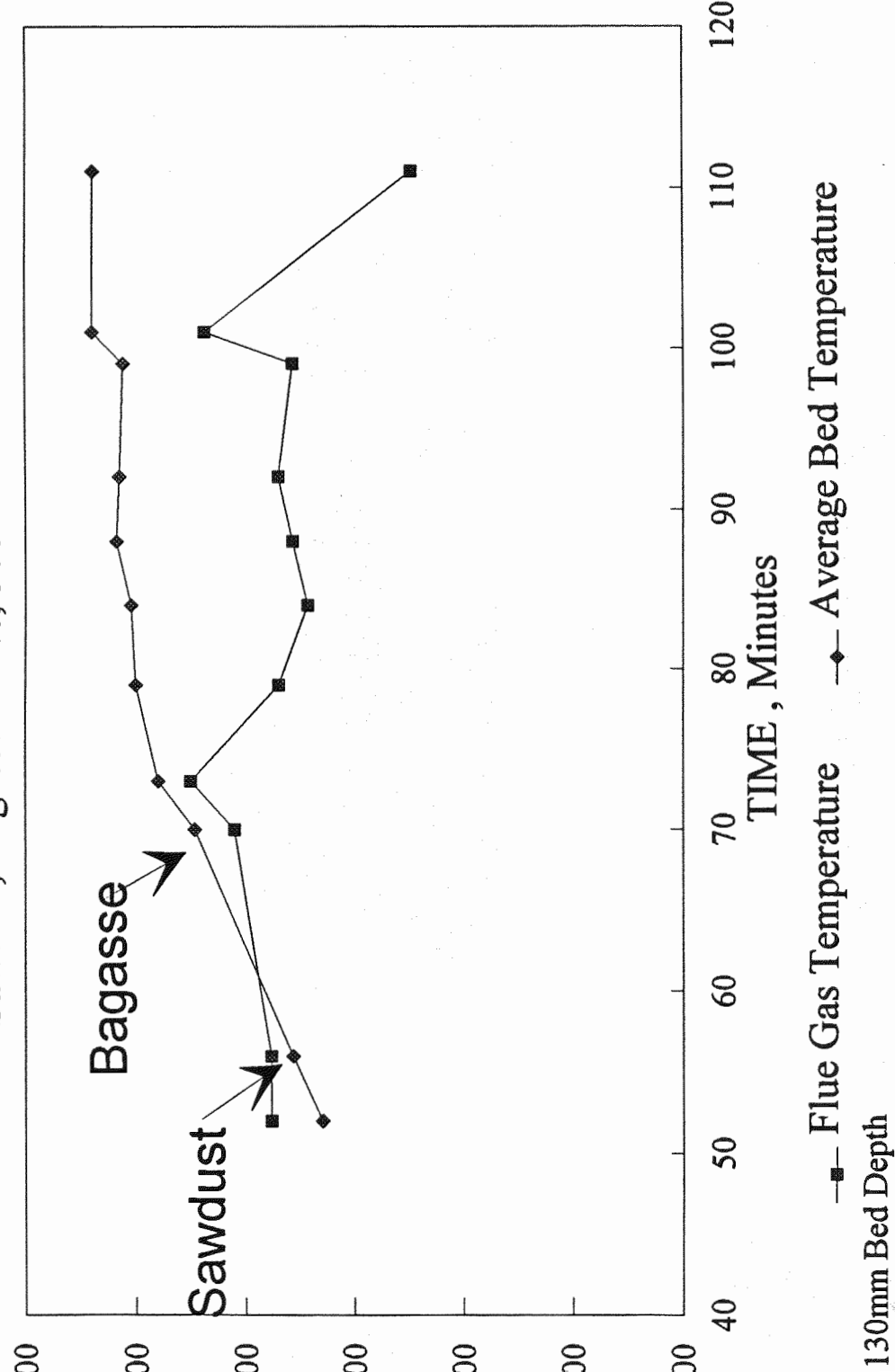


Fig.12.13 Temperatures: Shallow Bed, Chute Feed
 Coal, Sawdust, Bagasse Fibres, 300 micron Sand

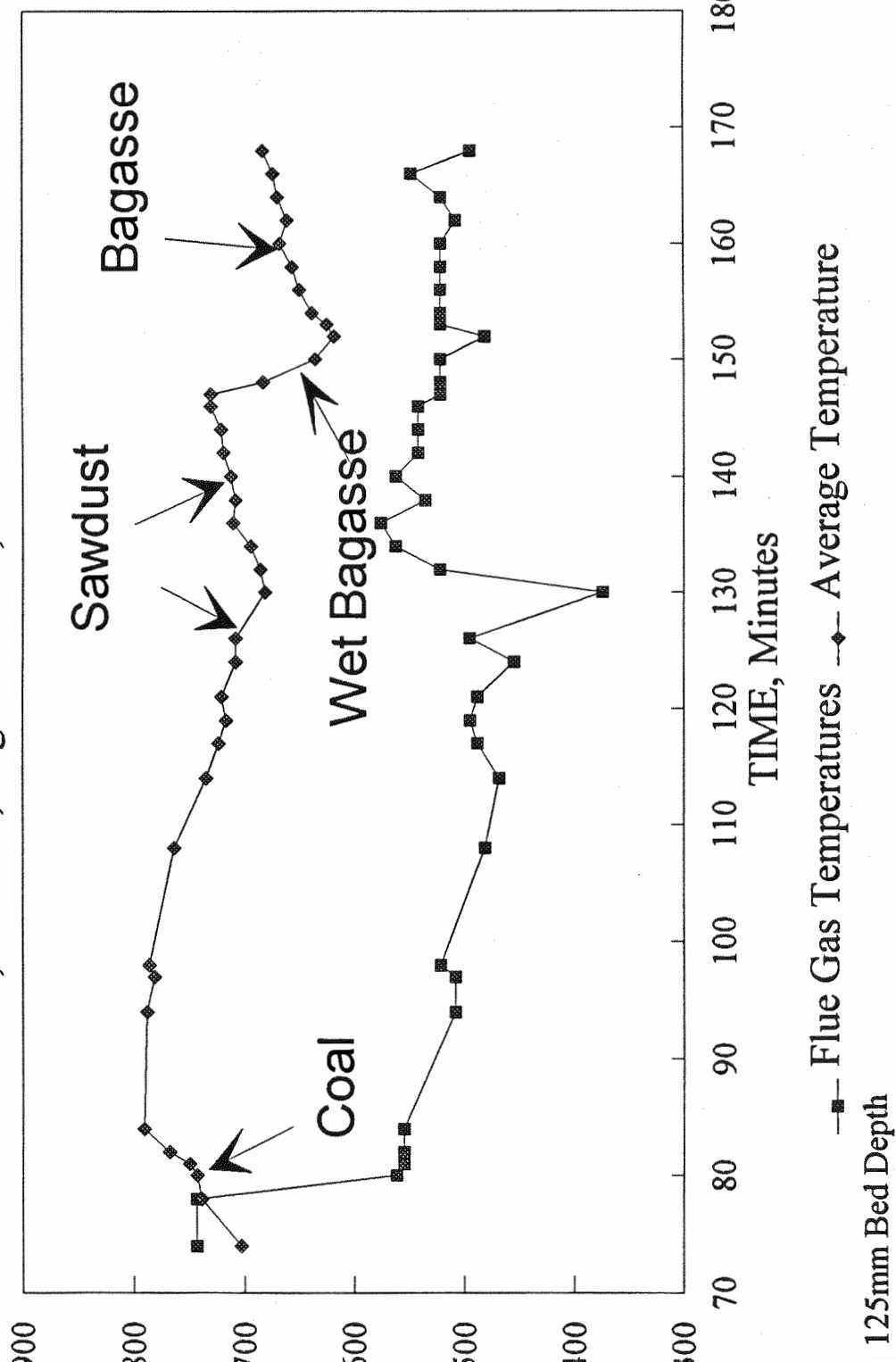


Fig.12.14 Temperatures: Deep bed, Screw Feed
Sawdust, 300 micron Sand

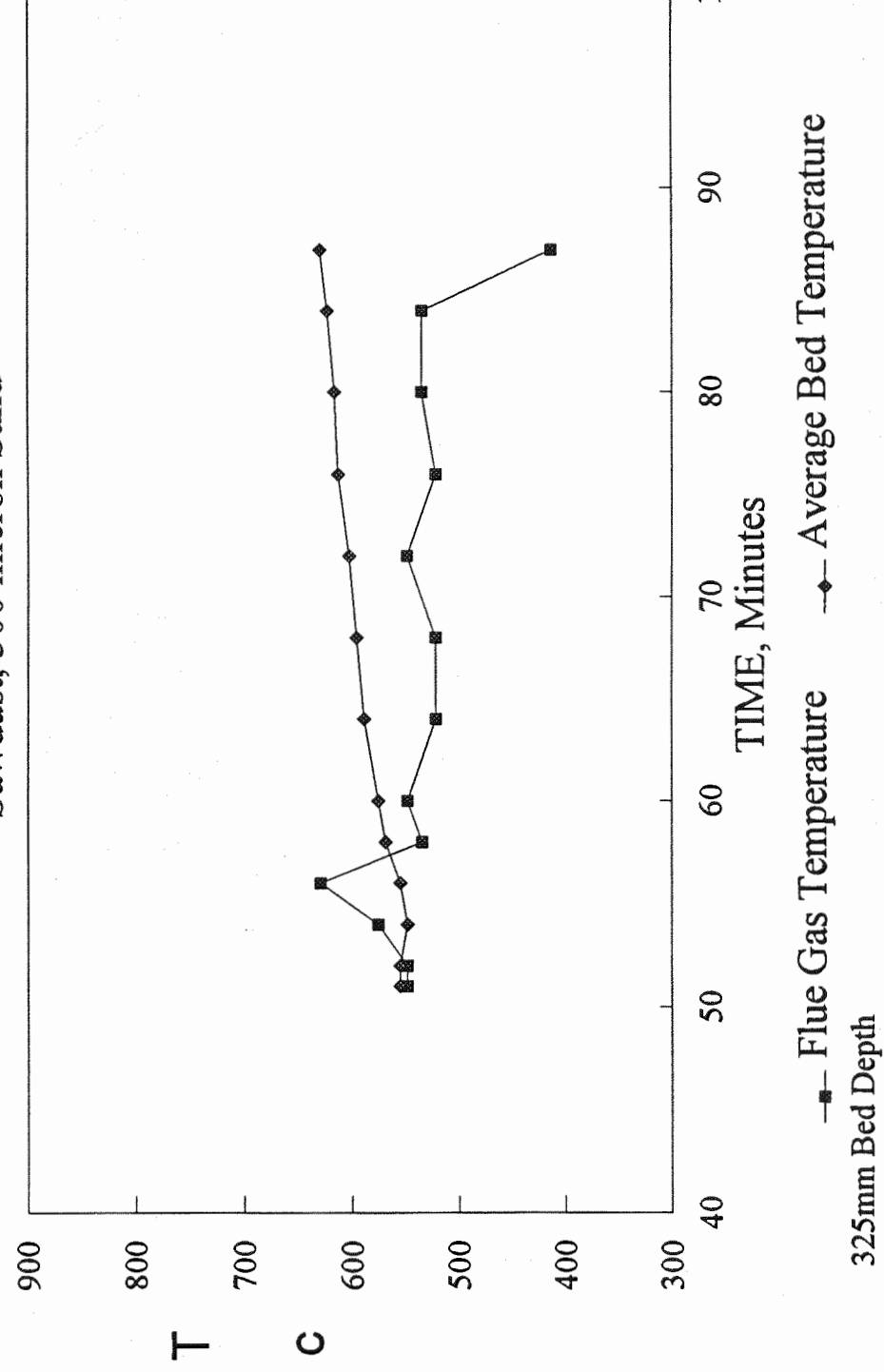


Fig.12.15 Temperatures: Deep Bed, Ingestor Feed
Sawdust, Bagasse, 300 micron Sand

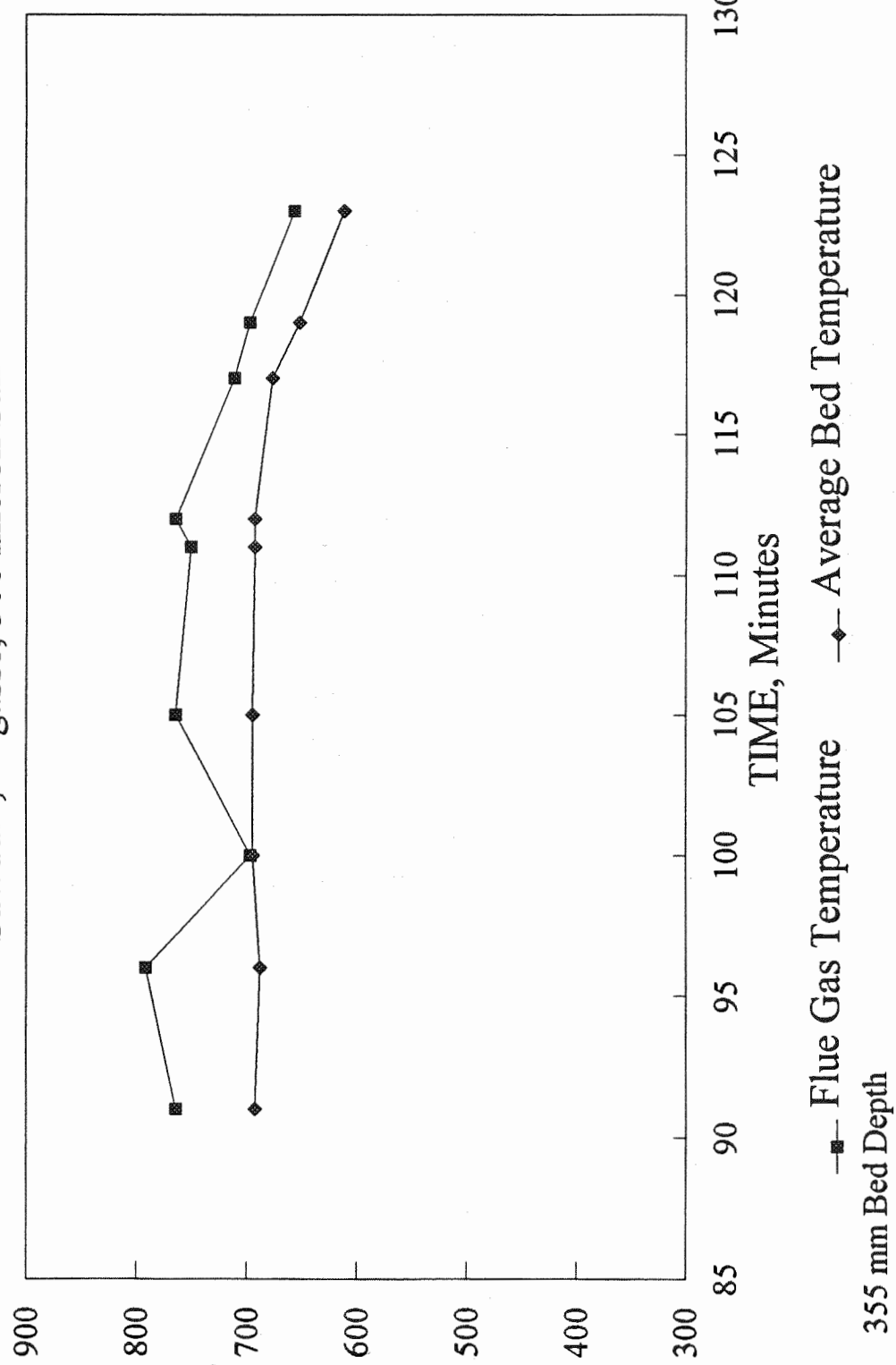


Fig.12.16 Temperatures: Modified Spouted Bed, Screw Feed
Sawdust, 530 micron Sand

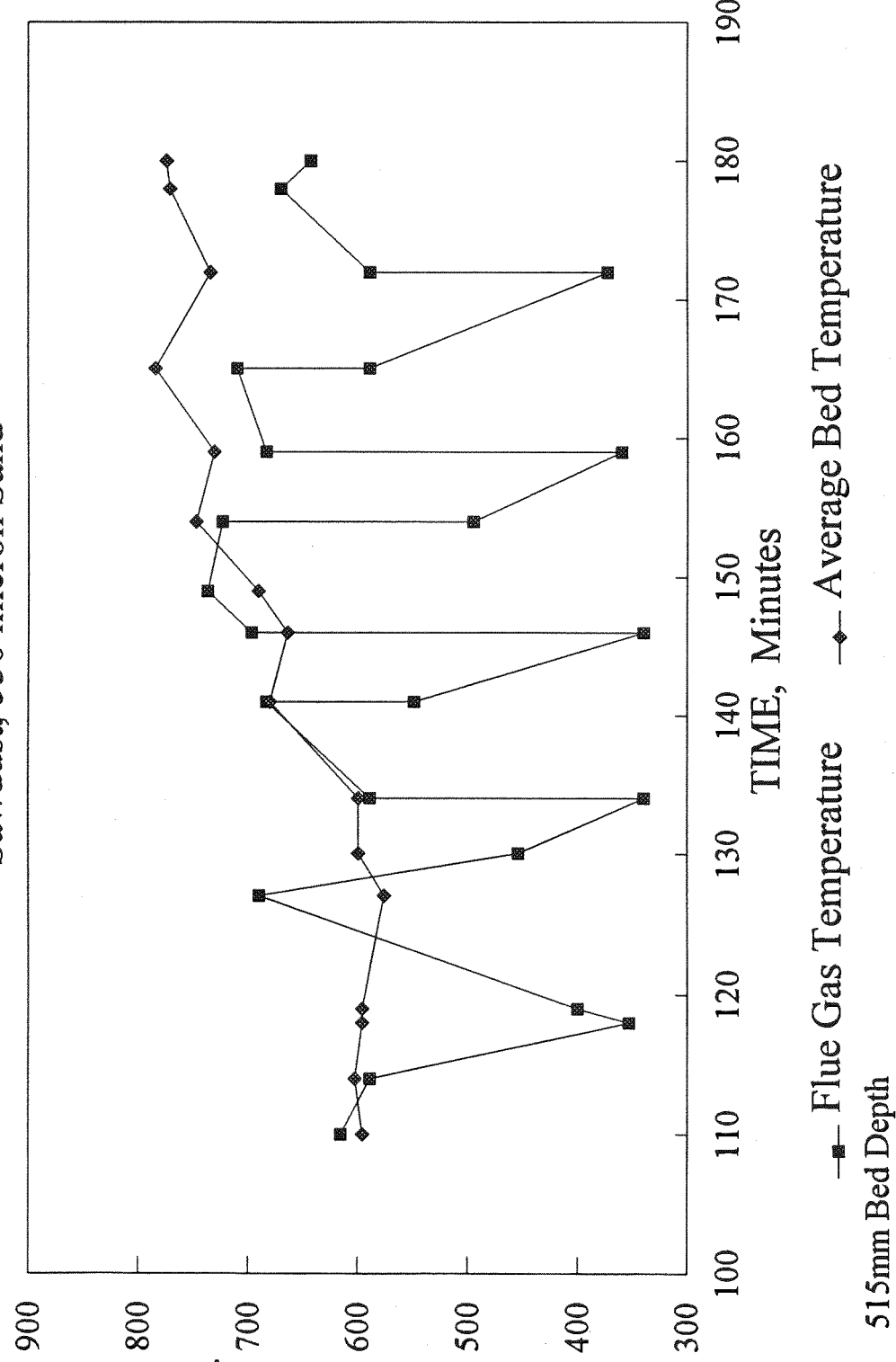


Fig.12.17 Temperatures: Modified Spouted Bed, Screw Feeder
Sawdust, 530 micron Sand

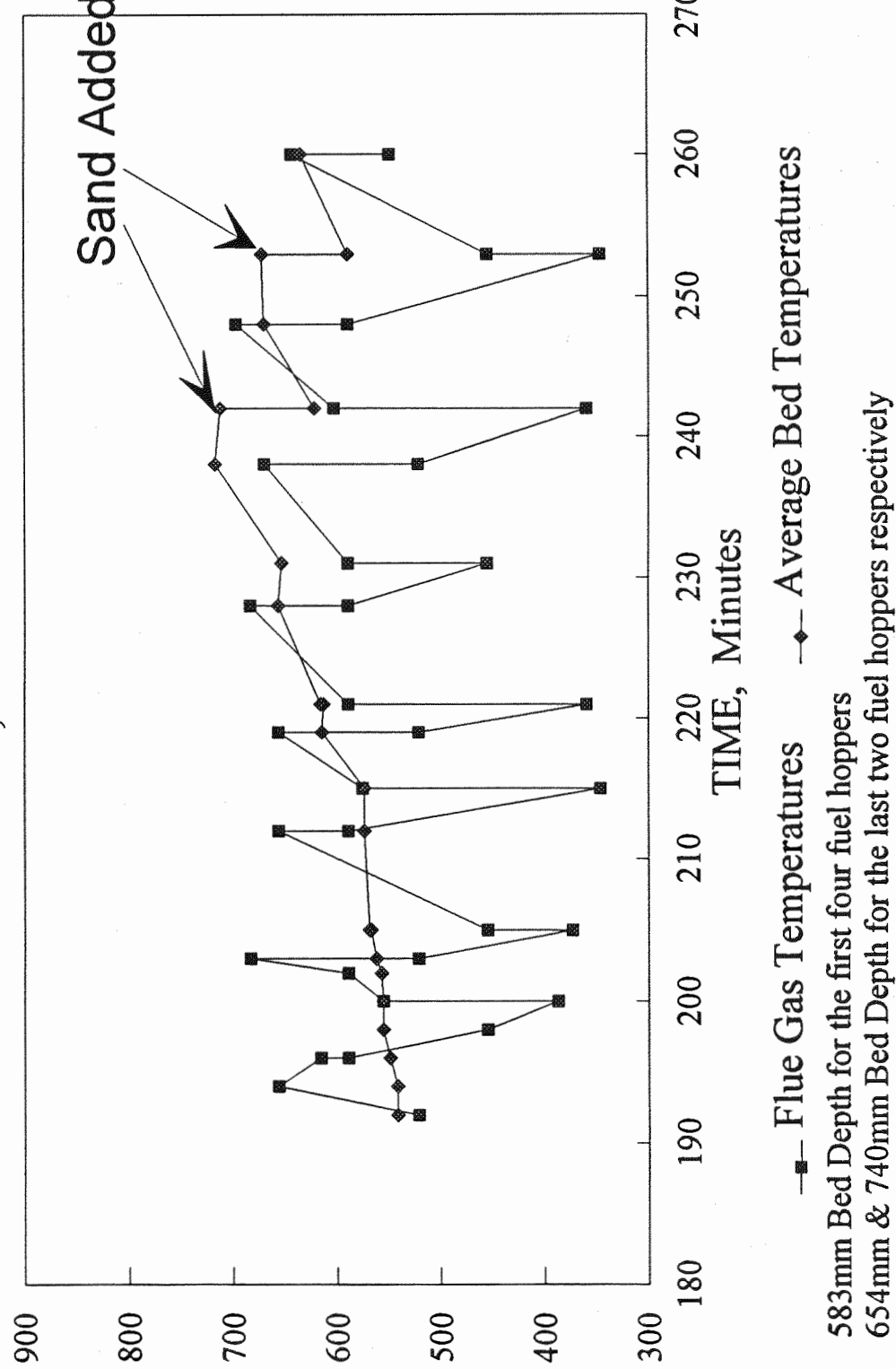


Fig.12.18 Combustion Efficiencies:Above Bed Feed

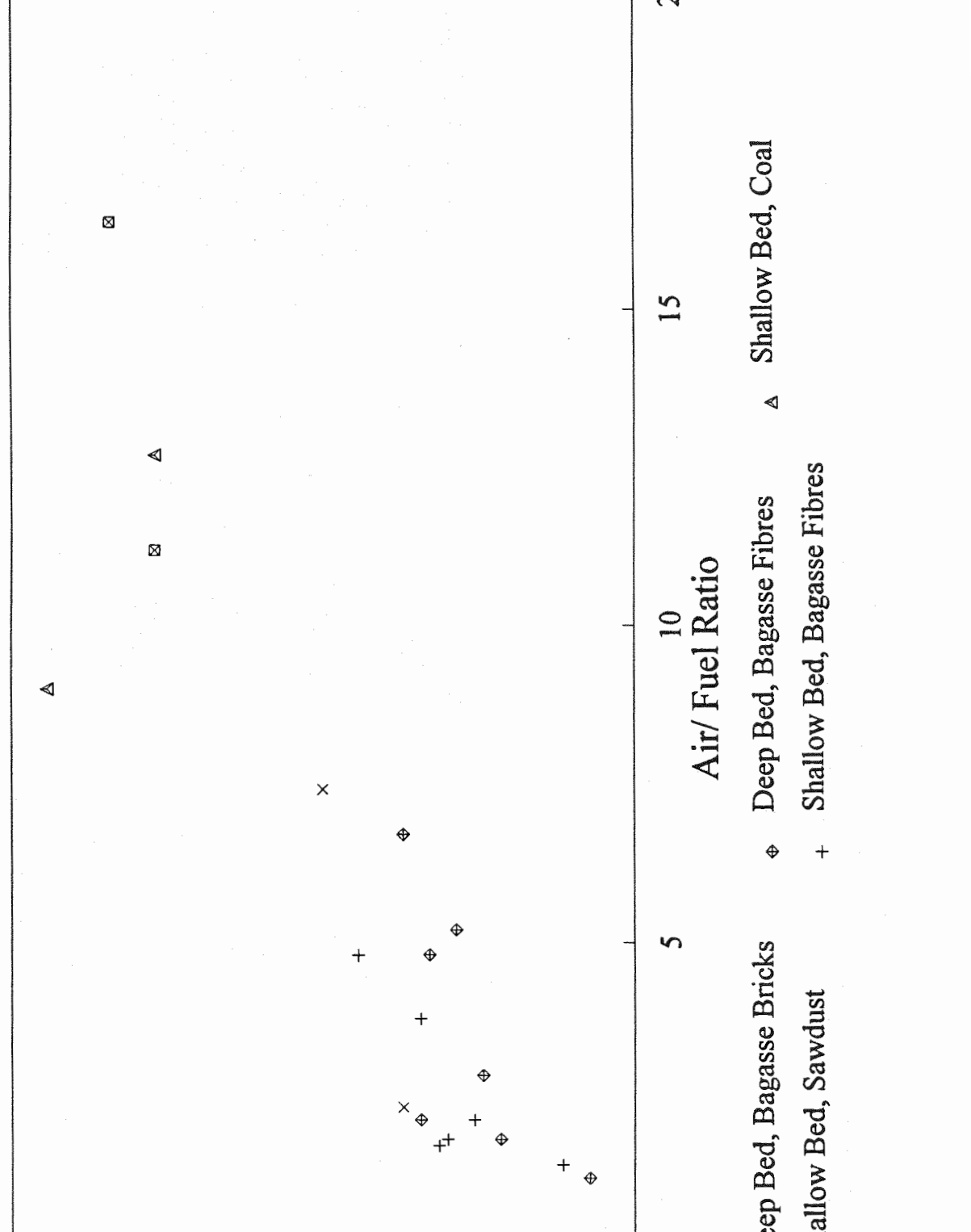


Fig.12.19. Fluidized Bed Efficiencies: Above Bed Feed

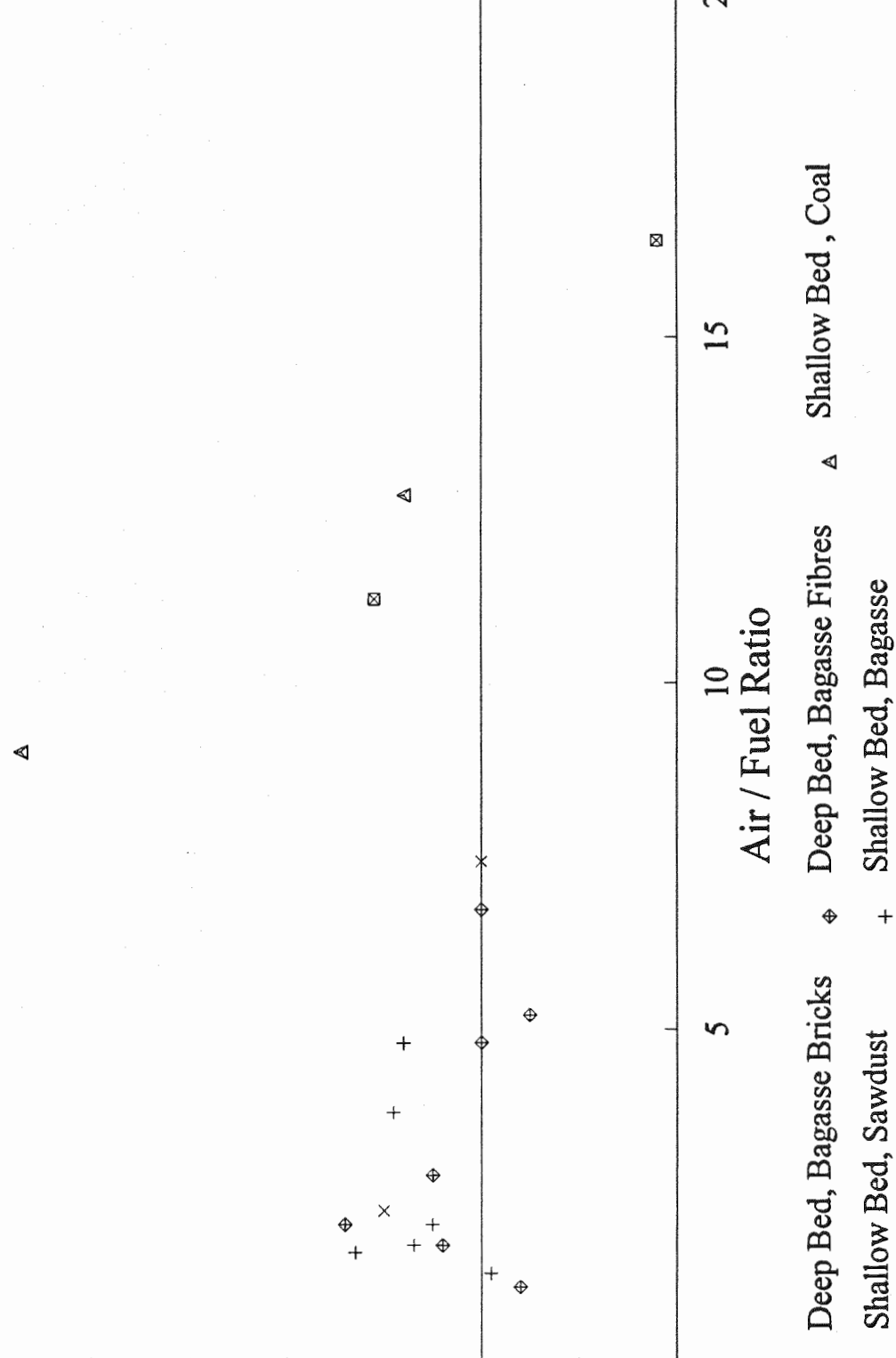


Fig. 12.20 Overall Bed Efficiencies: Above Bed Feed

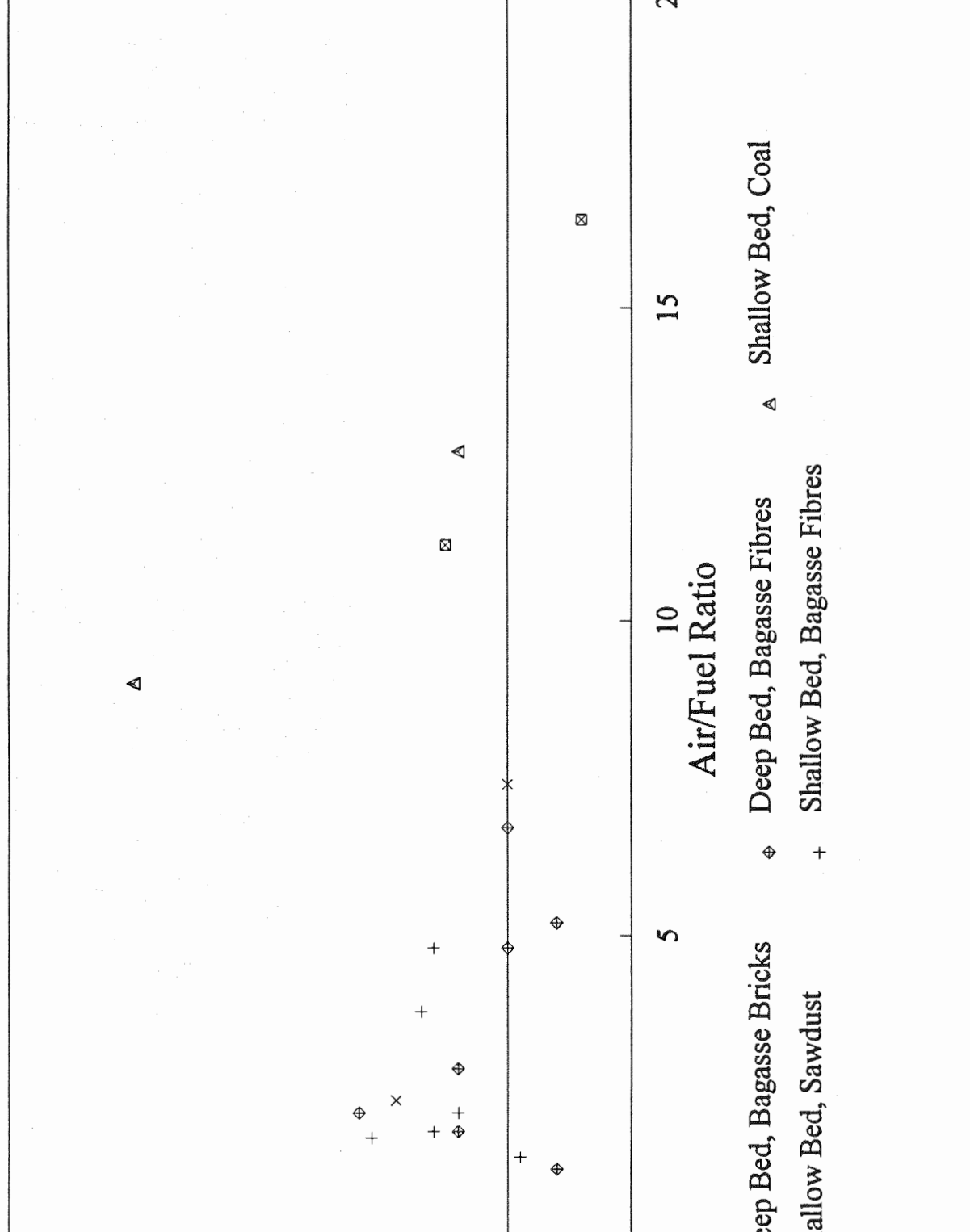


Fig.12.21 Combustion Efficiencies: Ingestor Feed

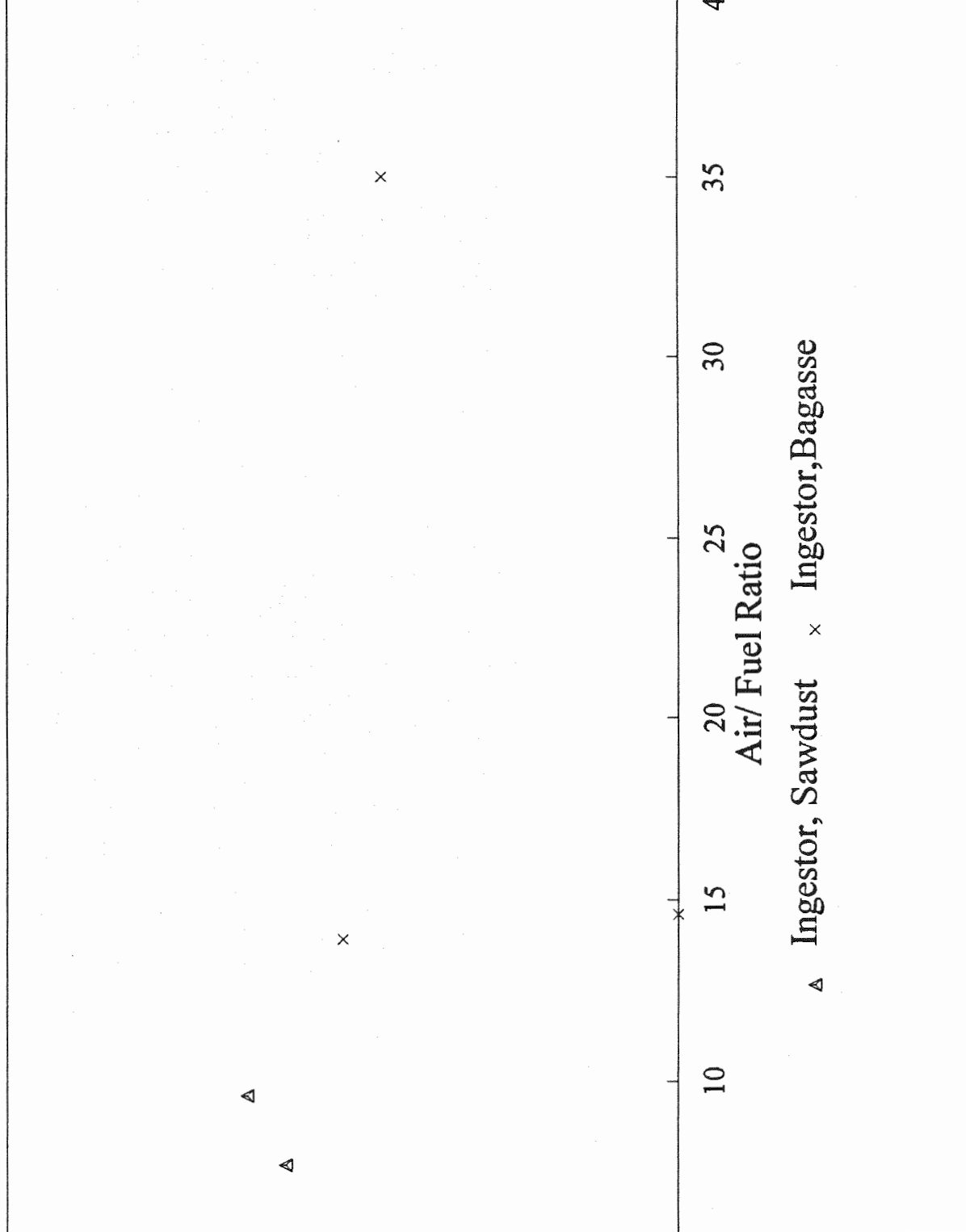


Fig.12.22 Fluidized Bed Efficiencies: Ingestor Feed

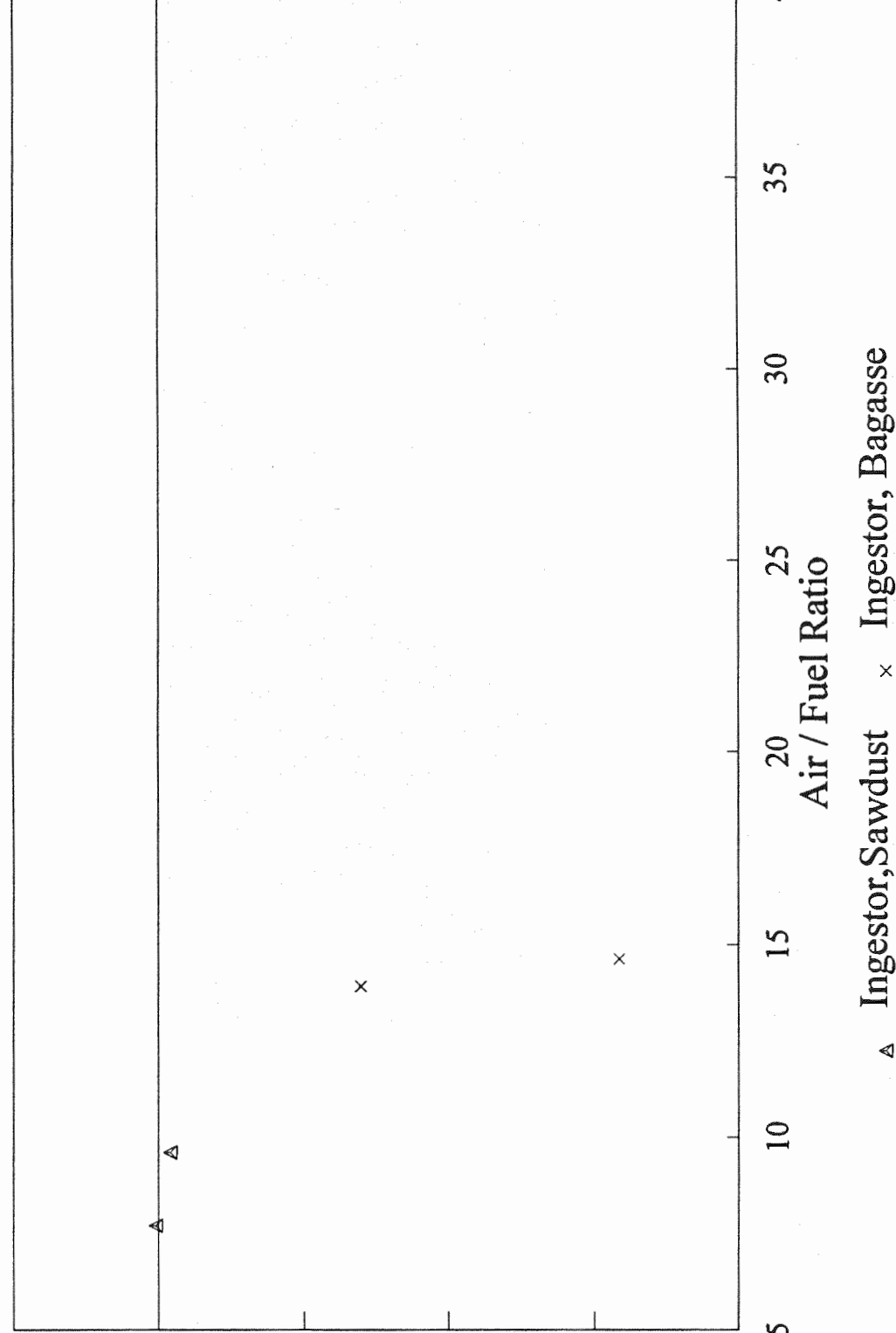


Fig.12.23 Overall Bed Efficiencies: Ingestor Feed

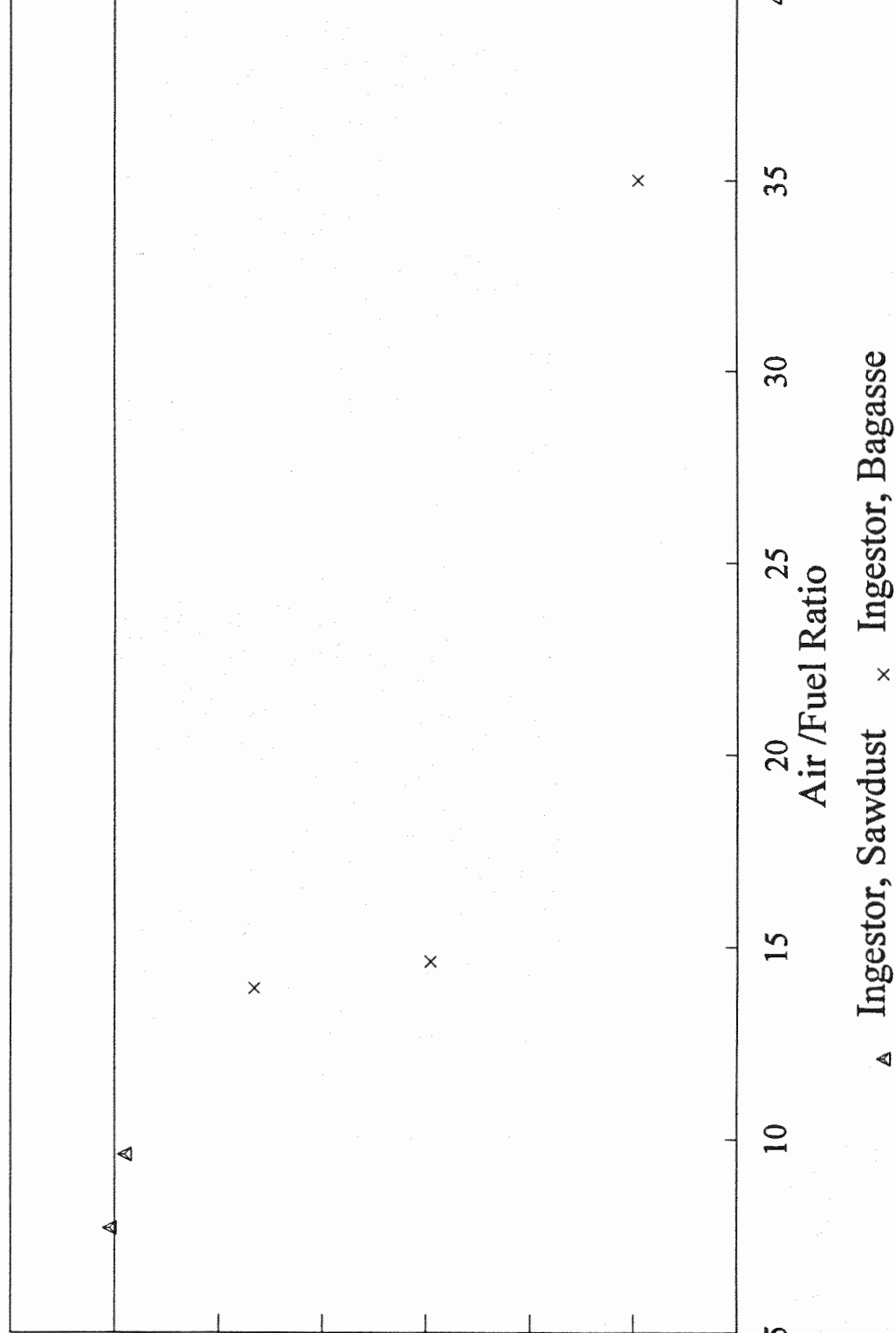


Fig.12.24 Combustion Efficiencies: Below Bed Feed

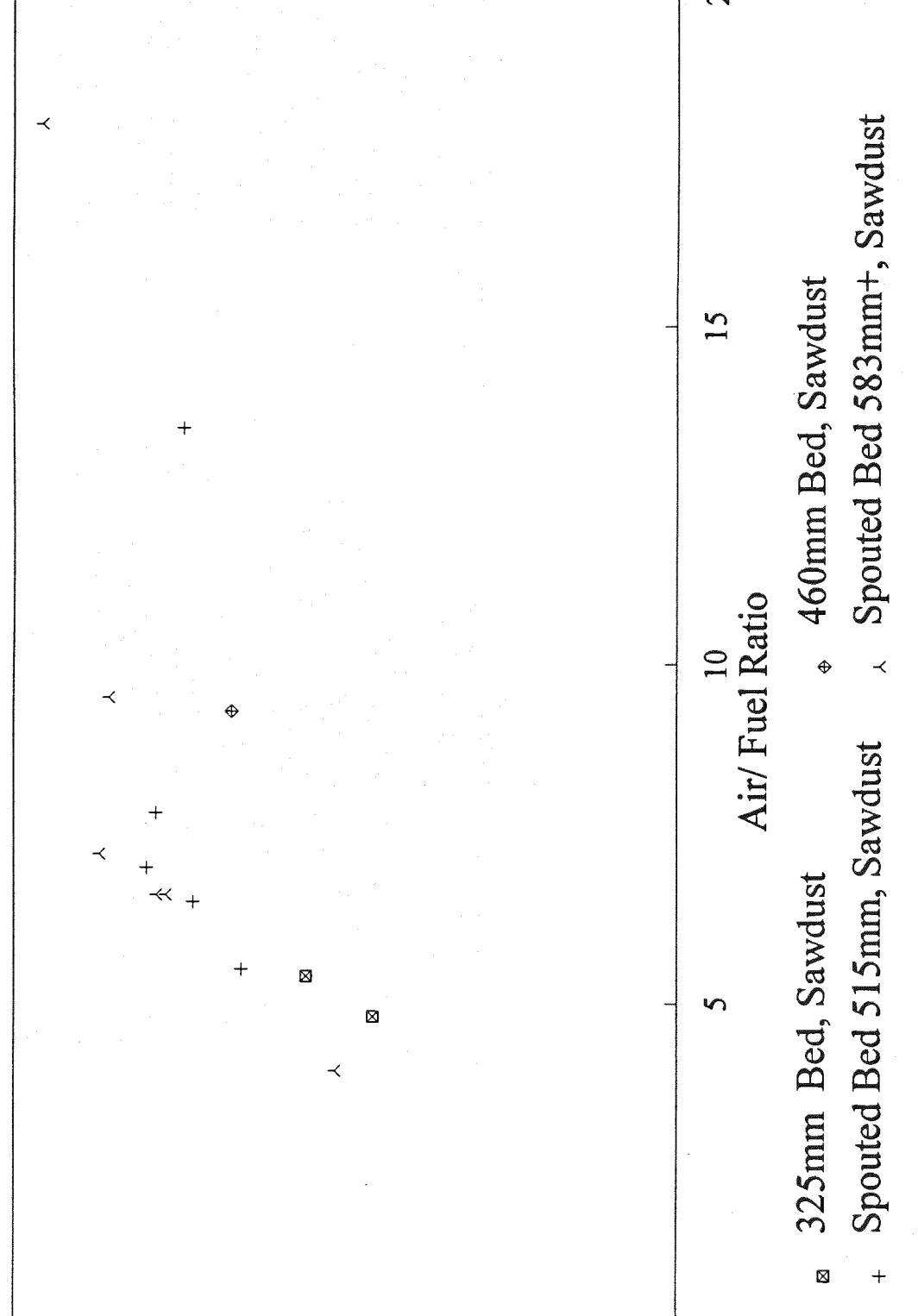
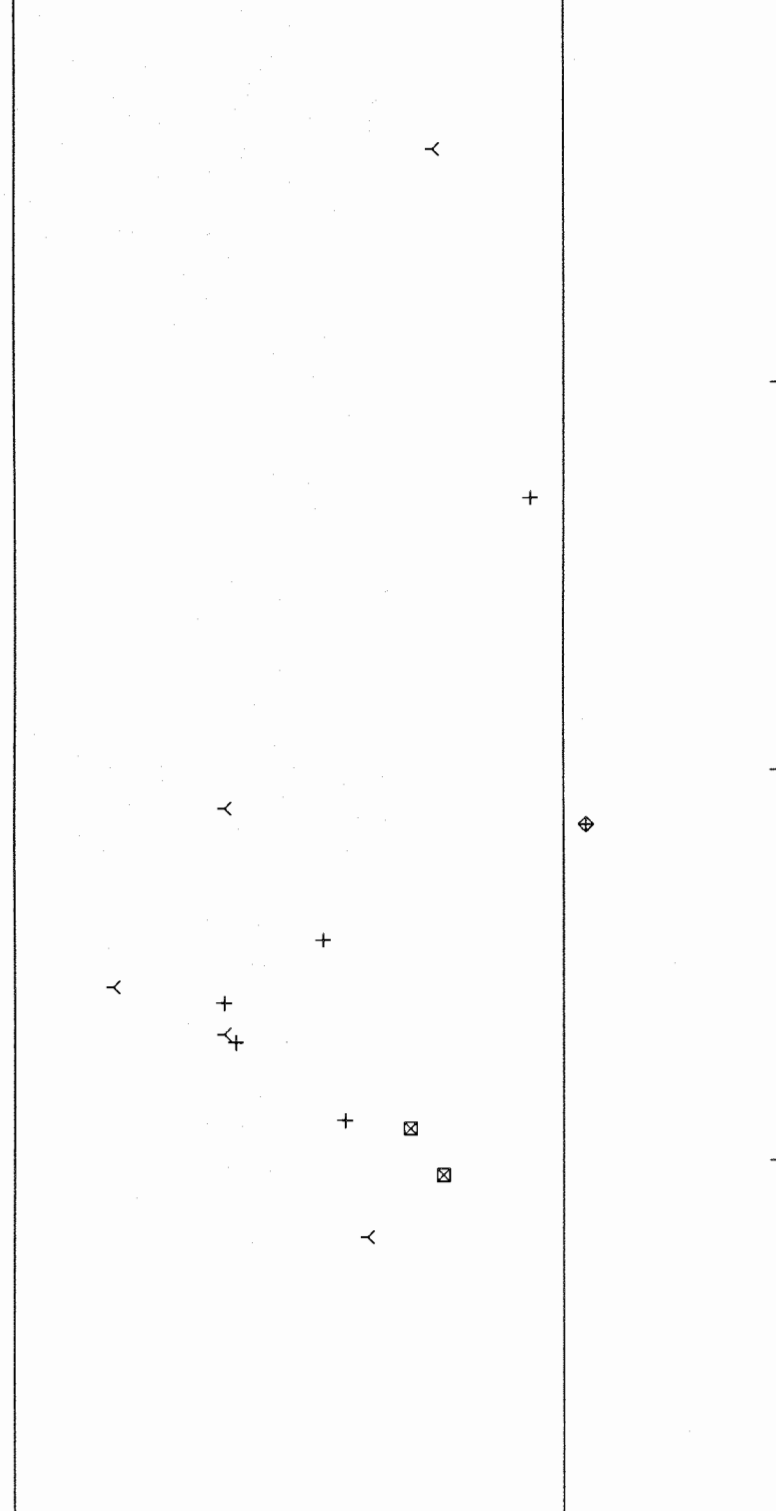


Fig. 12.25 Fluidized Bed Efficiencies: Below Bed Feed



	5	10	15	20
Air / Fuel Ratio				
325mm Bed, Direct Screw Feed, Sawdust	◆	◆	◆	◆
515mm Spouted Bed , Sawdust	×	×	×	×

Fig.12.26 Overall Bed Efficiencies: Below Bed Feed

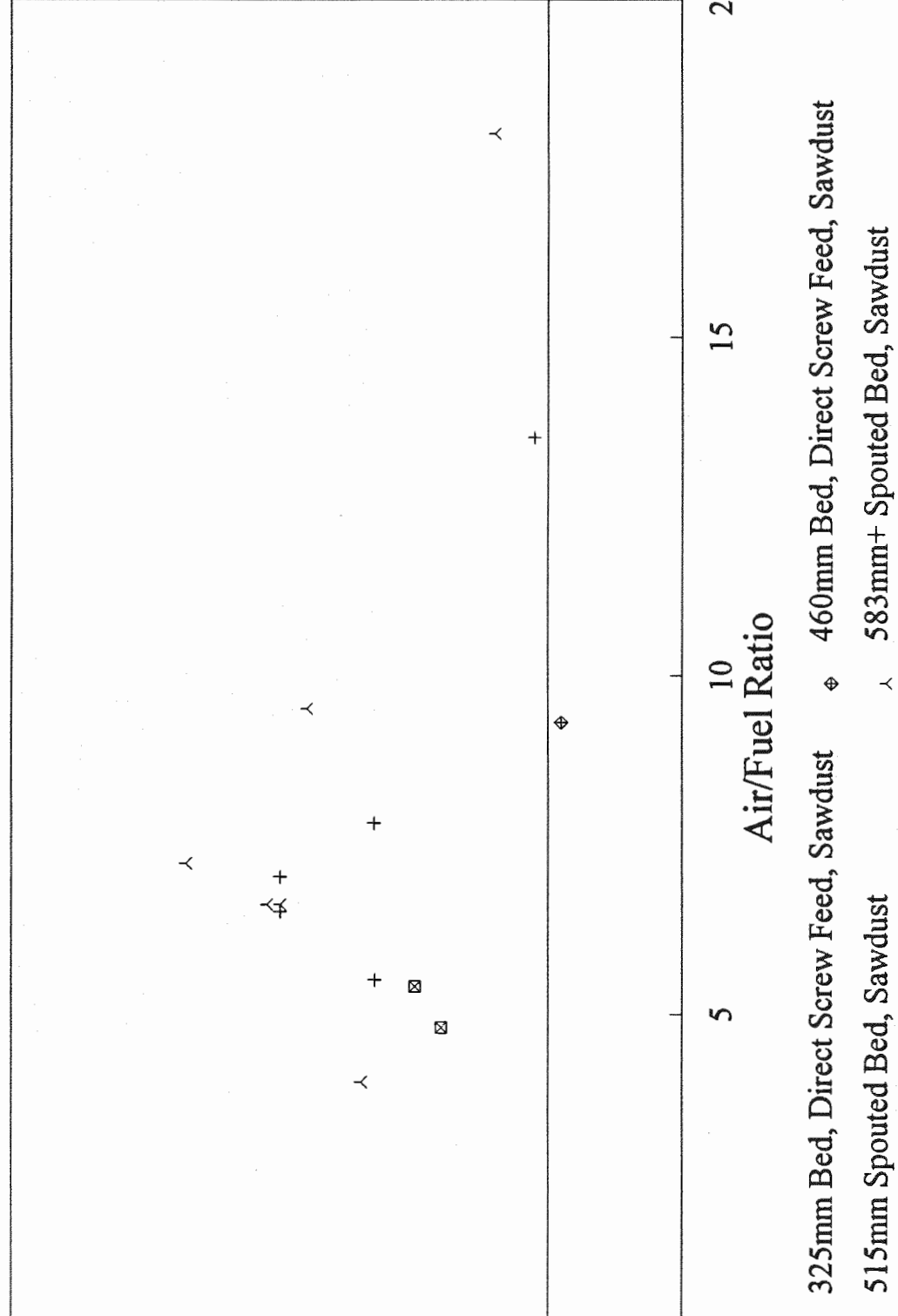


Fig.12.27 Combustion Efficiency, Depth Characteristic

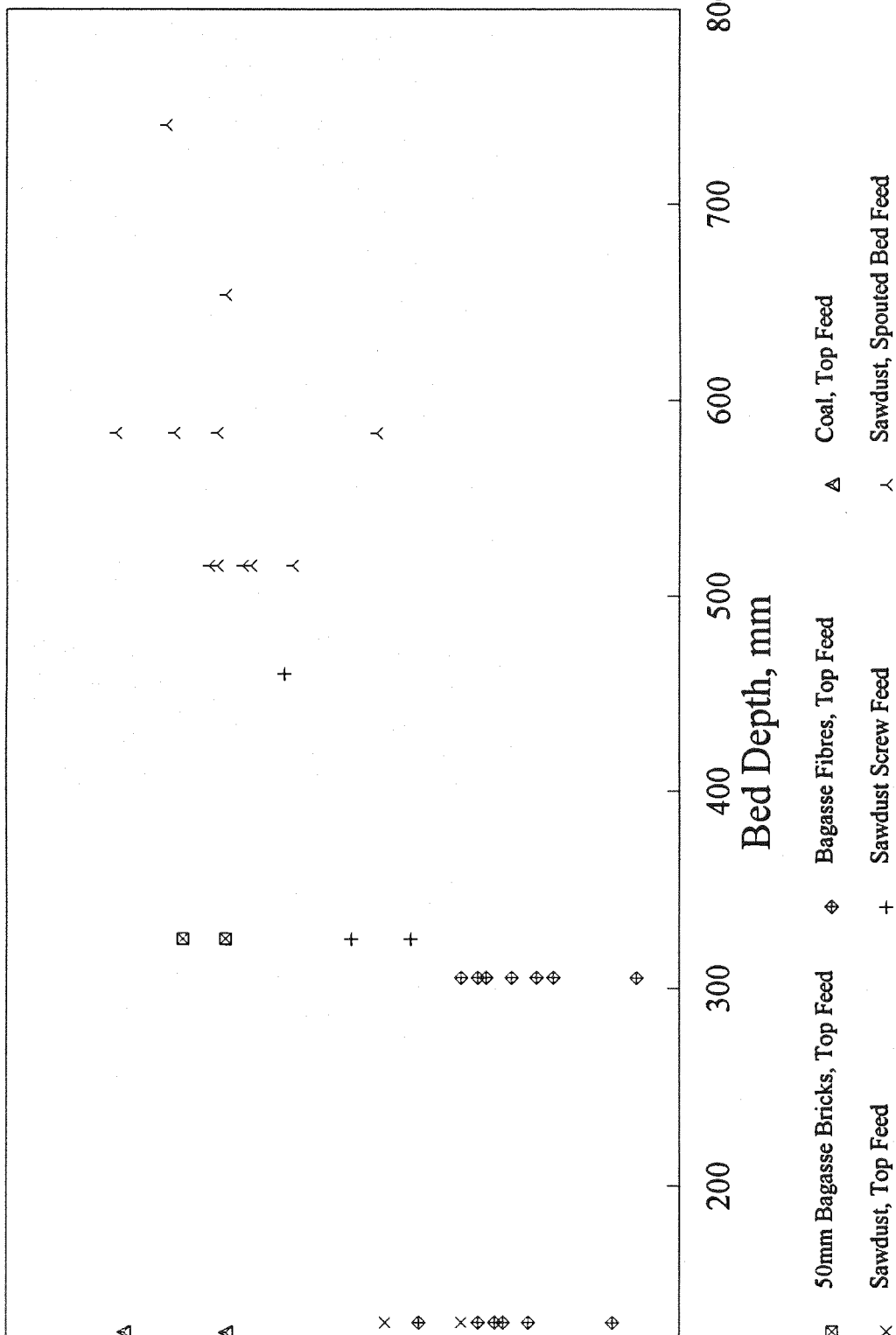


Fig.12.28 Overall Bed Efficiency, Depth Characteristic

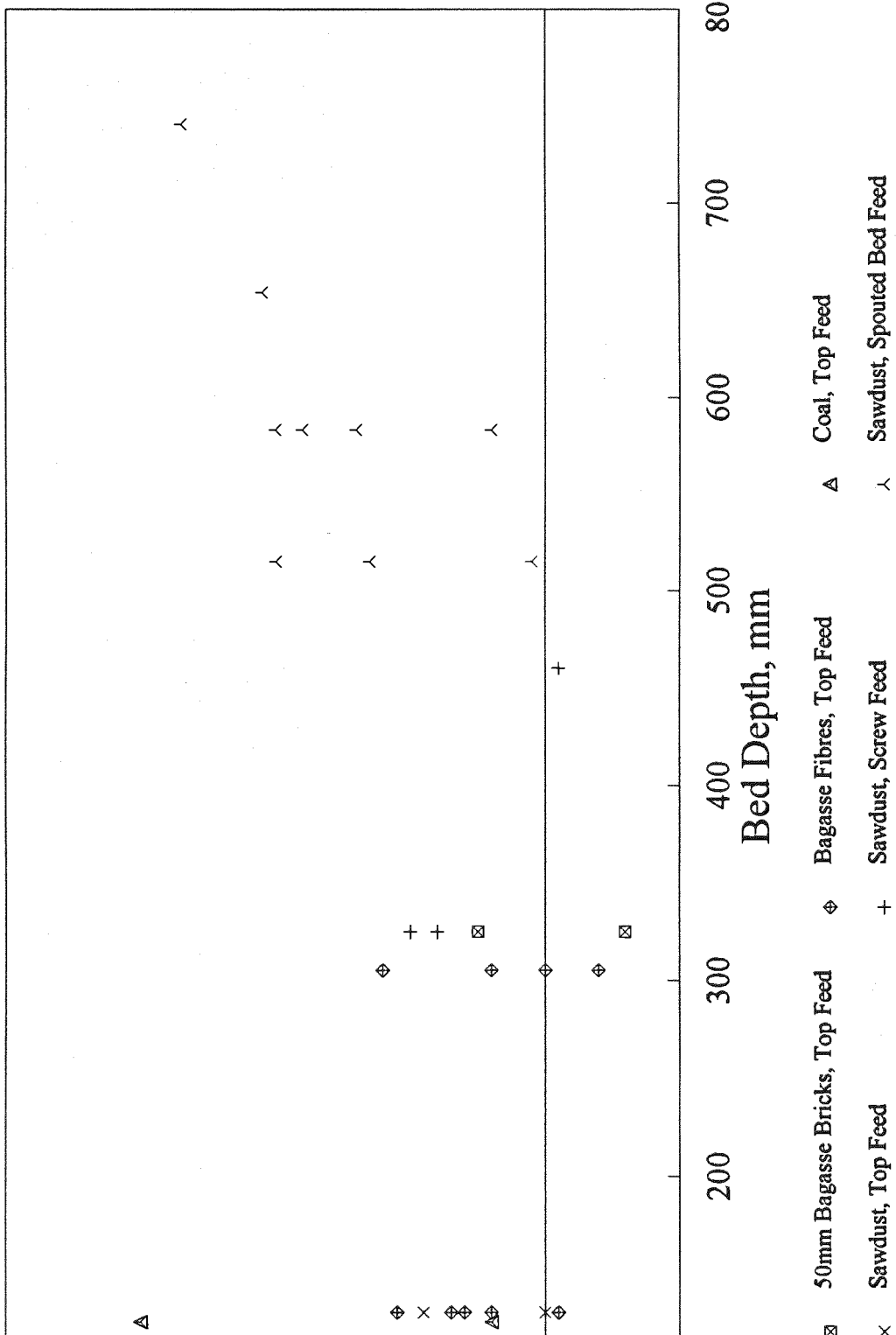


Fig.12.29 Heat Flux: Above Bed Feed Systems

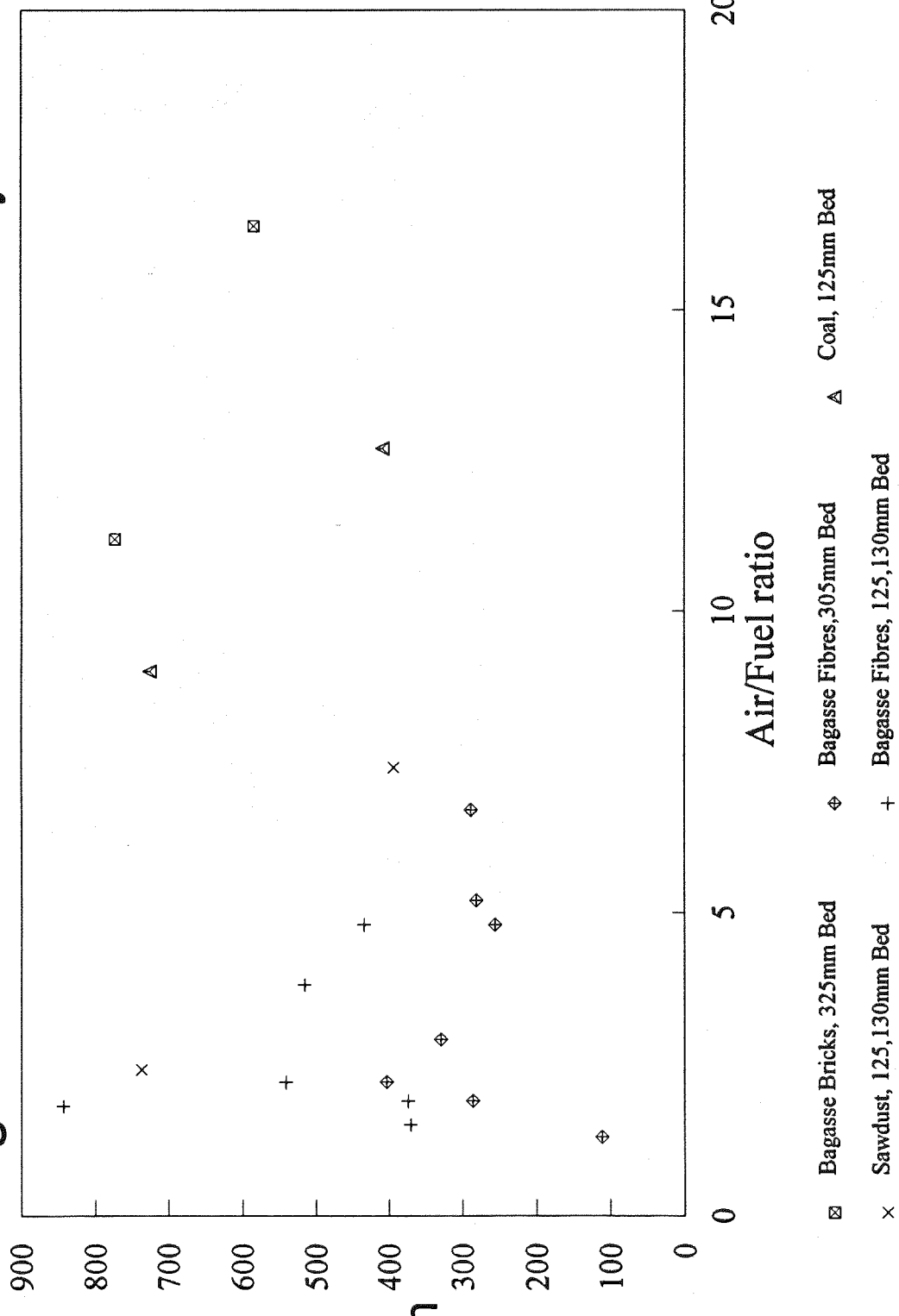


Fig.12.30 Heat Flux: Below Bed Feed Systems

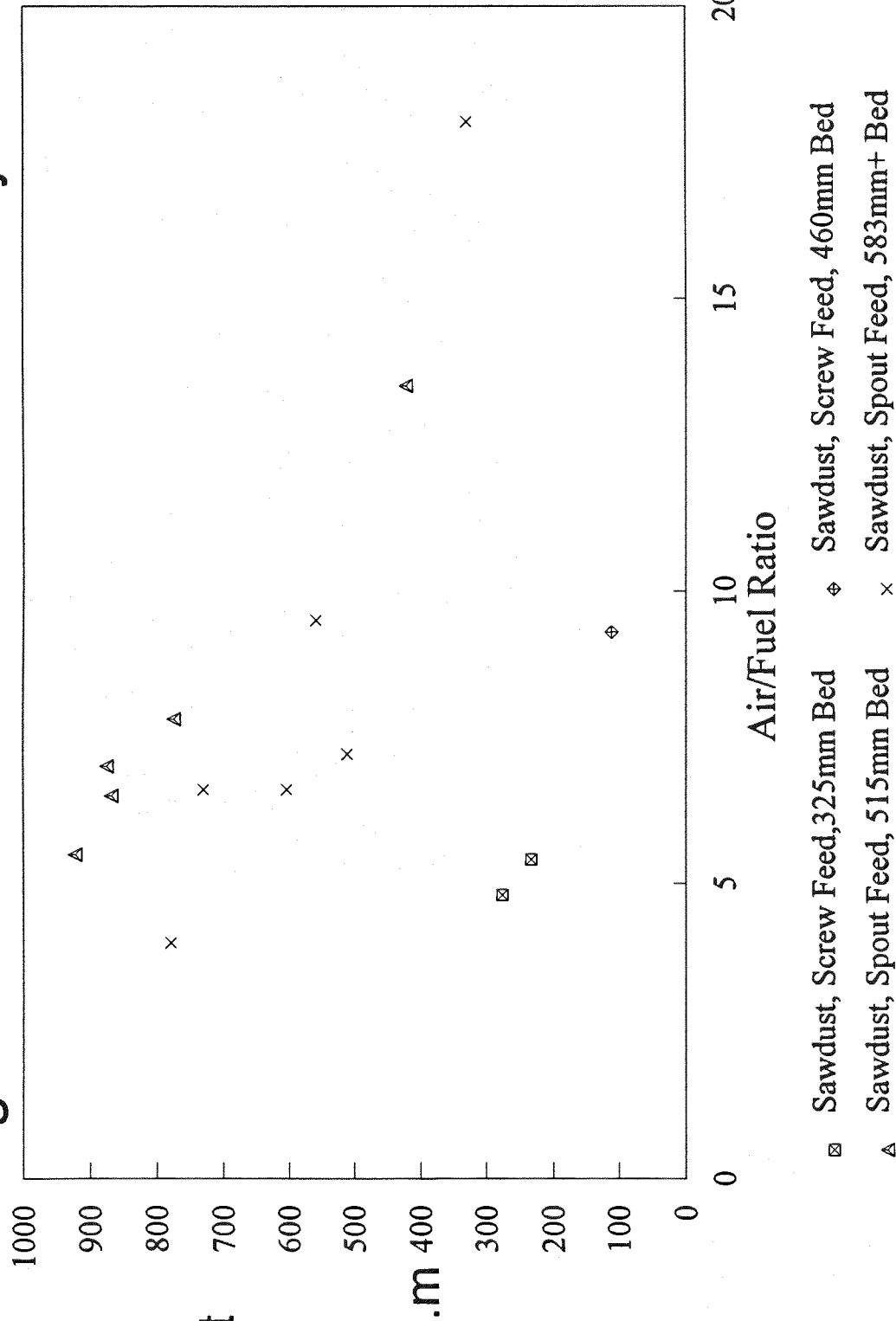


Fig.12.31 Proposed Devolatilizer/Partial Gasifier with Pressurised Fuel Feed

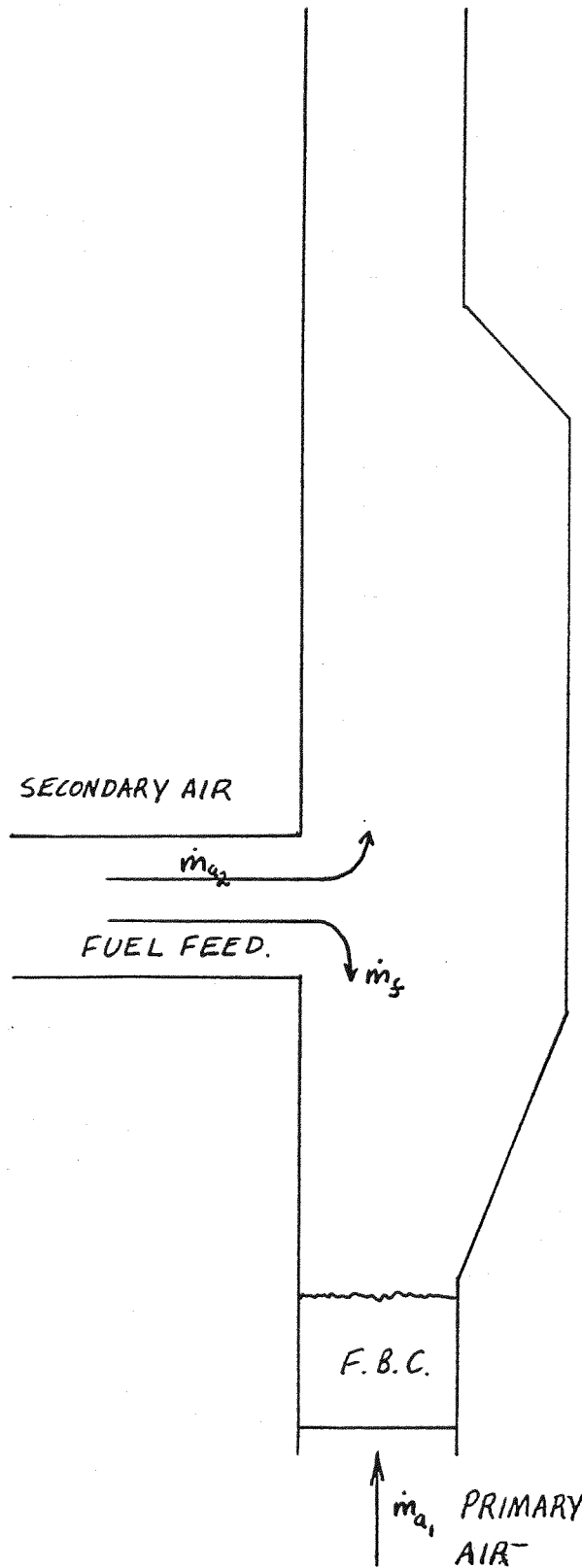


Fig.12.32 Proposed Devolatilizer/Partial Gasifier with Mechanical Fuel Feed

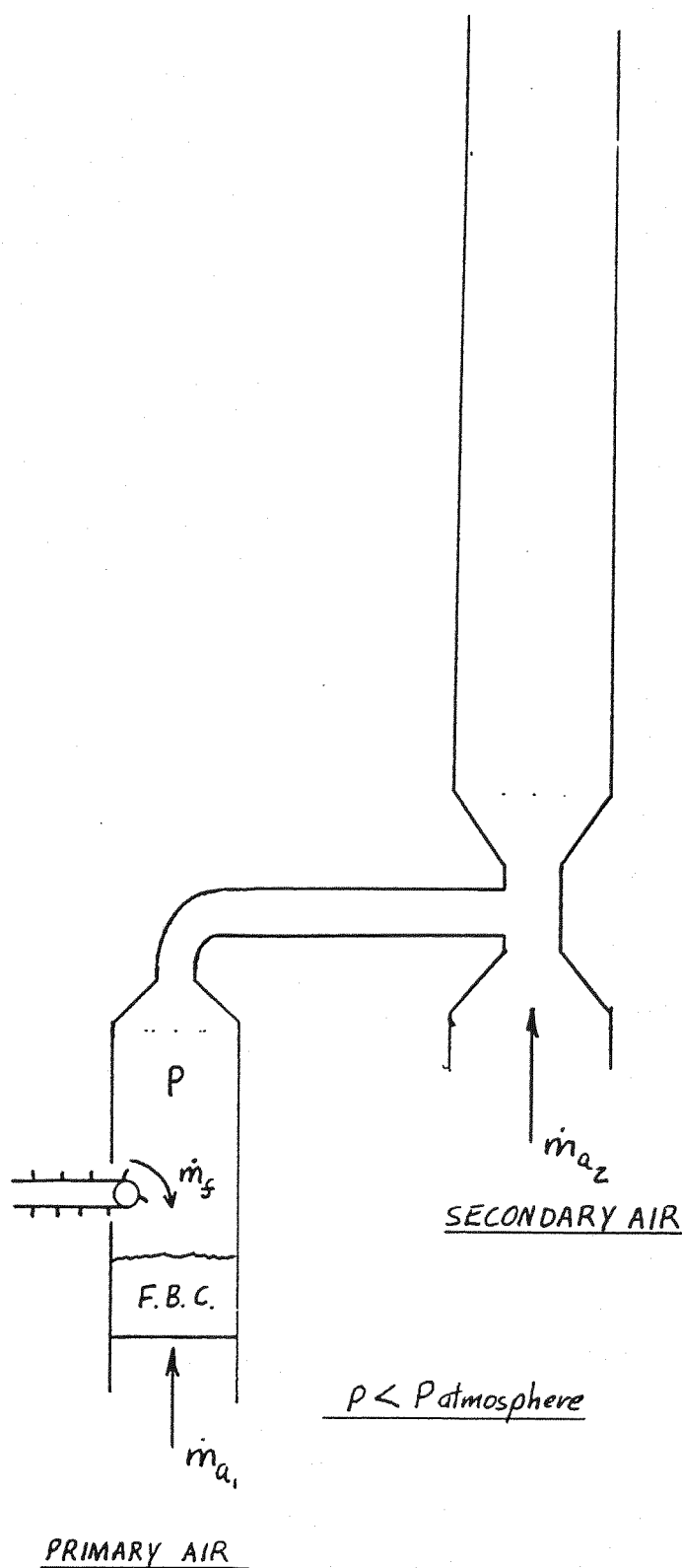


Fig.12.33 Proposed Pre- Gasification Combustor with Secondary Air

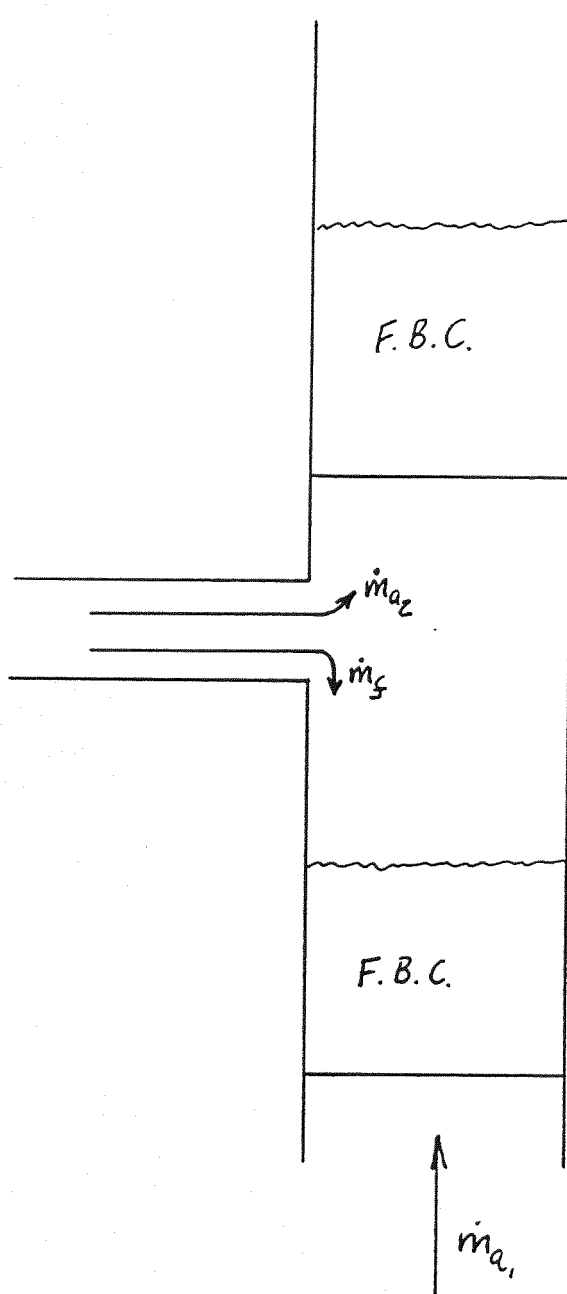


Fig.12.34 Proposed Pre- Gasification Combustor without Secondary Air

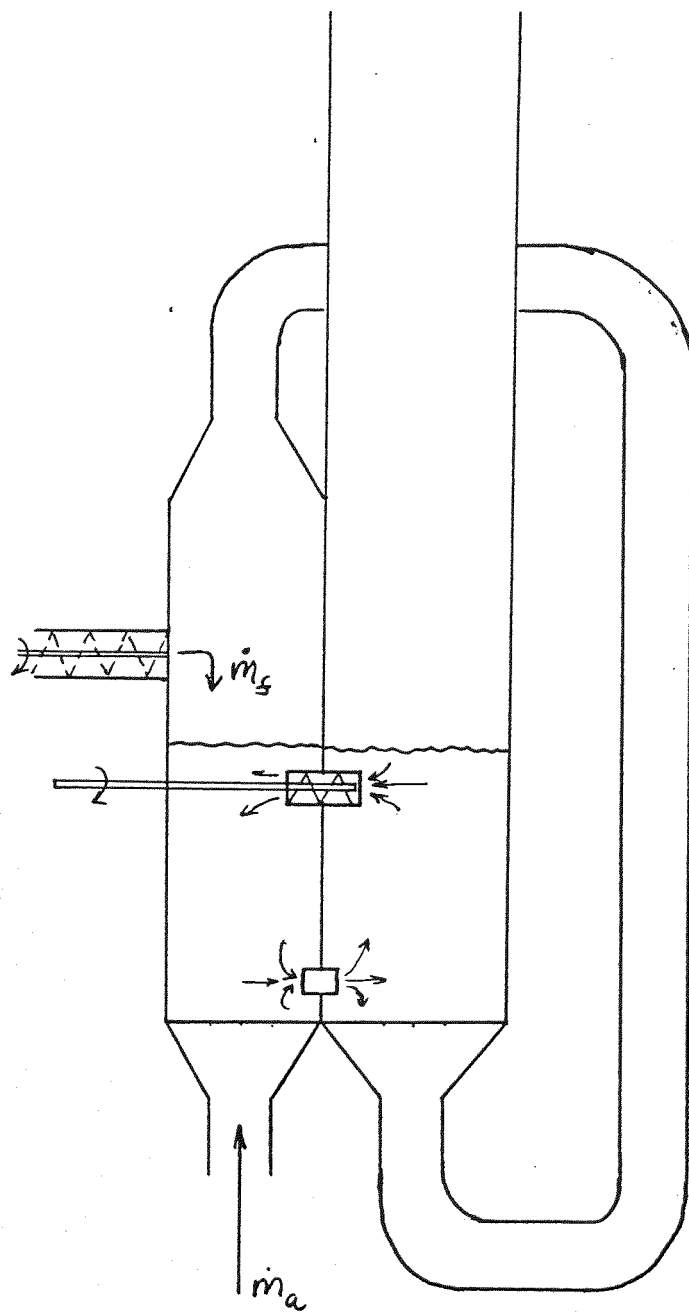


Fig.12.35 Proposed Modified Spouted Bed with Fuel/Air Pre-heated

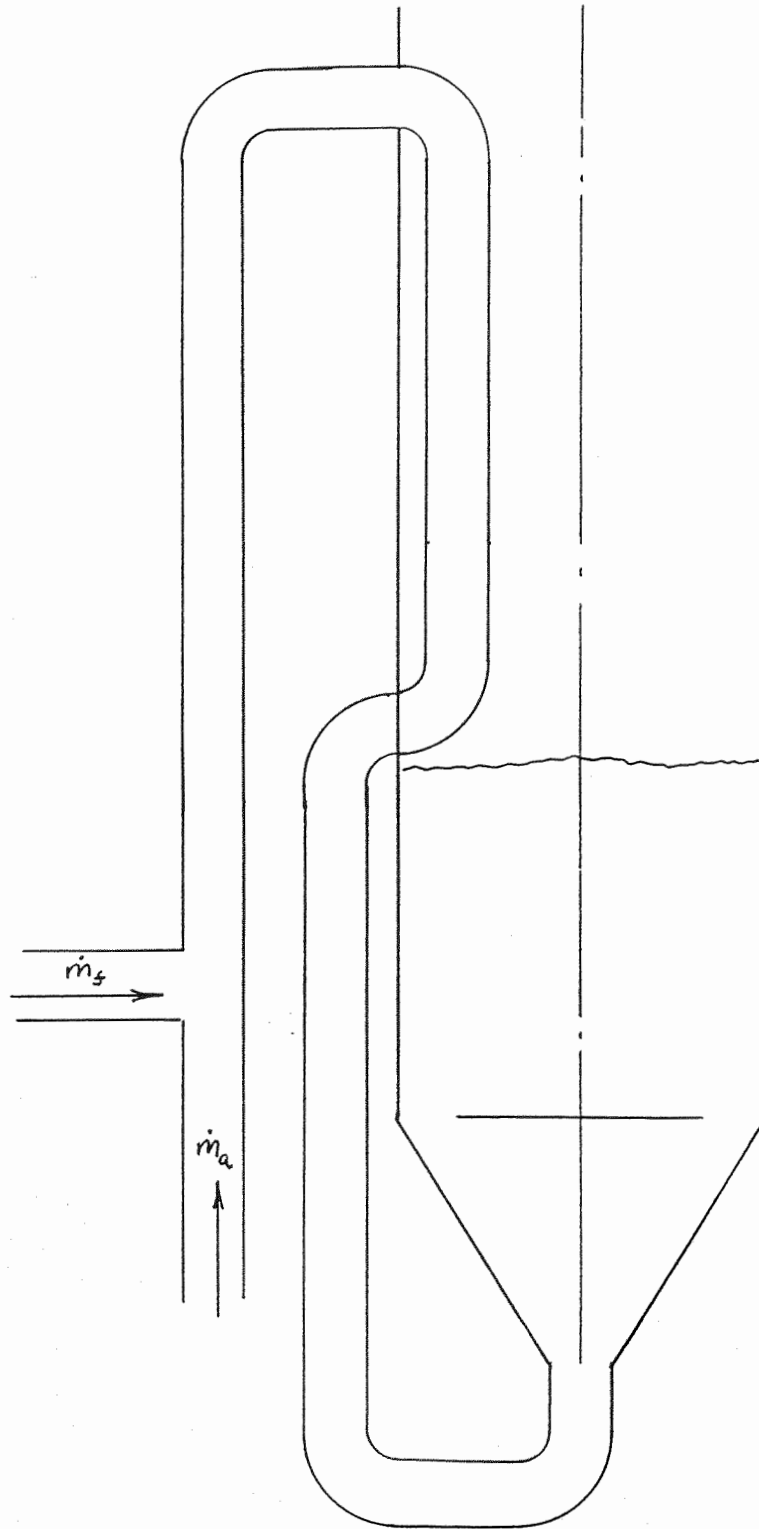


Fig.12.36 Proposed Modified Dual Chamber Spouted Bed

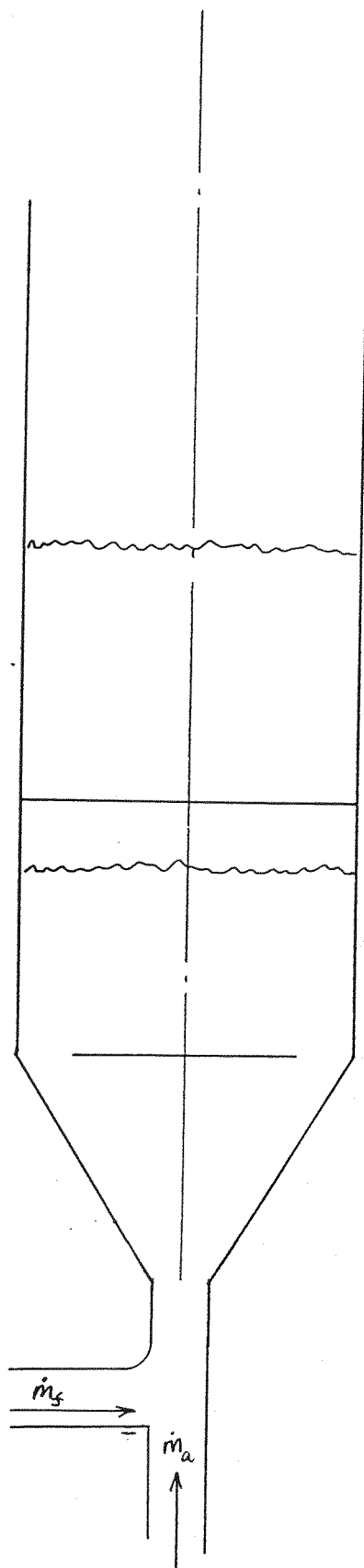


Fig.12.37 Proposed Modified Spouted Bed with Bubble Controls

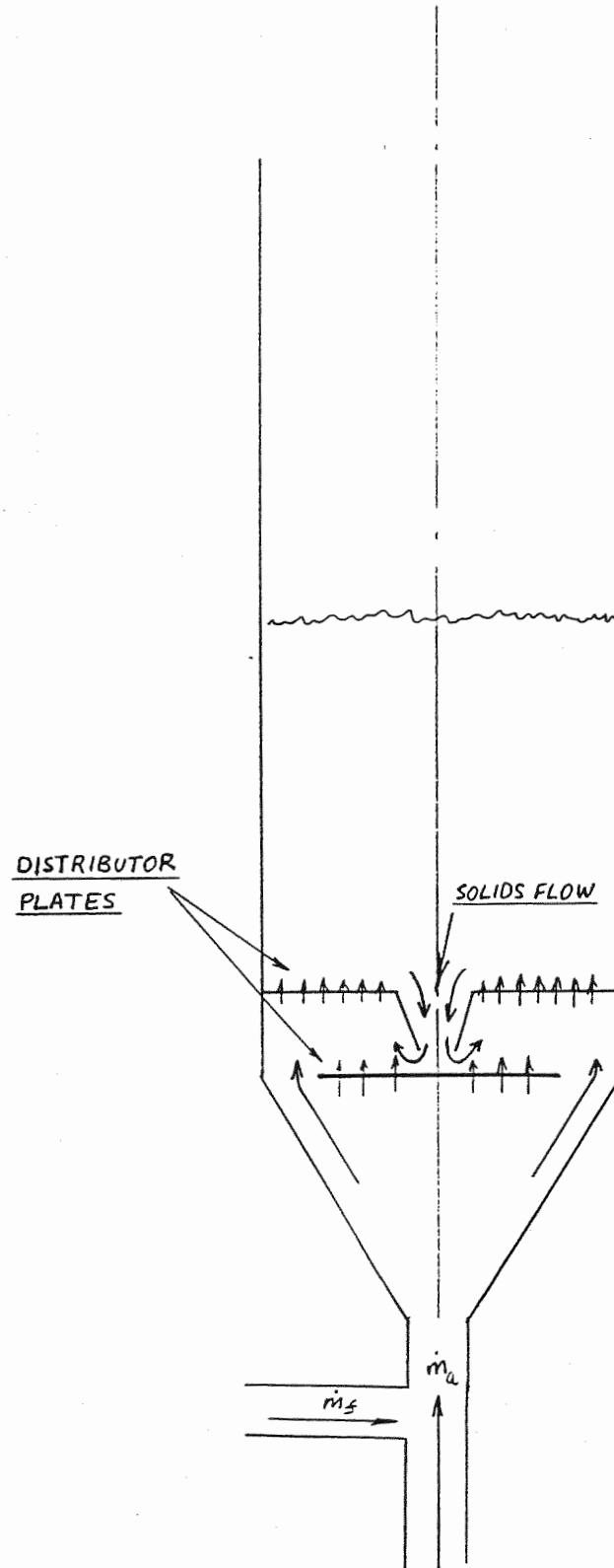


Fig.12.38 Proposed Spouted Bed with Multi-Point Fuel Feed

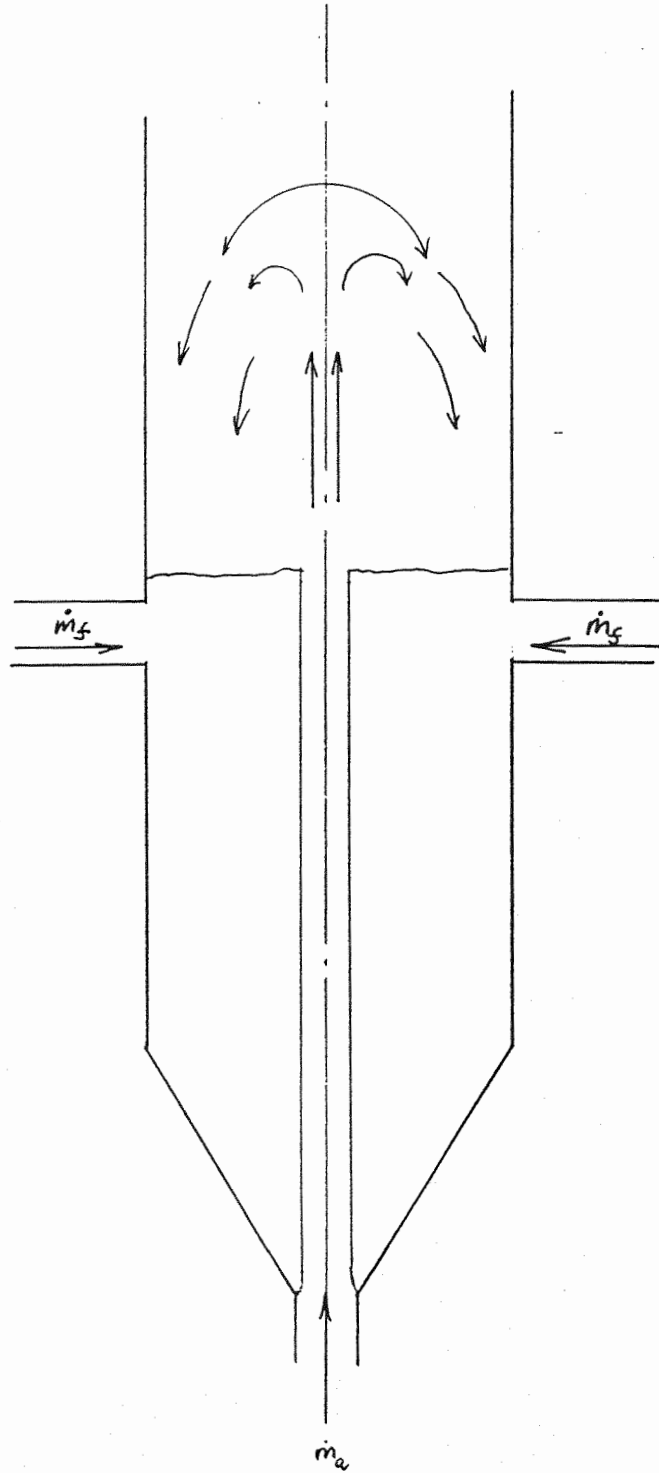


Fig.12.39 Proposed Improved Ingestor with Above Tube feed

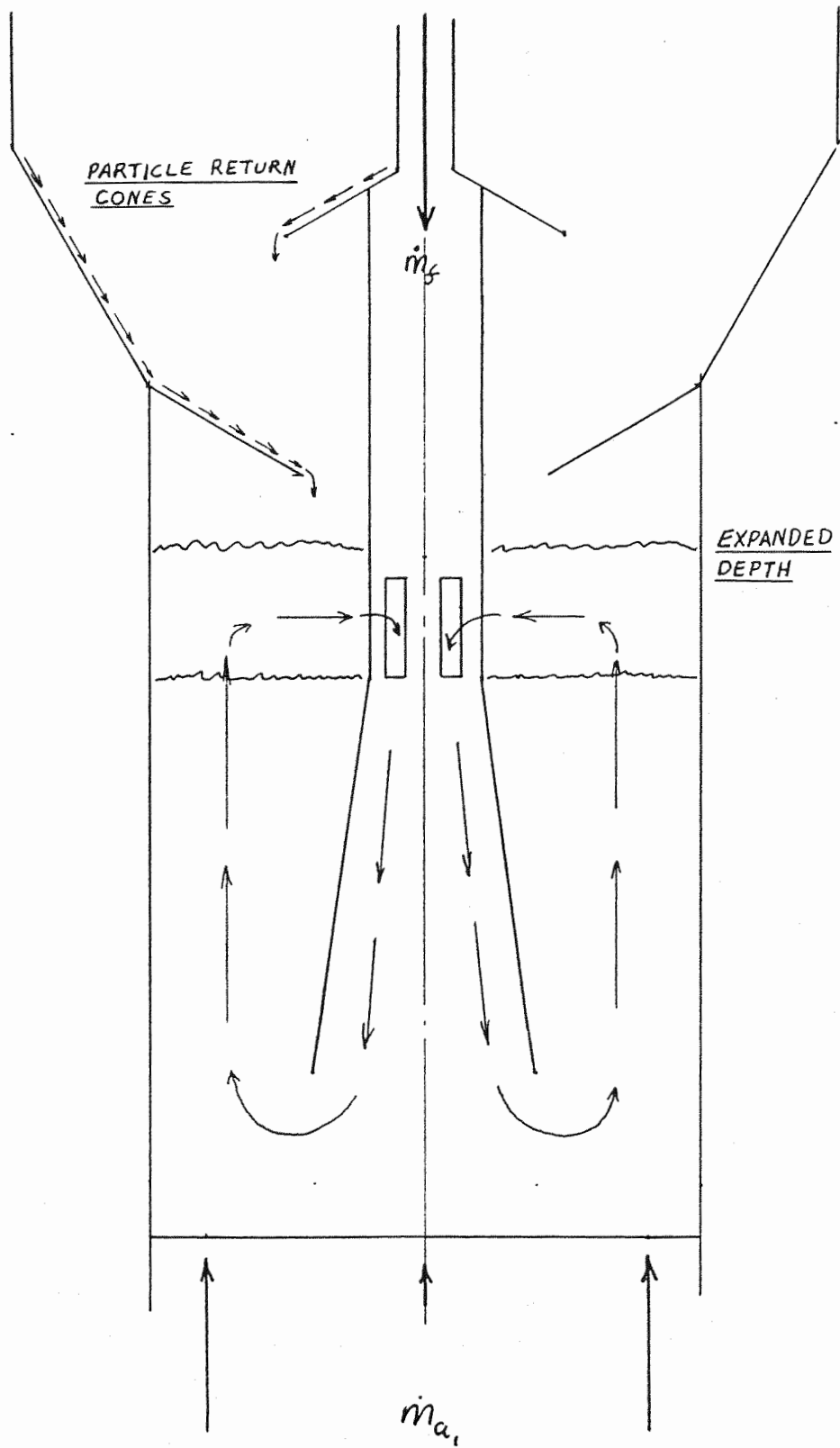
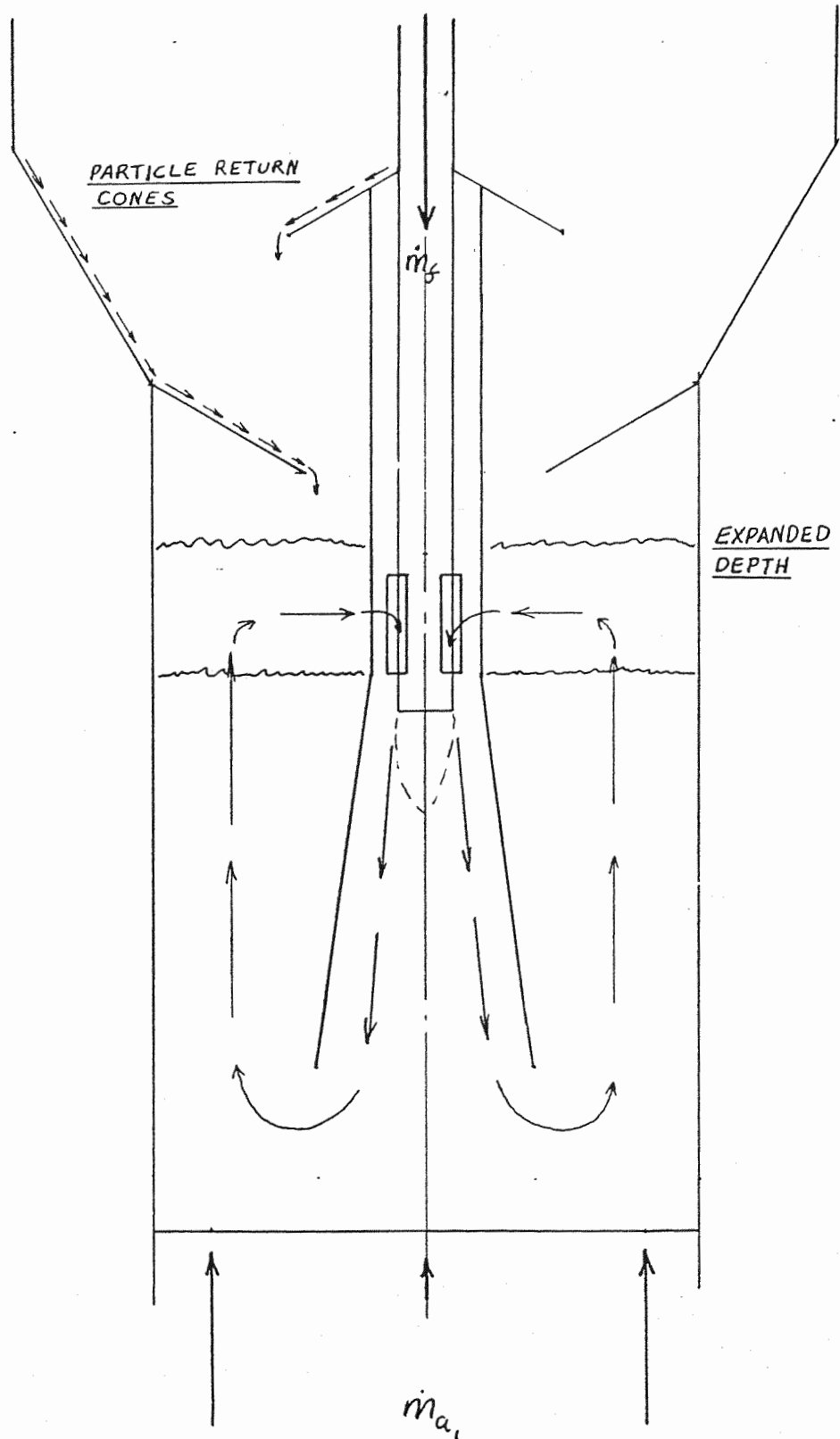


Fig.12.40 Proposed Improved Ingestor with Pneumatic Fuel-Air Jet Injection.



Fluidized Bed Combustion of Waste Material

Volume 2 of 2

Appendices

by

Colin Robert Cole

Submitted in fulfilment of the requirements for the
degree of

Master of Engineering (Mechanical)

at the

University of Central Queensland.
Rockhampton.

Department of Mechanical Engineering

James Goldston Faculty of Engineering

Submitted : January, 1994

CENTRAL QUEENSLAND
UNIVERSITY - LIBRARY

Table of Contents

Title Page	i
Table of Contents	ii
List of Tables	iii
List of Figures and Illustrations	iii
 A. Sample Calculations	
(a) Theoretical Calculations	1
(b) Results Calculations	12
(c) Iterative Spreadsheet Calculations	25
 B. Experimental Data and U_f/U_{mf} Charts	28
 C. Equipment Drawings and Photographs	69
 D. Equipment Data	108
 E. Fuel Properties	116
 F. Sand Properties	128
 G. Combustor Operation Instructions and Charts	138
 H. Equipment Design Calculations	145
 I. Commissioning Notes	152

List of Tables

Table.A1-A2	Iterative Calculations	25
Table.B1-B24	Flow Visualisation Data	28
Table.B25-B33	Combustion Data	40
Table D1	Combustor Specific Heat and Wall Losses	109
Table E1	Typical Fuel Properties	116
Table E2-E5	Fuel Particle Fall Estimates	119
Table E6-E11	Fuel Particle Heat Transfer	119
Table E12-E13	Miscellaneous Tables	121
Table F1-F2	Typical Sand Properties	128
Table F3-F6	Sand Particle Size Analysis Tables	129
Table F7-F14	Sand Theoretical Voidage, Bubble Fraction and Mixing	130
Table H1	Fluidized Bed Combustor Materials Costs	151

List of Figures and Illustrations

Fig. B1-B17	Temperature and U_f/U_{mf} Charts	52
Fig. C1-C13	Flow Visualisation Equipment Drawings	69
Fig. C14-C31	Combustor Equipment Drawings	82
Fig. C32-C46	Photographs	100
Fig. D1-D8	Equipment Data Graphs	110
Fig. E1-E5	Fuel Particle Analysis Graphs	123
Fig. E6-E7	Fuel Particle Heat Transfer Graphs	126
Fig. E8	Minimum Combustion Efficiency for Sustained Operation on Cellulose Fuels	127
Fig. G1-G9	Operation Charts	140

Appendix A : Sample Calculations

(a) Theoretical Calculations

Interpolations

Air and water properties that are usually obtained from property tables are not readily useable for large numbers of repetitive calculations using a spreadsheet. A typical calculation is minimum fluidization velocity which requires a different viscosity value for each temperature. The problem was solved by taking data from Mayhew.Y.R and Rogers.G.F.C., Thermodynamic and Transport Properties of Fluids, and fitting the data to usually three straight line correlations. Errors in correlations were checked and are stated in each case. The accuracy of such an approach far exceeds normal manual interpolations:

(a) Specific Heat of Air, kJ/kg.K

Correlations $C_p = 0.000077 T + 0.981848$ for $T = 275$ to 400 K
 $C_p = 0.000228 T + 0.915644$ for $T = 400$ to 900 K
 $C_p = 0.000168 T + 0.973186$ for $T = 900$ to 1250 K

Maximum Error 0.12%

(b) Dynamic Viscosity of Air, Pa.s $\times 10^5$

Correlations $\mu = 0.004483 T + 0.499343$ for $T = 275$ to 400 K
 $\mu = 0.003125 T + 1.120182$ for $T = 400$ to 900 K
 $\mu = 0.002365 T + 1.787643$ for $T = 900$ to 1250 K

Maximum Error 1.0 %

(c) Thermal Conductivity of Air, kW/m.K $\times 10^5$

Correlations $k = 0.007495 T + 0.374152$ for $T = 275$ to 400 K
 $k = 0.005688 T + 1.215236$ for $T = 400$ to 900 K
 $k = 0.004429 T + 2.3255$ for $T = 900$ to 1250 K

Maximum Error 1.0%

(d) Enthalpy of Steam at 1bar. kJ/kg

Correlations $h = 1.534429 T + 2351.9$ for $T = 100$ to 500 C
 $h = 1.94175 T + 2129.3$ for $T = 500$ to 1300 C

Maximum Error 0.6%

Equivalent Particle Diameter

For a non-spherical particle of diameter 1mm and length 10mm, equivalent particle diameter is given by(Eq.3.1):

$$d_p = \left[\frac{6 V_p}{\pi} \right]^{(1/3)} = \left[\frac{6 (\pi (1)^2 / 4) (10)}{\pi} \right]^{(1/3)} = 2.466 \text{ mm}$$

Surface Mean Particle Size

Using typical coarse grade river sand data(Eq.3.6).

$$\bar{d}_p = \frac{1}{\sum \left[\frac{x}{d_p} \right]} = \frac{1}{\left(\frac{.003}{112.5} + \frac{0.082}{225} + \frac{0.141}{362.5} + \frac{0.297}{512.5} + \frac{0.473}{890} \right)}$$

$$= 530 \text{ microns}$$

Sphericity

Using the same data(Eq.3.2)

$$\phi = \frac{(\text{Surface area sphere})}{(\text{Surface area particle})} = \frac{\pi (2.466)^2}{2\pi (1)^2 / 4 + \pi (1) (10)} = 0.579$$

Voidage

Using typical sand data, bulk density is 1450 kg/m³ and particle density 2300 kg/m³. (Eq.3.3)

$$\epsilon = 1 - \frac{\rho_f}{\rho_p} = 1 - \frac{1450}{2300} = 0.37$$

Specific Surface

Using typical sand data of $\phi = 0.95$, $d_p = 300$ micron, specific surface on particle volume basis is (Eq.3.4,3.5):

$$a' = \frac{6}{\phi d_p} = \frac{6}{(0.95)(300/10^6)} = 21053 m^{-1}$$

Using the same data a more useful specific surface is on bed volume basis:

$$a = \frac{6(1-\epsilon)}{\phi d_p} = \frac{6(1-0.37)}{(0.95)(300/10^6)} = 13263 m^{-1}$$

Minimum Fluidization Velocity

Using typical data for 300 micron sand at 27 C. (Eq.3.26)

$$U_{mf} = \frac{\bar{d}_p^2 (\rho_p - \rho_g) g}{1650 \mu_g} = \frac{(300/10^6)^2 (2300 - 1.2) 9.81}{(1650)(1.846)(10^{-5})}$$

$$U_{mf} = 0.067 \text{ m/sec}$$

Particle Terminal Velocity (Spherical Particles)

Terminal velocities must be calculated for discrete particle diameters, not surface mean particle sizes which are useful only for fluidization calculations. (Eq.3.28)

$$U_t = \left[\frac{4}{225} \frac{(\rho_p - \rho_g)^2 g^2}{\rho_g \mu_g} \right]^{(1/3)} d_p$$

Evaluating for 100 micron sand at 27 C gives:

$$U_t = \left[\frac{4}{225} \frac{(2300-1.2)^2 (9.81)^2}{(1.2) (1.846) (10^{-5})} \right]^{(1/3)} (100/10^6) = 0.742 \text{ m/sec}$$

Particle Terminal Velocity (Non-Spherical Particles)

Corrections must be made for the shape of particles that cannot be approximated to a sphere. The simplest method of obtaining theoretical terminal velocities for non-spherical shapes is to first calculate the velocity independent group (Eq.3.76):

$$C_d Re_p^2 = \frac{4 g d_p^3 \rho_g (\rho_p - \rho_g)}{3 \mu_g^2}$$

$$= \frac{4 (9.81) (2.466/10^3)^3 (1.2) (540-1.2)}{3 (1.846/10^5)^2} = 3.73 \times 10^5$$

Then using the data presented in Kunii et al, reproduced in Fig.E5, Appendix E, and $\phi=0.6$ the Reynolds number corresponding to terminal velocity is read off as $Re_p=300$. The terminal velocity is then (Eq.3.77)

$$U_t = \frac{Re_p \mu_g}{d_p \rho_g} = \frac{(300) (1.846/10^5)}{(2.466/10^3) (1.2)} = 1.87 \text{ m/sec}$$

The velocity calculated for this data using spherical particle formula would be equal to 6.95 m/sec, illustrating the correction needed. Terminal velocities for samples of bagasse and sawdust using the above method are calculated and used to present Cumulative Mass Conveyed graphs in Figs. E2 & E4 (Appendix E).

Bubble Fraction and Mixing

Theoretical values of bubble fraction and solids turnover rate can be derived from Ergun's equation and the relationship (Eq.3.37):

$$\delta = 1 - \frac{L_{mf}}{L_f} = \frac{\epsilon_f - \epsilon_{mf}}{1 - \epsilon_{mf}}$$

The above equation can be re-arranged to give :

$$L_f = L_{mf} \frac{(1 - \epsilon_{mf})}{(1 - \epsilon_f)}$$

Which substituting into Ergun's equation (Eq.3.7) gives:

$$\frac{\Delta P}{L_{mf}(1 - \epsilon_{mf})} (1 - \epsilon_f) = 150 \frac{(1 - \epsilon_f)^2}{\epsilon_f^3} \frac{\mu_g U_f}{(\phi \bar{d}_p)^2} + 1.75 \frac{(1 - \epsilon_f)}{\epsilon_f^3} \frac{\rho_g U_f^2}{\phi \bar{d}_p}$$

Which for a fluidized bed reduces to :

$$\rho_p g = 150 \frac{(1 - \epsilon_f)}{\epsilon_f^3} \frac{\mu_g U_f}{(\phi \bar{d}_p)^2} + \frac{1.75}{\epsilon_f^3} \frac{\rho_g U_f^2}{\phi \bar{d}_p}$$

Which is a quadratic in U_f . For a given value of ϵ_f , the equation can be solved for U_f . The operational point U_f can therefore be related to voidage, expanded bed depth and bubble fraction. Since it is easier to solve for U_f than ϵ_f , it is useful to tabulate voidage, velocity, bubble fraction etc as is done in Appendix F. eg Substituting the values $\epsilon_f = 0.6$, $d_p = 300$ micron, $\mu_g = 1.846/10^5$, $\rho_g = 1.2 \text{ kg/m}^3$, $\phi = 0.95$ gives:

$$22563 = 63130.536 U_f + 34113.06 U_f^2$$

$$\text{or } U_f^2 + 1.8506 U_f + 0.6614 = 0$$

Which, of course, can be solved in the usual way to give:

$$U_f = 0.2811 \text{ m/sec}$$

Having found U_f for various ϵ_f , it is necessary to estimate the bubble velocity before the turnover rate can be calculated. For usual operations (Eq.3.39):

$$u_B = \frac{U_f - (1-\delta) U_{mf}}{\delta} = \frac{(0.2811 - (1-0.333)(0.667))}{0.333}$$

$$u_B = 0.727 \text{ m/sec}$$

The turnover rate for sand can then be calculated given that the bubble / wake volume ratio α is known to be 0.25 and the turnover rate is given by (Eq.3.35):

$$J = \alpha \delta u_B \rho_p (1 - \epsilon_{mf}) = (0.25)(0.333)(0.727)(2300)(1 - 0.4)$$

$$J = 83 \text{ kg/m}^2 \cdot \text{sec}$$

Bed Pressure Drop when Fluidized

For a typical sand bed of diameter 489mm and depth 300mm (Eq.3.9).

$$\Delta P = \frac{m}{A_t \rho_p} (\rho_p - \rho_g) g = \frac{(1450) (0.1878) (0.3)}{(0.1878) (2300)} (2300 - 1.2) 9.81$$

$$\Delta P = 4265 \text{ Pa}$$

Bed Solids-Gas Equilibrium Depth

The equation relating inlet and outlet temperatures in Section No. can be re-arranged to give (Eq.3.43):

$$\ln \left[\frac{T_{g_i} - T_B}{T_{g_e} - T_B} \right] = \frac{Nu_p 6 (1 - \epsilon_m) L_m}{Pr Re_p \phi \bar{d}_p}$$

If we consider thermal equilibrium is reached when the gas solids temperature difference is reduced by 99%. The equation then simplifies to:

$$L_m = \frac{4.605 Pr Re_p \phi \bar{d}_p}{6 Nu_p (1 - \epsilon_m)}$$

Using typical data from Combustor Run No. 5

$$L_m = \frac{(4.605) (0.639) (0.37) (0.95) (300/10^6)}{(0.0082) (0.6) 6} = 0.011 \text{ m}$$

Heat Transfer Coefficients

(a) Gas-to-Particle

For a bed of 300 micron sand operating at 627 C (Eq.3.40)

$$h_{gp} = 0.03 \frac{k_g}{d_p} Re_p^{1.3} = \frac{0.03 (6.276/10^2) (0.37)^{1.3}}{300/10^6} = 1.7 W/m^2.K$$

(b) Particle-to-Particle

For the same bed conditions and fuel size 2mm. (Eq.3.41)

$$h_{pp} = \frac{2k_g}{d_{pf}} + \frac{0.016}{\sqrt{d_p}} = \frac{2 (6.276/10^5)}{0.002} + \frac{0.016}{\sqrt{300/10^6}}$$

$$h_{pp} = 0.986 kW/m^2.K = 986 W/m^2.K$$

Particle Residence Time.

Particle residence time of a cellulose particle in a Fluidized Bed combustor is given by (Eq.3.90):

$$\Delta t = \frac{\phi d_{pf} \rho_{pf} \bar{C}_{pf}}{6 h_{pp}} \ln \left[\frac{T_B - T_{p1}}{T_B - T_{p2}} \right]$$

$$= \frac{(0.6) (0.002) (540) (2400)}{6 (1000)} \ln \left[\frac{600-100}{600-300} \right] = 0.13 \text{ sec}$$

Bed Behaviour Index

Using Data from Combustion Run No.5 (Eq.3.30,3.31)

$$\zeta = Fr_{mf} Re_{p_{mf}} \left(\frac{\rho_p - \rho_g}{\rho_g} \right) \left(\frac{L_{mf}}{d_t} \right)$$

$$= \frac{(0.15)^2 0.37}{(300/10^6) 9.81} \frac{(2300 - .4)}{0.4} \frac{(0.13)}{(0.489)}$$

$$= 36 \therefore \text{smooth}$$

Estimating Maximum Spouting depth

Taking 530micron sand, inlet diameter 50mm, Bed diameter 489mm, estimates are then:

$$L_{m_{\max}} = 0.72 (.489)^2 / 0.05 = 9.56 \text{ m Eq.3.22}$$

$$L_{m_{\max}} = 0.67 (.489)^{4/3} / (530/10^6)^{1/3} = 3.2 \text{ m Eq.3.23}$$

And there are other correlations see Section 3.2. What is significant is the inconsistency between the results.

Fluidized Bed Wall Heat Transfer Q_{lw}

Taking a 125mm bed it is necessary to consider the insulated wall and the uninsulated area where the gas burners are fitted (300mmx300mm)

Insulated Wall Area

$$h_{conv} = 1.25\theta^{1/3} \quad \text{taking } \theta = 50^\circ\text{C}$$

$$= 4.6 \text{ W/m}^2.\text{K}$$

Taking $h_{wall} = 200 \text{ W/m}^2.\text{K}$, $k_{steel} = 48.5 \text{ W/mK}$, $k_{insl} = 0.098 \text{ W/m.K}$

$$\frac{1}{U} = \frac{1}{4.6} + \frac{1}{200} + \frac{0.1}{0.098} + \frac{0.01}{48.5}$$

$$U = 0.81 \text{ W/m}^2.\text{K}$$

Similarly for the uninsulated area, but taking the outside surface temperature at 50°C , giving $h_{conv} = 9.75 \text{ W/m}^2.\text{K}$

$$\frac{1}{U} = \frac{1}{9.75} + \frac{1}{200} + \frac{0.01}{48.5}$$

$$U = 9.3 \text{ W/m}^2.\text{K}$$

The Heat Transfer for the 125mm of bed wall is therefore estimated at 600C as:

$$Q_{1w} = (\pi (0.7) (0.125) - (0.3) (0.125)) (0.81) (600-25)$$

$$+ (0.3) (0.125) (9.3) (600-25) = 310 \text{ Watts}$$

Estimation of C_{pBe} from other Test Data

If the C_{pBe} value is known for one bed it can be deduced for another using the following process.

Taking C_{pBe} for a 300 mm bed at 1.29, Sand mass is 88.5 kg.

Equating heat capacities:

$$m_B C_{pBe} = m_B C_{pp} + m_{steel} C_{psteel} \text{ which gives}$$

$$88.5 C_{pBe} = (88.5) (0.7) + m_{steel} (0.46)$$

$$\text{Equivalent } m_{steel} = 113.5 \text{ kg}$$

Estimating the volume of steel contacting the sand in the 300mm bed and for a 125mm bed (based on bed plate and wall steel) it is found that the reduction in steel volume is 41.4% therefore the new C_{pBe} is (ie reducing steel mass to 58.6% of original):

$$C_{pBe} = ((34) (0.7) + (0.586) (113.5) (0.46)) / 34$$

$$C_{pBe} = 1.6 \text{ kJ/kg.K}$$

(b) Results Calculations

Air Volumetric Flow Measurement

(a) British Standard Nozzle

Air Flow at free air conditions is given by the Manufacturers formula:

$$\dot{V} = 74.97 k A \sqrt{\frac{h T}{P_a}}$$

where $k = 0.96$
 $A =$ Throat Area of Nozzle dia = 74.95mm
 $h =$ mm of water
 $T =$ Ambient Temperature K
 $P_a =$ Atmospheric pressure Pa.

Since a digital pressure gauge was used instead of the water manometer and 1 mm of water equals 9.81 Pascals the equation becomes:

$$\dot{V} = 74.97 k A \sqrt{\frac{p T}{g P_a}}$$

where $p =$ digital pressure reading in Pa.
 $g =$ gravitational acceleration m/sec²

Considering the original equipment was readable +/-1mm, measurements of air flow corresponding to pressures less than 10 Pascals were not regarded as reliable. A typical calculation would be: eg $p = 50$ Pascals, $T = 300$ K, $P_a = 101300$ Pa.

$$\dot{V} = (74.97) (0.96) \frac{(\pi 0.07495^2)}{4} \sqrt{\frac{(50) (300)}{(9.81) (101300)}}$$

$$\dot{V} = 0.039 \text{ m}^3/\text{sec}$$

Experimental Uncertainty of result

Uncertainties of instruments used are:

Digital pressure gauge	2 Pa
Temperature	1 K
Atmospheric pressure	50Pa

Percentage uncertainty is then :

$$\Delta \dot{V} (\%) = 100 \times \sqrt{[(2/50)^2 + (1/300)^2 + (50/101300)^2]}$$

$$\Delta \dot{V} (\%) = 4 \%$$

(b) Pitot - Static Tube Measurements

The usual equation for incompressible flow is :

$$U = \sqrt{\frac{2(p_s - p_o)}{\rho}}$$

The more exact equation for compressible flow is :

$$\frac{U^2}{2} = C_{pa} T_s \left[1 - \left[\frac{p_o}{p_s} \right]^{\frac{(\gamma-1)}{\gamma}} \right]$$

In both equations P_s is stagnation pressure and P_o is static pressure. A comparison of the results from the two equations for typical data and as pitot-static pressure differences were not large no significant difference in the results were obtained. For simplicity the equation for incompressible flow was used. Air density was calculated using the usual formula:

$$\rho_g = \frac{P_o}{R T}$$

A typical calculation is therefore:

$$\begin{aligned} P_o &= 101399 \text{ Pa} \\ P_s &= 101432 \text{ Pa} \\ P_a &= 101300 \text{ Pa} \\ T &= 300 \text{ K} \\ R &= 287 \text{ kJ/kg.K} \end{aligned}$$

$$\rho = \frac{(101399)}{(287)(300)} = 1.18 \text{ kg/cu.m}$$

$$U = \sqrt{\frac{2(132-99)}{1.18}} = 7.48 \text{ m/sec}$$

The pitot-static tube was used on the flow visualisation test rig in a 21mm diameter tube fitted to the air-flow from the 190mm diameter bed. The flowrate was approximated from the pitot-static tube result which gives the maximum velocity in the tube. The approximation was taken from:

$$\frac{U_{\max}}{U_{\text{average}}} = 1 + 4.07 \sqrt{\frac{f}{8}}$$

Where friction factor f is obtained from the moody diagram. While in theory each calculation would require a calculation of Reynolds number and factor f , in practice it is only necessary to obtain an average factor f for the regime of flows being considered. For 7.48 m/sec, Reynolds number is 10300, f is 0.04 assuming a relative roughness of 0.007. The ratio of maximum velocity to average velocity of 1.29. The flowrate is then given by:

$$\dot{V} = \frac{(7.48) \pi (0.021)^2}{(4)(1.29)} = 0.002 \text{ m}^3/\text{sec}$$

Experimental Uncertainty of Result.
Air density uncertainty

$$\Delta \rho (\%) = 100 \times \sqrt{[(1/300)^2 + (50/101300)^2]} = 0.3\%$$

Velocity uncertainty

$$\Delta U (\%) = 100 \times \sqrt{[(0.3/100)^2 + (2/33)^2]} = 6 \%$$

Flowrate Uncertainty

$$\Delta \dot{V} (\%) = 100 \times \sqrt{[2(0.5/21)^2 + (6/100)^2 + (0.01/1.28)^2]}$$

$$\Delta \dot{V} (\%) = 7\%$$

(c) Rotameter Measurements

The rotameter used is calibrated in cfm which can be converted to m³/sec by multiplying by the conversion factor 4.5/10⁴ m³/sec per cfm.

The uncertainty of measurement is estimated at +/- 1cfm. which is +/- 0.5 l/sec or in the range 2 to 10 % depending on the operating point in the 5-50 cfm, 2-22.5 l/sec range.

Air Mass Flowrate

Air mass flowrate is obtained by simply multiplying the FAD by the density of ambient air in the case of the B.S. Nozzle and the rotameter. Due to the use of a dust bag downstream from the pitot-static tube density for the calculation using the pitot static tube has to be calculated based on static pressure. The calculation is then:

$$\dot{m}_a = \rho_g \dot{V}$$

eg.

$$\dot{m}_a = (1.18) (0.039) = 0.046 \text{ kg/sec}$$

The uncertainty of air mass flow depends on where the volume flow reading was obtained. eg

Mass Flow uncertainties are:

Ex B.S. Nozzle	4%
Ex. Rotameter	2-10% depending on operation point
Ex. Pitot-Static Tube.	2-10% depending on operating point

Superficial Velocities

(a) Flow Visualisation Equipment.

$$U_f = \frac{\dot{V}}{\pi (d_t/2)^2} = \frac{0.002}{\pi (0.19/2)^2} = 0.071 \text{ m/sec}$$

For very deep beds eg $L_m > 500 \text{ mm}$ a slight correction will be obtained if average actual bed gas density is considered in a similar way to calculations for the combustor. For most shallow bed conditions it is sufficient to assume free air density in the bed. Uncertainty of Result is :

$$\Delta U_f (\%) = 100 \times \sqrt{(7/100)^2 + 2(1/190)^2} = 7\%$$

(b) Combustion Equipment

For cold bed conditions:

$$U_f = \frac{\dot{m}_a}{\rho_a \pi (d_t/2)^2} = \frac{0.046}{1.18 \pi (0.489/2)^2} = 0.208 \text{ m/sec}$$

For operations at 600 C

$$U_f = \frac{\dot{m}_a}{\rho_a \pi (d_t/2)^2} = \frac{0.046}{0.4 \pi (0.489/2)^2} = 0.612 \text{ m/sec}$$

Uncertainty of result.

As for flow visualisation equipment, uncertainties will be in the range 5 to 10%.

Fuel Flow Measurement

Equivalent mass flow of fuel is calculated by dividing the mass of the batch by the time elapsed. eg

$$\dot{m}_f = \frac{m_f}{\Delta t} = \frac{1200}{600} = 2 \text{ grams/sec}$$

Uncertainty of results

(a) Batch Feed :	mass batch	300-1500 grams
	mass unc.	10 grams
	time period	10 minutes
	time unc.	0.5 minutes

For a flow rate of 2 grams/sec over a test period of 10 minutes the uncertainty would be:

$$\Delta \dot{m}_f (\%) = 100 \times \sqrt{[(10/1200)^2 + (0.5/10)^2]} = 5 \%$$

(b) Screw Feeder:	mass hopper	3000 grams
	mass unc.	300 grams

$$\Delta \dot{m}_f (\%) = 100 \times \sqrt{[(250/3000)^2 + (0.5/10)^2]} = 10 \%$$

Temperature Measurement

(a) Chart Plotter - Thermocouple Measurements

Chart plotter readings to +/-0.1 division. 0.1 division = 0.5mV

Correlation of Thermocouples is given by equation:

$$T = 134.66 (\text{ChartReading}) + 50$$

eg, For a chart reading of 5.5, voltage is 27.5mV, but using equation directly gives:

$$T = 134.66 (5.5) + 50 = 790C$$

Uncertainty of result.

Chart uncertainty:	0.1 division
Typical % @ 5.5	2 %

(b) Digital Thermometer

Reading uncertainty	1 C
Typical % @ 600C	0.2%

Pressure Measurement

Digital Pressure gauges allowed readings of ± 1 Pascal
Uncertainty of Drop Pressure Calculations are therefore ± 2 Pascals.

Heat Transfer Calculations

(a) Heat Supplied to Air Q_a

$$Q_a = \dot{m}_a \bar{C}_{pa} (T_B - T_o)$$

For $T_B = 600$ C, $T_o = 27$ C, air mass flow of 0.028 kg/sec

Firstly, Evaluating C_{pa} at the two temperatures gives 1.005 and 1.1147, Average C_{pa} is 1.060 kJ/kg.K.

Heat Transferred to the air is therefore:

$$Q_a = (0.028) (1.060) (600 - 27) = 17 \text{ kW}$$

Uncertainty of result,

Taking uncertainties	mass flow	5%
	Temperature	2%

$$\Delta Q_a (\%) = 100 \times \sqrt{(5/100)^2 + (3/575)^2} = 5 \%$$

(b) Heat supplied to Fuel Q_f, Q_w

The calculation is identical to that above except for the addition of α which must be supplied from other calculations.

$$\alpha_f Q_f = \alpha_f \dot{m}_f C_{pf} (T_B - T_o)$$

eg.

$$\alpha_f Q_f = (1) (0.0046) (2.4) (600 - 27) = 6.3 \text{ kW}$$

if Moisture content of fuel was 25% then :

Calculating the enthalpy of steam and water as 3294.3kJ/kg and 113.1 kJ/kg, the calculation is:

$$\alpha_w Q_w = \alpha_w \dot{m}_w (h_B - h_o)$$

$$\alpha_w Q_w = (1) (0.25) (0.0046) (3294.3 - 113.1) = 3.6 \text{ kW}$$

Uncertainty percentages for both fuel and moisture calculations will be the same. Uncertainty in moisture content reading is considered negligible.

Uncertainty of result,
Taking Uncertainties

Mass flow	5% Batch feed
Mass flow	10% Screw feed
Temperature	2%

For Batch feed

$$\Delta Q_f (\%) = 100 \times \sqrt{(5/100)^2 + (3/575)^2} = 5 \%$$

For Screw feed

$$\Delta Q_f (\%) = 100 \times \sqrt{(10/100)^2 + (3/575)^2} = 10 \%$$

(c) Heat supplied to the bed solids Q_B

$$Q_B = m_B C_{pBe} \frac{(T_{B_2} - T_{B_1})}{(t_2 - t_1)}$$

$$Q_B = (80) (1.2) \frac{(650 - 600)}{(3600 - 3000)} = 8 \text{ kW}$$

The most uncertain term in the equation is C_{pBe} which is obtained by iterative calculations from data from two different run periods. From the consistency of the values obtained it is estimated to have an uncertainty of 10%.

Uncertainty of Results is therefore:

Taking uncertainties as	Mass	1kg
	C_{pBe}	10%
	Temperature	10%
	Time	5%

$$\Delta Q_B (\%) = 100 \times \sqrt{((1/80)^2 + (10/100)^2 + (10/100)^2 + (.5/10)^2)}$$

$$\Delta Q_B (\%) = 15 \%$$

(d) Total Heat Release in the Bed

The total heat release is just the sum of all the individual heat transfers:

$$Q_{total} = Q_a + Q_B + \alpha_f Q_f + \alpha_w Q_w + Q_{lw}$$

Assuming Q_{lw} is 0.8 kW,

$$Q_{total} = 17 + 8 + 6.3 + 3.6 + 0.8 = 35.7 \text{ kW}$$

Uncertainty is:

$$\Delta Q_{total} (\%) = \frac{\sqrt{(0.85^2 + 1.2^2 + .63^2 + .36^2 + 0.08^2)}}{35.7} \times 100 = 5 \%$$

(e) Combustion Efficiency

which is , using $CV = 19500 \text{ kJ/kg}$; (Eq.3.49)

$$\eta_c = \frac{Q_{total}}{\dot{m}_f CV} = \frac{35.7}{(0.0046)(19500)} = 0.398 \text{ or } 40\%$$

The uncertainties are:

$$\Delta \eta_c (\%) = 100 \times \sqrt{((5/100)^2 + (10/100)^2 + (0.5/19.5)^2)} = 11\%$$

(f) Fluidized Bed Efficiency

The maximum useful heat release to the bed must first be calculated (Eq.3.55):

$$Q_{B_{max}} = \dot{m}_f CV - (Q_a + \alpha_f Q_f + \alpha_w Q_w + Q_{lw})$$

eg.

$$Q_{B_{max}} = (0.0046)(19500) - (17 + 6.3 + 3.6 + 0.8) = 62 \text{ kW}$$

Then Fluidized Bed Efficiency is (Eq.3.59):

$$\eta_B = \frac{Q_B}{Q_{B_{max}}} = \frac{8}{62} = 0.129 \text{ or } 13\%$$

Uncertainty of Results.

$$\Delta (\dot{m}_f CV) = (89.7) \sqrt{\left(\frac{1}{10}\right)^2 + \left(\frac{.5}{19.5}\right)^2} = 9.3 \text{ kW}$$

$$\Delta Q_{B_{\max}} = \sqrt{(9.3^2 + (\sqrt{(.85^2 + .63^2 + .36^2 + .08^2)})^2} = 9.4 \text{ kW}$$

$$\Delta \eta_B (\%) = 100 \times \sqrt{(9.4/62)^2 + (15/100)^2} = 0.213 \text{ or } 21\%$$

(g) Operating Ratio.

Firstly the maximum possible useful heat transfer must be calculated (Eq.3.57).

$$Q_{B_{th\max}} = \dot{m}_f (CV - (T_B - T_O) \left(\left(\frac{\dot{m}_a}{\dot{m}_f} \right)_{st} \bar{C}_{pa} + \alpha_f C_{pf} \right)$$

eg

$$Q_{B_{th\max}} = (.0046) (19500 - (600 - 27) ((5.09) (1.06) + (2.4)))$$

$$Q_{B_{th\max}} = 69.2 \text{ kW}$$

Operating Ratio is then simply. (Eq.3.58):

$$O_r = \frac{Q_{B_{\max}}}{Q_{B_{th\max}}} = \frac{62}{69.2} = 0.896 \text{ or } 90 \%$$

Uncertainty of Result.

$$\Delta Q_{B_{th\max}} (\%) = 100 \times \sqrt{(10/100)^2 + (500/15000)^2} = 11 \%$$

$$\Delta O_r (\%) = 100 \times \sqrt{(11/100)^2 + (9.4/62)^2} = 19\%$$

(h) Overall Bed Efficiency
(Eq.3.60)

$$\eta_{BC} = \frac{Q_B}{\dot{m}_f CV} = \frac{8}{89.7} = 0.089 \text{ or } 9\%$$

Uncertainty of result.

$$\Delta \eta_{BC} (\%) = 100 \times \sqrt{(9.3/89.7)^2 + (15/100)^2} = 0.182 \text{ or } 18\%$$

(i) Packed Bed Heat Flux
(Eq.3.45)

$$\psi = \frac{\dot{m}_f CV \eta_c}{A_t L_m} = \frac{(0.0046) (19500) (0.4)}{(0.1878) (0.30)} = 637 \text{ kW/m}^3$$

The uncertainty of the result is:

$$\Delta \psi (\%) = 100 \times \sqrt{(0.1^2 + 0.1^2 + 0.02^2 + 0.001^2 + 0.003^2)}$$

$$\Delta \psi = 15\%$$

Air/Fuel Ratio

Using typical data gives:

$$\text{Air/fuel ratio} = \frac{\dot{m}_a}{\dot{m}_f} = \frac{0.028}{0.0046} = 6.09$$

The uncertainty of the result is:

$$\Delta (\text{Air/Fuel}) \% = 100 \times \sqrt{(0.1^2 + 0.1^2)} = 15 \%$$

(c) Iterative Spreadsheet Calculations

Determination of C_{pBe} from Cooldown Data

Table A1 : Iterative Determination of C_{pBe}

Ref .No .	Time mins	Temp C	Q_a kW	Energy Stored in Bed, kW	Q_B kW**	Q_{tot} kW
1	112	501		54702		
2	118	467	7.59	50858	-10.68	-3.09
3	128	427	6.87	46246	-7.69	-0.82
4	134	407	6.51	43940	-6.41	0.11
5	138	387	6.15	41634	-9.61	-3.45
6	147	353	5.57	37790	-7.12	-1.55
					Average Q_{tot} is	-1.759
7	148	353	0	37790	0	0
8	178	330	0	35168	-1.456	-1.456
				h_{conv} A	0.0046	
				Calculate Average Q_i in Per.2-6	1.76	
				Selected C_{pBe}	1.29	
				$m_B C_{pBe}$	114.17	

** Calculated on the change in energy stored during the time from the Ref.No. preceding to the present instant.

Calculation Procedure (See Vol.1 Section 3.41, Eqs.3.63-3.66)

Select C_{pBe} and calculated $m_B C_{pBe}$ using known mass of sand Q_B is calculated from the change in energy stored divided by time. The energy stored is obtained from the $m_B C_{pBe}$ value selected and obtained iteratively.

The total heat release in the bed Q_{tot} is firstly summed and averaged in this case from $t = 118$ mins to $t = 147$ mins. The average Q_{tot} during cooldown must be slightly negative and will equal the wall convection losses since the heat removed in the flue gases plus wall losses must equal the heat lost from the bed. (note: This is the cooling period with airflow)

The $h_{conv}A$ for the combustor found by dividing the average Q_{tot} by the average combustor-surroundings temperature difference from $t = 148$ mins to $t = 178$ mins (note: This is the cooling period without airflow)

Having found $h_{conv}A$ a calculation of the wall loss Q_l is made for the period $t = 118$ mins to $t = 147$ mins and compared with the figure calculated for Q_{tot} . If they are equal, as shown, calculations are complete. If they are not equal a new value for C_{pBe} is chosen, which modifies $m_B C_{pBe}$, which in turn changes Q_B etc and the process is repeated until the calculated Q_l equals the actual Q_l for the period of cooling with air. The resulting C_{pBe} is taken as the equivalent specific heat for bed structure and solids. The process is greatly facilitated by the use of a spreadsheet.

Estimated Particle Fall Times.

Calculations were done iteratively to calculate approximate fall times and then average h_{gp} values to generate approximate values for particle temperature at bed entry for continuously fed fuel particles. The iterative calculation was necessary as the fall distances were relatively short and particles did not reach terminal velocities in most cases. Calculations are as detailed in Vol.1, Section.3.43. An example

Table A2. Fuel Particle Fall Time and Distance Estimation

Fuel Data per particle									
Bagasse					Si units				
Type	Length	Diameter	Density	Sphericity	4412 micron	0.004412 m	543 micron	0.000543 m	540 kg/cu.m
300 micron	400 mm	0.135 m/s	0.37 kg/cu.m	4.00E-05 Pa.s	0.61	0.614017	1250 micron	0.00125 m	5.5E-07 kg
675 C	9.48E-03 kg/sec	A	2.145 Volume	Mass	5.5E-07 kg	1.0E-09 cu.m	5 %	5 %	5 %
Re	p	C	d	C	Relative Velocity	Drag Force	Absolute Velocity	Velocity Increment	Distance Increment
Spherical					m/sec	N	m/sec	m/sec	m
d	C	d	C	d	actual	actual	0	0	0
7.9645	2.1627	17.2245	8.3205	6.7320	0.1350	1.4E-07	-0.47742	0.477422	-0.02387
3.7394	2.2251	8.3205	6.7320	6.1363	0.6124	1.4E-06	-0.84095	0.363529	-0.04205
2.9622	2.2726	6.7320	6.1363	5.8768	0.9760	2.9E-06	-1.07092	0.229972	-0.05355
2.6648	2.3027	6.1363	5.8768	5.7583	1.2059	4.0E-06	-1.19898	0.128055	-0.05995
2.5337	2.3195	5.8768	5.7583	5.7032	1.3340	4.7E-06	-1.26479	0.065809	-0.06324
2.4734	2.3281	5.7583	5.7032	5.6775	1.3998	5.1E-06	-1.29712	0.03233	-0.06486
2.4453	2.3323	5.7032	5.6775	5.6655	1.4321	5.2E-06	-1.31264	0.015517	-0.06563
2.4322	2.3343	5.6775	5.6655	5.6598	1.4476	5.3E-06	-1.32347	0.007362	-0.06617
2.4260	2.3353	5.6655	5.6598	5.6572	1.4550	5.4E-06	-1.32511	0.003474	-0.06626
2.4231	2.3357	5.6598	5.6572	5.6559	1.4585	5.4E-06	-1.32587	0.001635	-0.06631
2.4218	2.3360	5.6572	5.6559	5.6554	1.4601	5.4E-06	-1.32624	0.000768	-0.06632
2.4211	2.3361	5.6559	5.6554	5.6551	1.4609	5.4E-06	-1.32648	0.000361	-0.06633
2.4208	2.3361	5.6554	5.6551	5.6549	1.4612	5.4E-06	-1.32652	0.00017	-0.06633
2.4207	2.3361	5.6551	5.6550	5.6549	1.4614	5.4E-06	-1.32654	0.00008	-0.06633
2.4206	2.3361	5.6550	5.6549	5.6549	1.4615	5.4E-06	-1.32654	0.000037	-0.06633
2.4206	2.3361	5.6549	5.6549	5.6549	1.4615	5.4E-06	-1.32654	0.000018	-0.06633
2.4206	2.3362	5.6549	5.6549	5.6549	1.4615	5.4E-06	-1.32654	-0.00013	1.061232
17.0670									
17.0668									
17.0664									
17.0654									
17.0634									
17.0592									
17.0503									
17.0312									
16.9906									
16.9046									
16.7234									
16.3459									
15.5774									
14.0821									
11.3966									
7.1515									
1.5765									
Average					Average				
Total					Total				
Distance					Distance				
Increment					Increment				
m					m				
0					0				
-0.02387					-0.02387				
-0.06592					-0.06592				
-0.11946					-0.11946				
-0.17941					-0.17941				
-0.24265					-0.24265				
-0.30751					-0.30751				
-0.37314					-0.37314				
-0.43914					-0.43914				
-0.50531					-0.50531				
-0.57157					-0.57157				
-0.63786					-0.63786				
-0.70418					-0.70418				
-0.7705					-0.7705				
-0.83682					-0.83682				
-0.90315					-0.90315				
0.158086					0.158086				

Appendix B : Experimental Data and U_f/U_{mf} Charts

TABLE B1. Flow Visualisation Data 180 micron Sand

Ambient Conditions			PRESSUR	101670 Pa		
			TEMP	24.5 C		
			DENSITY	1.19 kg/cu.m		
Bed Conditions			Sand size	180 microns		
			Umf	0.024 m/s		
			Distributor	100 mesh		
			Bed Depth	330 mm		
MOTOR SPEED Hz	PITOT Pa Pa	STATIC Pa	PITOT TEMP C	BELOW PLATE Press.kPa	BED BASE PRES kPa	BED TOP PRESS kPa
0		0	0	0	0	0
17	72	68	24	4.72	4.48	0.51
18	117	106	25	5.14	4.85	0.84
19	168	151	24	5.63	5.32	1.23
20	217	192	24	6.15	5.82	1.68
20	240	213	24	6.09	5.75	1.45
21	278	247	24	6.67	6.31	2.13
				0	0	0

TABLE B2. Flow Visualisation Data 180 micron Sand

Ambient Conditions			PRESSURE	101670 Pa		
			TEMP	24.5 C		
			DENSITY	1.19 kg/cu.m		
Bed Conditions			Sand size	180 microns		
			Umf	0.024 m/s		
			Bed depth	440 mm		
			Distributor	Mesh and packed bed.		
MOTOR SPEED Hz	PITOT Pa Pa	STATIC Pa	PITOT TEMP C	BELOW PLATE Press.kPa	BED BASE PRES kPa	BED TOP PRESS kPa
0		0	0	0	0	0
17	42	40	25	4.81	4.69	0.27
18	47	44	25	5.31	5.2	0.33
19	63	59	25	5.89	5.73	0.47
20	82	75	25	6.45	6.22	0.66
21	133	115	25	7.07	6.74	1.13
22	193	173	25	7.55	7.22	1.67
23	238	211	25	8.11	7.73	2.11
24	284	252	25	8.74	8.37	2.69

TABLE B3. Flow Visualisation Data 180 micron Sand

Ambient Conditions			PRESSUR	101670 Pa		
			TEMP	24.5 C		
			DENSITY	1.19 kg/cu.m		
Bed Conditions			Sand size	180 microns		
			Umf	0.024 m/s		
			Distributor	100 mesh		
			Bed depth	590 mm		
MOTOR SPEED Hz	PITOT Pa Pa	STATIC Pa	PITOT TEMP C	BELOW PLATE Press.kPa	BED BASE PRES kPa	BED TOP PRESS kPa
0		0	0	0	0	0
18	41	38	25	6.81	6.65	0.35
19	46	43	25	7.58	7.43	0.42
20	68	59	25	8.35	8.1	0.7
21	105	94	25	9.1	8.83	1.06
22	165	149	25	9.77	9.47	1.82
23	218	196	25	10.44	10.08	2.41
24	280	245	25	11.26	10.88	3.2

TABLE B4. Flow Visualisation Data 180 micron Sand

Ambient Conditions		PRESSUR	101350 Pa					
		TEMP	25 C					
		DENSITY	1.18502 kg/cu.m					
Bed Conditions		Sand size	180 microns					
		Umf	0.0246 m/s					
		Bed depth	185 mm					
		Distributor	Mesh and packed bed.					
Bagasse Added		Nil						
MOTOR SPEED Hz	PITOT Pa Pa	STATIC Pa	PITOT TEMP C	BELOW PLATE Press.kPa	BASE PRES kPa	BED TOP PRESS kPa	Bed Depth expanded mm	Comments
0		0	0	0	0	0	185	Good Mixing
15	12	11	24	1.66	1.51	0.02	185	
16	16	13	24	1.9	1.72	0.02	185	
17	19	16	24	2.15	1.96	0.03	190	
18	29	24	24	2.37	2.13	0.05	195	
19	85	73	24	2.46	2.24	0.15	200	
19.5	108	85	24	2.53	2.29	0.18	200	
20	131	98	24	2.63	2.38	0.22	205	Turbulent
21	183	145	24	2.77	2.49	0.32	210	

TABLE B5. Flow Visualisation Data 180 micron Sand

Ambient Conditions		PRESSUR	101350 Pa					
		TEMP	25 C					
		DENSITY	1.185 kg/cu.m					
Bed Conditions		Sand size	180 microns					
		Umf	0.024 m/s					
		Bed depth	185 mm					
		Distributor	Mesh and packed bed.					
Bagasse Added		47.6grams added to base of bed						
MOTOR SPEED Hz	PITOT Pa Pa	STATIC Pa	PITOT TEMP C	BELOW PLATE Press.kPa	BASE PRES kPa	TOP PRESS kPa	Bed Depth expanded mm	Comments
0		0	0	0	0	0		
15	20	17	24	1.65	1.46	0.03	185	
16	25	22	24	1.89	1.7	0.04	185	
17	30	26	24	2.13	1.9	0.05	185	
18	35	30	24	2.37	2.12	0.05	190	
19	41	36	24	2.61	2.34	0.06	195	
20	130	102	24	2.89	2.36	0.2	200	
21	180	137	24	2.79	2.5	0.3	200	
20	125	99	24	2.63	2.36	0.2	205	Good Mixing
19	78	69	24	2.46	2.2	0.12	210	Dead Spot
18	40	31	24	2.32	2.09	0.07	210	Remained
28	693	423	24	4.31	3.72	1.4	265	All mixed

TABLE B6. Flow Visualisation Data 180 micron Sand

Ambient Conditions		PRESSUR	101350 Pa					
		TEMP	25 C					
		DENSITY	1.185 kg/cu.m					
Bed Conditions		Sand size	180 microns					
		Umf	0.024 m/s					
		Bed depth	190 mm					
		Distributor Mesh and packed bed.						
Bagasse Added		47.6 grams pre-mixed						
MOTOR SPEED Hz	PITOT Pa Pa	STATIC Pa	PITOT TEMP C	BELOW PLATE Press.kPa	BASE PRES kPa	BED TOP PRESS kPa	Bed Depth expanded mm	Comments
0		0	0	0	0	0		
15	16	13	25	1.67	1.5	0.04	190	
16	20	16	25	1.9	1.71	0.04	190	
17	24	20	25	2.14	1.93	0.04	190	
18	60	38	25	2.29	2.09	0.05	190	
19	105	85	25	2.4	2.18	0.18	195	
20	150	110	25	2.56	2.28	0.25	200	
21	193	135	25	2.74	2.48	0.31	205	Good Mixing

TABLE B7. Flow Visualisation Data 180 micron Sand

Ambient Conditions		PRESSURE		101350 Pa				
		TEMP		25 C				
		DENSITY		1.185 kg/cu.m				
Bed Conditions		Sand size		180 microns				
		Umf		0.024 m/s				
		Bed depth		190 mm				
		Distributor		Mesh and packed bed.				
Bagasse Added		47.6 grams added and premixed.						
		46.3grams added to top						
MOTOR SPEED Hz	PITOT Pa Pa	STATIC Pa	PITOT TEMP C	BELOW PLATE Press.kPa	BASE PRES kPa	TOP PRESS kPa	Bed Depth expanded mm	Comments
0		0	0	0	0	0		
16	20	17	25	1.9	1.74	0.04	190	
17	23	20	25	2.15	1.97	0.04	190	
18	34	27	25	2.37	2.15	0.07	190	
19	102	80	25	2.42	2.2	0.18	200	
20	152	120	25	2.56	2.03	0.24	205	
21	195	151	25	2.75	2.25	0.34	205	Good Mixing

TABLE B8. Flow Visualisation Data 180 micron Sand

Ambient Conditions		PRESSURE	101350 Pa					
		TEMP	25 C					
		DENSITY	1.185 kg/cu.m					
Bed Conditions		Sand size	180 microns					
		Umf	0.024 m/s					
		Bed depth	195 mm					
		Distributor	Mesh and packed bed.					
Bagasse Added		93.9 grams added and premixed.						
MOTOR SPEED Hz	PITOT Pa Pa	STATIC Pa	PITOT TEMP C	BELOW PLATE Press.kPa	BASE PRES kPa	TOP PRESS kPa	Bed Depth expanded mm	Comments
0		0	0	0	0	0		
16	34	29	25	1.84	1.63	0.06	195	
17	48	41	25	2.06	1.73	0.08	195	
18	65	55	25	2.25	1.79	0.1	190	
19	102	87	25	2.42	1.91	0.17	195	
20	150	120	25	2.56	2.06	0.26	200	Sticky mix
21	200	152	25	2.75	2.23	0.36	205	Good Mixing

TABLE B9. Flow Visualisation Data 180 micron Sand

Ambient Conditions		PRESSUR	101350 Pa					
		TEMP	25 C					
		DENSITY	1.185 kg/cu.m					
Bed Conditions		Sand size	180 microns					
		Umf	0.024 m/s					
		Bed depth	195 mm					
		Distributor	Mesh and packed bed.					
		Ingestion time	22.5 seconds					
Bagasse Added		93.9 grams added and premixed.						
		43.4grams added to top, Bed started at U>Umf						
MOTOR SPEED Hz	PITOT Pa Pa	STATIC Pa	PITOT TEMP C	BELOW PLATE Press.kPa	BASE PRES kPa	BED TOP PRESS kPa	Bed Depth expanded mm	Comments
0		0	0	0	0	0		
21	200	152	25	2.75	2.23	0.36	205	A
22	275	201	25	2.87	2.28	0.48	210	B
23	320	231	25	3.12	2.44	0.61	220	C
24	386	268	25	3.35	2.66	0.73	230	D
0	0	0	0	0	0	0	0	
0	0	A/ Dead zone developed					0	
0	0	B/ Dead Zone still there					0	
0	0	C/ Small dead zone remaining					0	
		D/ Good Mixing						

TABLE B10. Flow Visualisation Data 180 micron Sand

Ambient Conditions		PRESSUR	101350 Pa					
		TEMP	25 C					
		DENSITY	1.185 kg/cu.m					
Bed Conditions		Sand size	180 microns					
		Umf	0.024 m/s					
		Bed depth	195 mm					
		Distributor	Mesh and packed bed.					
Bagasse Added		137.3 grams added and premixed.						
MOTOR SPEED Hz	PITOT Pa Pa	STATIC Pa	PITOT TEMP C	BELOW PLATE Press.kPa	BASE PRES kPa	TOP PRESS kPa	Bed Depth expanded mm	Comments
0		0	0	0	0			
16	53	45	25.5	1.77	1.45	0.09	195	
17	72	61	25.5	1.96	1.58	0.12	195	
18	95	81	25.5	2.17	1.72	0.17	198	
19	121	98	25.5	2.36	1.84	0.22	198	
20	148	117	25.5	2.58	1.99	0.26	200	
21	229	172	25.5	2.69	2.11	0.41	205	70% mix
22	282	206	25.5	2.87	2.29	0.53	210	
24	388	270	25.5	3.34	2.66	0.75	230	good mix
		0	0	0	0			

TABLE B11. Flow Visualisation Data 180 micron Sand

Ambient Conditions		PRESSUR	101350 Pa					
		TEMP	25 C					
		DENSITY	1.185 kg/cu.m					
Bed Conditions		Sand size	180 microns					
		Umf	0.024 m/s					
		Bed depth	210 mm					
		Distributor	Mesh and packed bed.					
Bagasse Added		234.6 grams added and premixed.						
		Ingestion time of 97.3 g in 34 secs, Pp=388Pa, Ps=270Pa, proir to test						
MOTOR SPEED Hz	PITOT Pa Pa	STATIC Pa	PITOT TEMP C	BELOW PLATE Press.kPa	BED BAS PRES kPa	BED TOP PRESS kPa	Bed Dept expanded mm	Comments
0		0	0	0	0			
20	206	144	26	2.47	2.05	0.41	215	
21	360	263	26	2.44	2.14	0.72	225	
22	392	276	26	2.72	2.36	0.76	225	
24	494	331	26	3.2	2.77	0.97	230	
26	594	396	26	3.78	3.18	1.26	240	50% fluidized
28	710	464	26	4.34	3.44	1.51	250	
30	847	534	26	4.92	3.85	1.84	260	good mix
		0	0	0	0			

TABLE B12. Flow Visualisation Data 490 micron Sand

Ambient Conditions		PRESSURE		101000 Pa				
		TEMP		27 C				
		DENSITY		1.173 kg/cu.m				
Bed Conditions		Sand size		490 microns				
		Umf		0.178 m/s				
		Bed depth		215 mm				
		Distributor		Mesh and packed bed.				
Bagasse Added		nil						
MOTOR SPEED Hz	PITOT Pa Pa	STATIC Pa	PITOT TEMP C	BELOW PLATE Press.kPa	BASE PRES kPa	TOP PRESS kPa	Bed Depth expanded mm	Comments
11	132	99	27	1.76	1.58	0.24	215	good mixin
12	181	131	27	2.24	1.99	0.34	215	
13	224	158	27	2.6	2.32	0.42	215	
14	290	199	27	3.18	2.88	0.56	215	
15	348	228	27	3.64	3.26	0.68	215	
16	489	310	27	3.98	3.62	0.99	220	
17	602	375	27	4.49	3.97	1.2	225	
18	731	432	27	5.01	4.31	1.51	230	
19	854	498	27	5.55	4.57	1.79	240	
20	984	564	27	6.11	4.93	2.12	245	
21	1150	627	27	6.25	5.28	2.48	250	almost slugging
22	1295	694	27	7.42	5.69	2.86	250	

TABLE B13. Flow Visualization Data 490 micron Sand

Ambient Conditions			PRESSURE 101700 Pa					
			TEMP 23 C					
			DENSITY 1.197 kg/cu.m					
Bed Conditions			Sand size 490 microns					
			Umf 0.178 m/s					
			Bed depth 215 mm					
			Distributor Mesh and packed bed.					
Bagasse Added			44.9 grams to base					
MOTOR SPEED Hz	PITOT Pa Pa	STATIC Pa	PITOT TEMP C	BELOW PLATE Press.kPa	BASE PRES kPa	TOP PRESS kPa	Bed Depth expanded mm	Comments
				0				
12	193	147	22	2.2	2.05	0.31	215	
13	237	176	22	2.6	2.45	0.41	215	
14	377	257	22	3.16	2.94	0.69	215	
15	458	310	22	3.6	3.37	0.87	215	
16	546	349	22	4.13	3.85	1.06	215	
17	710	440	22	4.57	4.17	1.44	230	
18	821	498	22	5.03	4.45	1.65	235	
19	940	555	22	5.58	4.8	1.85	240	
20	1080	619	22	6.18	5.11	2.24	250	90% mixing
21	1230	693	22	6.83	5.54	2.61	255	
22	1384	744	22	7.48	5.87	2.93	255	
23	1505	802	22	8.08	6.22	3.27	260	
Bagasse Still not mixed								

TABLE B14. Flow Visualization Data 490 micron Sand

Ambient Conditions		PRESSUR	101700 Pa					
		TEMP	23 C					
		DENSITY	1.197 kg/cu.m					
Bed Conditions		Sand size	490 microns					
		Umf	0.178 m/s					
		Bed depth	215 mm					
		Distributor	Mesh and packed bed.					
Bagasse Added		44.9 grams		pre-mixed				
MOTOR SPEED Hz	PITOT Pa Pa	STATIC Pa	PITOT TEMP C	BELOW PLATE Press.kPa	BED BASE PRES kPa	BED T PRESS kPa	Bed Depth expanded mm	Comments
12	166	105	22	2.27	2.07	0.33	220	good mixin
14	305	184	22	3.25	3	0.64	220	
16	510	290	22	4.09	3.75	1.1	220	
18	749	405	22	5.06	4.46	1.66	230	
20	992	519	22	6.17	5.06	2.24	250	
22	1275	645	22	7.39	5.8	2.91	255	

TABLE B15. Flow Visualization Data 490 micron Sand

Ambient Conditions			PRESSURE 101700 Pa					
			TEMP 23 C					
			DENSITY 1.197 kg/cu.m					
Bed Conditions			Sand size 490 microns					
			Umf 0.178 m/s					
			Bed depth 215 mm					
			Distributor Mesh and packed bed.					
Bagasse Added			44.9 grams pre-mixed					
			56.9 grams added to top, mixed during run up					
MOTOR SPEED Hz	PITOT Pa Pa	STATIC Pa	PITOT TEMP C	BELOW PLATE Press.kPa	BASE PRES kPa	TOP PRESS kPa	Bed Depth expanded mm	Comments
12	191	130	22	2.27	2.12	0.36	220	slow ingest
14	298	194	22	3.33	3.1	0.59	220	
15	378	231	22	3.77	3.5	0.76	220	
16	519	310	22	4.14	3.82	1.06	230	
16	505	298	22	4.18	3.83	1.06	220	
17	665	380	22	4.63	4.2	1.41	230	all ingest
18	776	438	22	5.02	4.44	1.69	240	
19	902	486	22	5.53	4.71	1.97	245	dead zones good mix
20	1031	548	22	6.12	5.01	2.31	250	
22	1295	661	22	7.36	5.8	2.91	255	
24	1613	786	22	8.62	6.54	3.65	260	

TABLE B16. Flow Visualization Data 490 micron Sand

Ambient Conditions		PRESSUR	101700 Pa					
		TEMP	23 C					
		DENSITY	1.197 kg/cu.m					
Bed Conditions		Sand size	490 microns					
		Umf	0.178 m/s					
		Bed depth	240 mm					
		Distributor	Mesh and packed bed.					
Bagasse Added		101.8 grams	pre-mixed					
		43 grams	added to top, mixed during run up					
MOTOR SPEED Hz	PITOT Pa Pa	STATIC Pa	PITOT TEMP C	BELOW PLATE Press.kPa	BED BASE PRES kPa	BED T PRESS kPa	Bed Depth expanded mm	Comments
15	448	260	23	3.58	3.28	0.97	240	Channelling
	638	361	23	4.56	4.15	1.39	240	
20	1013	527	23	6.15	5.12	2.26	250	50%fluid 80% fluid good mix seperation
22	1315	653	23	7.32	5.8	2.97	250	
24	1637	784	23	8.57	6.55	3.76	255	
26	1960	910	23	9.93	7.01	4.58	265	
28	2330	1050	23	11.34	8.39	5.44	300	
22	1185	568	23	7.56	5.65	2.74	250	

TABLE B17. Flow Visualisation Data Centre Flow 490 micron Sand

Ambient Conditions		PRESSUR		102000 Pa		
		TEMP		26.5 C		
		DENSITY		1.19 kg/cu.m		
Bed Conditions		Sand size		490 microns		
		Umf		0.178		
		Distributor		Five caps in centre		
		Bed Depth		180 mm		
MOTOR SPEED Hz	PITOT Pa Pa	STATIC Pa	PITOT TEMP C	BELOW PLATE PRESS	BASE PRES KPA	TOP PRESS KPA
0		0	0	0	0	0
14	264	142	26	2.87	2.07	0.56
15	352	191	26	3.29	2.42	0.76
16	490	250	26	3.59	2.63	1.07
17	620	310	26	4.04	2.95	1.38
18	740	360	26	4.41	3.2	1.62
19	870	415	26	4.85	3.5	1.93
20	1010	470	26	5.32	3.82	2.25
21	1160	520	26	5.82	4.18	2.59
22	1293	573	26	6.32	4.5	2.91
23	1430	626	26	6.81	4.84	3.25
24	1594	682	26	7.36	5.2	3.6

TABLE B18. Flow Visualisation Data Centre Flow 490 micron Sand

Ambient Conditions		PRESSURE	101900 Pa			
		TEMP	27 C			
		DENSITY	1.18 kg/cu.m			
Bed Conditions		Sand size	490 microns			
		Umf	0.178			
		Distributor	Five caps in centre			
		Bed Depth	365 mm			
MOTOR SPEED Hz	PITOT Pa Pa	STATIC Pa	PITOT TEMP C	BELOW PLATE PRESS	BASE PRES KPA	TOP PRESS KPA
0		0	0	0	0	0
12	128	82	26	3.14	2.42	0.31
13	164	102	26	3.82	2.86	0.33
14	271	160	26	5.29	4.14	0.6
15	348	193	26	6.06	5	0.73
16	580	300	26	6.63	5.53	1.31
17	821	390	26	7.43	6.03	1.85
18	1000	450	26	8.04	6.48	2.35
19	1220	550	26	8.83	7	2.77
20	1450	638	26	9.75	7.65	3.37

TABLE B19. Flow Visualisation Data Small Cone 490 micron Sand

Ambient Conditions		PRESSUR		102000 Pa		
		TEMP		27 C		
		DENSITY		1.18 kg/cu.m		
Bed Conditions		Sand size		490 microns		
		Umf		0.178		
		Distributor		100 Mesh		
		Cone		Dias:76,114mm; Height:113mm		
		Bed Depth		245 mm		
MOTOR SPEED Hz	PITOT Pa Pa	STATIC Pa	PITOT TEMP C	BELOW PLATE PRESS	BASE PRES KPA	TOP PRESS KPA
0		0	0	0	0	0
11	134	85	26.5	2.03	1.9	0.26
12	207	128	26.5	2.72	2.54	0.44
13	271	161	26.5	3.19	2.99	0.57
14	412	233	26.5	4.08	3.86	0.9
15	556	303	26.5	4.6	4.31	1.21
16	695	371	26.5	5.24	4.73	1.56
17	867	444	26.5	5.91	5.2	1.95
18	1012	510	26.5	6.47	5.58	2.32
19	1200	575	26.5	7.19	6	2.74
20	1363	647	26.5	7.95	6.42	3.16

TABLE B20. Flow Visualisation Data Large Cone 490 micron Sand

Ambient Conditions		PRESSURE		102000 Pa		
		TEMP		27 C		
		DENSITY		1.18 kg/cu.m		
Bed Conditions		Sand size		490 microns		
		Umf		0.178		
		Distributor		100 Mesh		
		Cone		Dias:75,150mm; Height:214mm		
		Bed Depth		260 mm		
MOTOR SPEED Hz	PITOT Pa Pa	STATIC Pa	PITOT TEMP C	BELOW PLATE PRESS	BASE PRES KPA	TOP PRESS KPA
0		0	0	0	0	0
11	126	80	26.5	2.32	2.15	0.25
12	192	117	26.5	3.02	2.8	0.4
14	375	214	26.5	4.37	4.04	0.81
16	732	383	26.5	5.37	4.89	1.63
17	910	459	26.5	6.08	5.24	2.1
18	1020	510	26.5	6.71	5.58	2.4
19	1170	560	26.5	7.5	5.9	2.75
20	1350	641	26.5	8.34	6.34	3.17

TABLE B21. Flow Visualisation Data, Spouted Bed, Draft Tube, 490 micron Sand

Ambient Conditions			PRESSUR	101600 Pa		
			TEMP	29 C		
			DENSITY	1.17 kg/cu.m		
Bed Conditions			Sand size	490 microns		
			Umf	0.178		
			Distributor	Five Caps in Centre		
			Tube	Dia:104mm ID; Height: 445mm		
			Bed Depth	515 mm		
MOTOR SPEED Hz	PITOT Pa Pa	STATIC Pa	PITOT TEMP C	BELOW PLATE PRESS	BASE PRES KPA	TOP PRESS KPA
0		0	0	0	0	0
16	192	119	29	5.36	4.57	0.38
18	266	161	29	6.67	5.76	0.57
19	409	230	29	7.16	6.16	0.84
20	610	350	29	7.6	6.35	1.3
21	800	450	29	8.2	7	1.9
25	1690	800	29	10.53	8.75	3.6

TABLE B22. Flow Visualisation Data, Reverse Circulation, 490 micron Sand

Ambient Conditions			PRESSUR	101800 Pa		
			TEMP	27 C		
			DENSITY	1.18 kg/cu.m		
Bed Conditions			Sand size	490 microns		
			Umf	0.178		
			Distributor	Six Caps in Annulus		
			Bed Depth	110 mm		
MOTOR SPEED Hz	PITOT Pa Pa	STATIC Pa	PITOT TEMP C	BELOW PLATE PRESS	BASE PRES KPA	TOP PRESS KPA
0		0	0	0	0	0
11	198	126	26	1.63	1.22	0.39
12	278	167	26	2.1	1.68	0.57
13	404	225	26	2.39	2.04	0.84
14	571	310	26	2.89	2.41	1.26
15	693	363	26	3.27	2.68	1.52
16	830	420	26	3.69	3.02	1.85
17	970	483	26	4.15	3.35	2.2
18	1105	533	26	4.57	3.68	2.53
19	1252	594	26	5.05	4.03	2.87
20	1401	645	26	5.57	4.42	3.24

TABLE B23. Flow Visualisation Data, Reverse Circulation, 490 micron Sand

Ambient Conditions			PRESSUR	101800 Pa		
			TEMP	27 C		
			DENSITY	1.18 kg/cu.m		
Bed Conditions			Sand size	490 microns		
			Umf	0.178		
			Distributor	Six Caps in Annulus		
			Bed Depth	195 mm		
MOTOR SPEED Hz	PITOT Pa Pa	STATIC Pa	PITOT TEMP C	BELOW PLATE PRESS	BASE PRES KPA	TOP PRESS KPA
0		0	0	0	0	0
13	237	152	26	2.65	2.2	0.46
14	320	194	26	3.29	2.92	0.66
15	430	251	26	3.66	3.26	0.9
16	568	309	26	4.07	3.59	1.23
17	704	372	26	4.51	3.91	1.56
18	832	427	26	4.92	4.21	1.86
19	981	490	26	5.38	4.58	2.21
20	1135	550	26	5.89	4.98	2.58
21	1294	606	26	6.44	5.37	2.97
22	1440	665	26	6.96	5.76	3.37

TABLE B24. Flow Visualisation Data, Ingestor Tube, 490 micron Sand

Ambient Conditions			PRESSURE	102100 Pa		
			TEMP	26 C		
			DENSITY	1.19 kg/cu.m		
Bed Conditions			Sand size	490 microns		
			Umf	0.178 m/sec		
			Distributor	100 Mesh		
			Bed Depth	265 mm		
MOTOR SPEED Hz	PITOT Pa Pa	STATIC Pa	PITOT TEMP C	BELOW PLATE PRESS	BASE PRES KPA	TOP PRESS KPA
0		0	0	0	0	0
15	330	219	25	4.16	3.82	0.4
16	400	255	25	4.75	4.39	0.8
16.5	526	324	25	4.92	4.54	1.05
17	620	375	25	5.2	4.74	1.3
17.5	700	415	25	5.43	4.96	1.48
18.5	826	477	25	6.01	5.3	1.72
20	1030	570	25	6.95	5.9	2.21
22	1300	655	25	8.27	6.63	2.94

TABLE B25 Deep Bed , Combustor Run No. 1,

40

Ambient Conditions				Pressure		102200	Pa			
				Temperature		26	C			
Fluidized Bed Conditions				Sand Size		490 micron				
				Sand Type		Graded River Sand				
				Bed Depth		325 mm total depth				
				Configuration		19 Bubble Caps, Pattern No.2				
				Fuel		50 mm Bagasse Bricks,dry				
Time	Air Flowrate			Fuel Type	Fuel Qty	Temperatures C				Average Bed Temp
	B.S. Nozzle	Rota	Vol Flow FAD			Distance from FBC base plate mm			Spare	
t mins	p Pa	cfm	V l/sec			+50 prb 12 bed wall	+200 prb 12 bed wall	+300 prb 12 bed wall		
0	104	0	55.92	lpg	28kpa	0	0	0	0	0
17	104	0	55.92	lpg	0	76.933	210	232	0	232
28	104	0	55.92	lpg	0	130.8	280	313	0	313
34	90	0	52.02	lpg	0	164.47	315	360	0	360
39	75	0	47.49	lpg	0	191.4	354	400	0	400
58	75	0	47.49	lpg	0	305.87	480	562	0	562
64	60	0	42.48	lpg	0	332.8	520	582	0	582
78	62	0	43.18		grams	406.87	597	683	0	683
82	61	0	42.83	Bagasse	1030	433.8	580	663	0	663
86	60	0	42.48	Bricks	637	454	575	636	0	636
89	60	0	42.48		819	454	570	636	0	636
93	60	0	42.48		1293	454	565	636	0	636
99	60	0	42.48		1107	467.47	568	649	0	649
102	60	0	42.48		1396	467.47	575	656	0	656
107	60	0	42.48		1105	474.2	590	676	0	676
111	60	0	42.48		891	480.93	600	690	0	690
117	60	0	42.48		1205	494.4	605	696	0	696
126	60	0	42.48		1187	514.6	592	669	0	669
129	60	0	42.48		1461	514.6	578	683	0	683
141	60	0	42.48	Bagasse	574	521.33	568	643	0	643
146	60	0	42.48	Fibres	483	507.87	550	629	0	629
0	0	0	0		0	0	0	0	0	0

TABLE B26 Deep Bed , Combustor Run No. 2

Ambient Conditions				Pressure		102000		Pa			
				Temperature		24		C			
Fluidized Bed Conditions				Sand Size		490		micron			
				Sand Type		Graded River Sand					
				Bed Depth		305		mm total depth			
				Configuration		19 Bubble Caps, Pattern No.2					
				Fuel		Bagasse Fibres, Dry					
Time t mins	Air Flowrate			Fuel Type	Fuel Qty	Temperatures C				Flue Gas Temp bed	Average Bed Temp bed
	B.S.	Rota	Vol Flow			Distance from FBC base plate mm					
	Nozzle		FAD			+50	+200	+300	+300		
	p	cfm	V			Depth of Thermocouple into bed sand					
	Pa		l/sec			prb 12	prb 12	prb 12	prb 75		
						bed wall	bed wall	bed wall			
0	76	0	47.69	lpg	100kpa	70	111	144	0	420	82
4	60	0	42.38		0	77		151	0	488	89
6	60	0	42.38		0	78	130	164	0	521	96
9	49	0	38.29		0	84	142	178	0	555	106
17	49	0	38.29		0	97	180	218	0	555	133
24	49	0	38.29		0	111	215	245	0	555	153
25	42	0	35.45		0	111	212	252	0	555	156
38	36	0	32.82	lpg plus	0	144	290	340	353	589	353
59	25	0	27.35	B Bricks	100kpa	212	496	568	589	791	589
73	15	50	22.50			299	623	723	723	723	723
77	0	40	18.00	Bagasse	1000	326	605	710	717	723	717
81	0	40	18.00	Fibres	970	346	603	710	710	723	710
86	0	30	13.50		1000	366	593	710	710	723	710
91	0	30	13.50		1683	380	562	710	710	723	710
96	0	20	9.00		1360	393	574	723	723	791	723
100	0	20	9.00		1485	393	552	737	730	791	730
105	0	15	6.75		1898	400	535	764	764	804	764
110	0	15	6.75			393	524	750	811	791	750
111	0	20	9.00			393	520	746	815	723	746
114	0	20	9.00			387	517	741	845	656	741
117	0	20	9.00			380	514	737	878	616	737
123	0	30	13.50		0	360	507	717	669	562	717
128	0	50	22.50		0	357	566	656	643	535	656
145	38		33.72		0	366	450	515	481	414	515
156	38	0	33.72		0	360	360	414	387	346	414

TABLE B27 Shallow Bed , Combustor Run No. 4.

Ambient Conditions				Pressure		102000		Pa			
				Temperature		21		C			
Fluidized Bed Conditions				Sand Size		300		micron			
				Sand Type		Graded River Sand					
				Bed Depth		130		mm total depth			
				Configuration		42 Bubble Caps, Pattern No.4					
						2.5mm diameter inserts fitted					
				Fuel		Sawdust: 25% Moisture					
						Bagasse:1% Moisture					
Time	Air Flowrate			Fuel Type	Fuel Qty	Temperatures C					
	B.S. Nozzle	Rota Vol Flow	FAD			Distance from FBC base plate mm				Chimney Average	
t	p		V			+50	+50	+100	+200	+1500	Bed
mins	Pa	cfm	l/sec			Depth of Thermocouple into bed sand					Temp
						prb 12 bed wall	prb 75 bed	prb 75 bed	prb 12 flue	flue	bed
0	0	34	13.77	lpg	20kpa	94	218	218	319	454	218
2	0	34	13.77		0		232	249	360	535	244
13	0	22	8.91		0	131	366	366	488	568	366
22	0	22	8.91		0		447	447	562	582	447
35	0	18	7.29	flame failure		230	548	548	589	467	548
42	0	18	7.29				562	562	737	656	562
52	0	18	7.29		10kpa		629	629	764	676	629
56		17	6.89		Sawdust	3880	296	656	656	723	676
70		17	6.89	Bagasse	861	335	737	750	811	710	746
73	0	17	6.89		1165		784	777	750	750	779
79	0	17	6.89		0		791	804	784	669	800
84		17	6.89		916		804	804	791	643	804
88		17	6.89		1382	386	818	818	777	656	818
92		10	3.60		1225		824	811	777	669	815
99		13	4.97		0		764	831	696	656	811
101		13	4.97		1259	409	858	831	696	737	839
111		13	4.97		0	446	858	831	770	548	839
112		18	7.29			534	858	811	777	535	825
116		18	7.29			592	804	777	750	515	785
134		18	7.29			459	636	629	622	427	631
159		18	7.29			352	467	467	467	333	467
162		18	7.29		0		454	454	454	333	454
172		18	7.29		0		407	407	407	299	407
182		18	7.29		0		366	366	366	272	366
188		18	7.29		0	284	346	346	346	265	346

TABLE B28 Shallow Bed , Combustor Run No. 5, Page 1 of 2

Ambient Conditions				Pressure		101700	Pa				
				Temperature		21	C				
Fluidized Bed Conditions				Sand Size		300	micron				
				Sand Type		Graded River Sand					
				Bed Depth		125	mm total depth				
				Configuration		42 Bubble Caps, Pattern No.4 2.5mm diameter inserts fitted					
Time	Air Flowrate			Fuel Type	Fuel Qty	Temperatures C					
	B.S. Nozzle	Rota FAD	Vol Flo V			Distance from FBC base plate mm				Chimney	Average
t mins	p Pa	cfm	l/sec			+50 prb 12 bed wall	+50 prb 75 bed	+100 prb 75 bed	+200 prb 12 flue	+1500 flue	Bed Temp bed
0	0	40	18	lpg	10 kpa	15	70	77	265	562	75
24	0	30	13.5			130	286	279	366	622	281
41	0	25	11.25			212	441	434	535	636	436
56	0	25	11.25	lpg+coal	200g	0	542	542	629	656	542
59	0	25	11.25		200g	0	562	562	663	669	562
63		25	11.25		474g	0	589	589	683	683	589
67	0	25	11.25			0	622	622	723	710	622
71	0	23.5	10.58			421	663	663	744	744	663
74	0	18	8.1			465	703	703	791	744	703
78	COAL	18	8.1	Coal	269	420	730	744	797	744	739
80	ONLY	18	8.1	Only	269	0	730	750	797	562	743
81		18	8.1	3%moist	269	0	723	764	791	555	750
82		18	8.1		269	0	764	770	791	555	768
84		18	8.1			0	791	791	791	555	791
94		18	8.1		269	0	784	791	770	508	788
97		17.5	7.875		0	630	777	784	791	508	782
98		17.5	7.875		267	0	777	791	791	521	786
108		17.5	7.875		0	0	764	764	750	481	764
114		17.5	7.875			0	730	737	723	467	734
117		17.5	7.875	Sawdust	170	0	723	723	737	488	723
119		17.5	7.875	25%moi	170	0	717	717	723	494	717
121		17.5	7.875		170	583	717	723	723	488	721
124		17.5	7.875		170	0	703	710	723	454	708
126		17.5	7.875		170	0	703	710	717	494	708
130		17.5	7.875		170	0	676	683	690	373	681
132		17.5	7.875		170	0	676	690	703	521	685
134		17.5	7.875		340	0	690	696	710	562	694
136		17.5	7.875		477	0	710	710	696	575	710
138		17.5	7.875		245	462	703	710	723	535	708
140		17.5	7.875		245	0	703	717	717	562	712
142		17.5	7.875		245	442	710	723	723	542	719
144		17.6	7.92		245	0	717	723	730	542	721
146		17.6	7.92		0	0	730	730	710	542	730
147		17.6	7.92	Wet Bag	476	453	730	730	683	521	730
148		17.6	7.92	80%moi	1779MO	0	656	696	717	521	682
150		17.6	7.92		0	0	595	656	683	521	635
152		17.6	7.92		0	0	609	622	616	481	618
153		17.6	7.92	Bagasse	122	438	616	629	696	521	624

TABLE B28 Shallow Bed , Combustor Run No. 5, Page 2 of 2

Ambient Conditions				Pressure	101700	Pa					
				Temperature	21	C					
Fluidized Bed Conditions				Sand Size	300	micron					
				Sand Type	Graded River Sand						
				Bed Depth	125	mm total depth					
				Configuration	42 Bubble Caps, Pattern No.4 2.5mm diameter inserts fitted						
Time t mins	Air Flowrate			Fuel Type	Fuel Qty	Temperatures C					
	B.S. Nozzle	Rota p	Flo V			Distance from FBC base plate mm				Chimney	Average
			FAD			50	50	100	200	+1500	Bed
	Pa	cfm	l/sec			Depth of Thermocouple into bed sand				Temp	
						prb 12 bed wall	prb 75 bed	prb 75 bed	prb 12 flue	flue	bed
154		17.6	7.92	Bagasse	245	0	629	643	683	521	638
156		17.6	7.92	1%moist	245	0	649	649	683	521	649
158		17.6	7.92		245	0	656	656	683	521	656
160		17.6	7.92		245	0	663	669	683	521	667
162		17.6	7.92		387	390	656	663	683	508	660
164		17.6	7.92		387	0	669	669	683	521	669
166		17.6	7.92		387	0	669	676	710	548	674
168		17.6	7.92		197	0	683	683	710	494	683
169		17.6	7.92		0	0	690	676	683	494	681
170		17.6	7.92		0	0	683	676	649	481	679
184		18	8.1		0	372	609	595	575	400	600
198		18	8.1		0	0	508	508	467	292	508
210		18	8.1		0	0	414	414	387	259	414
222		18	8.1		0	0	346	346	319	225	346
234		18	8.1		0	0	299	299	265	198	299
246		18	8.1		0	0	252	252	239	185	252

TABLE B29 Deep Bed , Screw Feeder, Combustor Run No. 6.

Ambient Conditions				Pressure	102300	Pa					
				Temperature	22	C					
Fluidized Bed Conditions				Sand Size	300	micron					
				Sand Type	Graded River Sand						
				Bed Depth	325	mm total depth					
				Configuration	42 Bubble Caps, Pattern No.4 2.5mm diameter inserts fitted						
Time	Air Flowrate			Fuel Type	Fuel Qty	Temperatures C					
	B.S. Nozzle	Rota Flow	Vol Flow			Distance from FBC base plate mm				Chimney Average	
t mins	p Pa	cfm	FAD V l/sec			+50 prb 12 bed wall	+50 prb 75 bed	+300 prb 75 bed	+300 prb 12 flue	+1500 flue	Bed Temp
0	0	30	13.5	lpg	15kpa	24	212	218	225	656	215
18	0	23	10.35		0	117	373	373	360	723	373
48	0	23	10.35		0	257	575	555	575	683	564
50		23	10.35			0	548	562	548	575	555
51		23	10.35	Sawdust	1629	0	279	555	454	548	555
52		23	10.35	13.5% m		0	292	555	454	548	555
54	0	23	10.35			0	346	548	535	575	548
56		23	10.35		0		494	555	548	629	555
58		23	10.35		0		548	568	568	535	568
60		18	8.1		3375		575	575	575	548	575
64		18	8.1			0	589	589	589	521	589
68		18	8.1			0	595	595	595	521	595
72		18	8.1			0	602	602	602	548	602
76		18	8.1			0	616	609	602	521	612
80		18	8.1			0	616	616	602	535	616
84		18	8.1		0		622	622	622	535	622
87		18	8.1	Sawdust	finished	0	629	629	629	414	629
112		30	13.5	Started	Cooling	0	501	501	501	319	501
118		30	13.5			397	467	467	467	313	467
128		30	13.5			0	427	427	427	292	427
134		30	13.5			303	407	407	407	272	407
138		30	13.5				387	387	387	265	387
147		30	13.5			263	353	353	353	252	353
148	0	0	0	Convection		263	353	353	353	212	353
178	0	0	0	Cooling		222	319	340	313	138	330

TABLE B30 Deep Bed , Screw Feeder, Combustor Run No. 7

Ambient Conditions				Pressure	102300	Pa					
				Temperature	22	C					
Fluidized Bed Conditions				Sand Size	300	micron					
				Sand Type	Graded River Sand						
				Bed Depth	460	mm total depth					
				Configuration	42 Bubble Caps, Pattern No.4 2.5mm diameter inserts fitted						
Time t mins	Air Flowrate			Fuel Type	Fuel Qty	Temperatures C					
	B.S. Nozzle p Pa	Rota Vol Flow FAD V cfm l/sec	Distance from FBC base plate mm +50 +50 +300 +300 +1500			Chimney Average Bed Temp					
				prb 12 bed wall	prb 75 bed	prb 75 bed	prb 12 bed wall	flue	bed		
0	0	40	18.00	LPG	15kpa	24	111	50	117	974	62
2	0	30	13.50		0	24	117	50	124	1006	63
25	0	35	15.75		0	38	212	185	225	50	190
42		25	11.25			69	340	340	340	1181	340
54		22	9.90			94	427	346	427	1181	362
56		22	9.90	Bagasse	grams	126	414	346	441	1181	360
72	0	22	9.90	+LPG	1400	126	535	508	535	1235	513
92		22	9.90		0	194	629	622	636	1235	624
98		18	8.10		0	211	649	649	649	1208	649
112		18	8.10			307	696	696	710	1230	696
116	gasof	18	8.10			0	710	710	710	1230	710
120		18	8.10	Sawdust	2180	0	683	676	676	50	678
150		18	8.10			497	669	676	676	50	675
150		18	8.10	Screw Jammed		0	669	676	676	50	675
190		18	8.10	Start	cooling	0	589	589	589	346	589
218		18	8.10	Finish	cooling		474	474	474	279	474
234		0	0.00	Start	convecti	0	420	420	420	212	420
282		0	0.00	Finish	convecti	0	346	420	360	131	406

TABLE B31 Deep Bed , Reverse Ingestor Feed, Combustor Run No. 8

Ambient Conditions				Pressure		102300		Pa					
				Temperature		23		C					
Fluidized Bed Conditions				Sand Size		300		micron					
				Sand Type		Graded River Sand							
				Bed Depth		355		mm total depth					
				Configuration		34 Bubble Caps, Pattern No.5							
						2.5mm diameter inserts fitted to inner 6 caps							
Time t mins	Air Flowrate			Fuel Type	Fuel Qty	Temperatures C							
	B.S. Nozzle p Pa	Rota Vol Flow cfm	FAD V l/sec			Distance from FBC base plate mm				Chimney Average Bed Temp			
						+50	+50	+300	+300		+1500		
Depth of Thermocouple into bed sand													
				prb 12 bed wall		prb 75 bed		prb 75 bed		prb 12 flue		flue bed	
0	38		33.62	lpg	15kpa		104	104	104	616	104		
16	38		33.62		0	139	178	178	178	656	178		
18	38		33.62		0		185	185	185	656	185		
48		58	26.10			365	373	373	373	764	373		
78		44	19.80			521	609	609	609	764	609		
88		44	19.80			570	669	676	683	750	674		
91		44	19.80	Sawdust	3140	595	683	696	696	764	692		
96		44	19.80	17.5% m	0		683	690	690	791	687		
100		44	19.80		0	608	690	696	696	696	694		
105		44	19.80	Sawdust	1084	591	690	696	696	764	694		
111		44	19.80			0	683	696	696	750	692		
112		44	19.80	Bagasse	514	0	683	696	696	764	692		
117			35.34	dry	350	0	663	683	683	710	676		
119			42.59		350	0	643	656	656	696	651		
123			42.59			0	602	616	616	656	611		
124		cool	42.59	Start	cooling		589	609	602	575	602		
154		cool f	42.59	finish	cooling	0	333	346	346	360	342		
154		conv	0.00	start	convectio	0	333	346	346	360	342		
174		conv f	0.00	finish	convecti	0	319	346	340	225	337		
0		0	0		0	0	0	0	0	0	0		

TABLE B32 Spouted Bed with Baffle , Combustor Run No. 9, Page 1 of 2

Ambient Conditions				Pressure Temperature		***** 22		Pa C			
Fluidized Bed Conditions				Sand Size		530 micron					
				Sand Type		Graded River Sand					
				Bed Depth		515 mm total depth					
						300 mm cone depth					
				Configuration		Spouted Bed with Baffle Plate					
Time t mins	Air Flowrate			Fuel Type	Fuel Qty	Temperatures C					
	B.S. Nozzle p Pa	Rota Vol Flo FAD V cfm l/sec	Distance from FBC base plate					Chimne Averag Bed Temp			
			+100			+50	+200		+300	+1500	
			prb 12 bed wal			prb 75 bed	prb 75 bed		prb 12 flue	prb 12 flue	
0	64		43.64	lpg	15kpa	38	104	111	144	548	107
8	65		43.98			72	151	151	185	548	151
15	45		36.59			100	164	164	185	602	164
24	28		28.86			146	218	218	239	643	218
33	25		27.27			165	265	252	292	683	258
50	23		26.16			256	340	333	360	710	336
67	28		28.86			340	420	414	427	723	417
78	24		26.72			389	467	461	467	703	464
86	15	57	25.65			397	481	481	494	696	481
90		53	23.85	Sawdu		390	494	494	515	696	494
105		53	23.85	12%m		412	575	575	582	804	575
110		53	23.85	-4.75m	2933	0	595	595	595	616	595
114		0	0.00	Hopper	lost pri	0	602	602	589	589	602
118		0	0.00		feed	0	595	595	494	353	595
119		53	23.85	Hopper	1592	0	595	595	562	400	595
127		53	23.85				575	575	575	690	575
130		53	23.85				595	602	589	454	599
130		0	0.00				595	602	589	454	599
134		0	0.00			0	595	602	481	340	599
134		53	23.85	Hopper	2103	0	595	602	575	589	599
141		53	23.85			0	0	676	683	656	683
141		0	0.00			0	0	676	683	589	548
146		0	0.00			0	0	656	669	521	340
146		53	23.85	Hopper	2223	0	656	669	643	696	663
149		53	23.85			0	0	683	696	663	737
154		53	23.85			0	0	744	750	723	723
154		0	0.00			0	0	744	750	643	494
159		0	0.00			0	628	723	737	562	360
159		53	23.85	Hopper	2122	628	723	737	696	683	731
165		53	23.85			0	0	784	784	764	710
165		0	0.00			0	0	784	784	656	589
172		0	0.00			0	0	723	744	602	373
172		53	23.85	Hopper	2004	640	723	744	710	589	734
178		53	23.85			0	0	764	777	764	669
180		53	23.85			0	664	770	777	764	643
180		53	23.85	Coolin		0	664	770	777	764	643
181		53	23.85			0	664	744	757	750	555
185		53	23.85			0	0	683	696	703	521

TABLE B32 Spouted Bed with Baffle, Combustor Run No.9, page 2 of 2

Ambient Conditions				Pressure	101900	Pa					
				Temperature	22	C					
Fluidized Bed Conditions				Sand Size	530	micron					
				Sand Type	Graded River Sand						
				Bed Depth	515	mm total depth					
					300	mm cone depth					
				Configuration	Spouted Bed with Baffle Plate						
Time	Air Flowrate			Fuel Type	Fuel Qty	Temperatures C					
	B.S. Nozzle	Rota	Vol Flo FAD V l/sec			Distance from FBC base plate m					Chimne Averag
t mins	p Pa	cfm				100	50	200	300	+1500	Bed Temp
						Depth of Thermocouple into bed sand					
						prb 12	prb75	prb75	prb 12		
						bed wal	bed	bed	flue	flue	bed
190		53	23.85	Conve	0	579	629	636	643	488	633
200		53	23.85		0	515	521	535	555	427	529
206		53	23.85		0	480	467	481	501	387	475
212		53	23.85		0	449	434	447	467	366	441
212		0	0		0	449	434	447	441	333	441
215		0	0		0	0	441	447	414	286	444
225		0	0		0	0	447	434	360	245	440
232		0	0		0	398	447	427	340	232	436
260		0	0		0	343	427	373	252	171	398

TABLE B33 Spouted Bed with Baffle , Combustor Run No.10, Page 1 of 2

Ambient Conditions				Pressure		101800		Pa			
				Temperature		25		C			
Fluidized Bed Conditions				Sand Size		530		micron			
				Sand Type		Graded River Sand					
				Bed Depth		583		mm total depth			
						300		mm cone depth			
				Configuration		Spouted Bed with Baffle Plate					
Time t mins	Air Flowrate			Fuel Type	Fuel Qty	Temperatures C					
	B.S. Nozzle p Pa	Rota cfm	Vol Flo FAD V l/sec			Distance from FBC base plate m					Chimne Averag Bed Temp
						+100	+50	+200	+300	+1500	
						prb 12 bed wal	prb 75 bed	prb 75 bed	prb 12 flue	flue	bed
0	20		24.53	lpg	30kpa l	41	77	77	90	589	77
47	27		28.50			102	144	144	158	589	144
62	30		30.04			109	185	178	198	696	180
71	27		28.50			126	205	198	212	710	200
100	23		26.31			167	252	245	259	710	247
110	22		25.73			184	265	259	272	723	260
123	22		25.73			200	286	279	292	696	281
129	28		29.02			214	292	292	299	757	292
157	15	57	25.65			252	333	333	340	723	333
164		53	23.85	Bagass	855		340	346	346	723	345
172		53	23.85	+lpg	988		387	373	387	885	376
177		53	23.85		1064	291	427	427	427	885	427
181		53	23.85		1101	306	467	467	467	885	467
184		53	23.85	End	1008	0	501	501	501	858	501
189		53	23.85	Bagass		0	548	542	542	858	543
189		0	0.00				548	542	542	548	543
190		0	0.00	Sawdu	17%moist		535	542	528	447	540
192		53	23.85	Hop 1	1968		542	542	542	521	542
194		53	23.85		2468 le	0	542	542	542	656	542
196		53	23.85		500g	0	548	548	548	616	548
196		0	0.00		0	0	548	548	548	589	548
198		0	0.00		0	0	555	555	548	454	555
200		0	0.00		0	0	555	555	542	387	555
200		53	23.85			0	555	555	555	555	555
202		53	23.85		0	0	562	555	555	589	557
203		53	23.85		0	0	562	562	562	683	562
203		0	0.00		0	0	562	562	562	521	562
205		0	0.00		0		562	568	568	373	567
205		53	23.85	Hop 2	800		568	568	568	454	568
212		53	23.85		0	0	568	575	568	656	574
212		0	0.00		0	0	568	575	568	589	574
215		0	0.00		0	0	568	575	562	346	574
215		53	23.85	Hop 3	2009	0	568	575	575	575	574
219		53	23.85		0	0	609	616	609	656	614
219		0	0.00		0	0	609	616	609	521	614
221		0	0.00				602	616	589	360	612
221		53	23.85	Hop 4	2171		616	616	616	589	616
228		53	23.85		0	0	656	656	656	683	656

TABLE B33 Spouted Bed with Baffle, Combustor Run No.10, page 2 of 2

Ambient Conditions				Pressure		101800		Pa				
				Temperature		25		C				
Fluidized Bed Conditions				Sand Size		530		micron				
				Sand Type		Graded River Sand						
				Bed Depth		583		mm total depth				
						300		mm cone depth				
				Configuration		Spouted Bed with Baffle Plate						
Time t mins	Air Flowrate			Fuel Type	Fuel Qty	Temperatures C						
	B.S. Nozzle p Pa	Rota cfm	Vol Flo FAD V l/sec			Distance from FBC base plate m					Chimne	Averag
											Bed	
						Depth of Thermocouple into bed sand					Temp	
					prb 12	prb 12						
					bed wal	bed	bed	flue	flue	bed		
228		0	0		0	0	656	656	656	589	656	
231		0	0		0		643	656	629	454	653	
231		53	23.85	Hop 5	2163		643	656	656	589	653	
238		53	23.85		0		717	717	717	669	717	
238		0	0		0		717	717	717	521	717	
242		0	0	Sand	19416	514	696	717	676	360	712	
242		53	23.85	Hop 6	1880	514	616	622	622	602	621	
248		53	23.85		0		669	669	669	696	669	
248		0	0		0		669	669	669	589	669	
253		0	0	Sand	23394	512	656	676	649	346	671	
253		53	23.85	Hop 7	1995	512	589	589	595	454	589	
260		53	23.85		0	517	629	636	636	643	634	
260		53	23.85	Coolin	0	517	629	636	636	548	634	
266		53	23.85		0	0	602	602	616	508	602	
290		53	23.85		0	438	488	494	501	420	493	
290		0	0	Conve	0	438	488	494	501	360	493	
312		0	0		0	396	481	488	467	286	486	

Fig B1 Temperature vs Time.
Combustor Run No.1

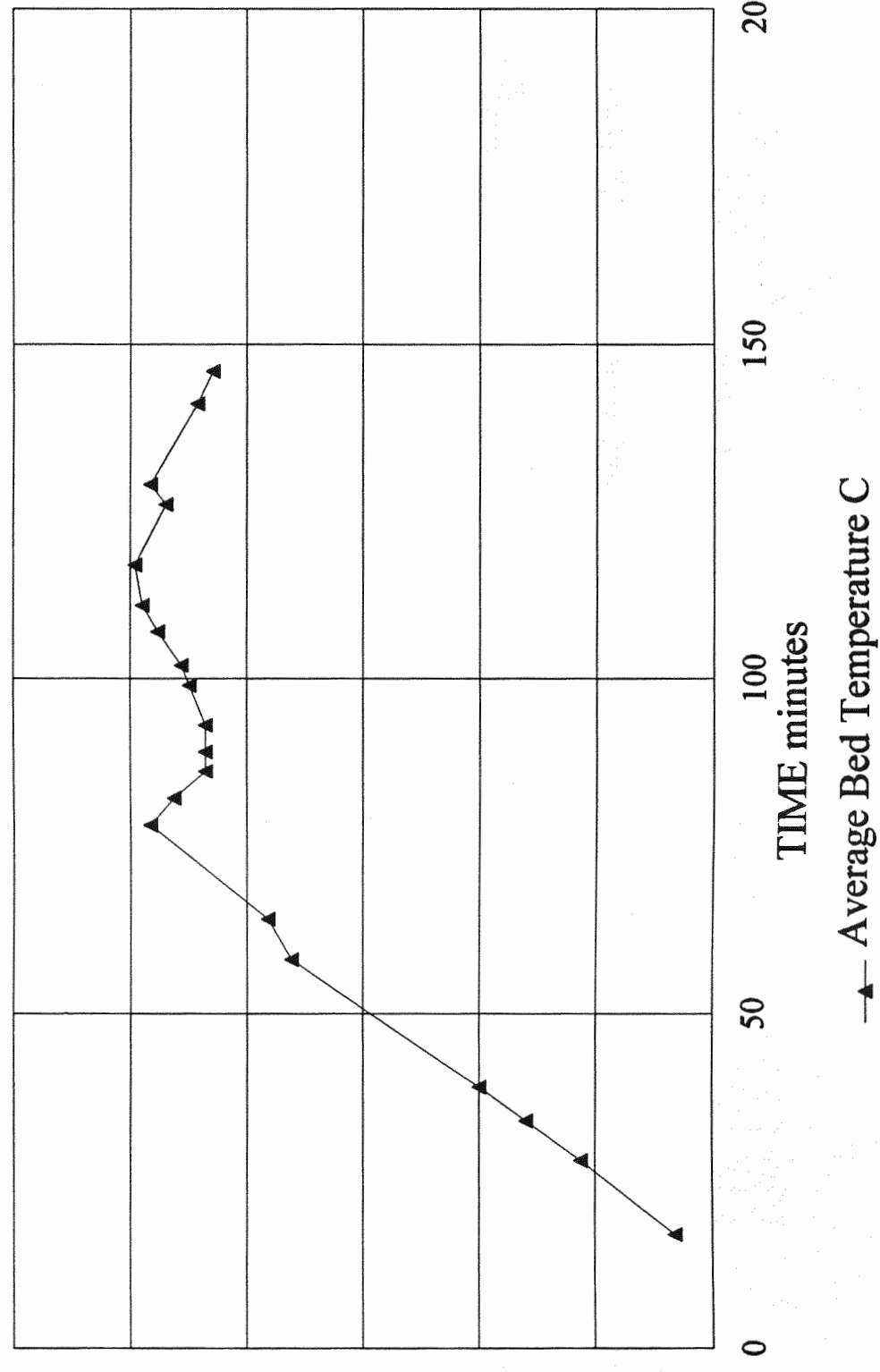


Fig. B2 U/Umf vs Time
Combustor Run No.1

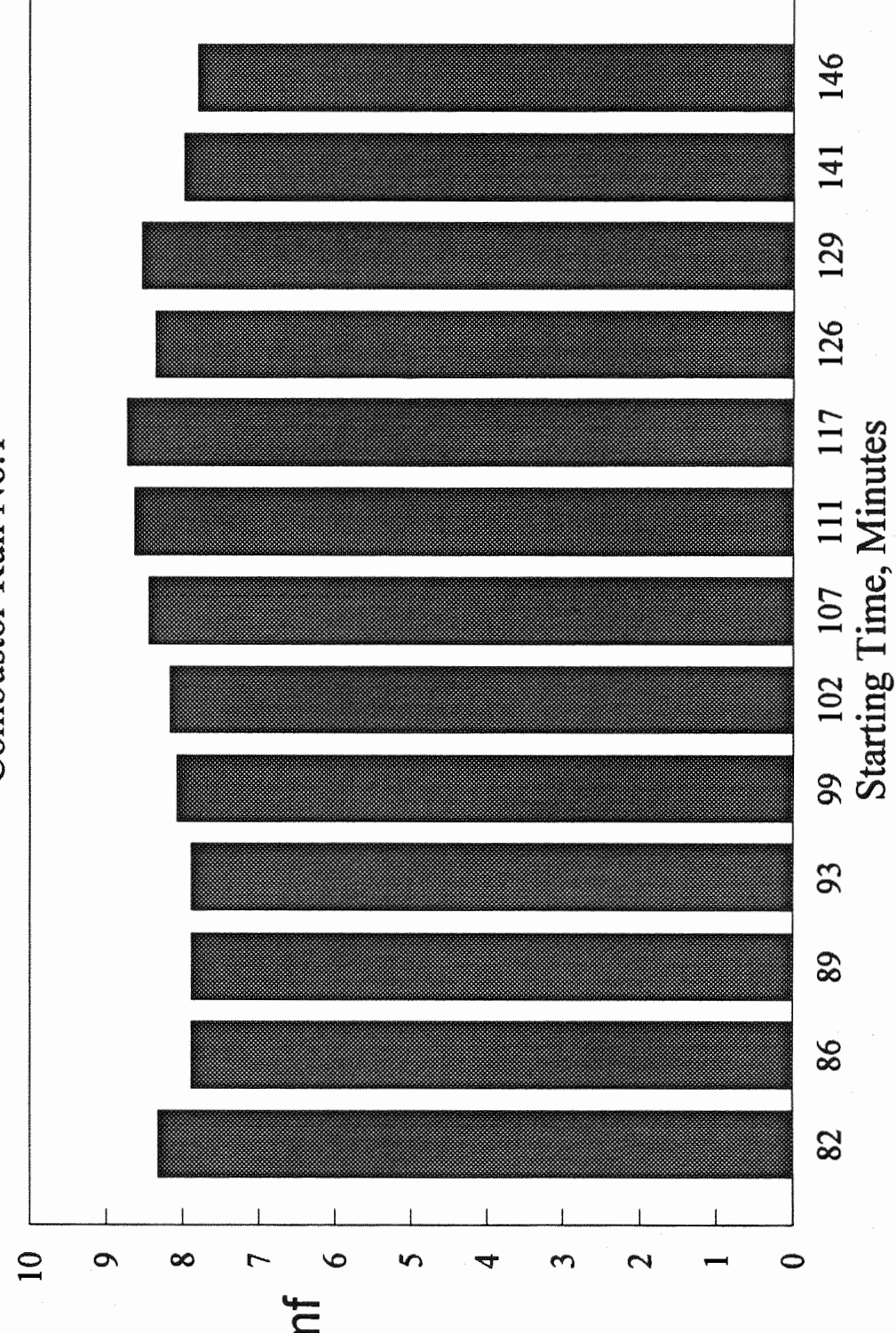


Fig. B3 Temperature vs Time
Combustor Run No.2

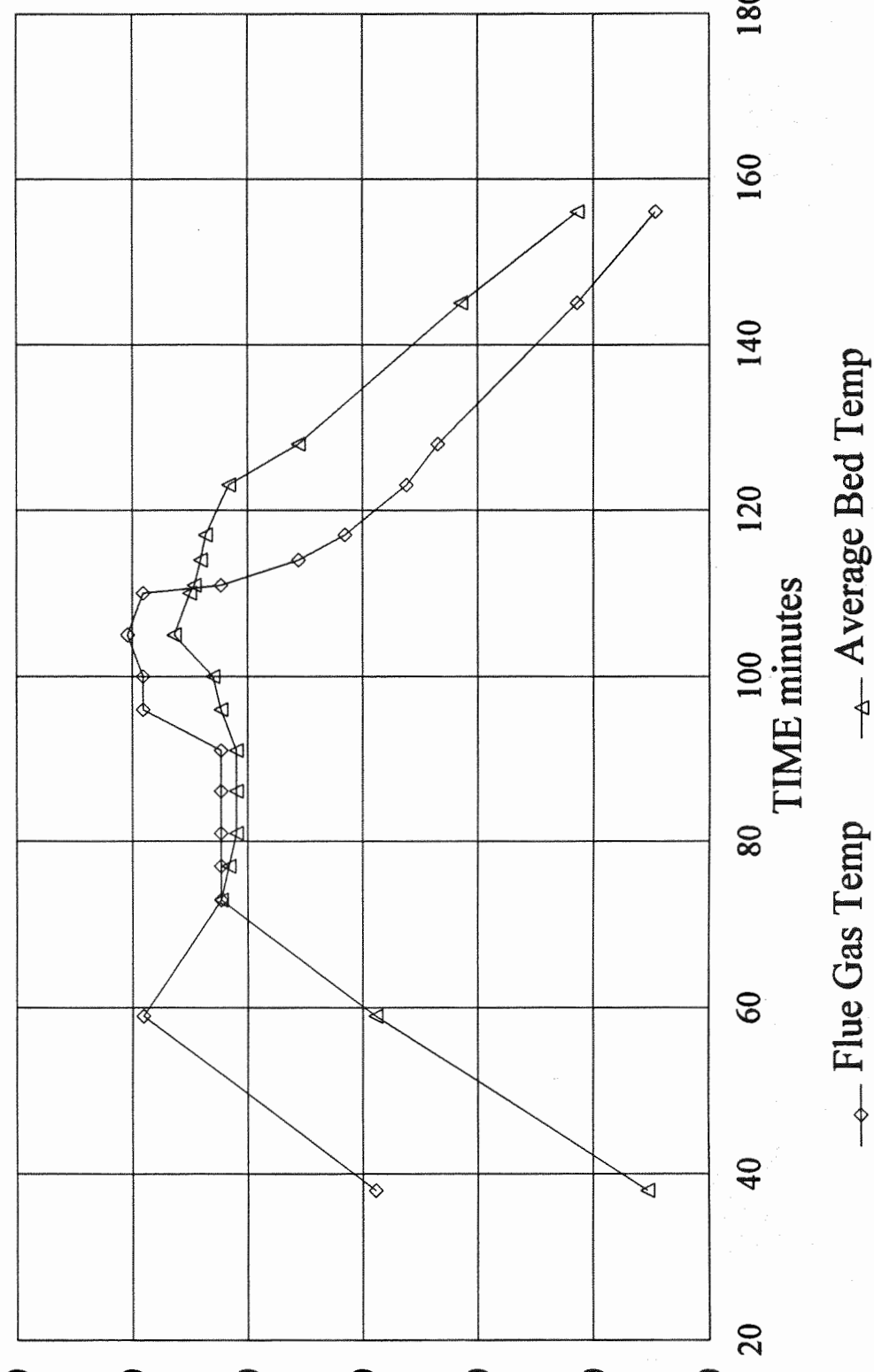


Fig. B4 Uf/Umf vs Time
Combustor Run No. 2

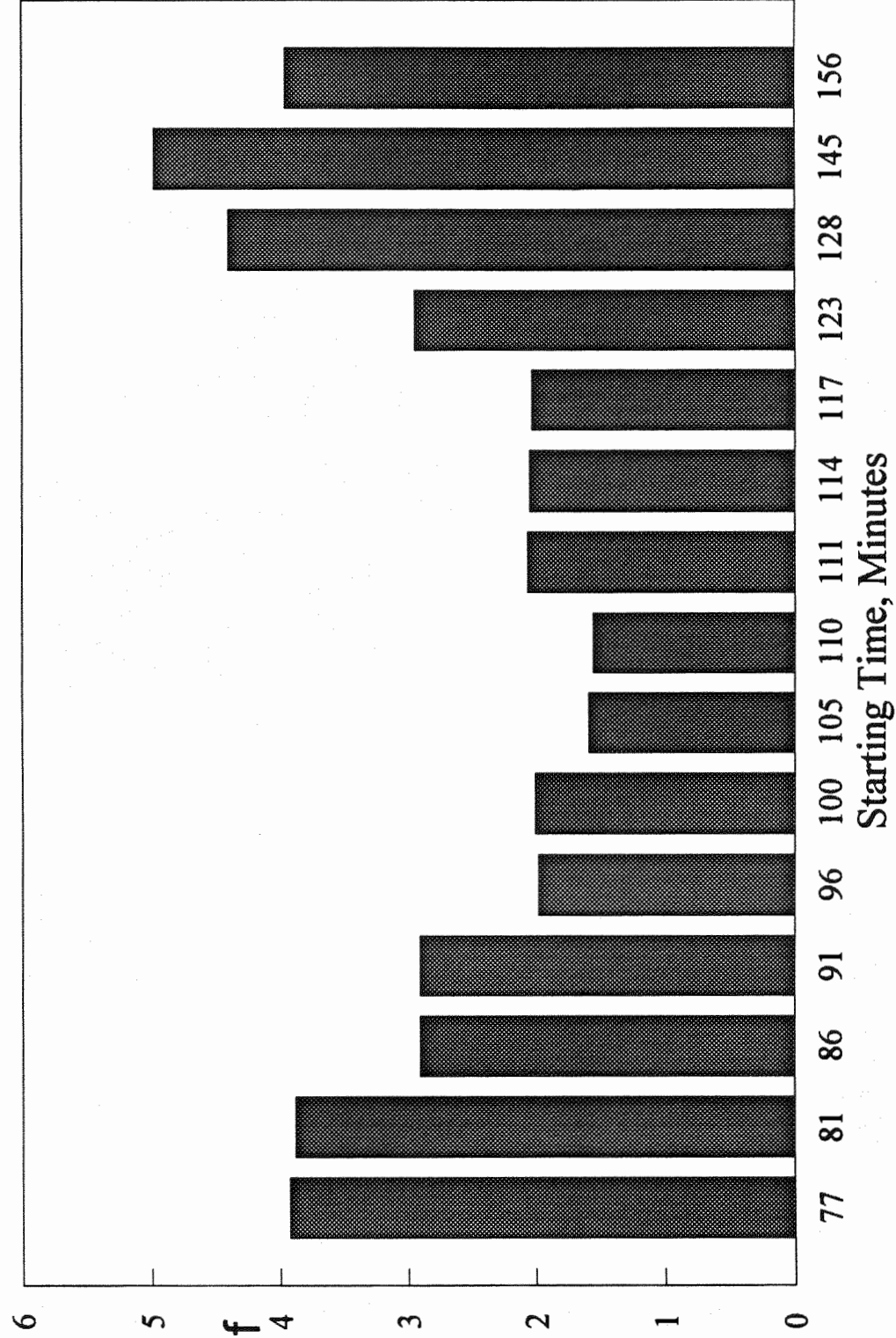


Fig. B5 Temperature vs Time
Combustion Run No.4

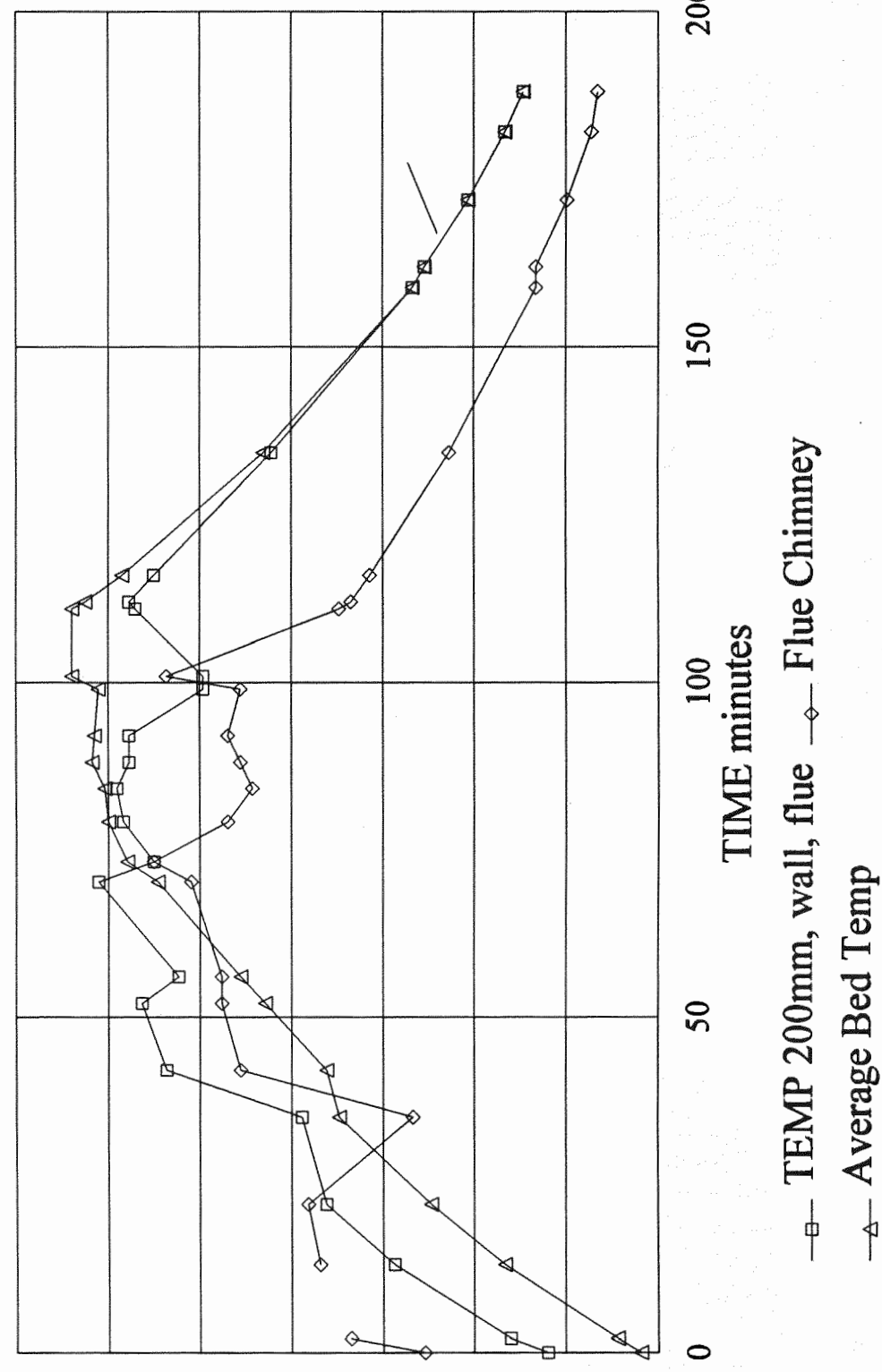


Fig. B6 Uf/Umf vs Time
Combustor Run No.4

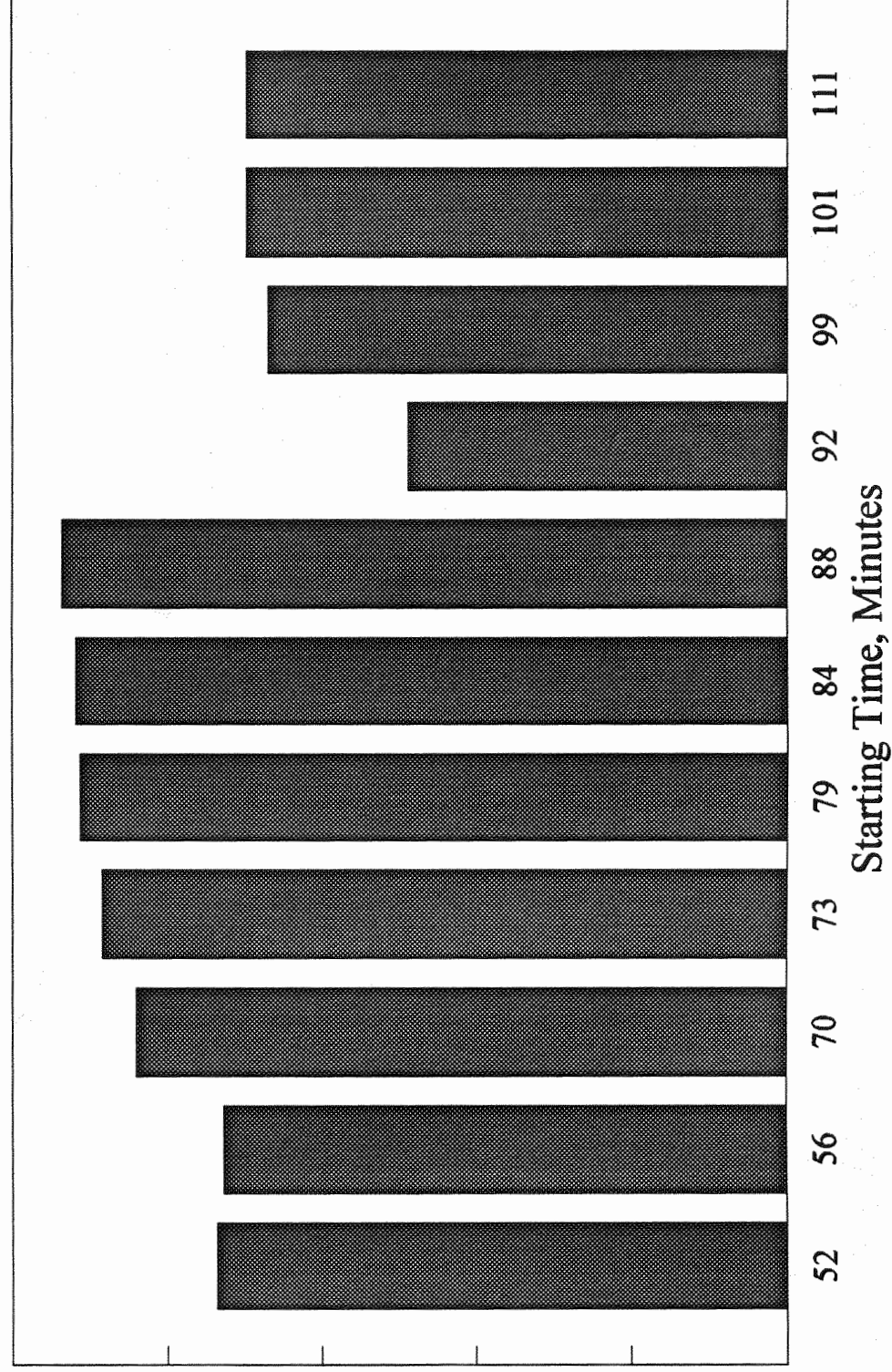


Fig. B7 Temperature vs Time
Combustor Run No.5

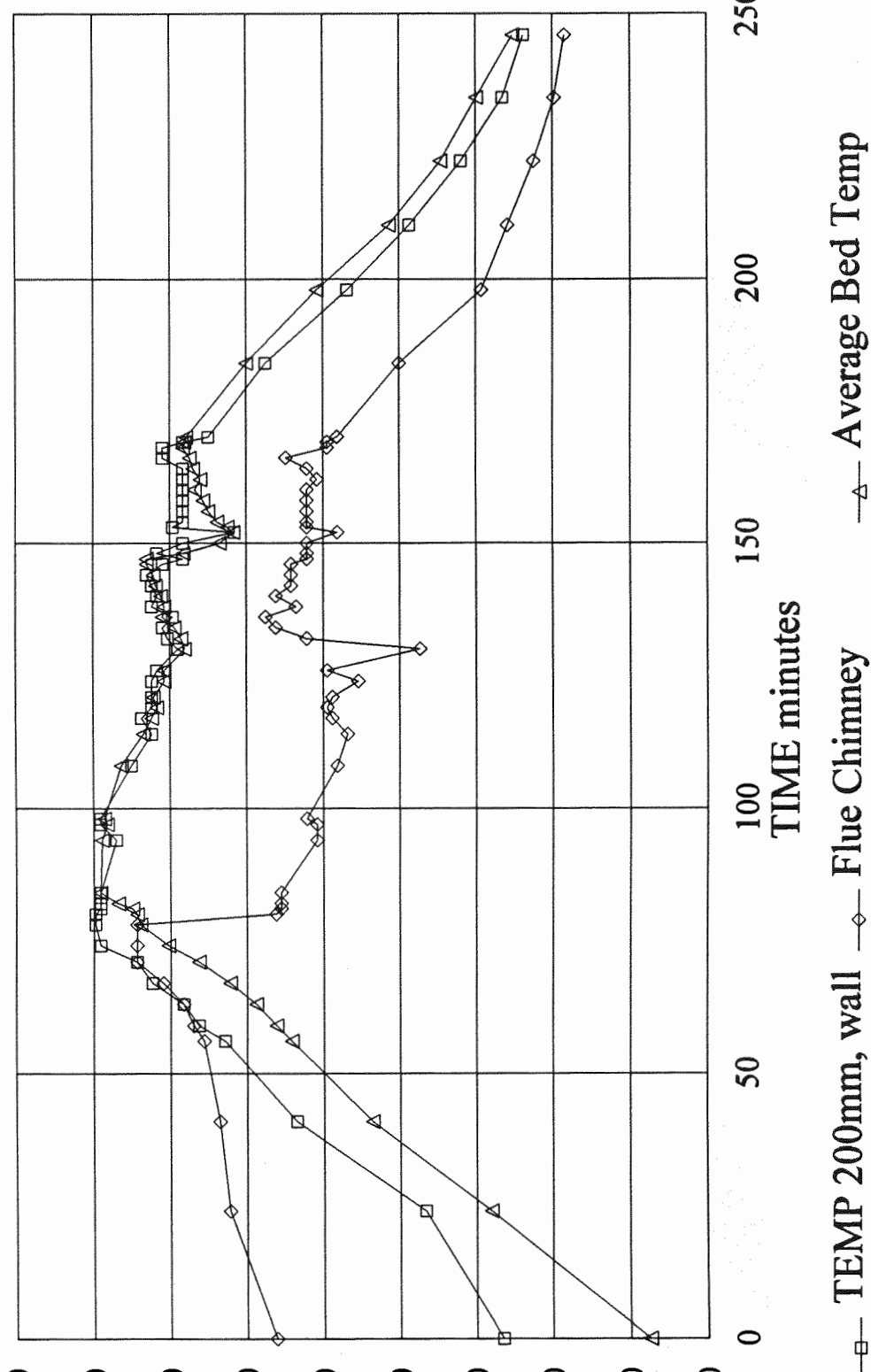


Fig .B8 Uf/Umf vs Time
 Combustor Run No.5

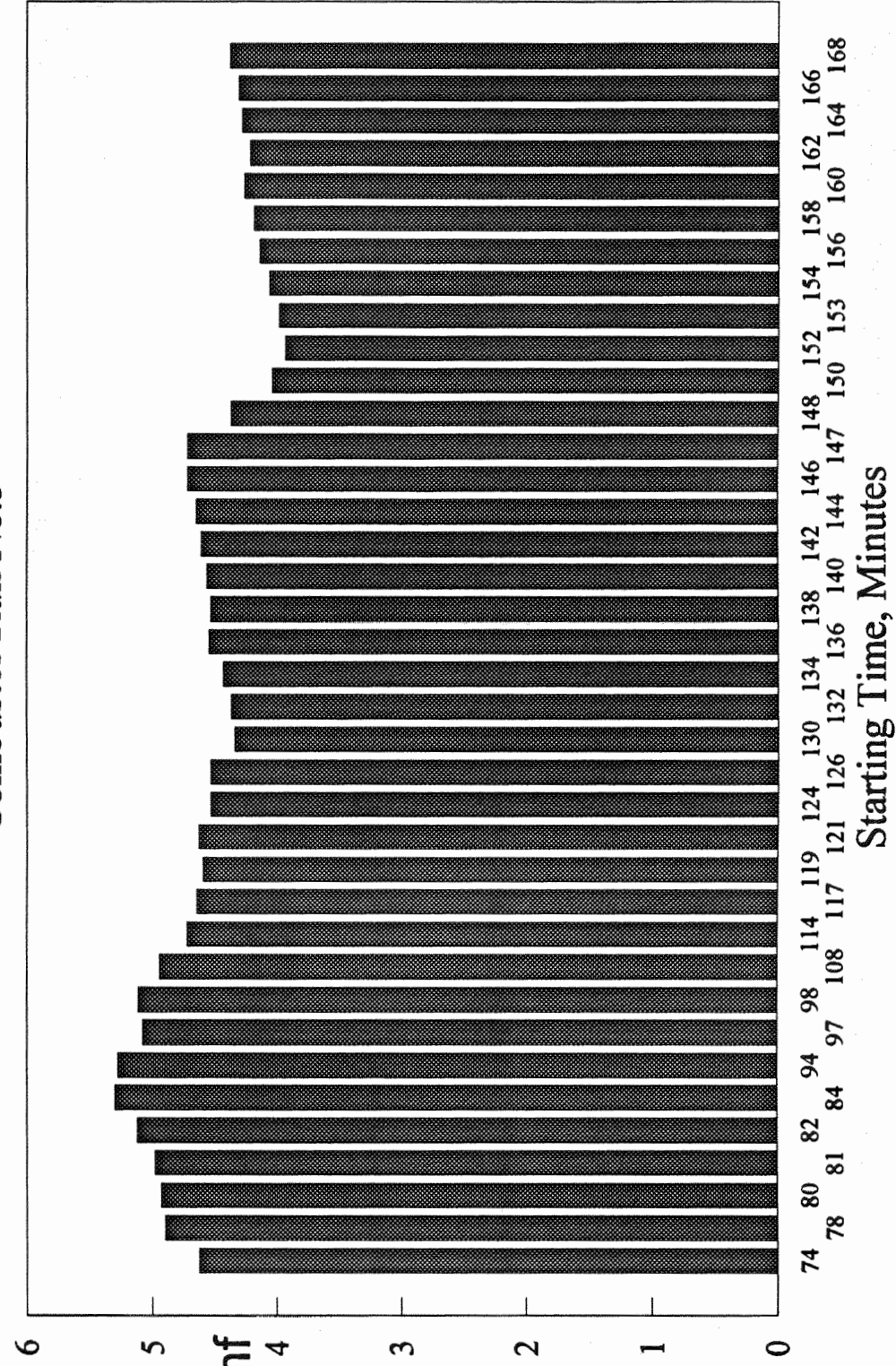


Fig B9 Temperature vs Time Combustor Run No.6

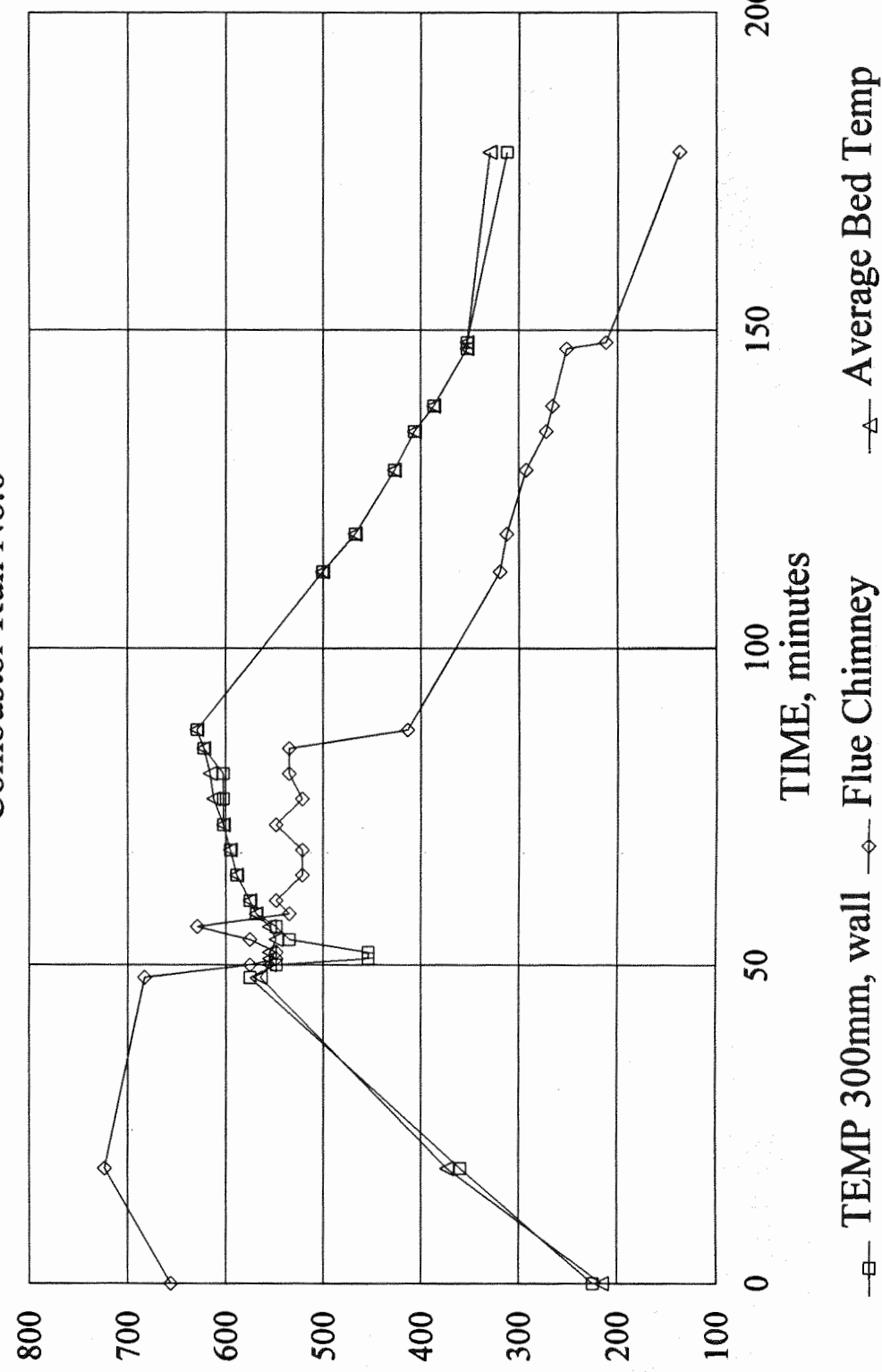


Fig. B10 Uf/Umf vs Time
Combustor Run No.6

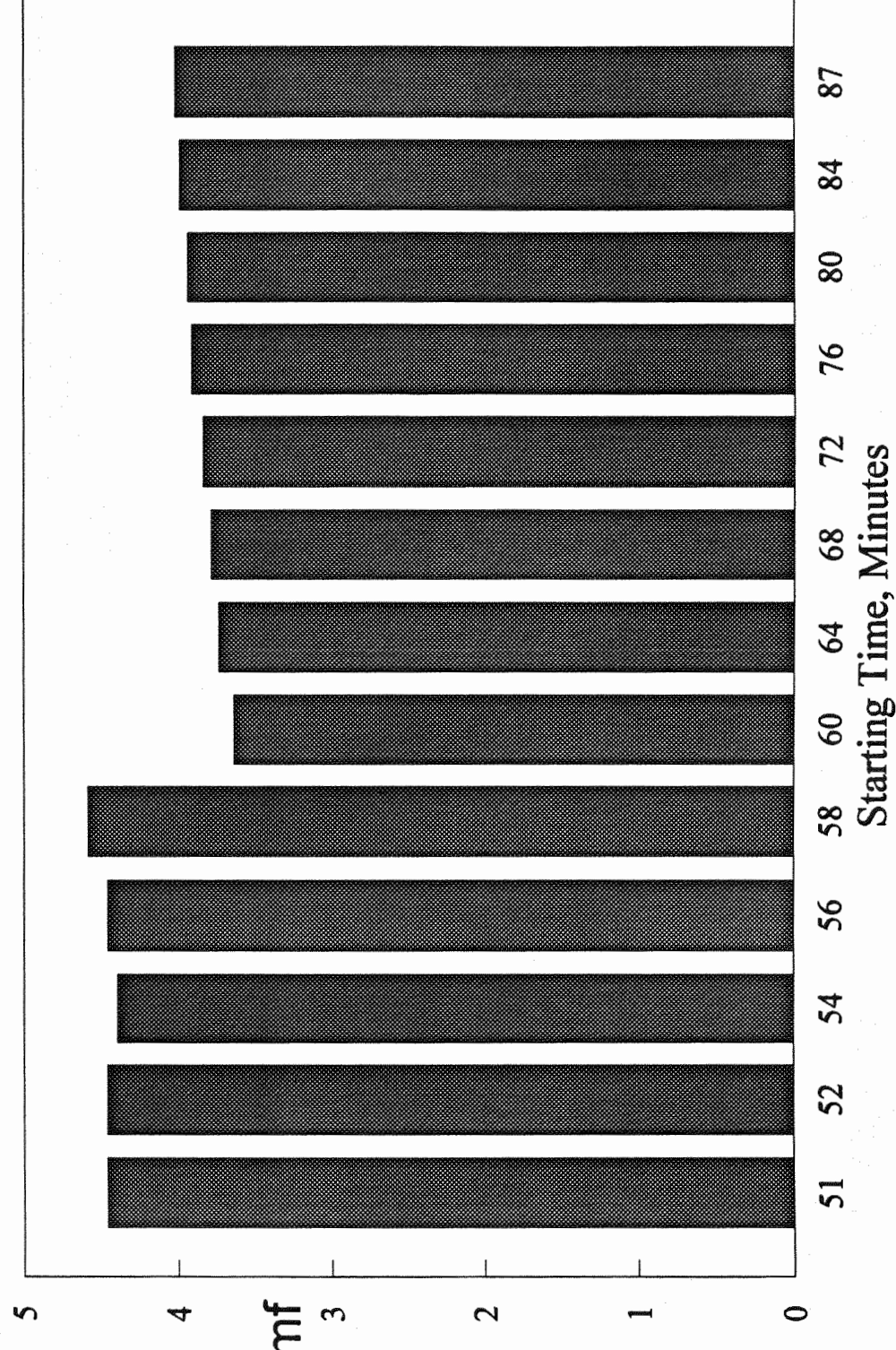


Fig. B11 Temperature vs Time
Combustor Run No.7

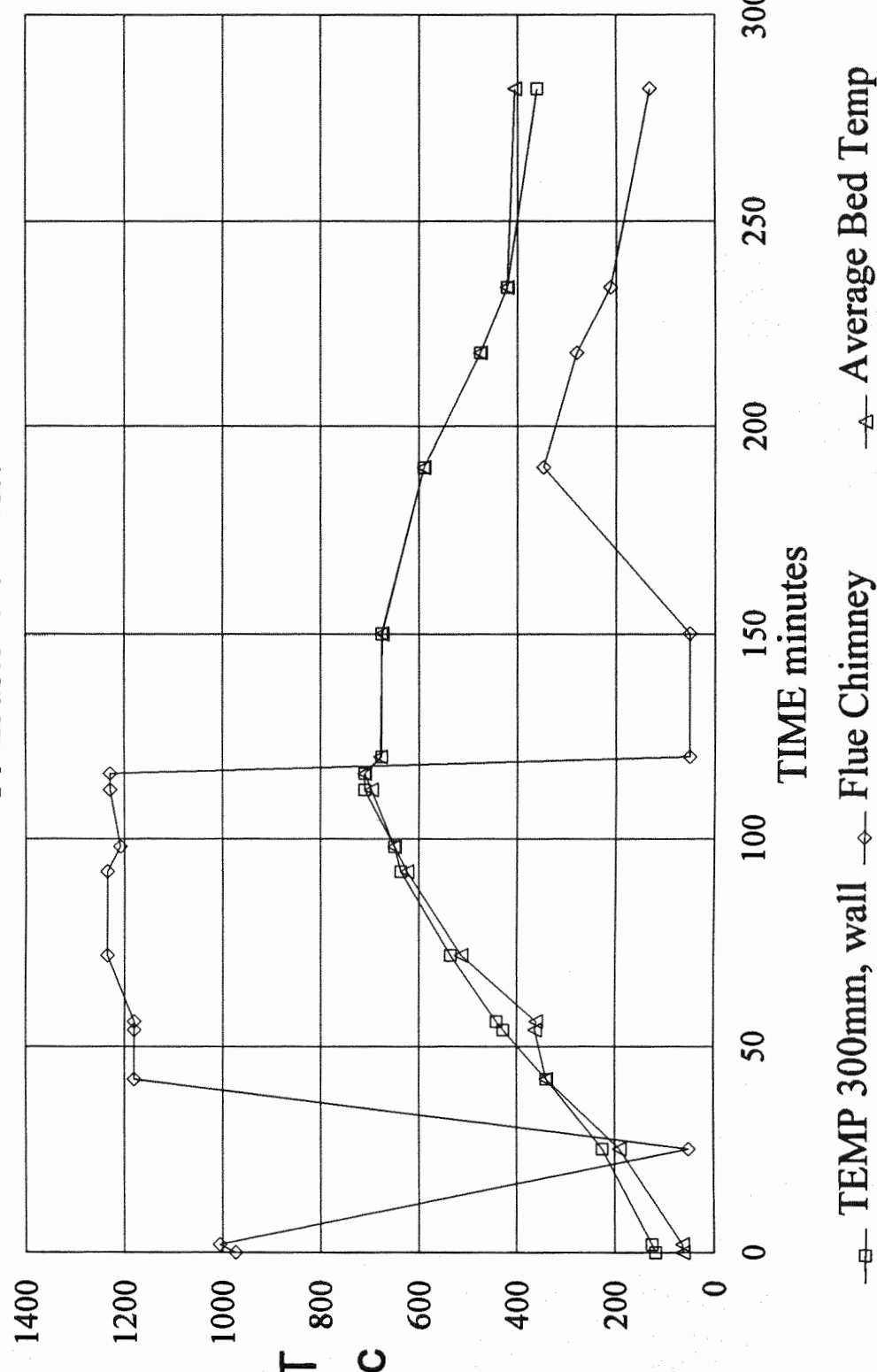


Fig. B12 Temperature vs Time
Combustor Run No.8

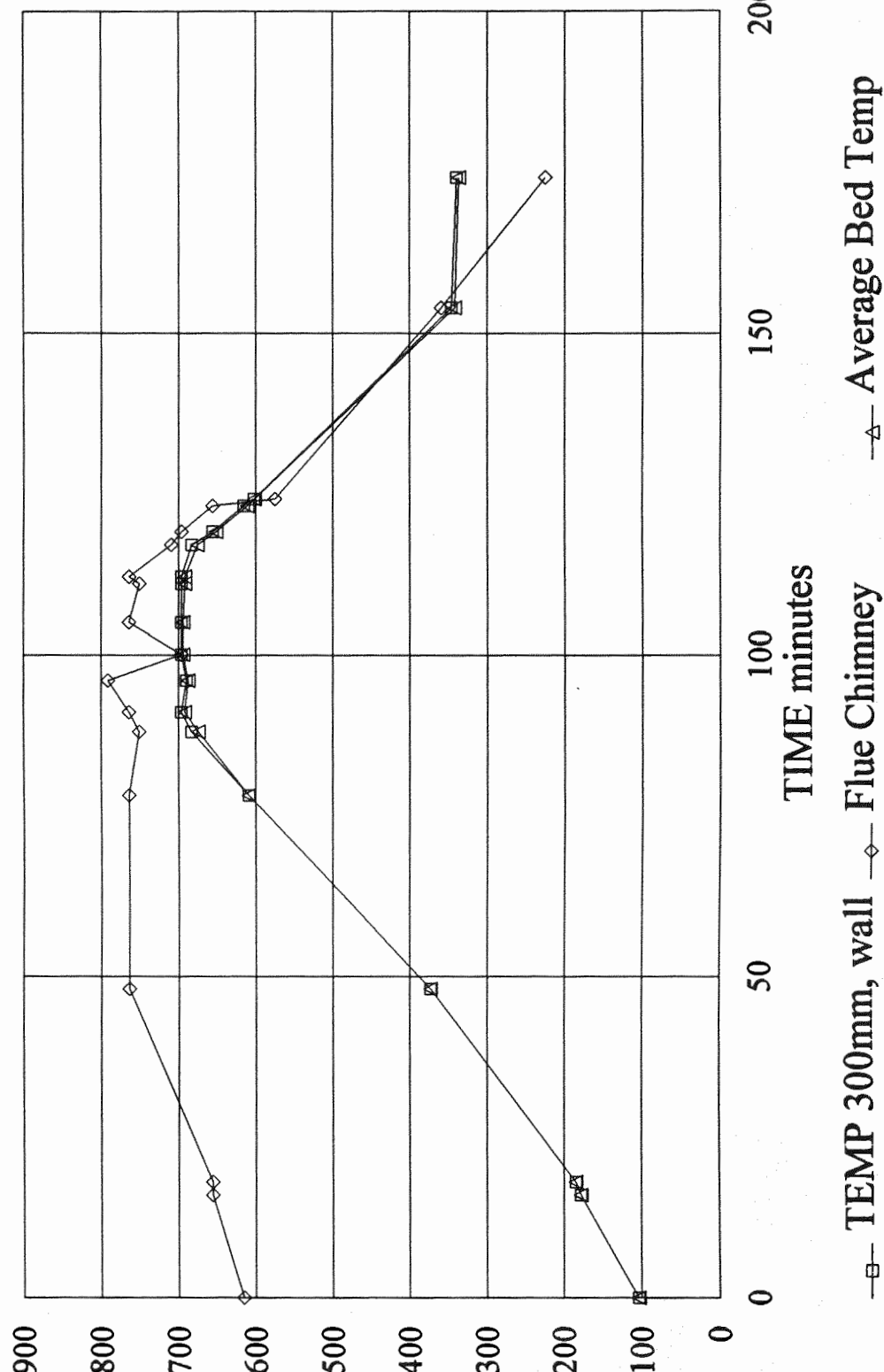


Fig.B13 U_f/U_{mf} vs Time
Combustor Run No.8

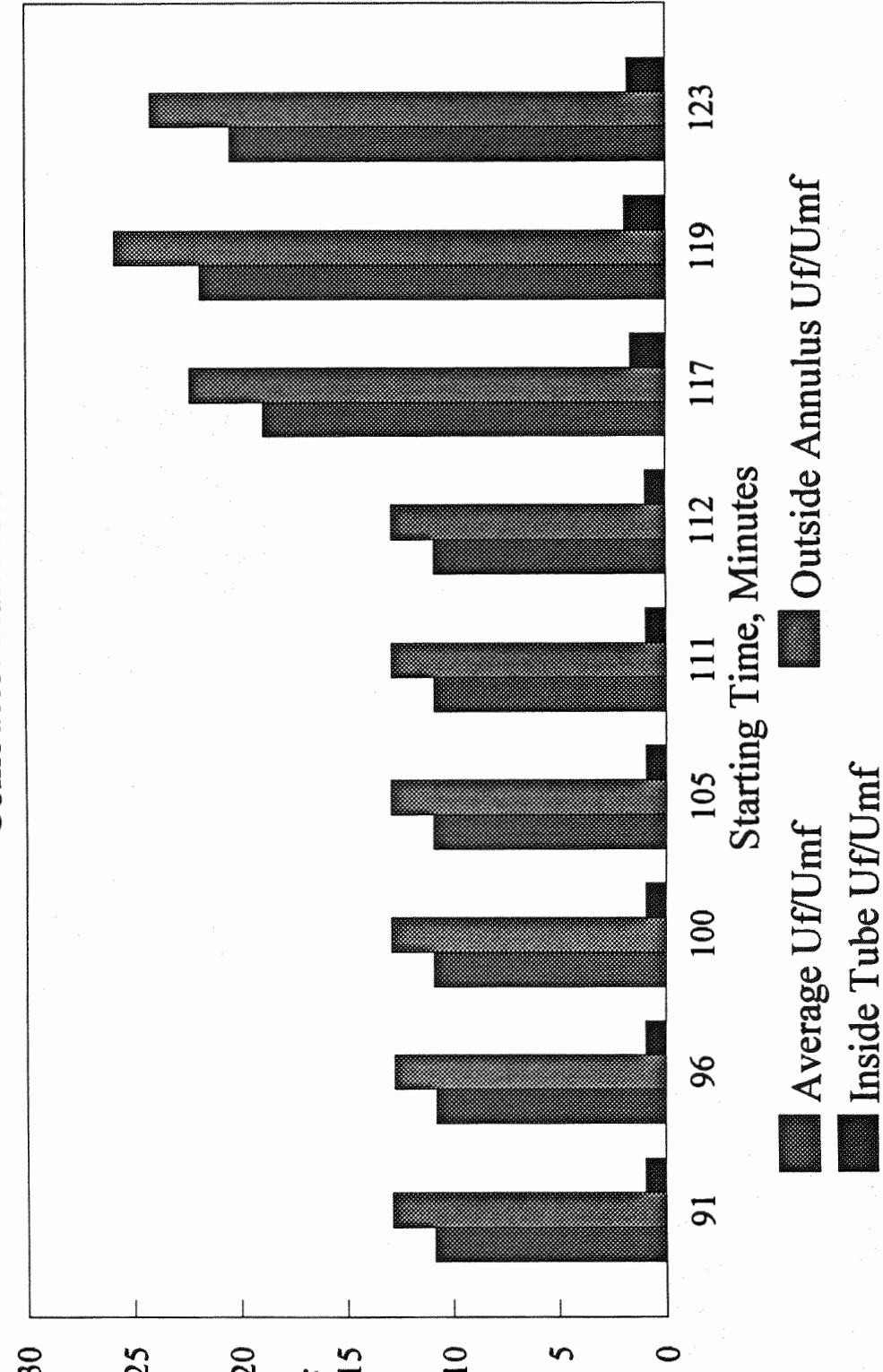


Fig.B14 Temperature vs Time

Combustor Run No.9

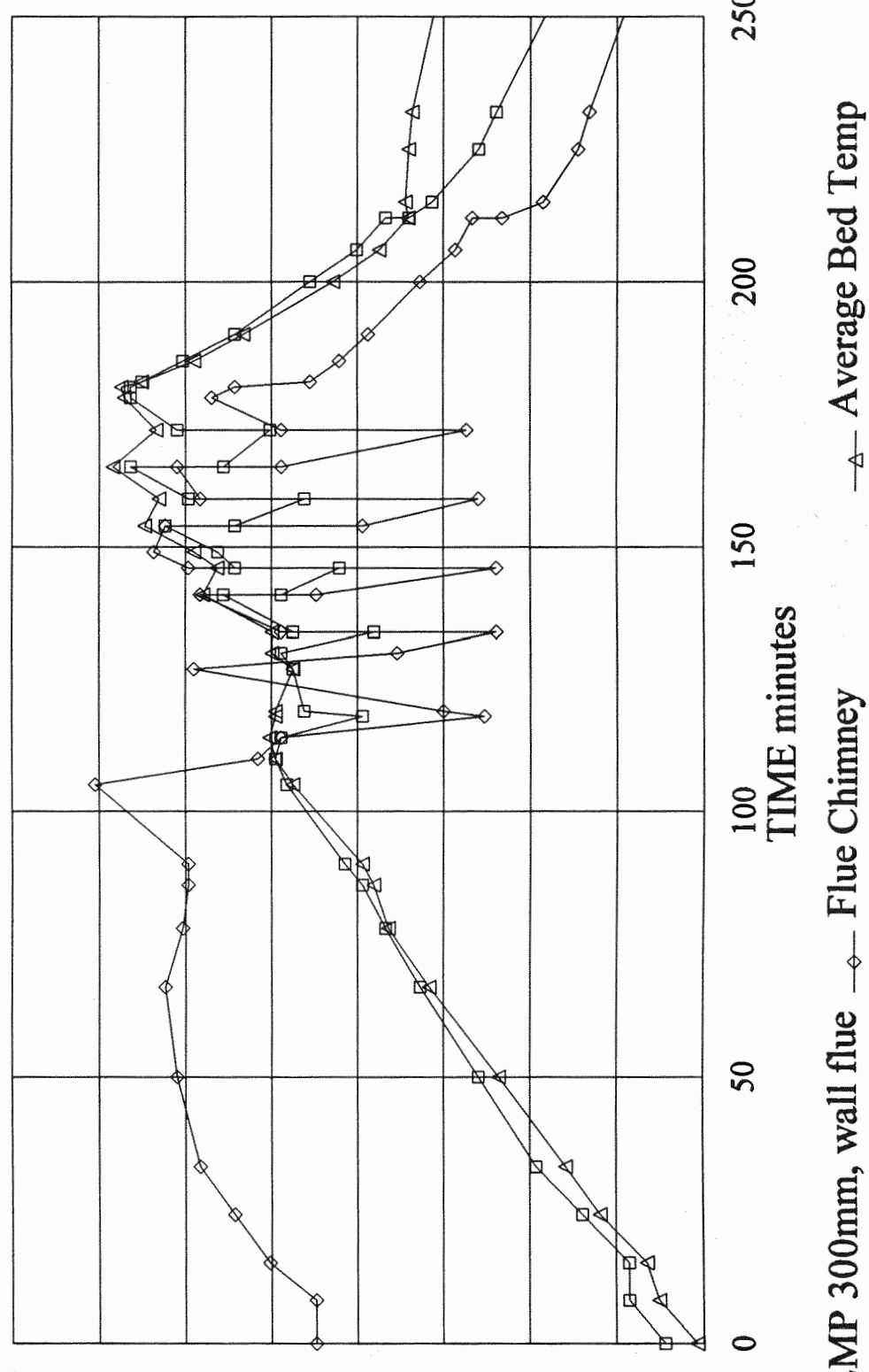


Fig. B15 U_f/U_{mf} vs Time
Combustor Run No.9

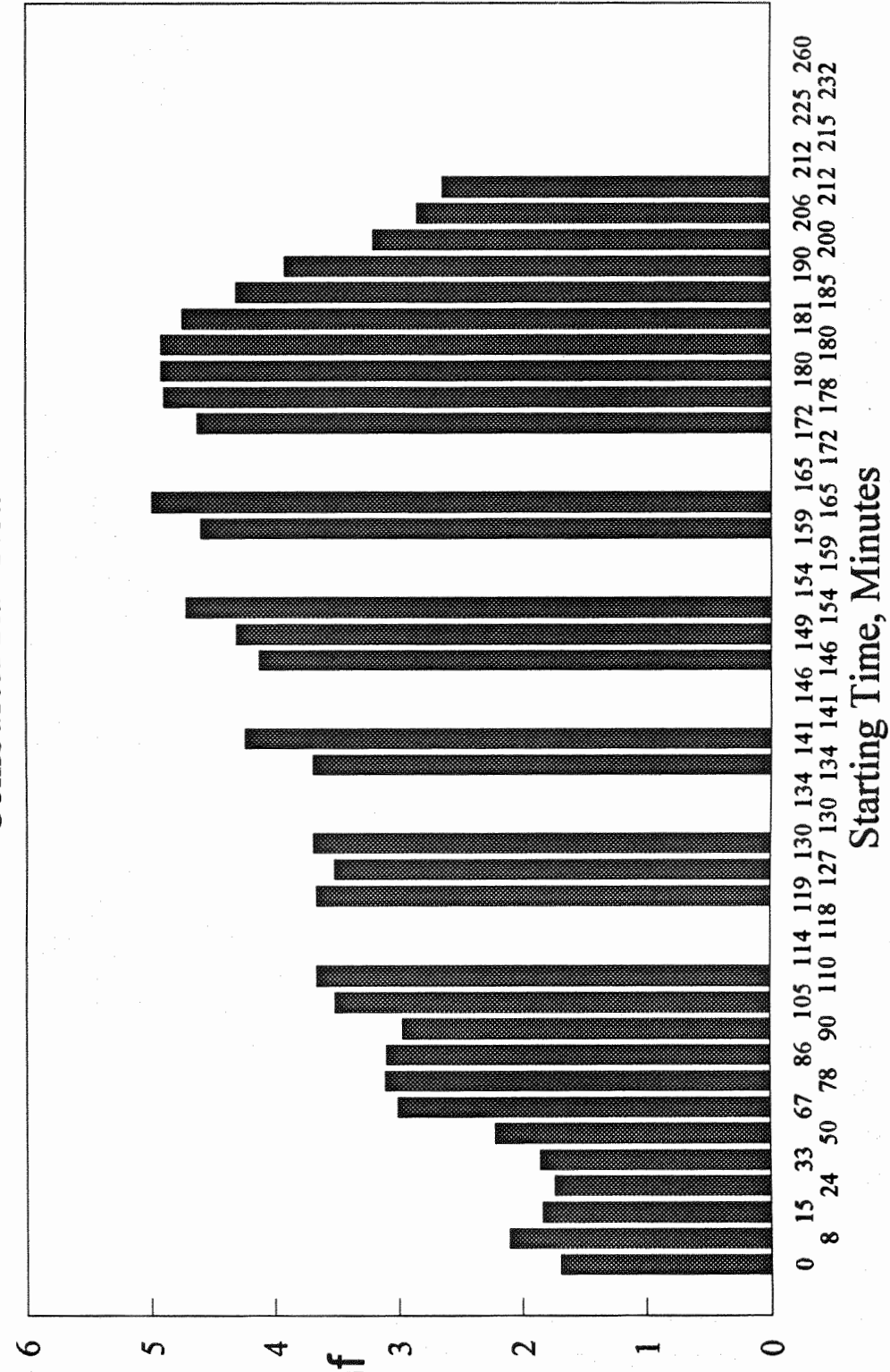


Fig.B16 Temperature vs Time Combustor Run No.10

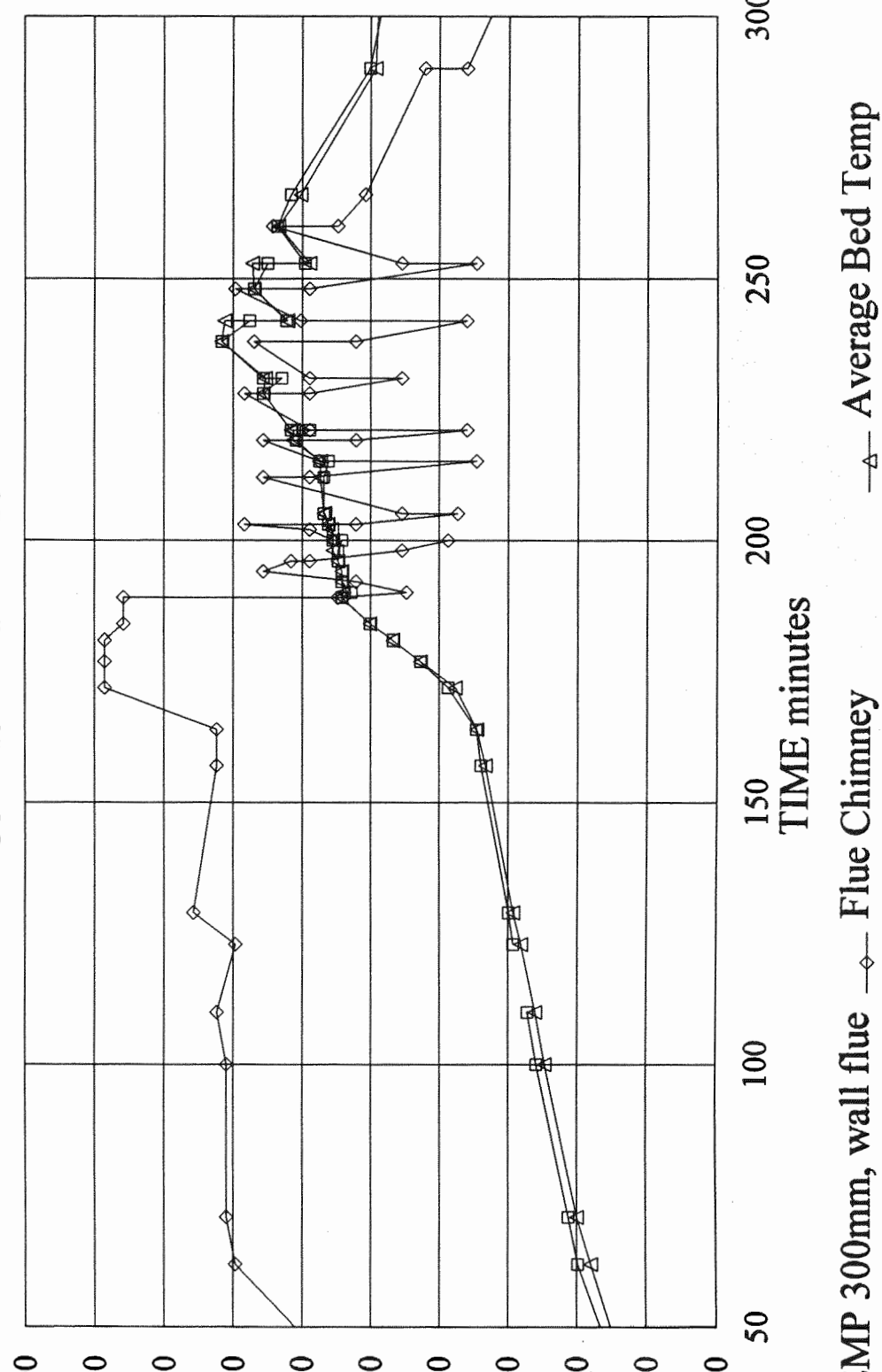
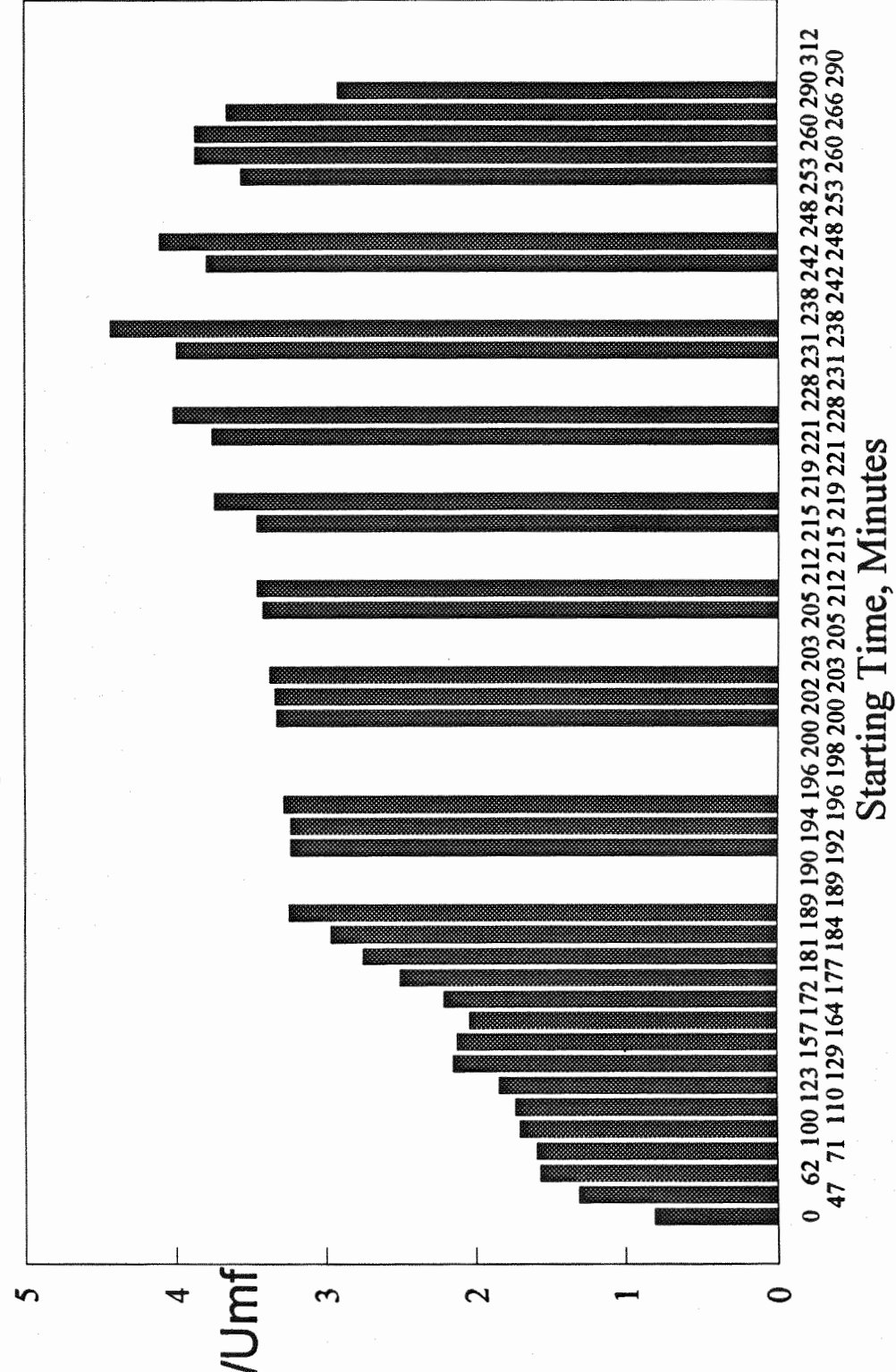


Fig.B17 U_f/U_{mf} vs Time
 Combustor Run No.10



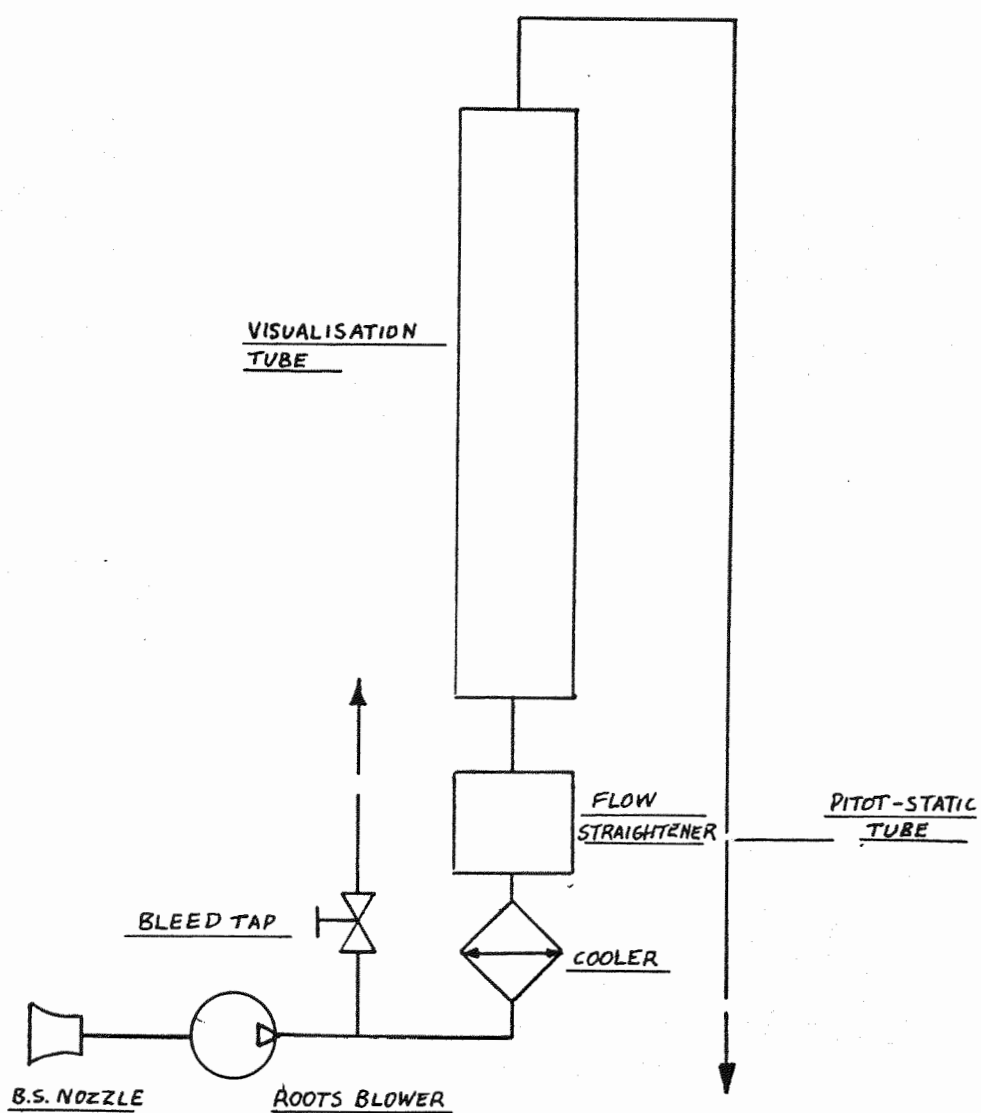
Appendix C : Equipment Drawings and PhotographsFig.C1 Flow Visualisation Schematic

Fig.C3 **Deep Bed Details, Mesh Distributor**

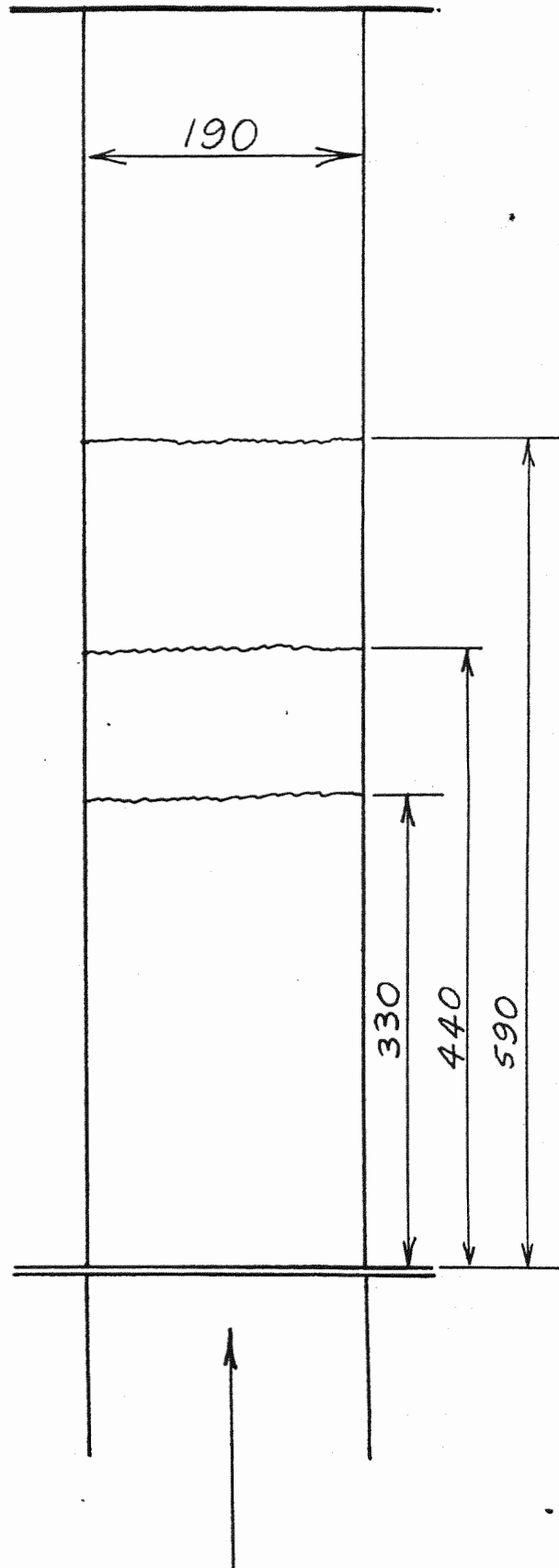


Fig.C4 **Bagasse-Sand Mixing Bed Details, Mesh Distributor**

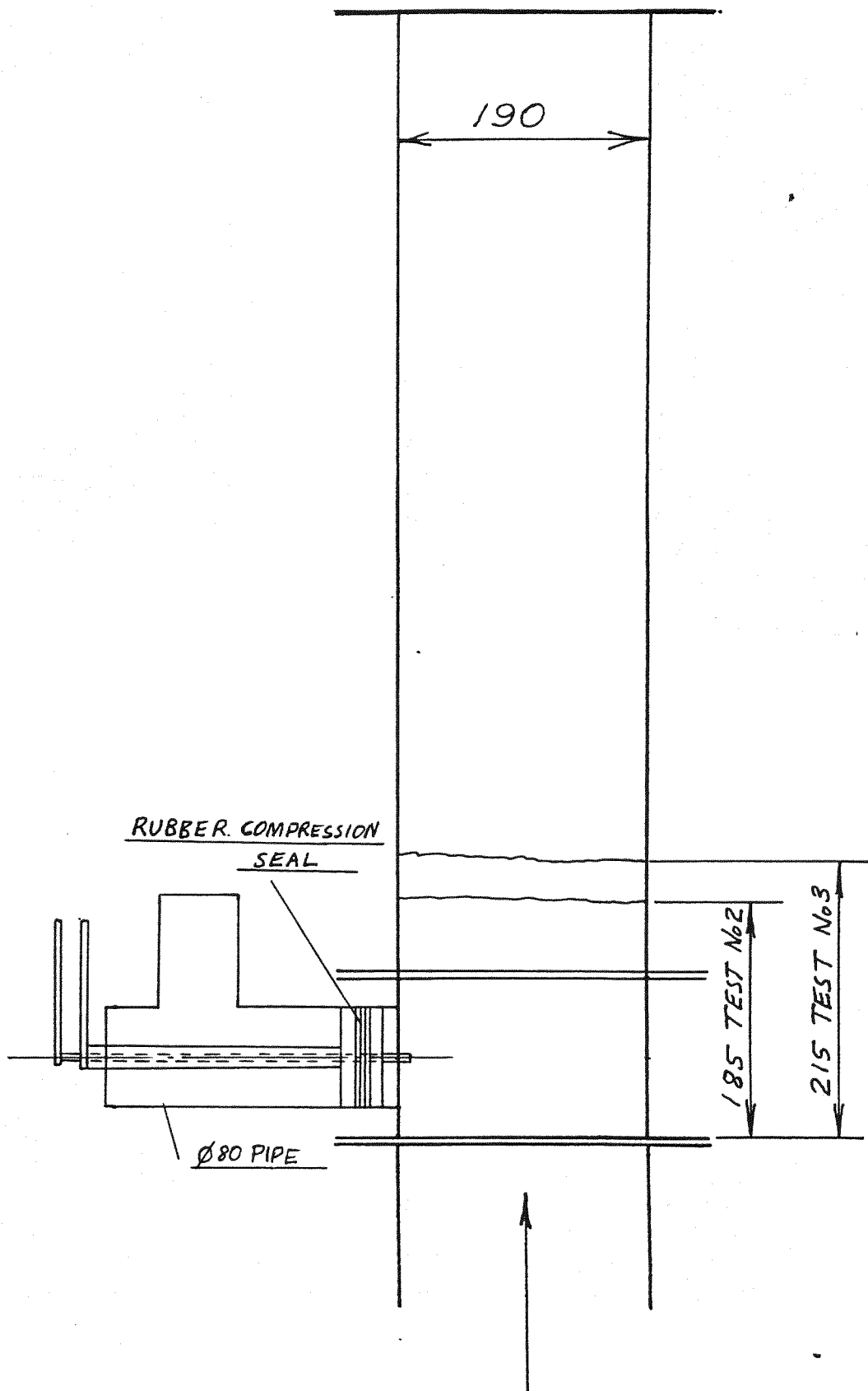


Fig.C5

Enhanced Mixing Bed Details, Central Flow Distributor

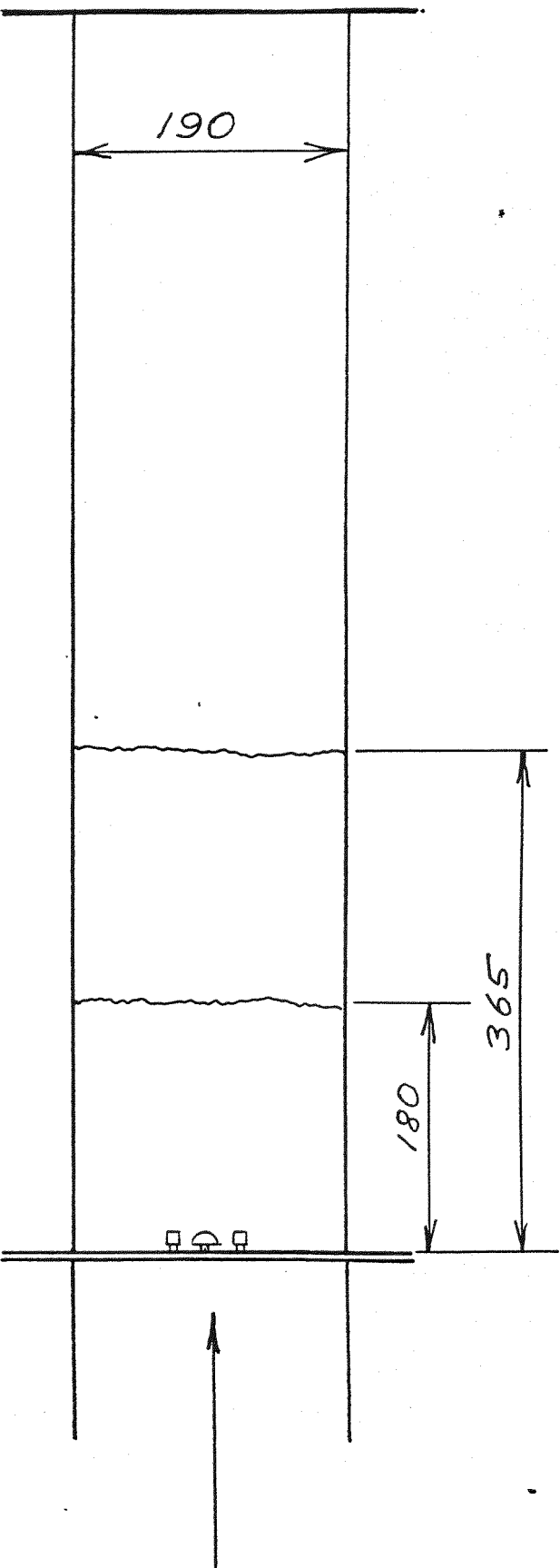


Fig.C6 **Enhanced Mixing Central Flow Distributor**

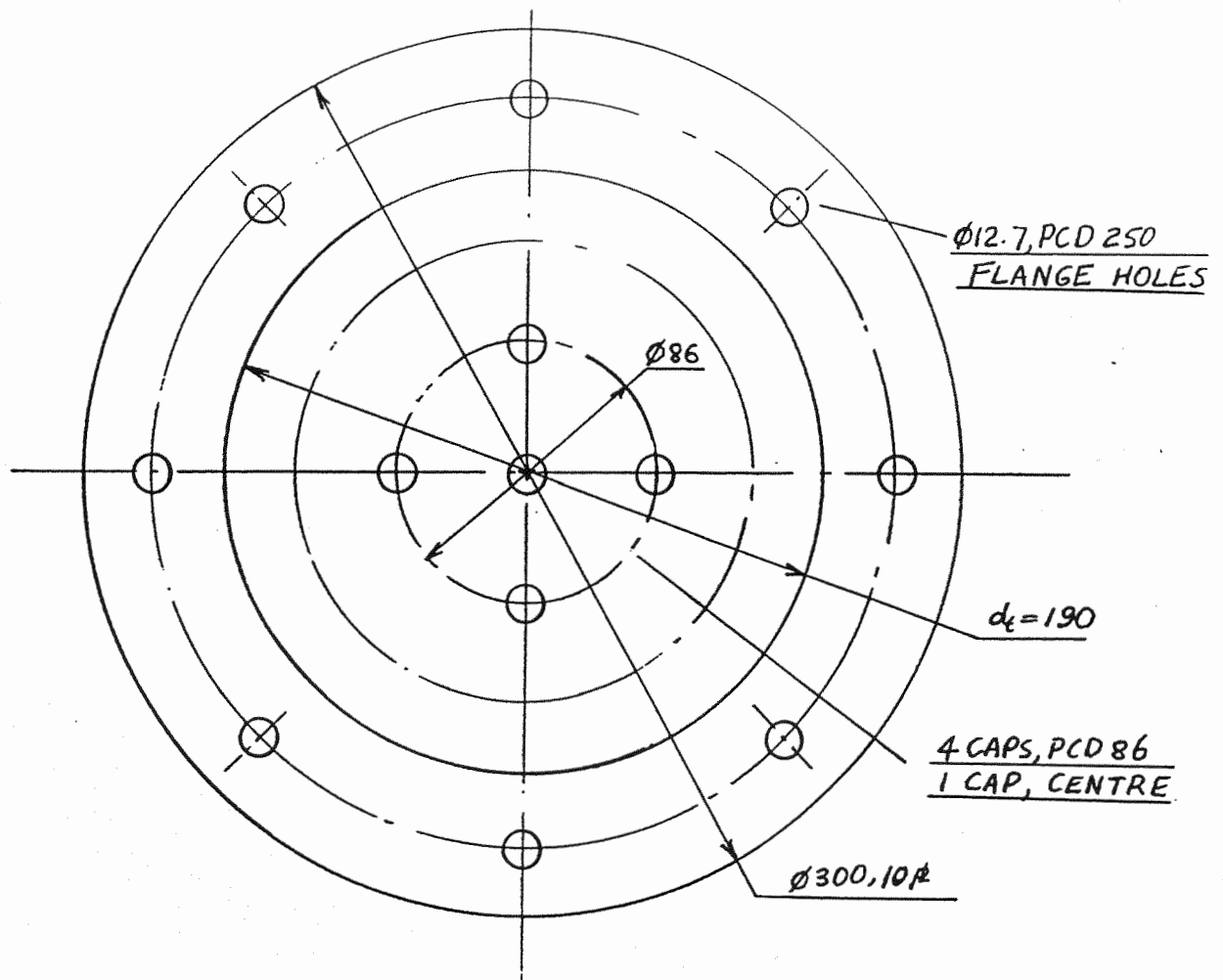


Fig.C8 **Draft Tube Central Flow Distributor**

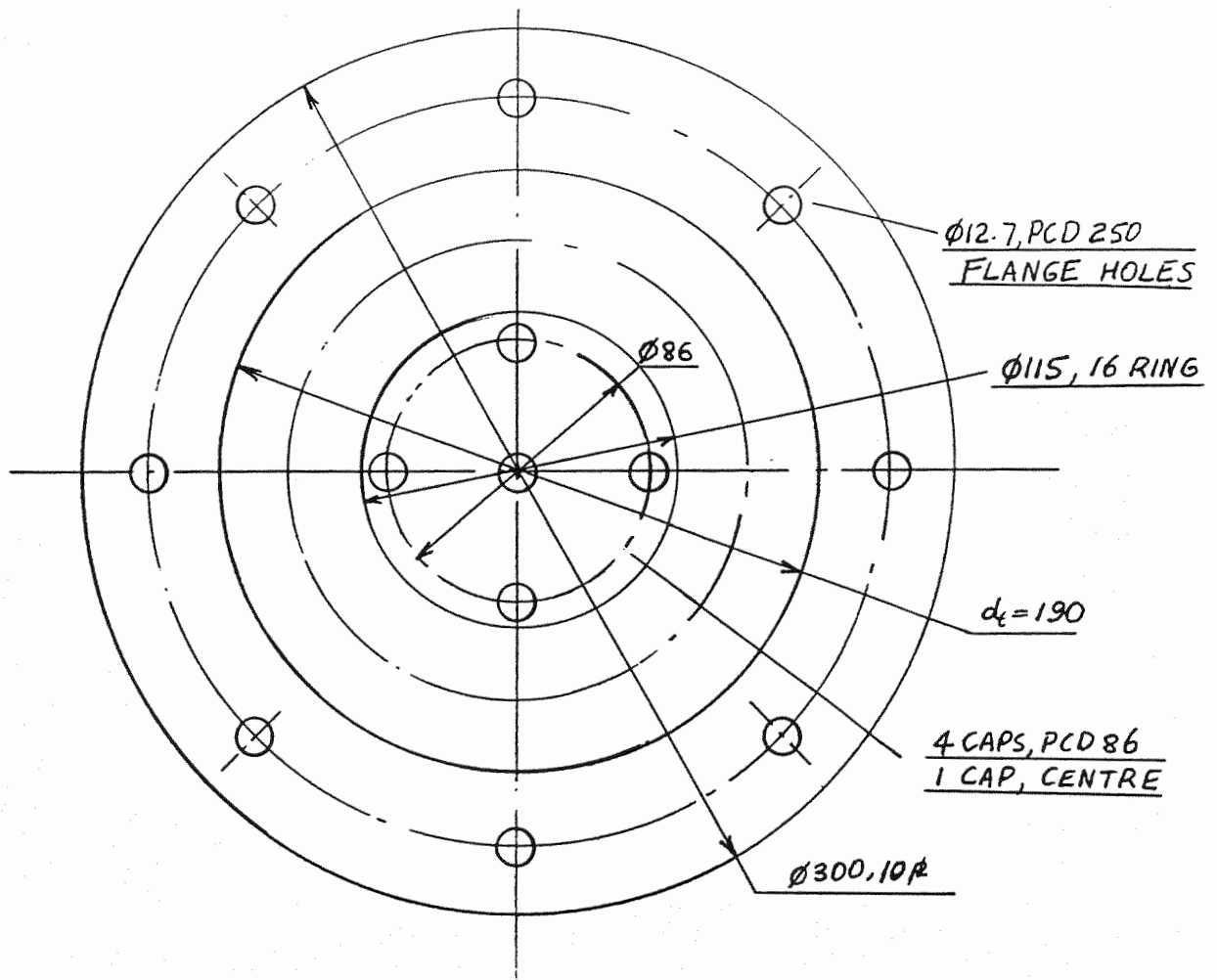


Fig.C9 **Enhanced Mixing Bed Details, Small Cone, Mesh Distributor**

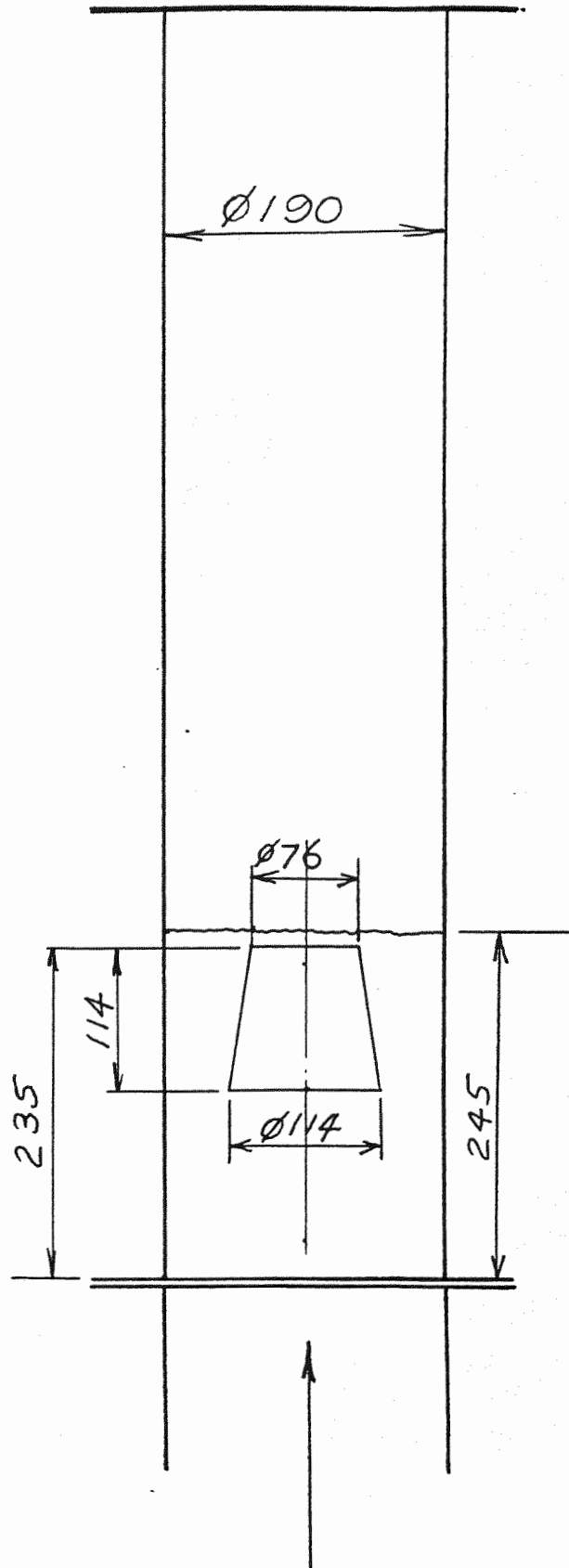


Fig.C10 **Enhanced Mixing Bed Details, Large Cone, Mesh Distributor**

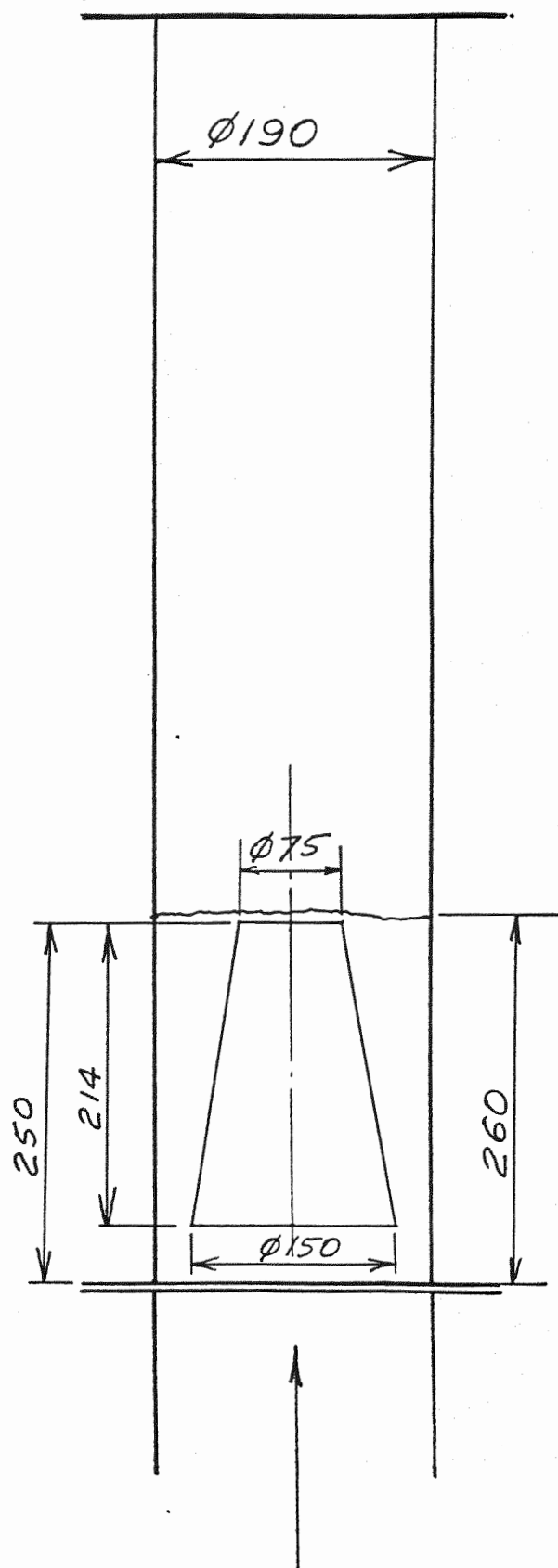


Fig.C11 **Reversed Mixing Bed Details, Annulus Flow**
Distributor

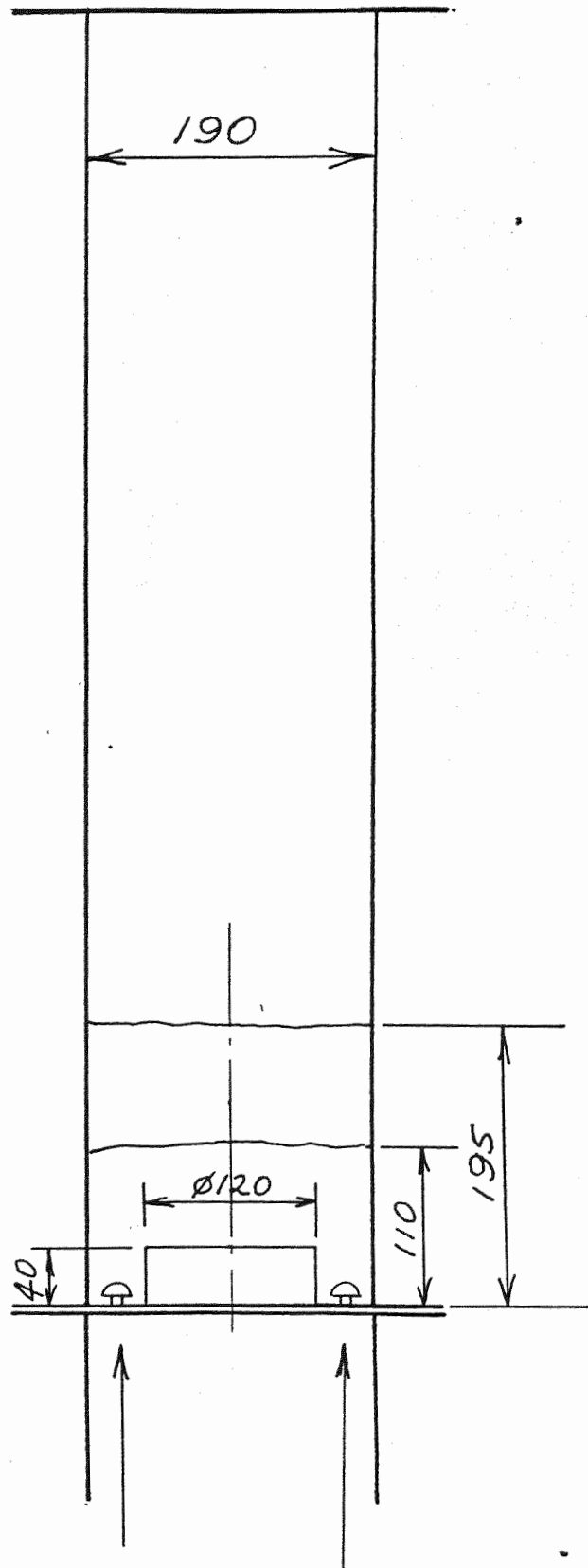


Fig.C12 **Reversed Mixing Flow Distributor**

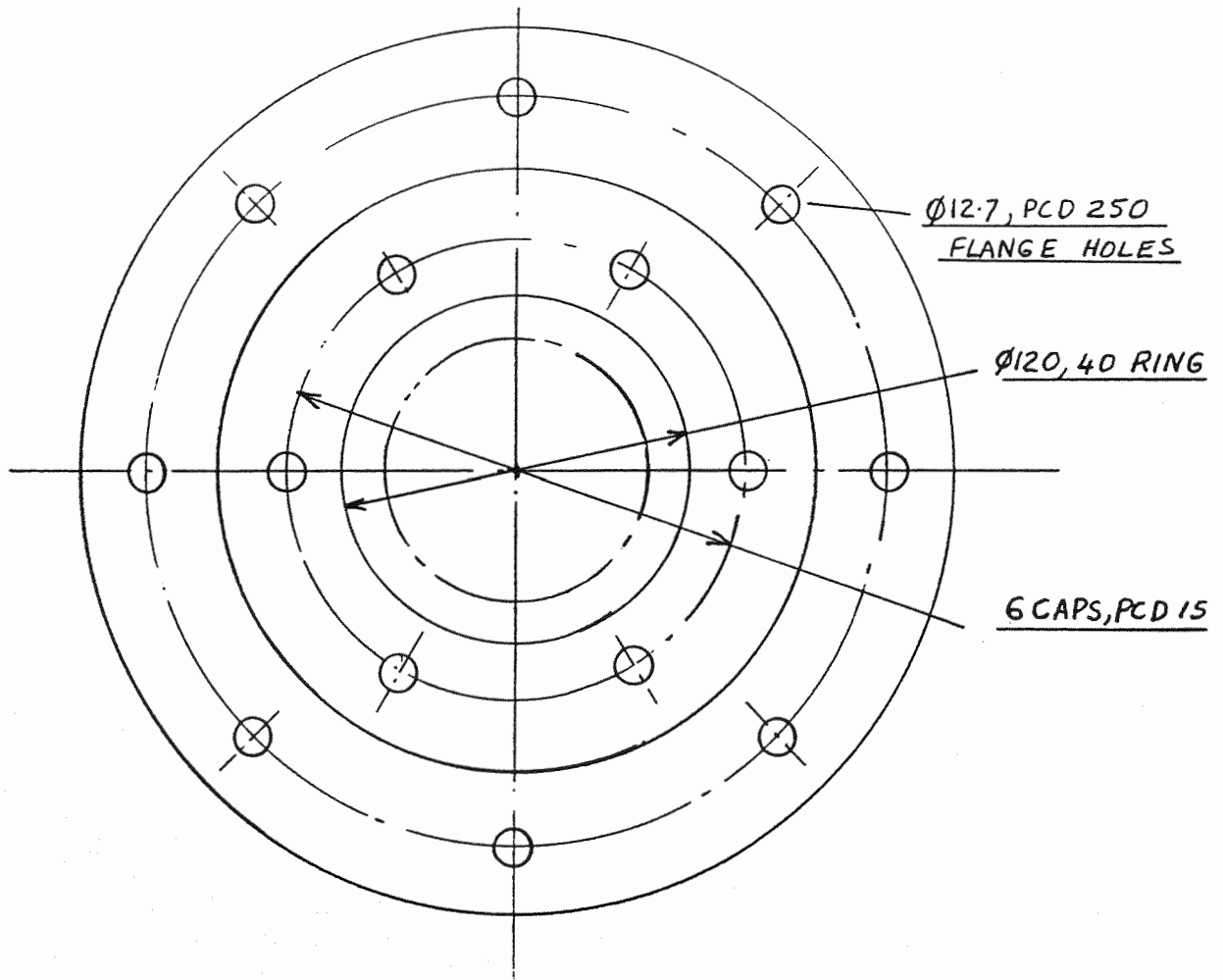


Fig.C13 Reversed Mixing Bed Details, Ingestor Tube, Mesh Plate

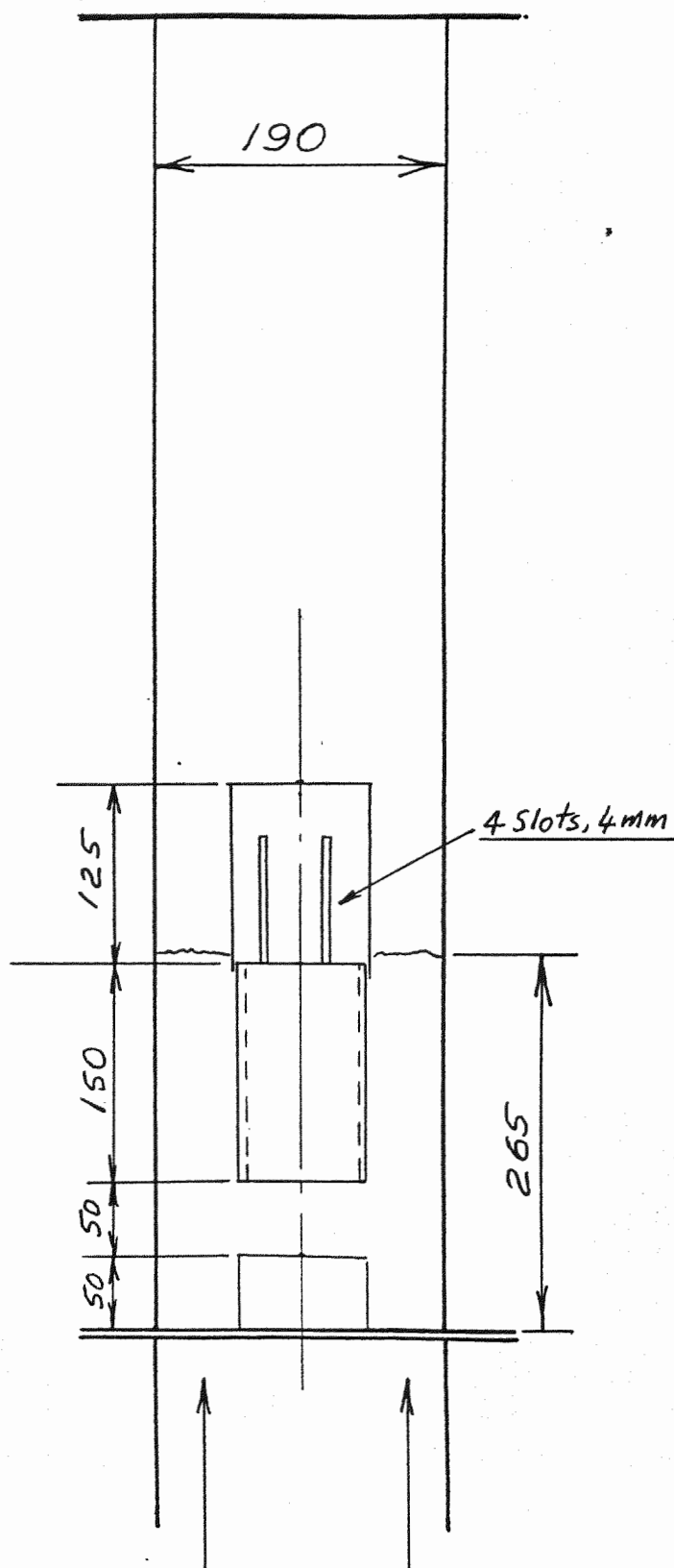


Fig.C14 Combustor Schematic

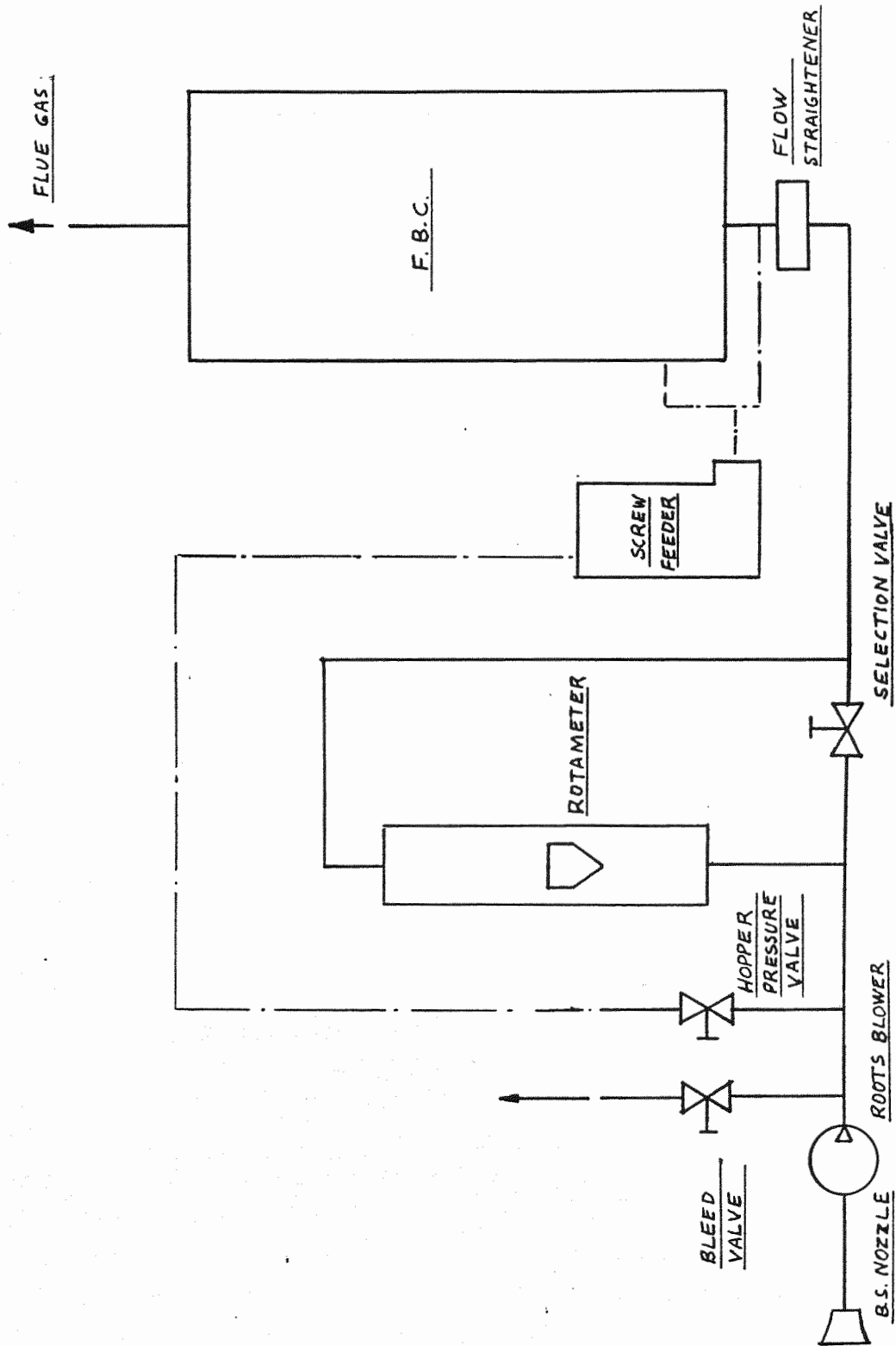


Fig.C16 Combustor Tube Details, Combustor Run 1 & 2

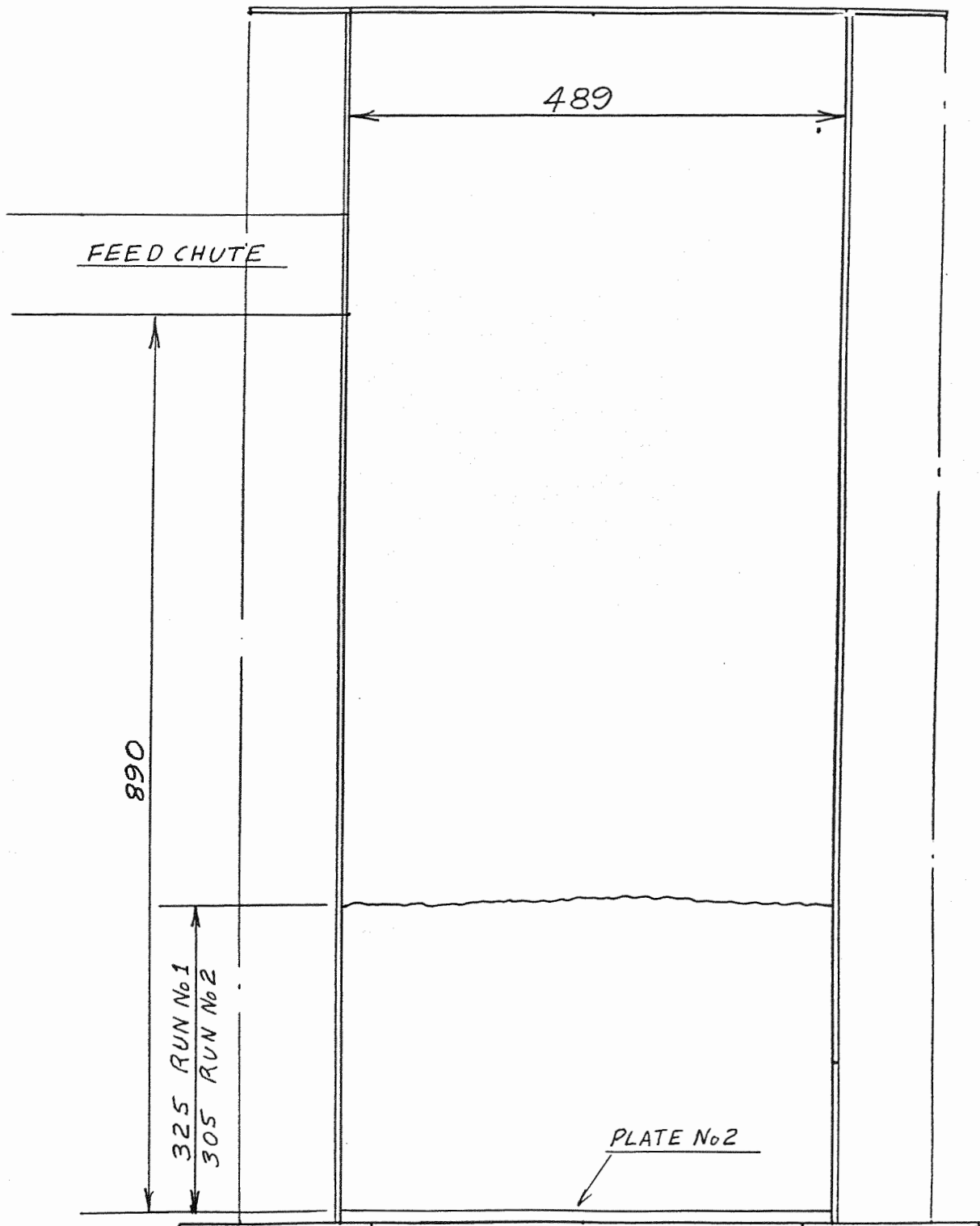


Fig.C17 **Combustor Tube Details, Combustor Run 3**

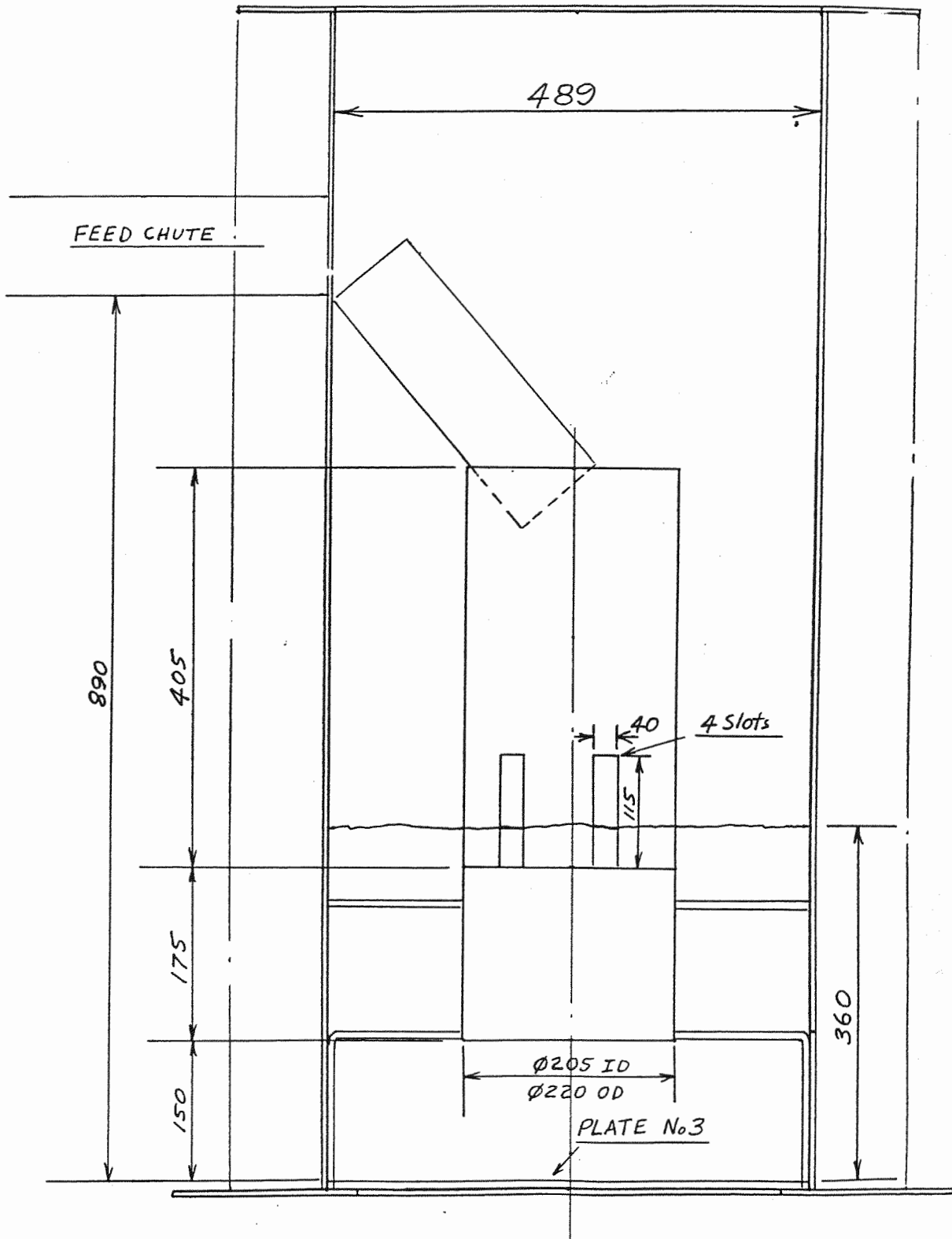


Fig.C18 Combustor Tube Details, Combustor Run 4 & 5

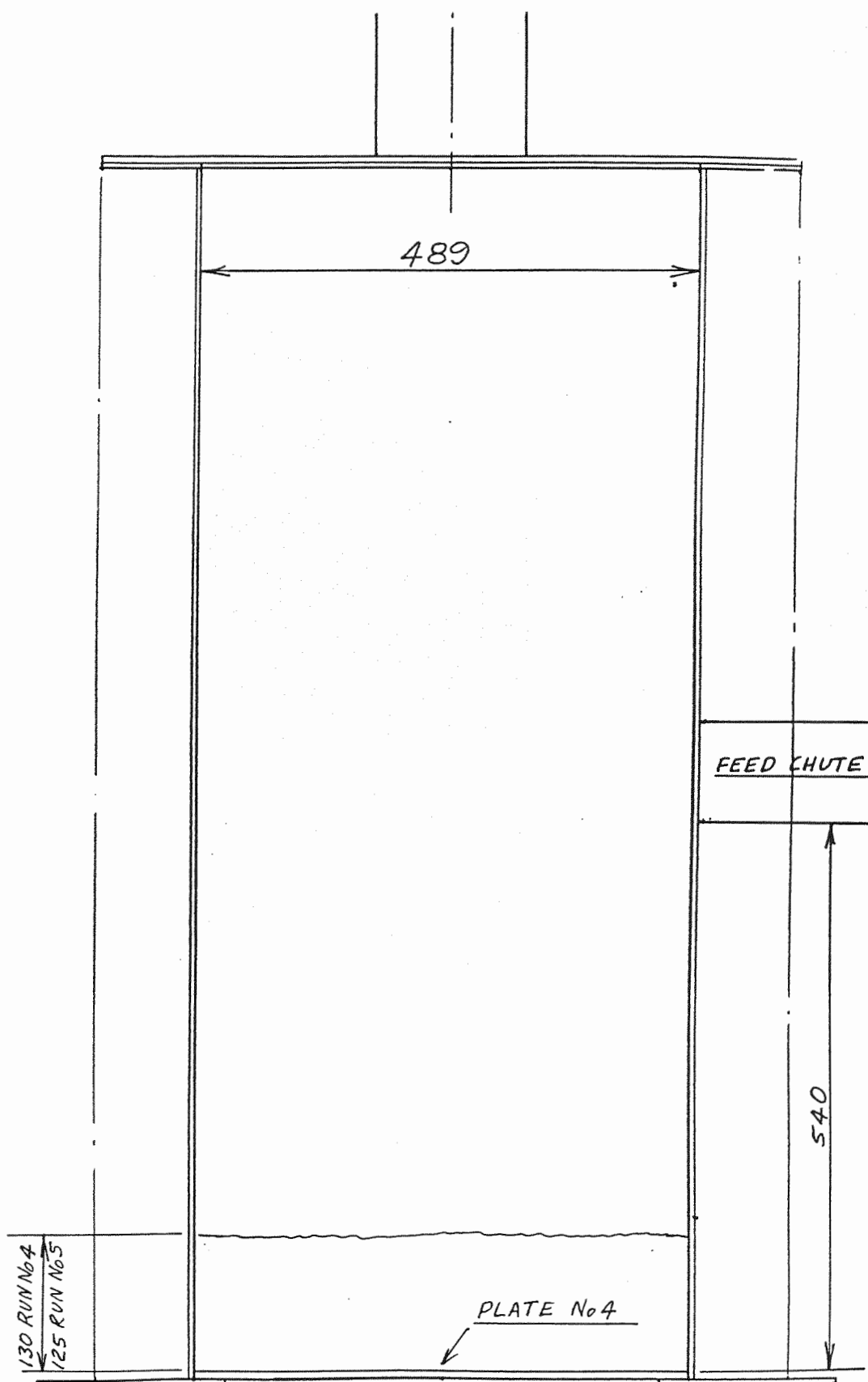


Fig.C19 Combustor Tube Details, Combustor Run 6 & 7

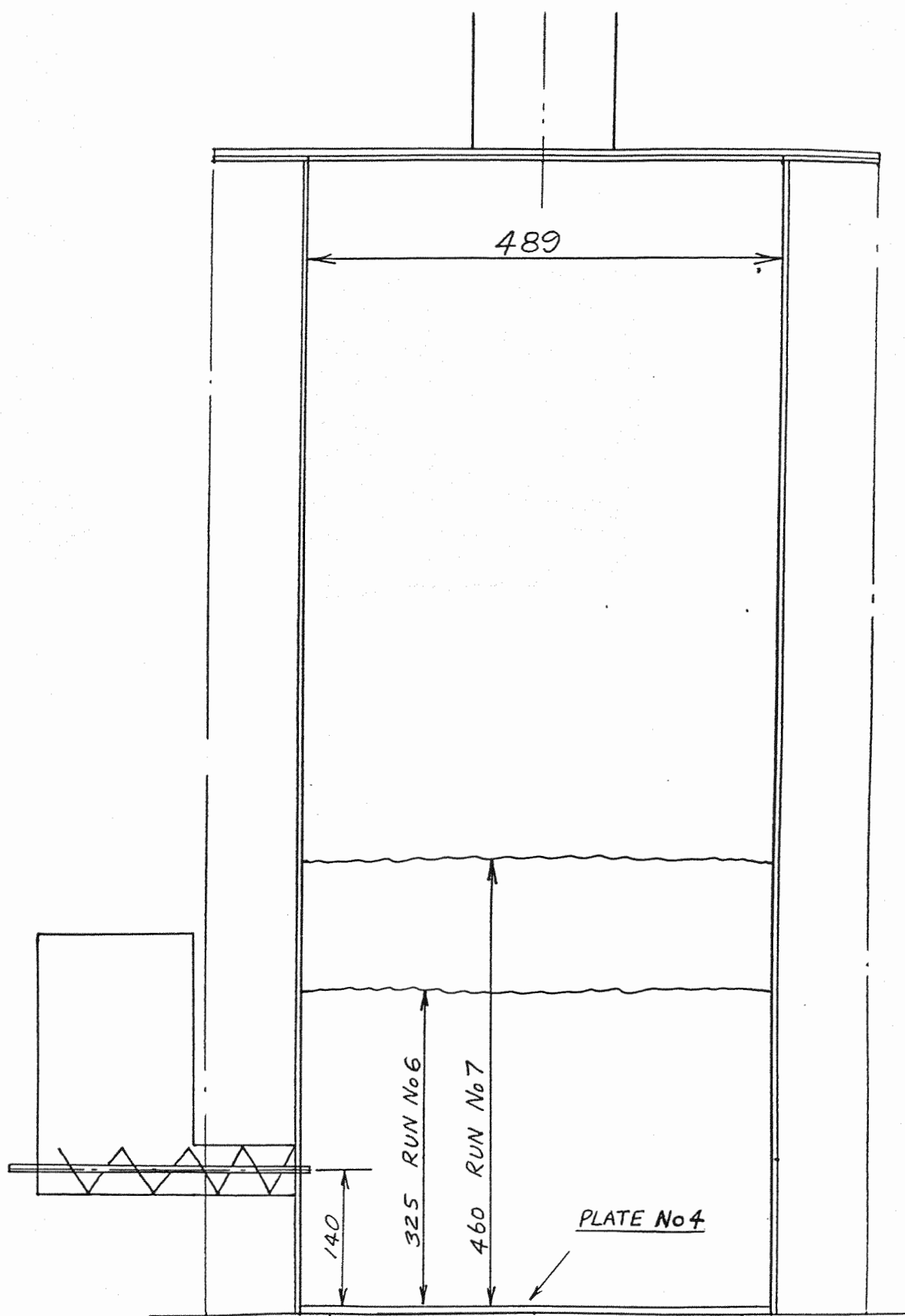


Fig.C21 Combustor Tube Details, Combustor Run 9 & 10

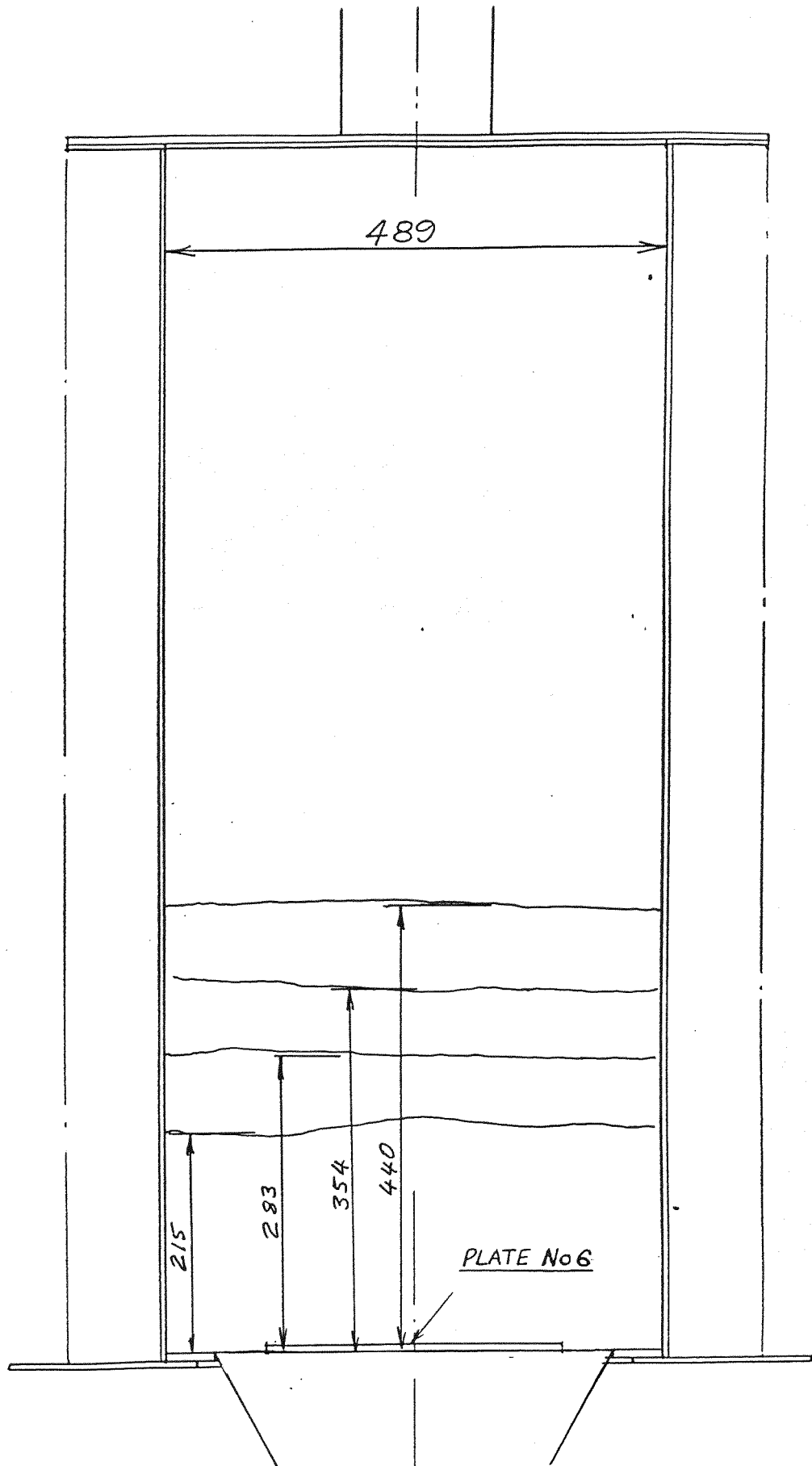


Fig.C22 Bubble Cap Locations,Distributor Plate No 1

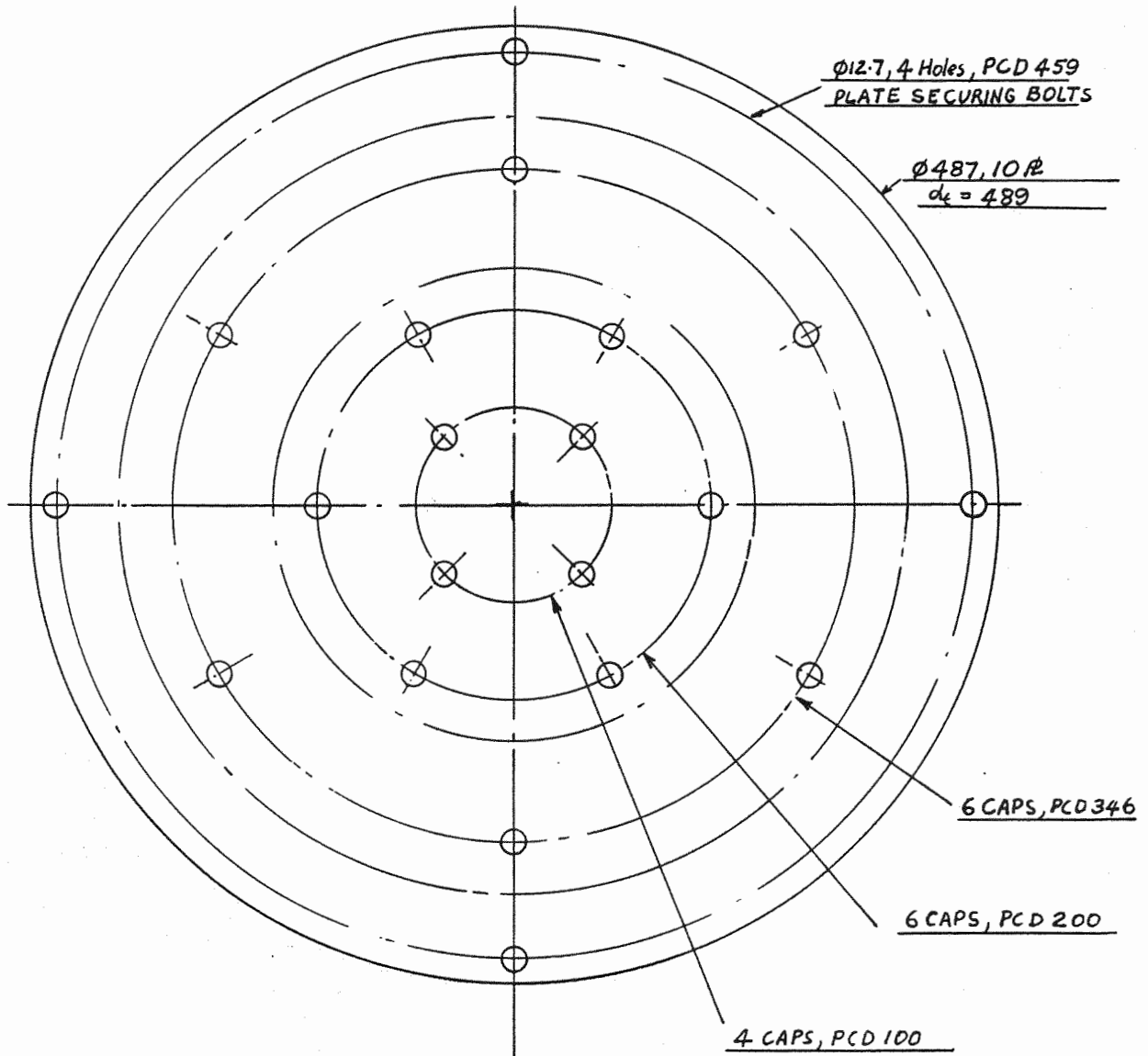


Fig.C23 Bubble Cap Locations,Distributor Plate No 2

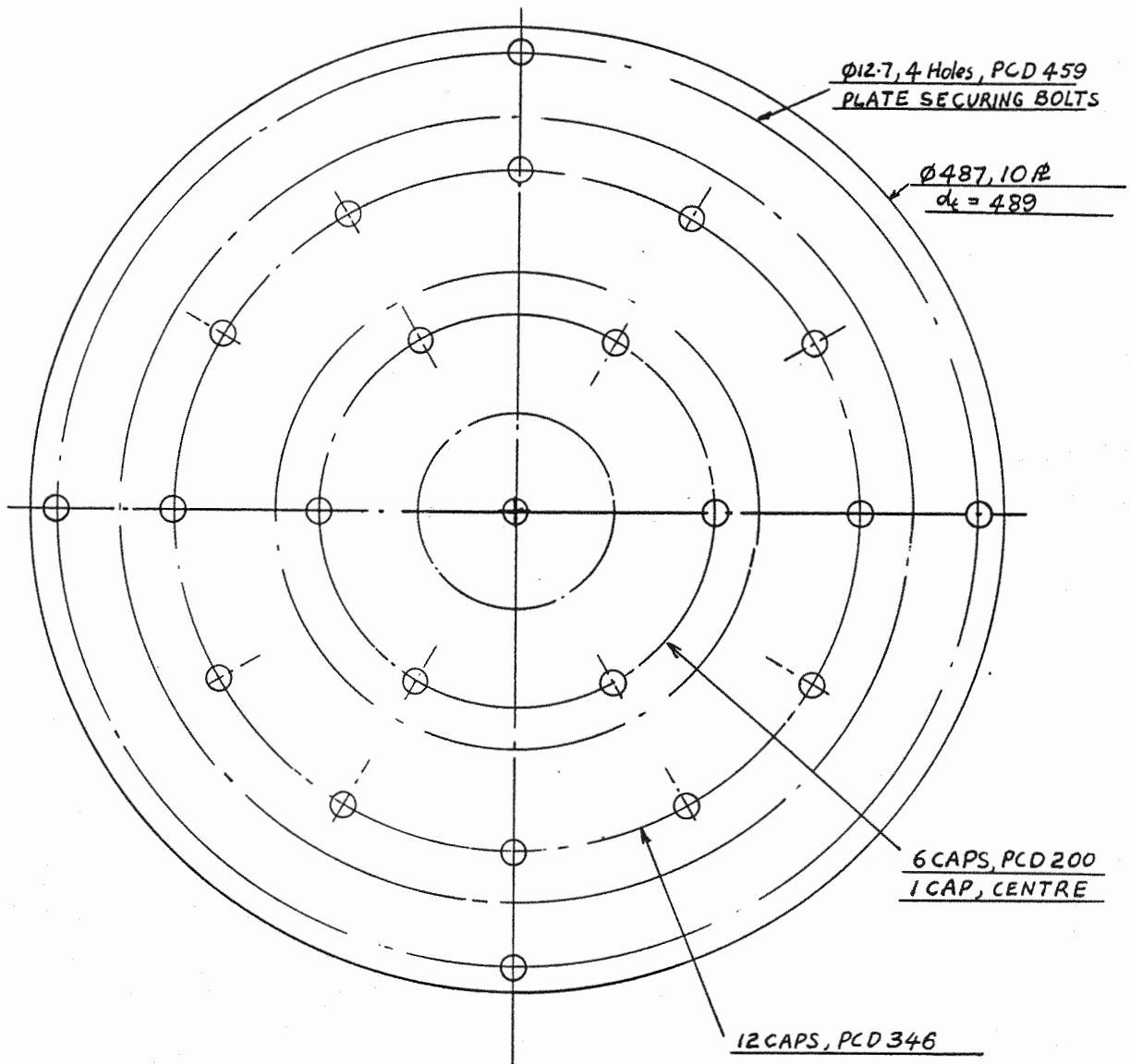


Fig.C24 Bubble Cap Locations,Distributor Plate No 3

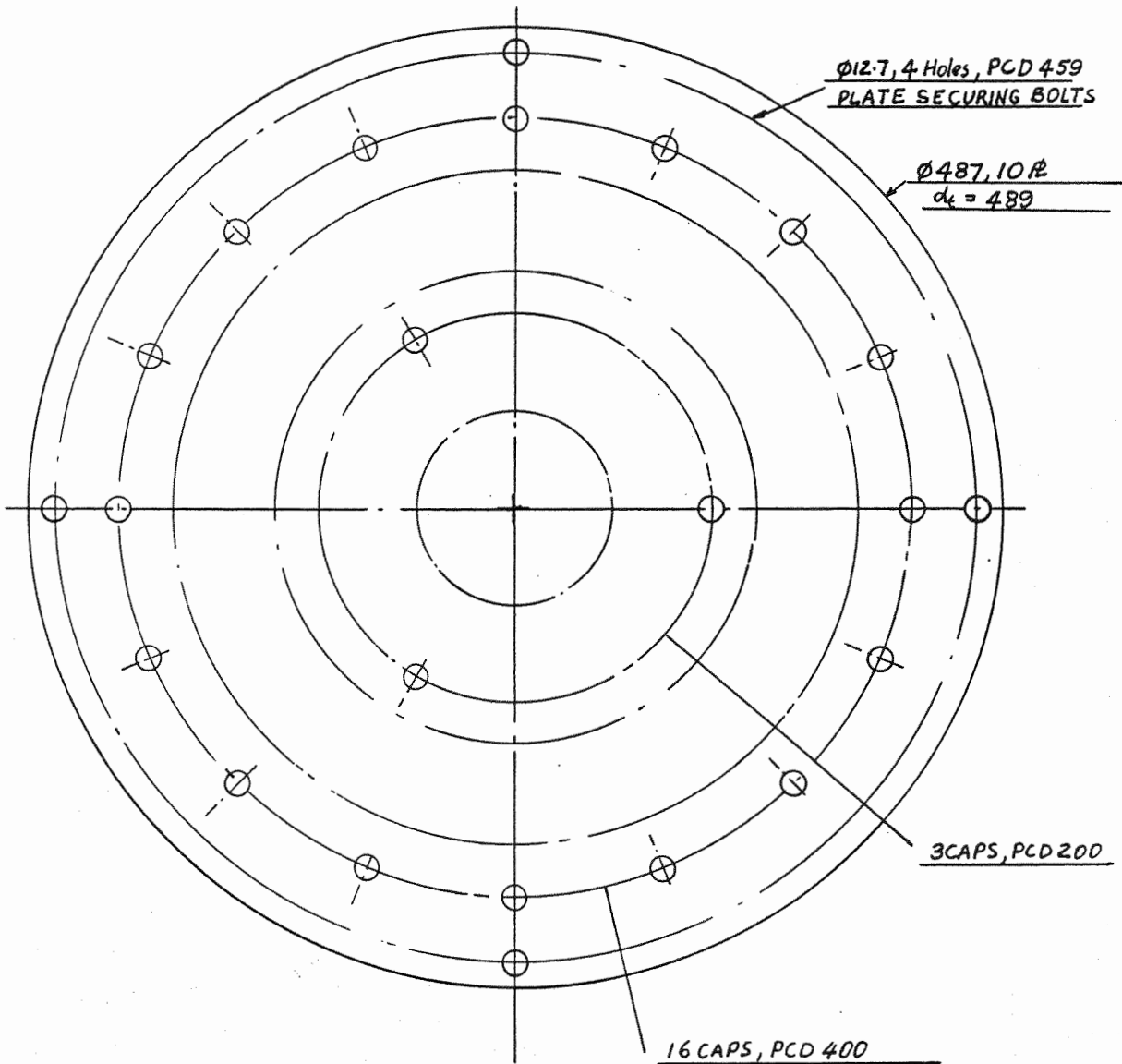


Fig.C25 Bubble Cap Locations,Distributor Plate No 4

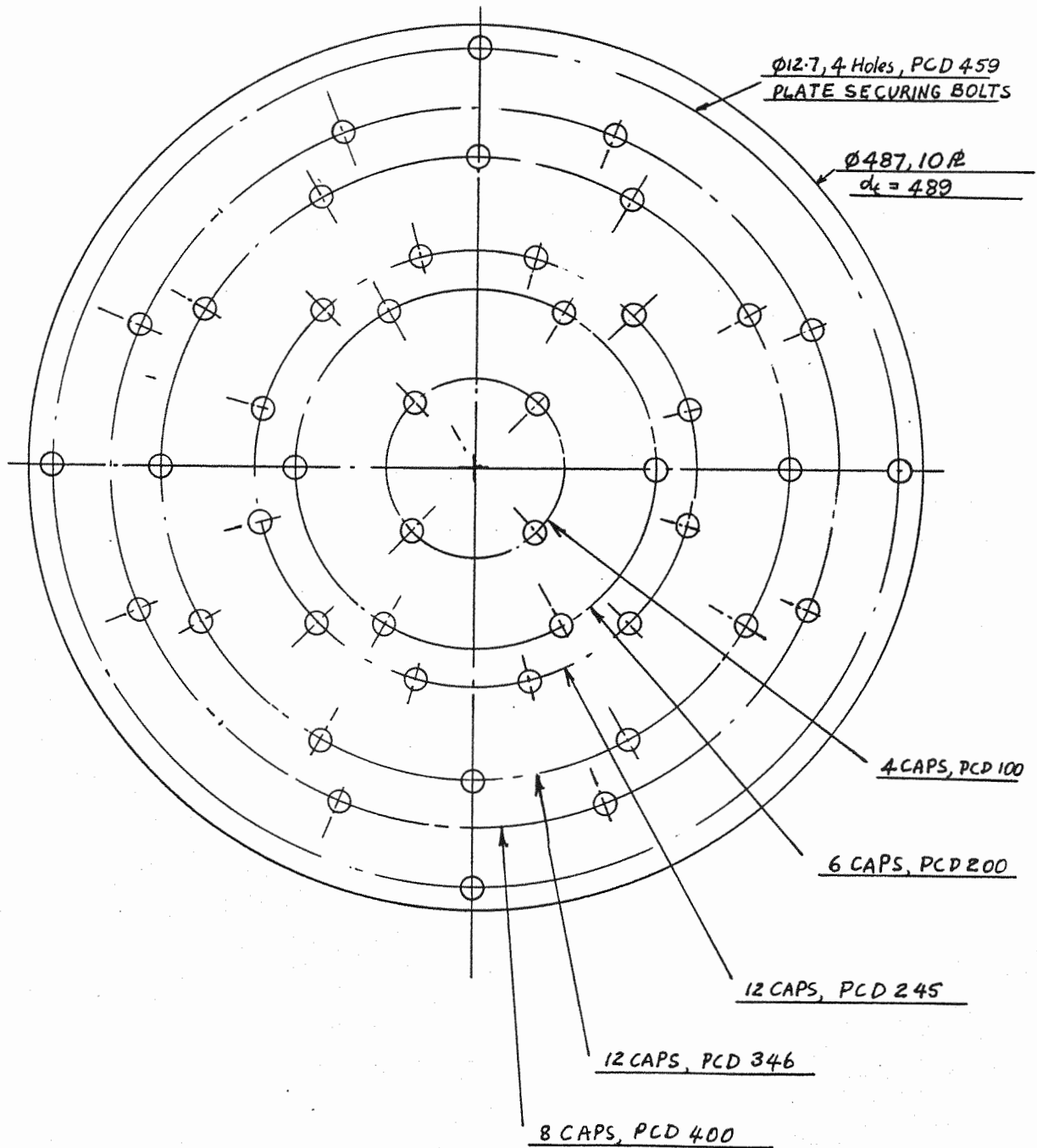


Fig.C26 Bubble Cap Locations,Distributor Plate No 5

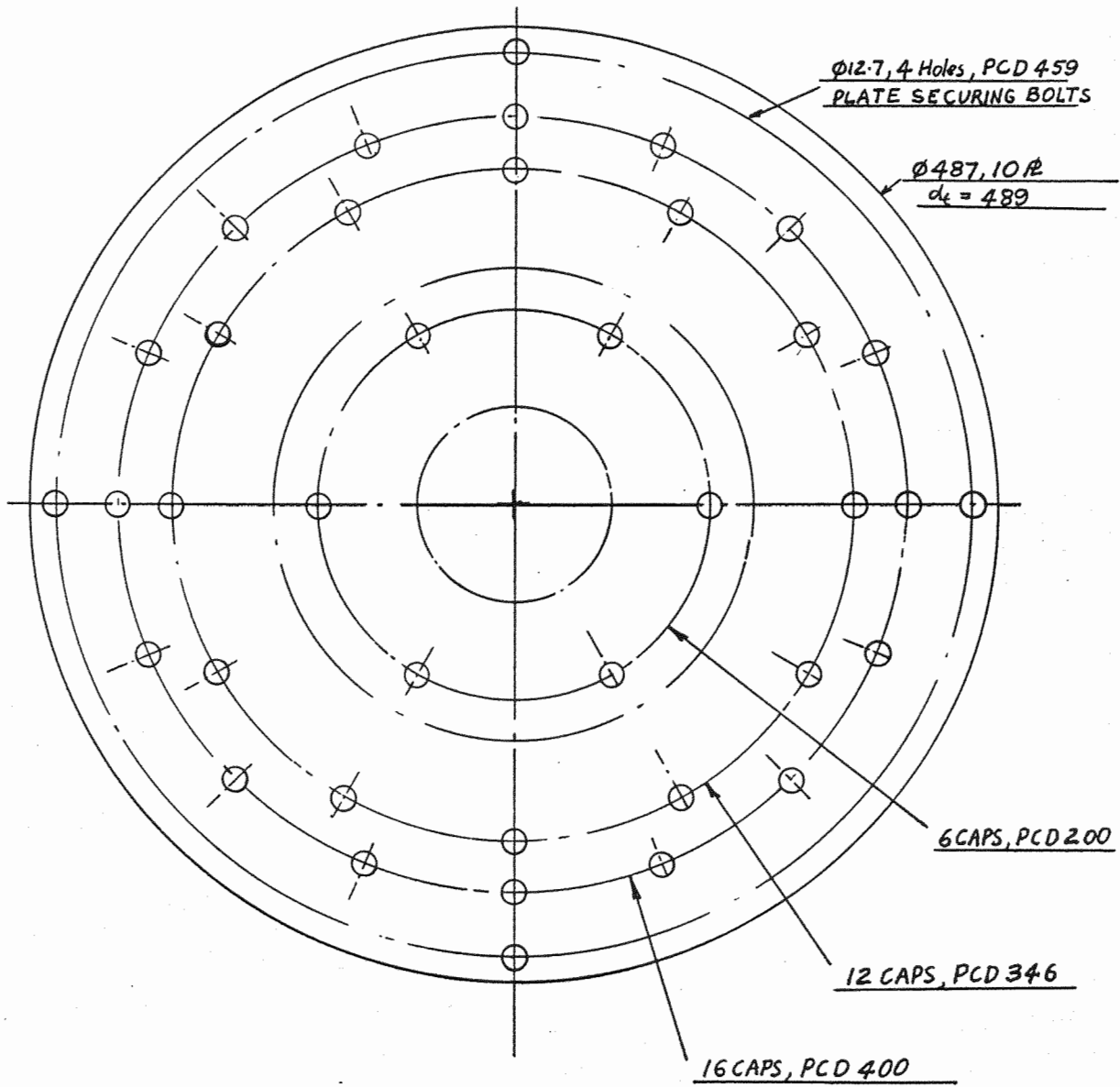


Fig.C27 Hole Locations,Distributor/Baffle Plate No 6

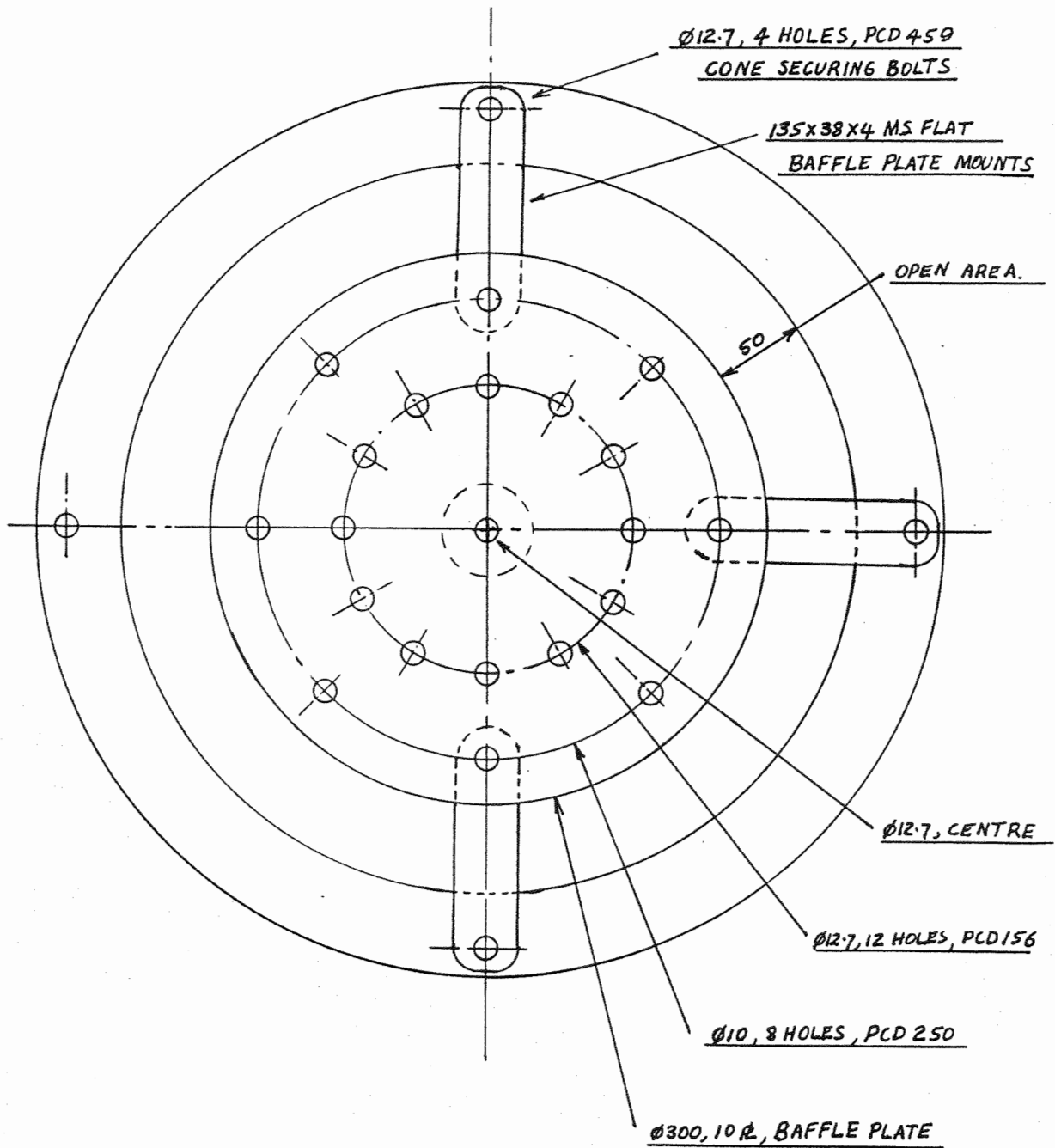


Fig.C28 **Modified Spouted Bed Cone Details**

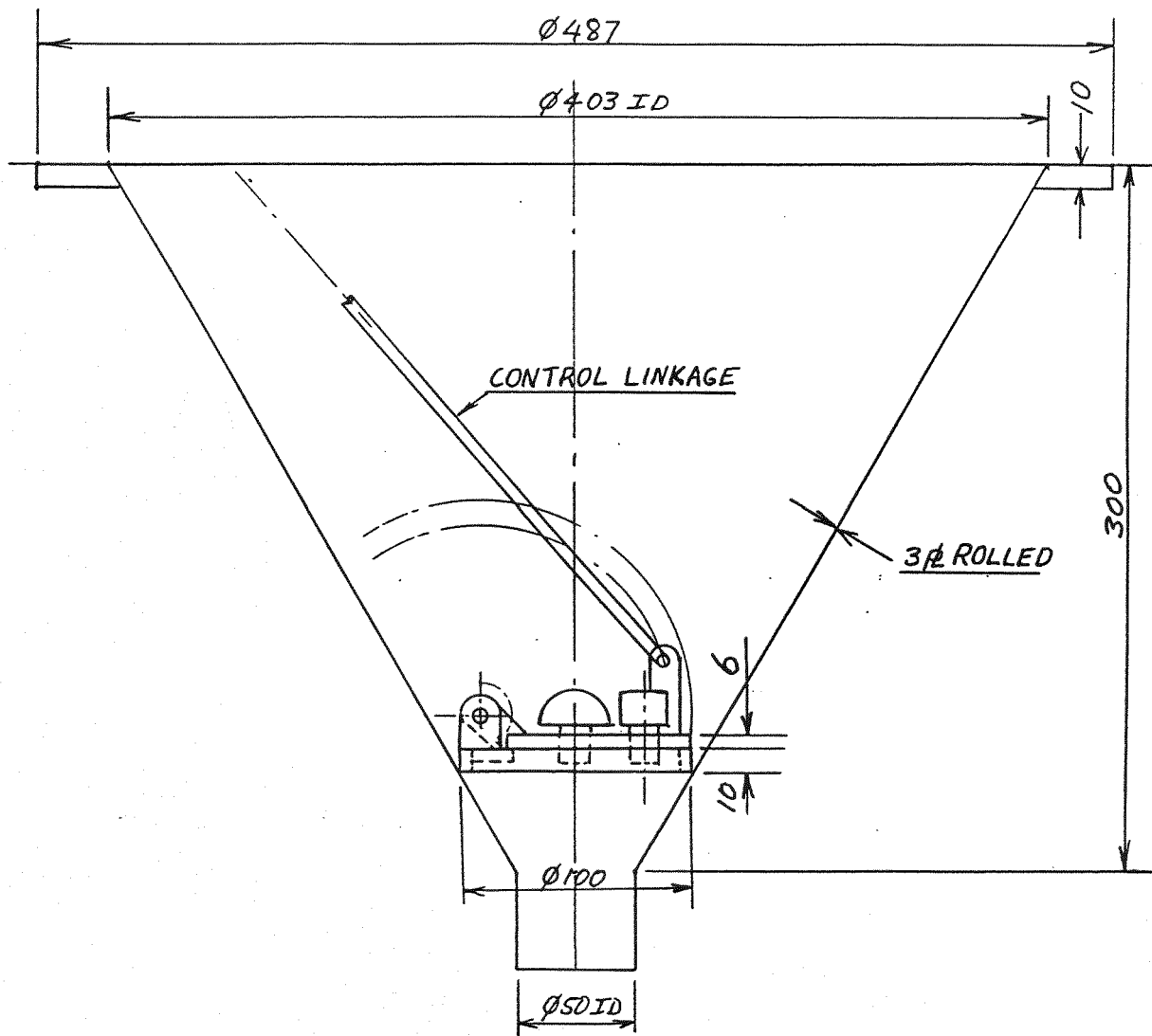
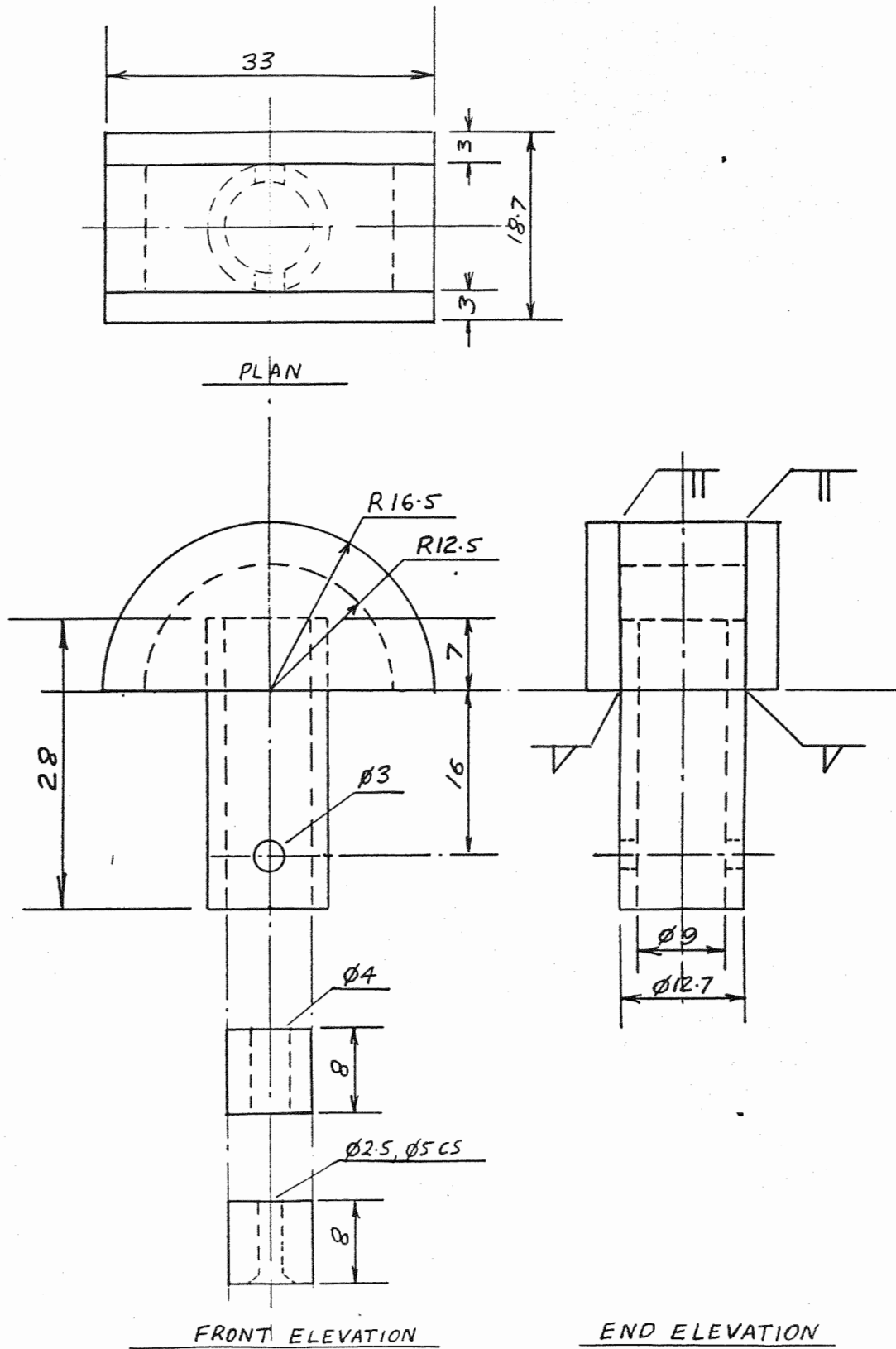


Fig.C29 **Bubble Cap Details**



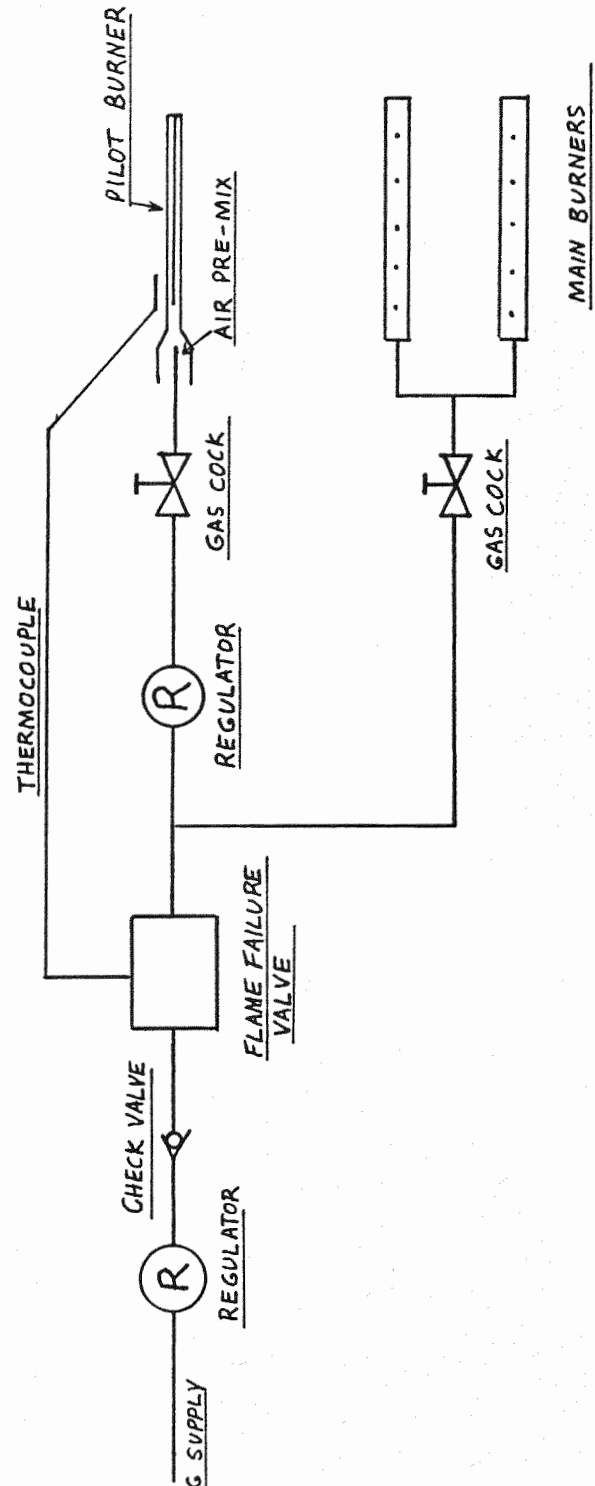


Fig.C31 Pilot and Main LPG Burner Details

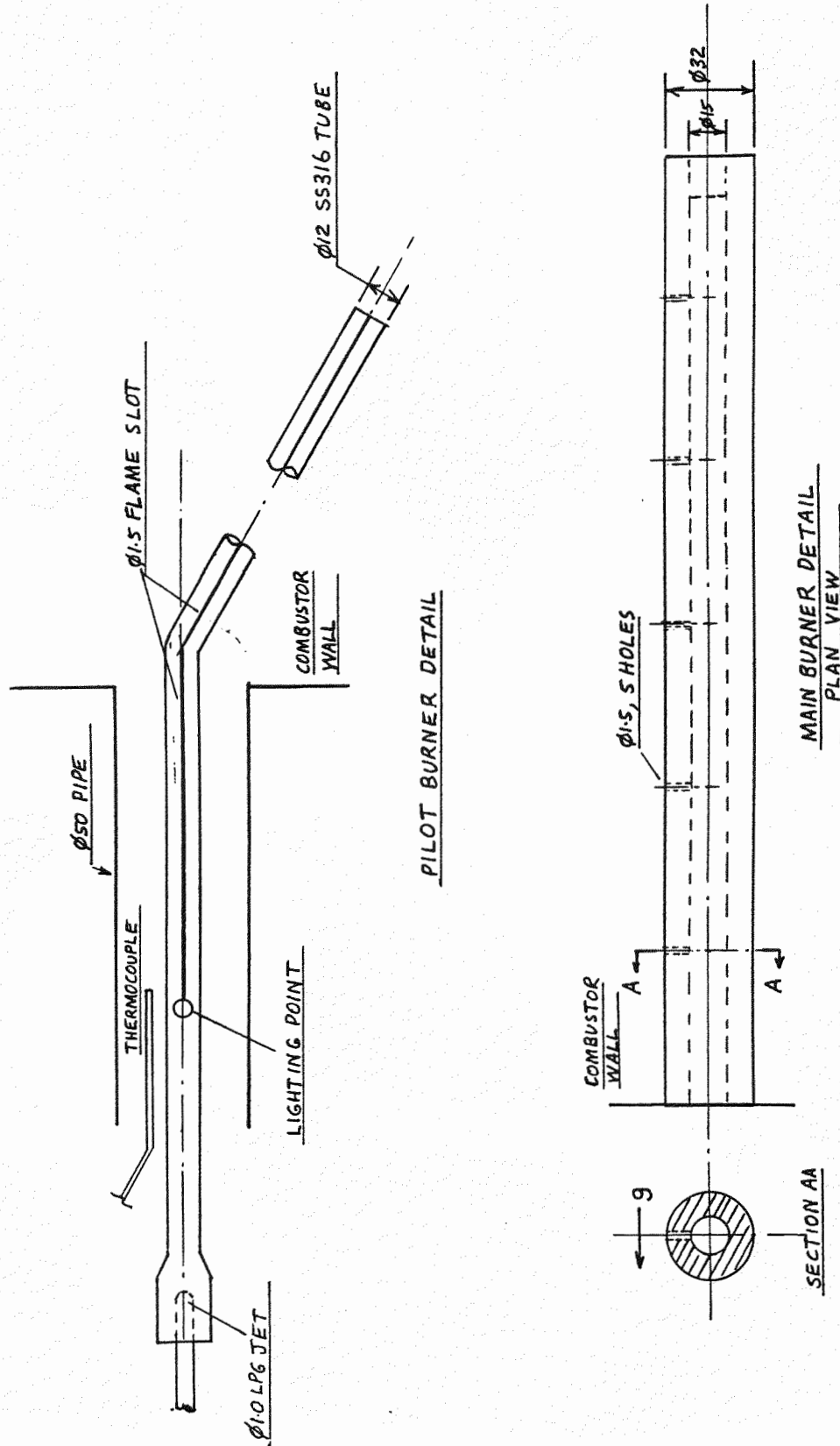


Fig.C32 **Flow Visualisation Test Rig.**



Fig.C33 **Base Fuel Introduction Plunger/Bed Solids Outlet**
and Flow Straightener.

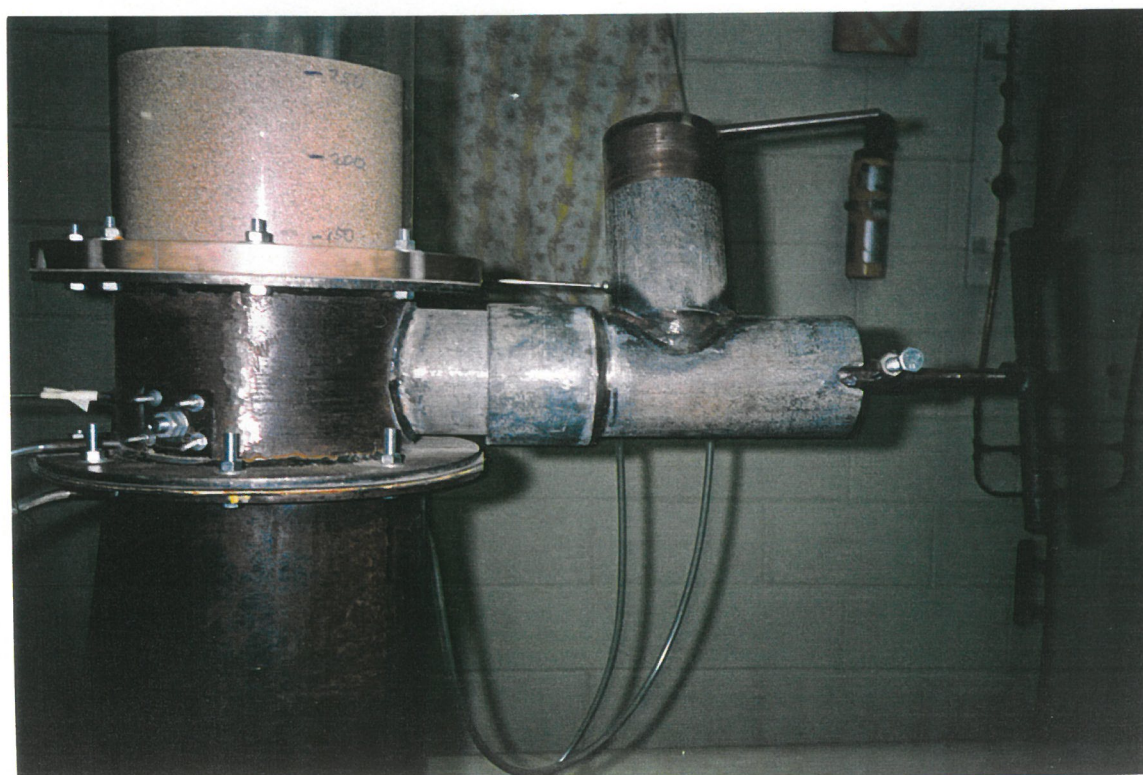


Fig.C34 **Fluidized Bed in Flow Visualisation Tube**

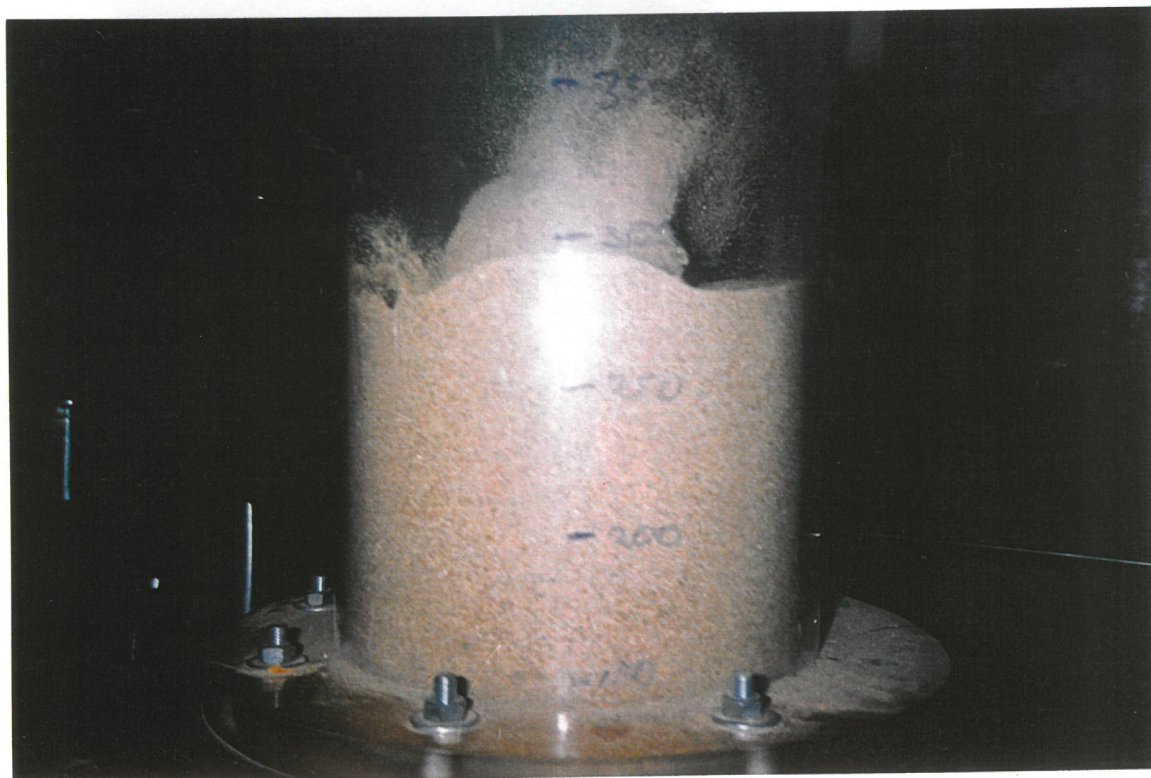


Fig.C35 **Pitot-Static Tube For Air Flow Measurement**

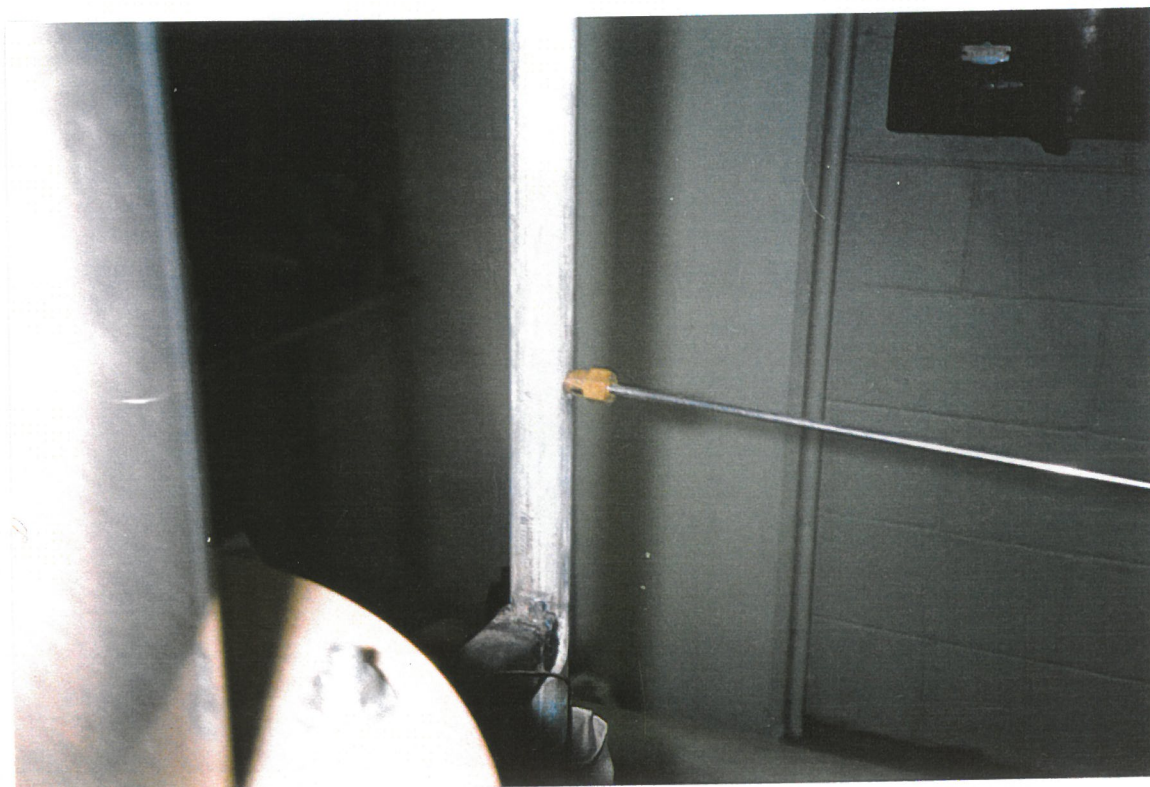


Fig.C36 **Fluidized Bed Combustor Test Rig**



Fig.C37 **Feed Chute and Observation Port**



Fig.C38 Fibrous, Particulate Bagasse



Fig.C39 Hardwood Sawdust



Fig.C40 Bagasse Combustion,Dry, Shallow Bed



Fig.C41 Sawdust Combustion,25% Moist, Shallow Bed



Fig.C42 **Pressurised Direct Screw Feeder**

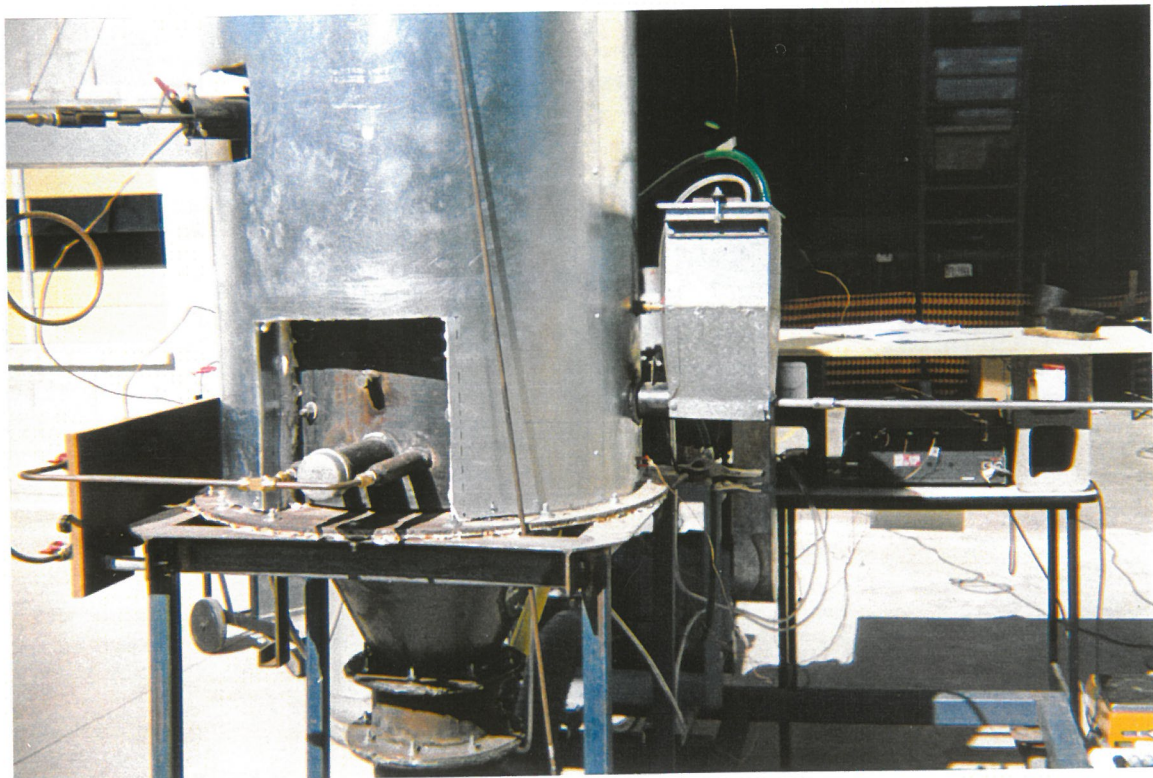


Fig.C43 **Fluidization For Ingestor Test, Plate Pattern No.5**

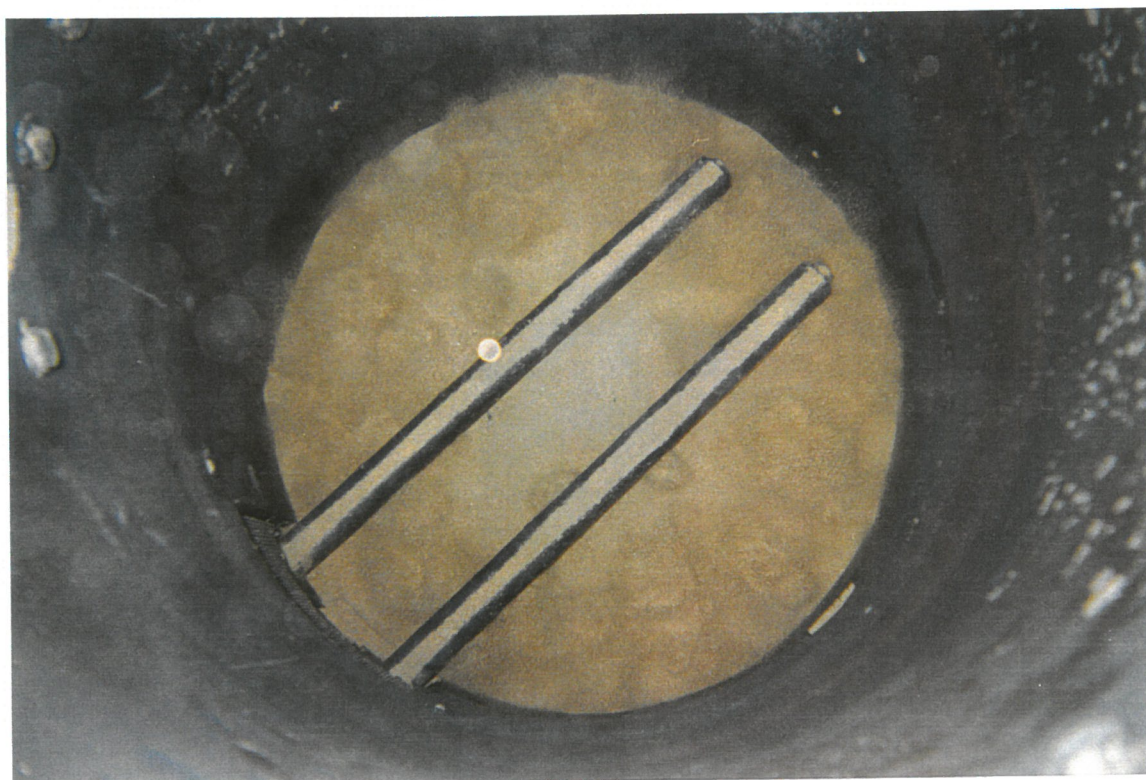


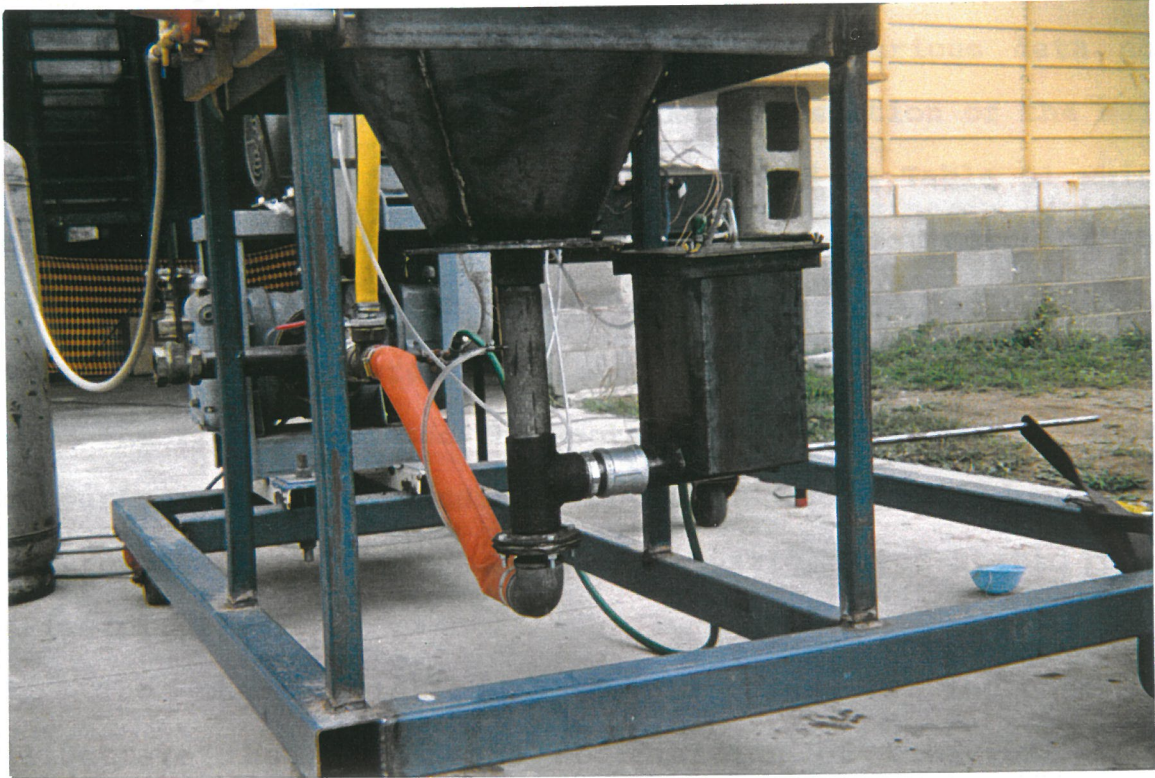
Fig.C44 **Ingestor Tube with Particle Control Cones**



Fig.C45 **Fluidized Bed Combustor fitted with Modified Spout Cone**



Fig.C46 Below Bed Screw Feed Hopper



Appendix D : Equipment Data

Explanatory Notes

The equipment data appendix includes various data not already included in the Equipment Details section of the main volume (Volume 1). The only table included is Table D1 which gives calculated and experimentally obtained estimates of the equivalent specific heat of the bed solids. (ie including the correction for bed steel.)

The figures include the Roots Blower Characteristic and a comparison of the readings obtained from the three air instruments used. (ie Rotameter, B.S.Nozzle, Pitot-Static Tube) (Figs.D1,D2)

The characteristic of bubble caps is included to illustrate the significant modification of behaviour of a compressible fluid even at low pressures. Further research could be pursued. Figure D3 shows the bubble cap characteristic K based on the velocity difference in the cap due to expansion. The gap in the data presented is due to the ranges over which instruments can be taken as reliable. The bubble cap pressure drops were measured with just one bubble cap in the flow visualisation rig. The significance of flow regime is clearly shown by the simple K and Pressure Drop results in Figs.D4,D5 and D6. The significance of entrance area is seen by the comparison of Figs. D4 and D7. It should be noted that the pressure drops in Fig D4 are still higher due to the larger entrance area, while the caps in Fig.D7 have been bushed to 4mm. The data combined serves as warning of the many difficulties in scaling up from test equipment to operational

Fluidized Bed Combustors. It was found that estimates based on single bubble cap data were so unreliable it was better to take an educated guess for the bubble cap bush size and test before combustion tests.

As no flow visualisation tests of a cone based spouted bed were completed in section A, the pressure drop characteristic for the spouted bed is included.(Fig.D8)

Table D1 : Combustor Specific Heat and Wall Losses

Configuration	Estimated Equivalent Specific Heat (Experiment -al) kJ/kg.K	Estimated Equivalent Specific Heat (Calculated) kJ/kg.K *(see note)	Estimated Bed Wall Loss @ 600C kW **(see note)
Shallow Bed,130mm	1.6	1.2	0.3
Deep Bed,300mm	1.3	1.06	0.75
Deep Bed,325mm	1.29	1.05	0.77
Deep Bed,460mm	0.92	1.0	0.91
Ingestor Bed,355mm	1.75	1.06	0.8
Spouted Bed,515mm	1.24	1.14	0.66
Spouted Bed,583mm	1.2	1.0	0.82
Spouted Bed,654mm	1.2	0.98	0.92
Spouted Bed,740mm	1.45	0.97	1.01

* Calculated estimates do not include bed expansion which means that steel mass used in calculation is less than actual, hence the lower values.

** Estimates for wall area contacting the sand bed material only. These values were used in calculations of below bed surface heat release.

Fig.D1 ROOTS BLOWERS DELIVERY CHARACTERISTIC

Ambient Temperature 28 C

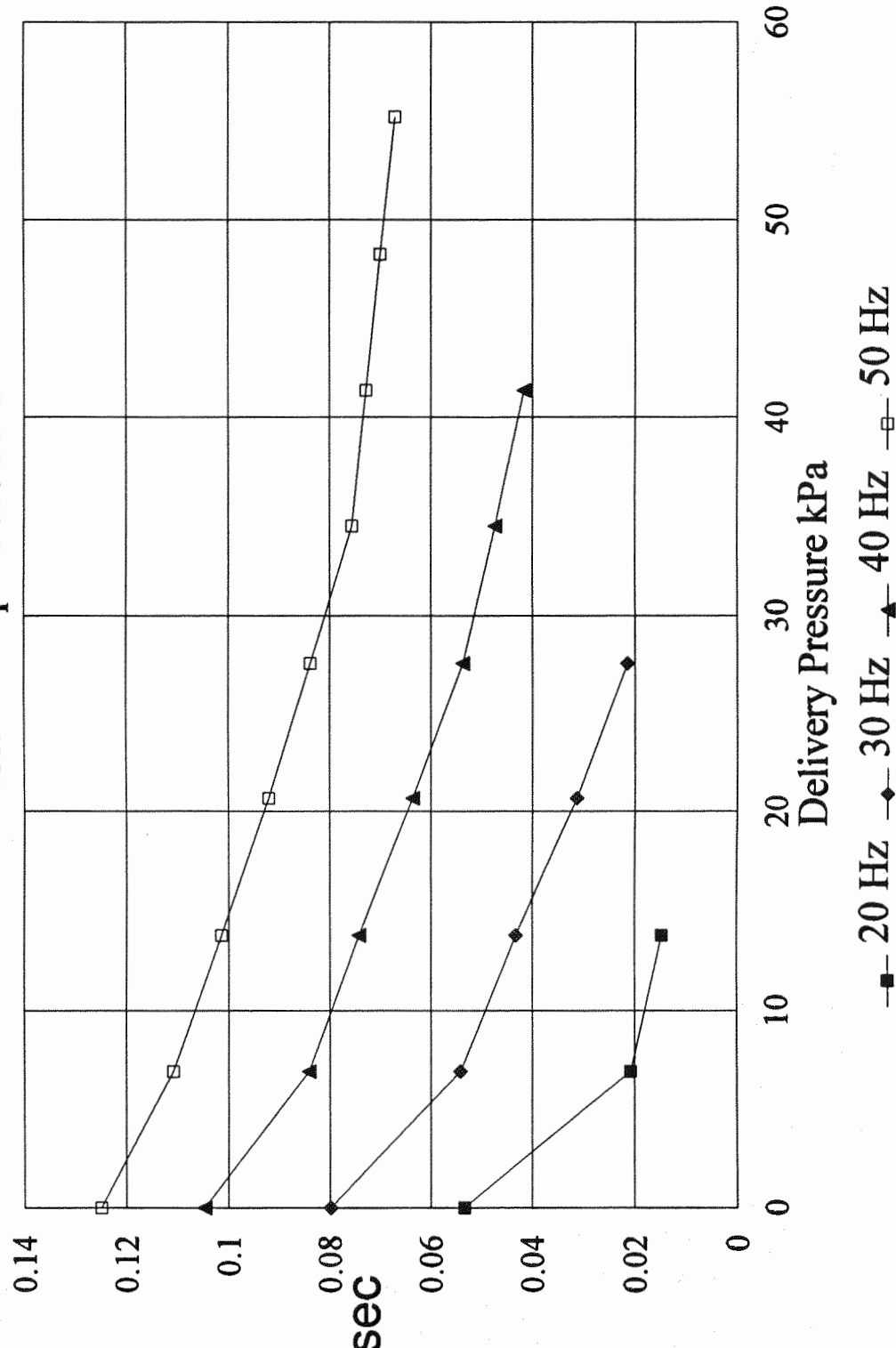


Fig.D2 AIR FLOW CU.M/S vs CU.M/S

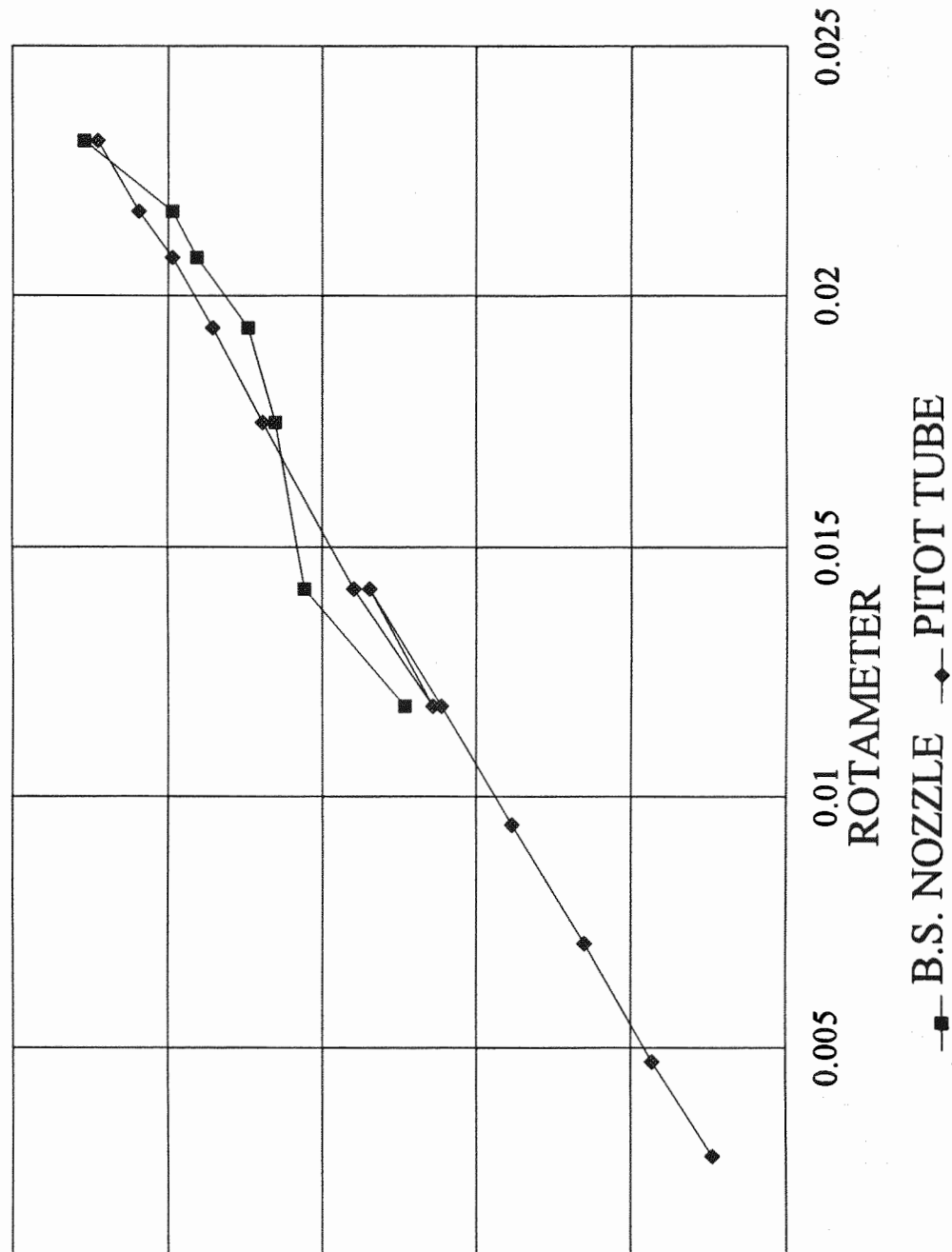
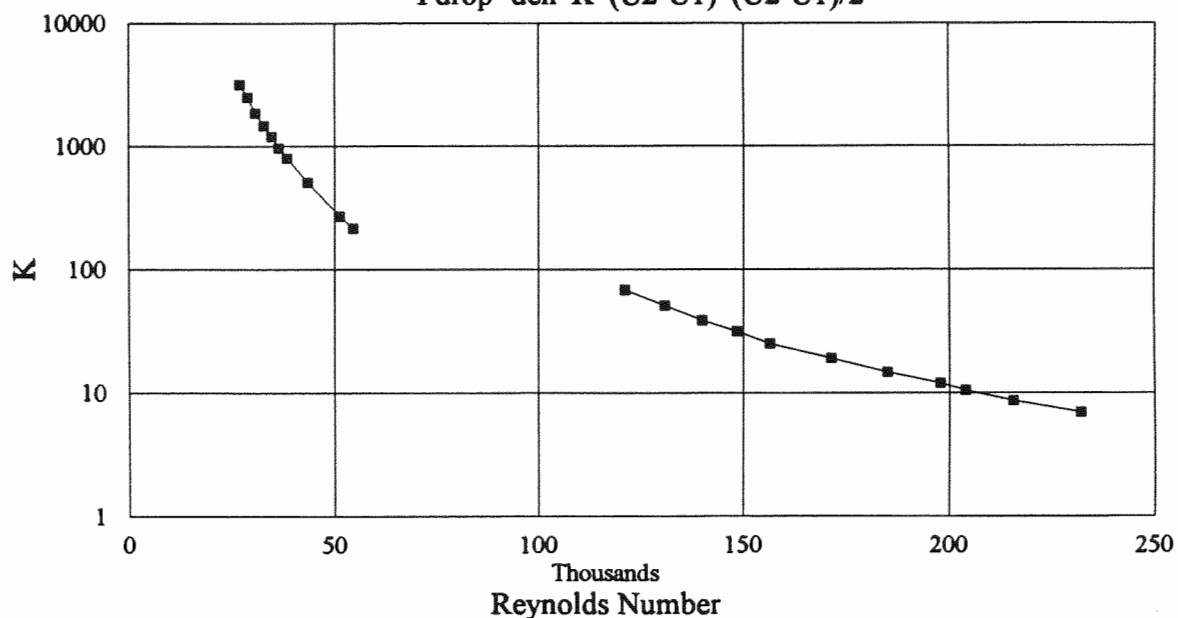


Fig.D3 Bubble Cap Discharge Characteristic

$$P_{\text{drop}} = \text{den} \cdot K \cdot (U_2 - U_1) \cdot (U_2 + U_1) / 2$$

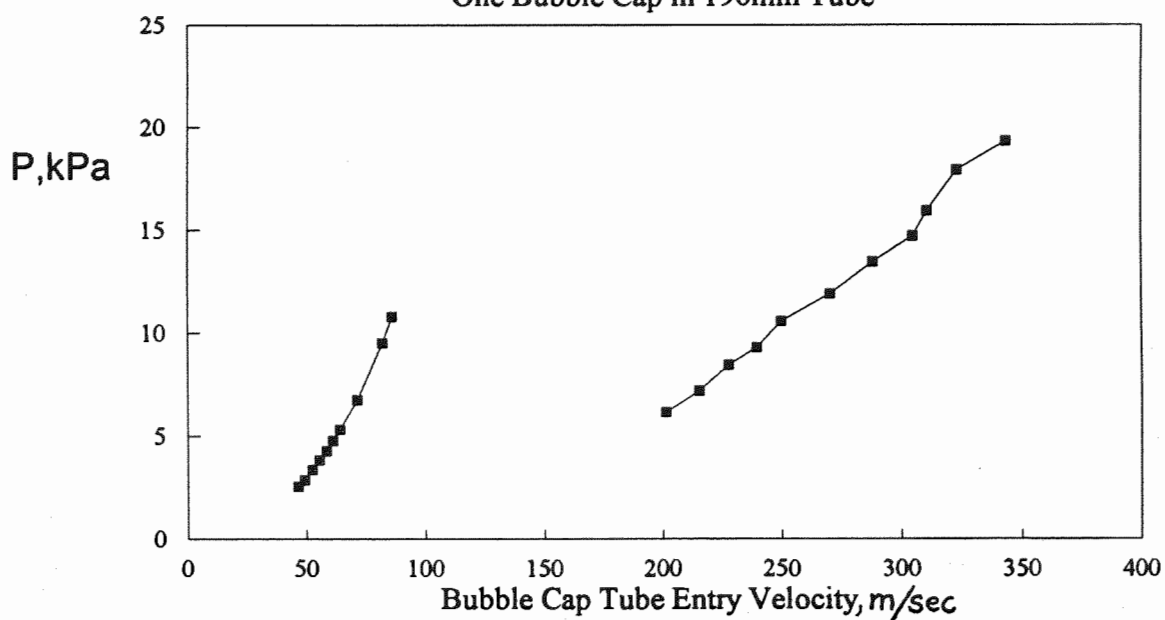


In cap tube, U_2 is Cap Tube exit Velocity, U_1 is cap tube entry velocity

Temperature 30 C, Bubble cap exit pressure ≤ 2 Pa gauge; Re is at cap inlet conditions; $d=9\text{mm}$

Fig.D4 Bubble Cap Pressure Drop

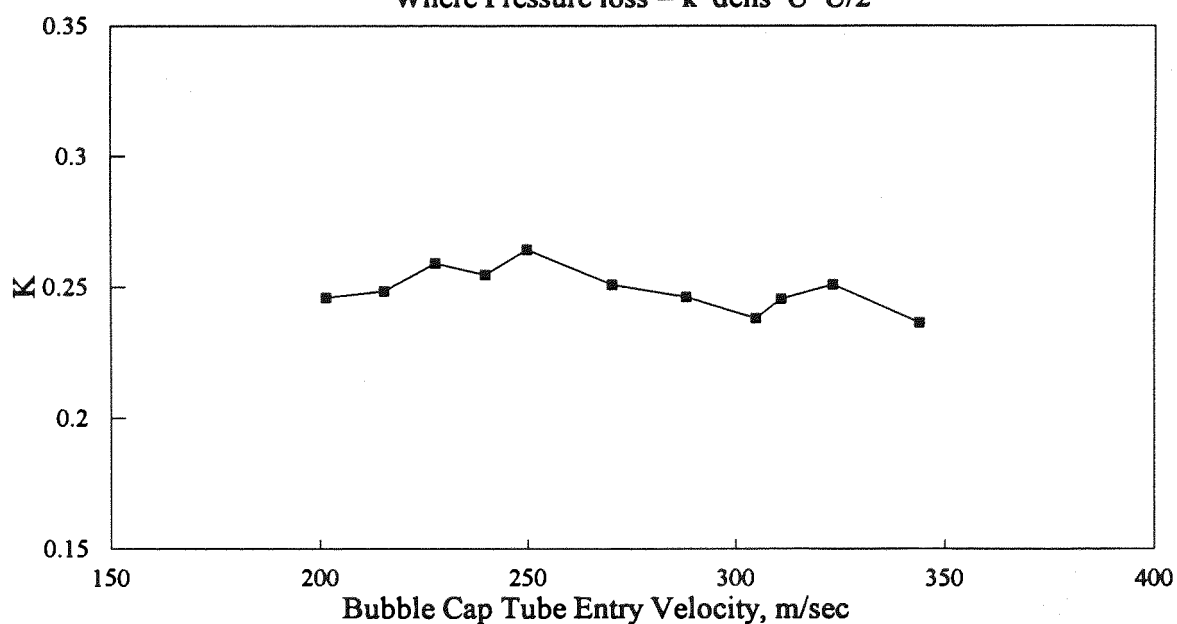
One Bubble Cap in 190mm Tube



Temperature, 30 C

Cap Exit Pressure ≤ 2 Pa gauge

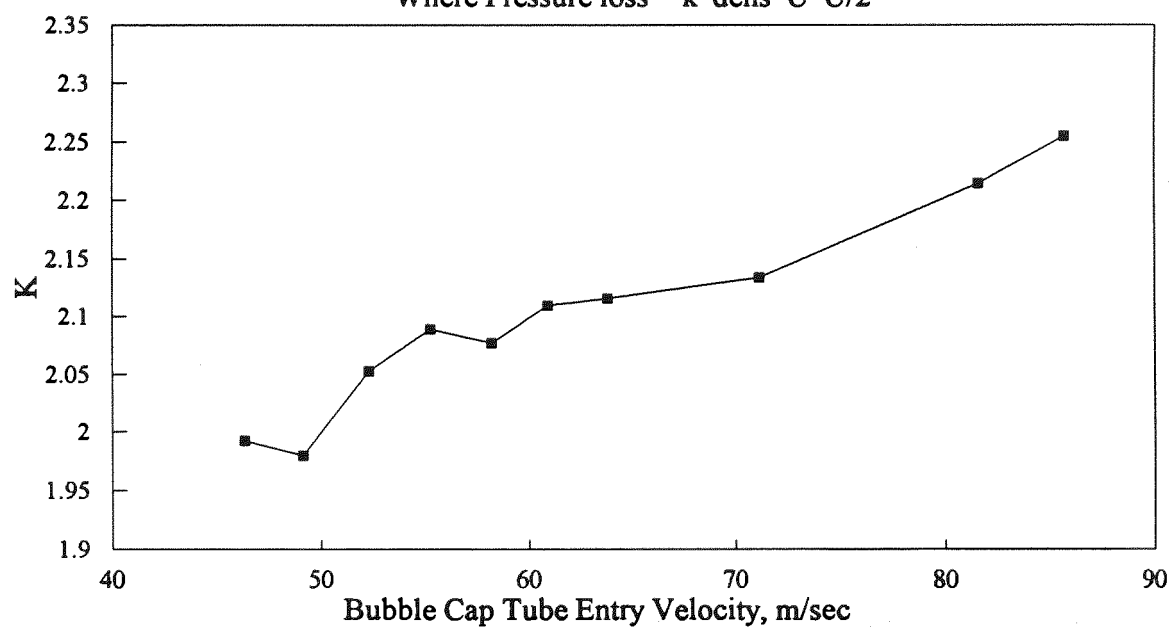
Fig.D5 Pressure Loss Coefficient K

Where Pressure loss = $k \cdot \text{dens} \cdot U \cdot U/2$ 

Temperature, 30 C

Cap Exit Pressure ≤ 2 Pa gauge

Fig.D6 Pressure Loss Coefficient K

Where Pressure loss = $k \cdot \text{dens} \cdot U \cdot U/2$ 

Temperature, 30 C

Cap Exit Pressure ≤ 2 Pa gauge

Fig.D7 Pressure Drop with 4mm Cap Inserts
19 Bubble Caps, Pattern No.3

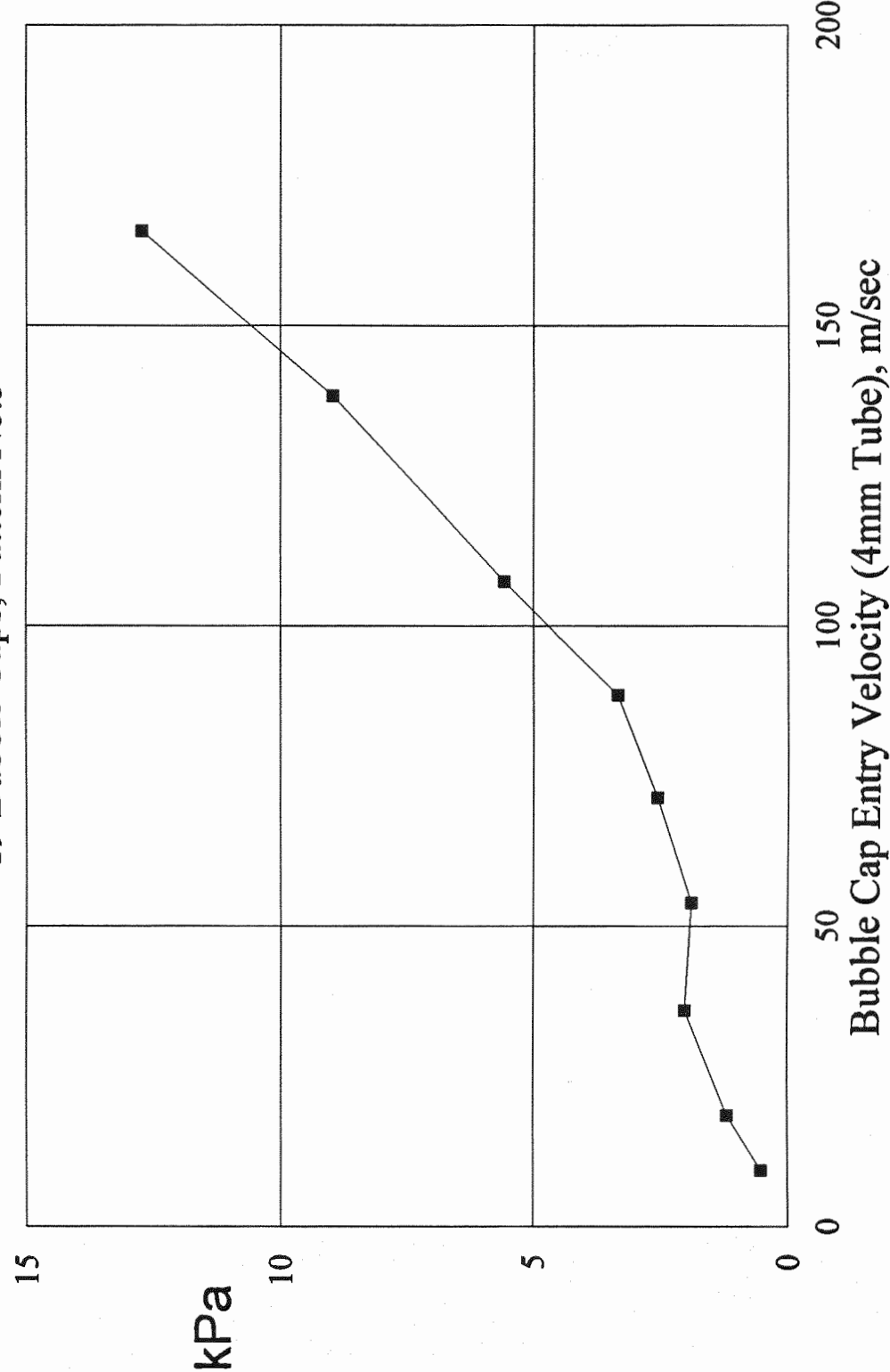
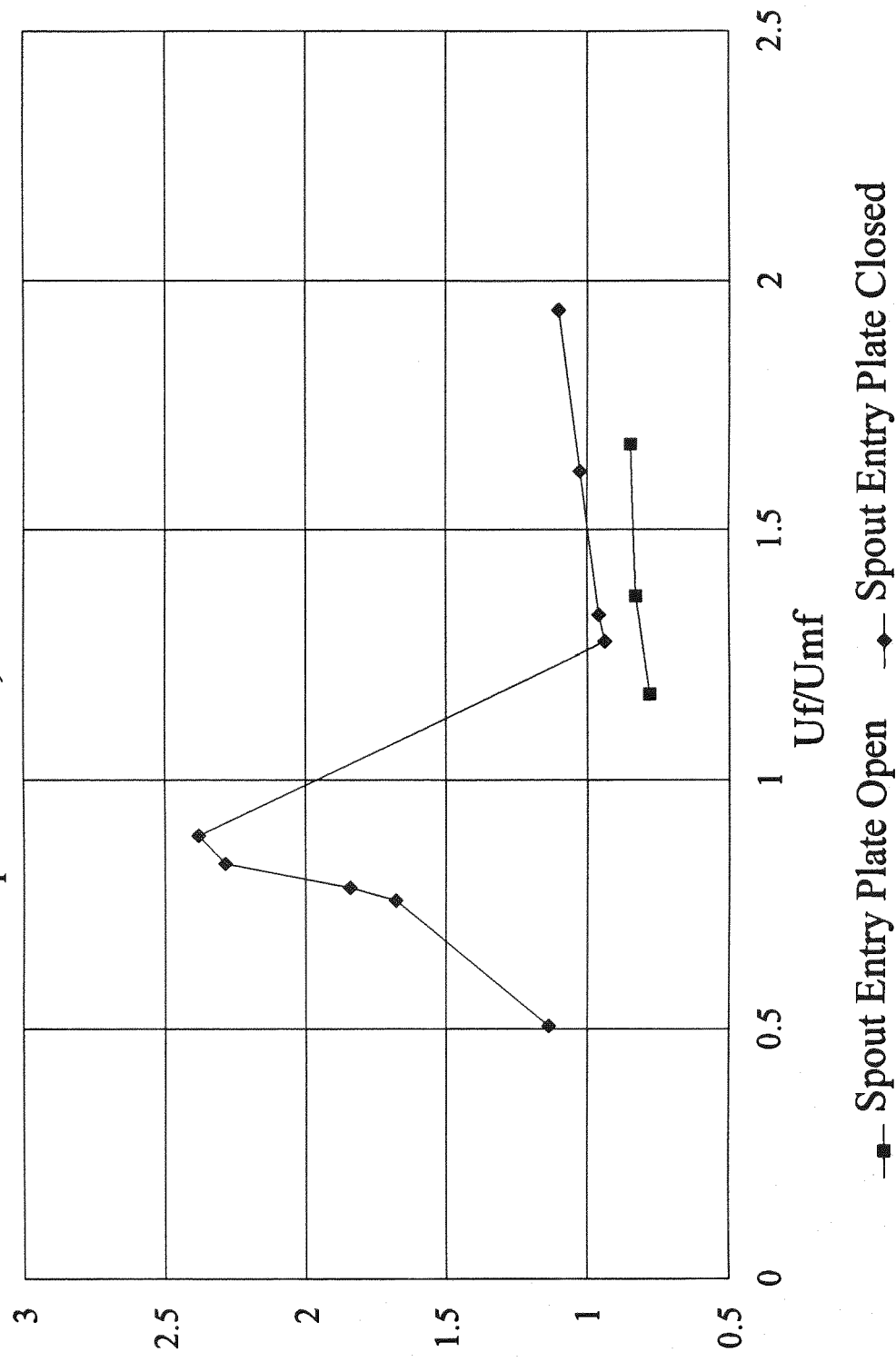


Fig. D8. Modified Spouted Bed Characteristic
Depth 740 mm, Sand 530 micron



Appendix E : Fuel Properties

Explanatory Notes

With fuels of high variability such as Bagasse and Sawdust a large section could be devoted to just analysing the fuel. As the project was not directed toward fuel analysis and the margins for successful operation would have to be large enough to cover a wide range of operating conditions a detailed analysis of fuel was not considered warranted. The data presented in this appendix is regarded as typical and where required was taken as representative in calculations

Table E1 Typical Fuel Properties

Item	Bagasse	Sawdust	Coal
High CV, MJ/kg	20.8*	21.7*	N/A
Low CV, MJ/kg	19.5*	20.4*	24
Particle Density, kg/m ³	540**	540**	N/A
Specific Heat kJ/kg.K	2.4**	2.4**	1.2

* From Bomb Calorimeter Tests at University of Central Queensland

** Values for wood as no other approximation was available

Table E2. Comparative Fuel Particle Fall Estimates: Dry Bagasse

117

Bed Conditions Fuel Conditions				Fall Distance	400 mm							
				Superficial Velocit	0.135 m/sec							
				Gas Temperature	675 C							
				Bed Sand Size	300 micron							
				Type	Bagasse							
				Particle density	540 kg/cu.m							
				Moisture Content	0 %							
				Continous Fuel Feed						Batch Feed Batch = 170gram		
d p micron	l/d	ϕ	Mass %	Fuel Fall Time secs	Fuel Drying Time secs	Fuel Residen Time(1) secs	h gp W/m2.K	h pp W/m2.K	Bed Entry Temp C	Fuel Residen Time secs	Bed Entry Temp C	
1082	8	0.62	80	0.45	0	0	191	1044	314	0.09	29	
3174	12	0.55	17	0.3	0	0.18	125	964	84	0.26	26	
7928	16	0.51	2	0.27	0	0.49	80	940	38	0.6	26	
9200	19	0.48	1	0.26	0	0.54	75	938	35	0.66	25	

(1) If particles reach the bed with $T_p < 300C$

Table E3. Comparative Fuel Particle Fall Estimates: Moist Bagasse

Bed Conditions				Fall Distance		400 mm							
				Superficial Velocit		0.135 m/sec							
				Gas Temperature		675 C							
				Bed Sand Size		300 micron							
				Type		Bagasse							
Fuel Conditions				Particle density		720 kg/cu.m							
				Moisture Content		25 %							
				Continous Fuel Feed						Batch Feed Batch = 170gram			
d p	l/d	ϕ	Mass	Fuel Fall Time secs	Fuel Drying Time secs	Fuel Residen Time(1) secs	h gp	h pp	Bed Entry Temp C	Fuel Residen Time secs	Bed Entry Temp C		
micron			%				W/m2.K	W/m2.K					
1082	8	0.62	80	0.38	0.08	0.029	200	1044	234	0.12	26		
3174	12	0.55	17	0.3	0.3	0.253	128	964	67	0.34	25		
7928	16	0.51	2	0.27	0.35	0.66	80	940	34	0.8	25		
9200	19	0.48	1	0.26	0.35	0.73	76	938	32	0.89	25		

(1) If particles reach the bed with $T_p < 300C$

Table E4. Comparative Fuel Particle Fall Estimates: Dry Sawdust

118

Bed Conditions				Fall Distance	400 mm							
				Superficial Velocity	0.135 m/sec							
				Gas Temperature	675 C							
				Bed Sand Size	300 micron							
				Fuel Conditions				Type	Sawdust			
Particle density	540 kg/cu.m											
Moisture Content	0 %											
				Continous Fuel Feed						Batch Feed Batch = 170grams		
d p	l/d	ϕ	Mass	Fuel Fall Time secs	Fuel Drying Time secs	Fuel Residen Time(1) secs	h gp	h pp	Bed Entry Temp C	Fuel Residen Time secs	Bed Entry Temp C	
micron			%				W/m2.K	W/m2.K				
156	2	0.85	11	N/A(2)	0	0		1757				
484	7	0.65	19	0.95	0	0	252	1193	654	0.036	37	
840	8	0.61	20	0.55	0	0	211	1078	446	0.066	30	
1164	8	0.62	26	0.4	0	0.012	185	1036	269	0.097	28	
1811	6	0.68	24	0.35	0	0.096	145	996	136	0.173	27	

(1) If particles reach the bed with $T_p < 300^\circ\text{C}$

(2) Particles of this size pneumaticall conveyed at 0.135m/sec

Table E5. Comparative Fuel Particle Fall Estimates: Moist Sawdust

Bed Conditions				Fall Distance 400 mm							
				Superficial Velocity 0.135 m/sec							
				Gas Temperature 675 C							
				Bed Sand Size 300 micron							
				Fuel Conditions							
				Type Sawdust							
				Particle density 720 kg/cu.m							
				Moisture Content 25 %							
				Continous Fuel Feed						Batch Feed Batch = 170grams	
d p	l/d	ϕ	Mass	Fuel Fall Time	Fuel Drying Time	Fuel Residen Time(1)	h gp	h pp	Bed Entry Temp	Fuel Residen Time	Bed Entry Temp
micron			%	secs	secs	secs	W/m2.K	W/m2.K	C	secs	C
156	2	0.85	11	N/A(2)		0		1757			
484	7	0.65	19	0.75	0.03	0	265	1193	600	0.05	31
840	8	0.61	20	0.5	0.06	0	222	1078	367	0.09	28
1164	8	0.62	26	0.4	0.095	0.04	193	1036	225	0.131	27
1181	6	0.68	24	0.3	0.21	0.152	149	996	100	0.231	25

(1) If particles reach the bed with $T_p < 300^\circ\text{C}$

(2) Particles of this size pneumaticall conveyed at 0.135m/sec

Table E6 Fuel-Particle hpp Values W/sq.m.K

Bed Temperature		400 C		
Thermal Conductivity of Air		0.051 W/mK		
Fuel dp microns	Sand Surface Mean Diameter (microns)			
	180	300	490	530
10	11393	11124	10923	10895
50	3233	2964	2763	2735
100	2213	1944	1743	1715
500	1397	1128	927	899
1000	1295	1026	825	797
5000	1213	944	743	715
10000	1203	934	733	705
50000	1195	926	725	697
100000	1194	925	724	696

119

Table E7 Fuel-Particle hpp Values W/sq.m.K

Bed Temperature		600 C		
Thermal Conductivity of Air		0.0615 W/mK		
Fuel dp microns	Sand Surface Mean Diameter (microns)			
	180	300	490	530
10	13493	13224	13023	12995
50	3653	3384	3183	3155
100	2423	2154	1953	1925
500	1439	1170	969	941
1000	1316	1047	846	818
5000	1217	948	747	720
10000	1205	936	735	707
50000	1195	926	725	697
100000	1194	925	724	696

Table E8 Fuel-Particle hpp Values W/sq.m.K

Bed Temperature		1000 C		
Thermal Conductivity of Air		0.0795 W/mK		
Fuel dp microns	Sand Surface Mean Diameter (microns)			
	180	300	490	530
10	17093	16824	16623	16595
50	4373	4104	3903	3875
100	2783	2514	2313	2285
500	1511	1242	1041	1013
1000	1352	1083	882	854
5000	1224	956	755	727
10000	1208	940	739	711
50000	1196	927	726	698
100000	1194	925	724	697

Table E9 Fuel-Particle Heat Transfer , kW/kg.K

Bed Temperature		400 C		
Thermal Conductivity of Air		0.051 W/mK		
Fuel dp microns	Sand Surface Mean Diameter (microns)			
	180	300	490	530
10	12658.4	12359.7	12136.5	12105.6
50	718.3	658.6	614.0	607.8
100	245.8	216.0	193.6	190.6
500	31.0	25.1	20.6	20.0
1000	14.4	11.4	9.2	8.9
5000	2.7	2.1	1.7	1.6
10000	1.3	1.0	0.8	0.8
50000	0.3	0.2	0.2	0.2
100000	0.1	0.1	0.1	0.1

120

Table E10 Fuel-Particle Heat Transfer , kW/kg.K

Bed Temperature		600 C		
Thermal Conductivity of Air		0.0615 W/mK		
Fuel dp microns	Sand Surface Mean Diameter (microns)			
	180	300	490	530
10	14991.7	14693.1	14469.8	14438.9
50	811.7	751.9	707.3	701.1
100	269.2	239.3	217.0	213.9
500	32.0	26.0	21.5	20.9
1000	14.6	11.6	9.4	9.1
5000	2.7	2.1	1.7	1.6
10000	1.3	1.0	0.8	0.8
50000	0.3	0.2	0.2	0.2
100000	0.1	0.1	0.1	0.1

Table E11 Fuel-Particle Heat Transfer , kW/kg.K

Bed Temperature		1000 C		
Thermal Conductivity of Air		0.0795 W/mK		
Fuel dp microns	Sand Surface Mean Diameter (microns)			
	180	300	490	530
10	18991.7	18693.1	18469.8	18438.9
50	971.7	911.9	867.3	861.1
100	309.2	279.3	257.0	253.9
500	33.6	27.6	23.1	22.5
1000	15.0	12.0	9.8	9.5
5000	2.7	2.1	1.7	1.6
10000	1.3	1.0	0.8	0.8
50000	0.3	0.2	0.2	0.2
100000	0.1	0.1	0.1	0.1

Table E12. Predicted Mean Surface Diameters for Sand Bagasse Mixtures
using existing theory

Mean Bagasse Diameter	Mean Sand Diameter	Bagasse by Mass	Bagasse by Particle Volume	Mean by Mass	Mean by Volume
microns	microns	%	%	microns	microns
1255	180	0	0	180	180
1255	180	0.65	2.693936	181.0078	184.25171
1255	180	1.287	5.196796	182.0065	188.385882
1255	180	1.88	7.413758	182.9461	192.205901
1255	180	3.22	12.06071	185.1055	200.738019
50000	180	3.22	12.06	185.9666	204.584009
1255	180	75	90	503.3983	785.73913
1255	490	0	0	490	490
1255	490	0.501	2.089305	491.501	496.320948
1255	490	1.13	4.591954	493.3986	504.110452
1255	490	1.6	6.380028	494.826	509.82729

Table E13. Minimum Combustion Efficiency for Sustained Operation without Useful Heat Yield

Moisture		Bed Temperatures C		
CV(kJ/kg)=	19500	400	600	1000
Stoichiometric	0	15	23	40
	0.1	16	25	43
	0.2	17	27	48
	0.3	18	30	54
	0.4	20	34	61
	0.5	23	39	72
	0.6	28	47	88
	0.7	35	61	
	0.8	49	88	
	0.9	93		
30% excess air	0	18	28	48
	0.1	19	29	52
	0.2	20	32	56
	0.3	21	35	62
	0.4	23	38	70
	0.5	26	44	81
	0.6	31	52	97
	0.7	38	66	
	0.8	52	93	
	0.9	96		

Fig.E1 Particle Analysis: Bagasse

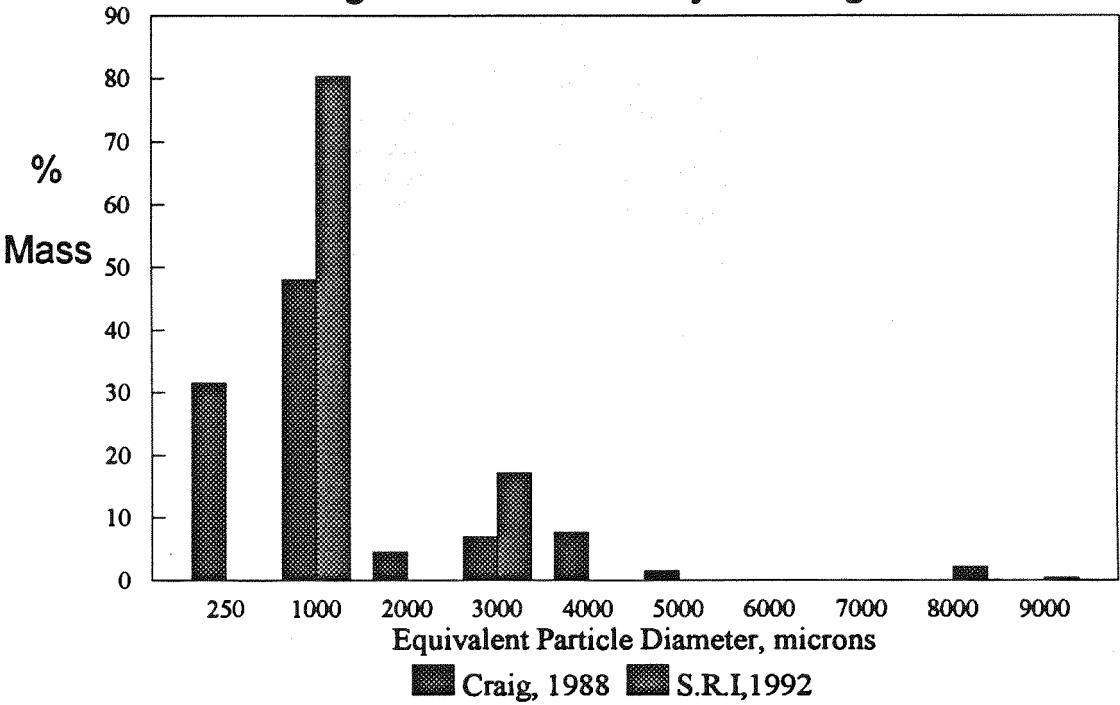
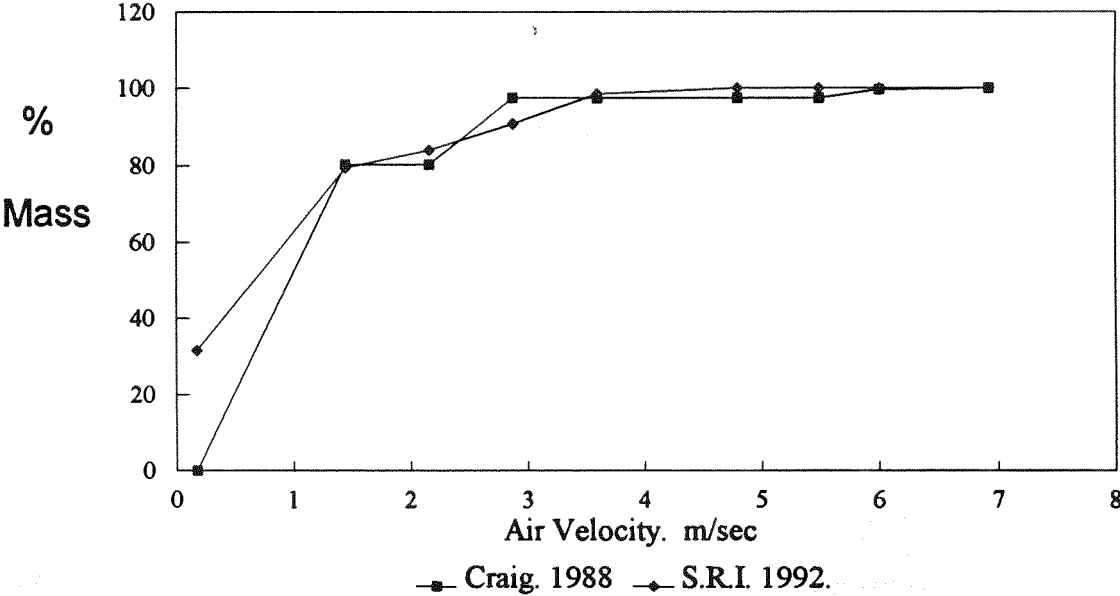


Fig.E2.Cumulative Mass Bagasse Conveyed vs Air Velocity
Operating Temperature : 600 C



Assumes : Particle Density = 540 kg/cu.m
Assumes: Sphericity = 0.6

Fig.E3 Particle Analysis: Sawdust

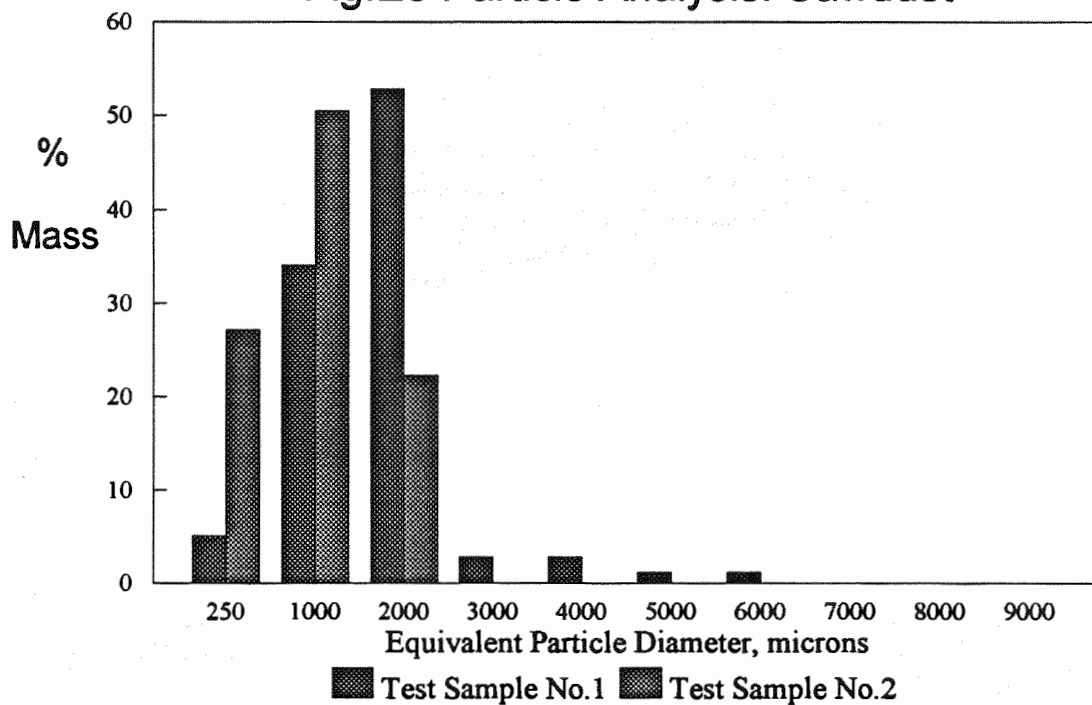
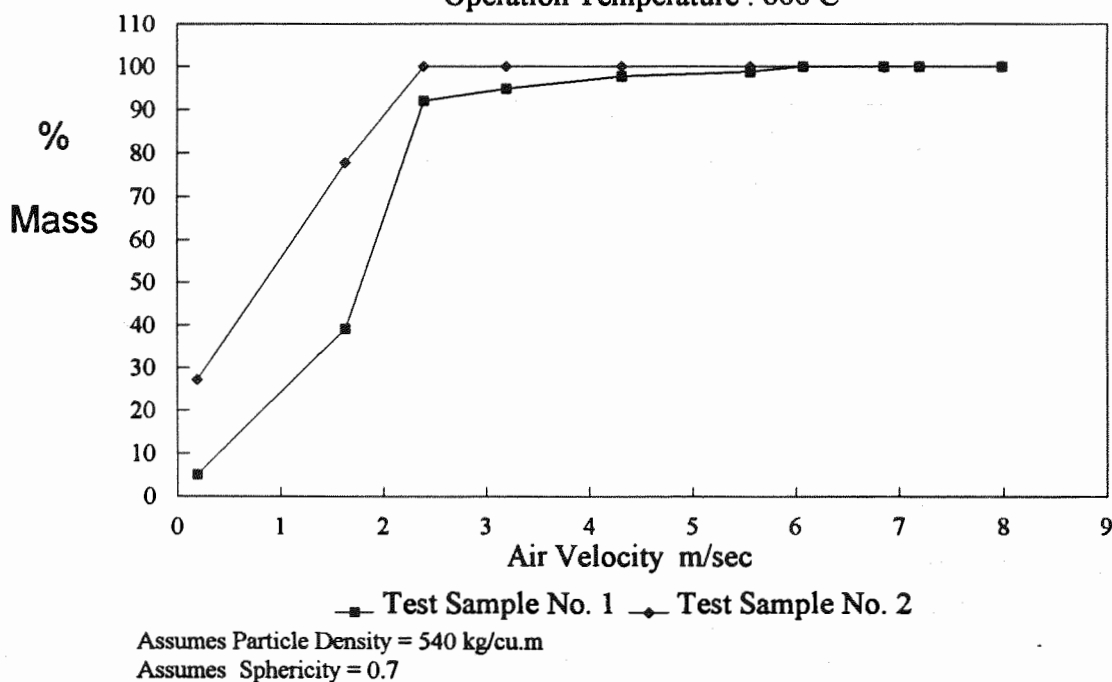
Fig.E4 Cumulative Mass Sawdust Conveyed vs Air Velocity
Operation Temperature : 600 C

Fig.E5. Chart for Calculating the Terminal Velocity of Particles falling Through Fluids.
 (Ref. Kunii.D & Levenspiel.O, p77)
 (Enlarged and grid lines added by author)

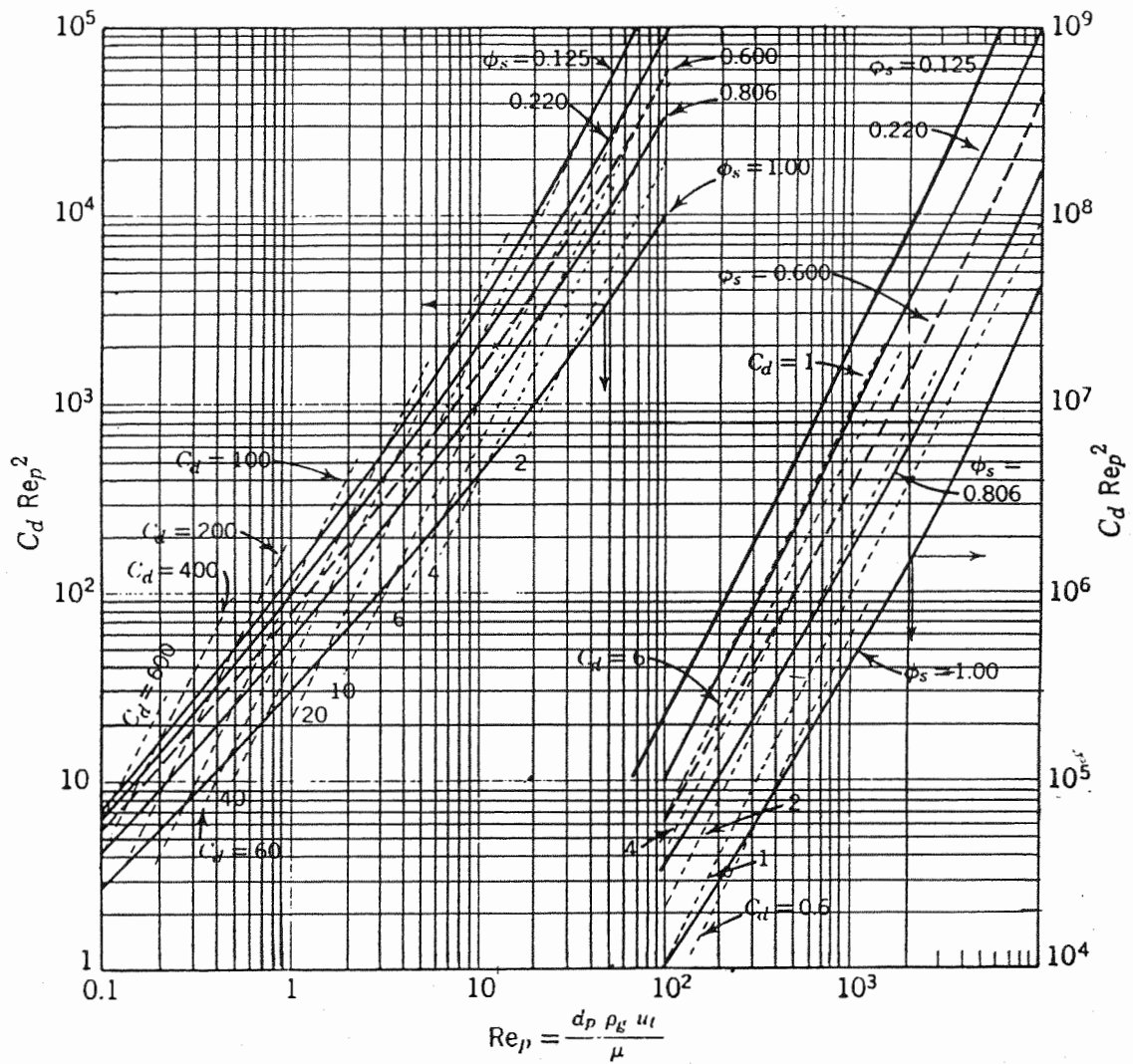


Fig.E6 Particle-Particle Heat Transfer Coefficient

Bed Temperature 600 C

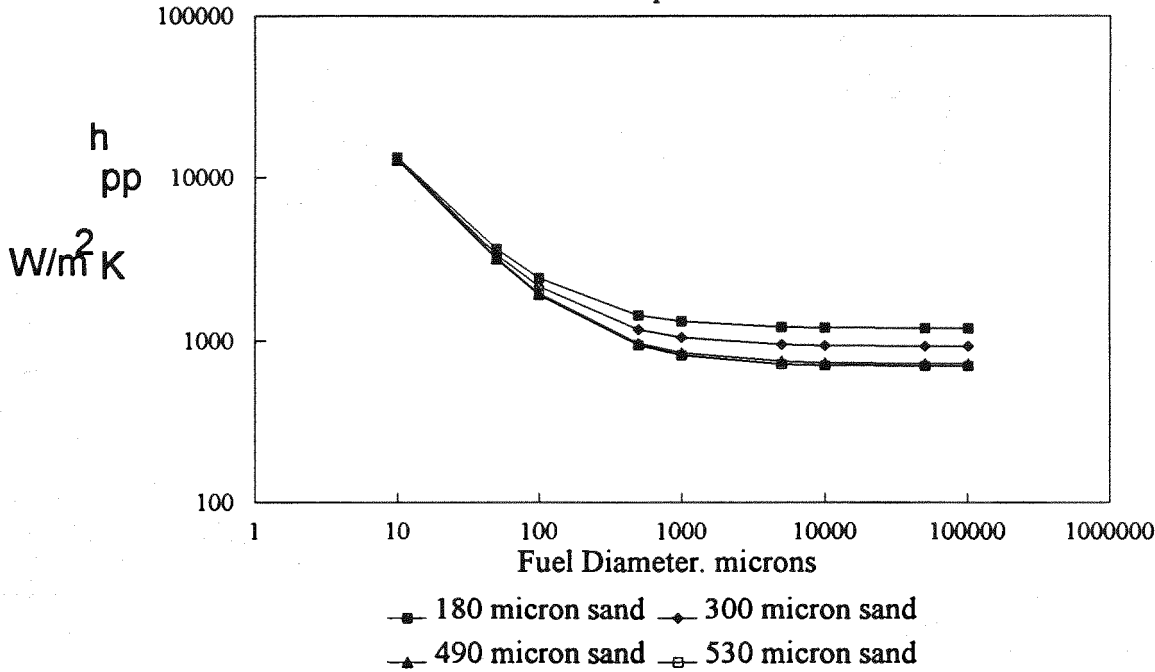
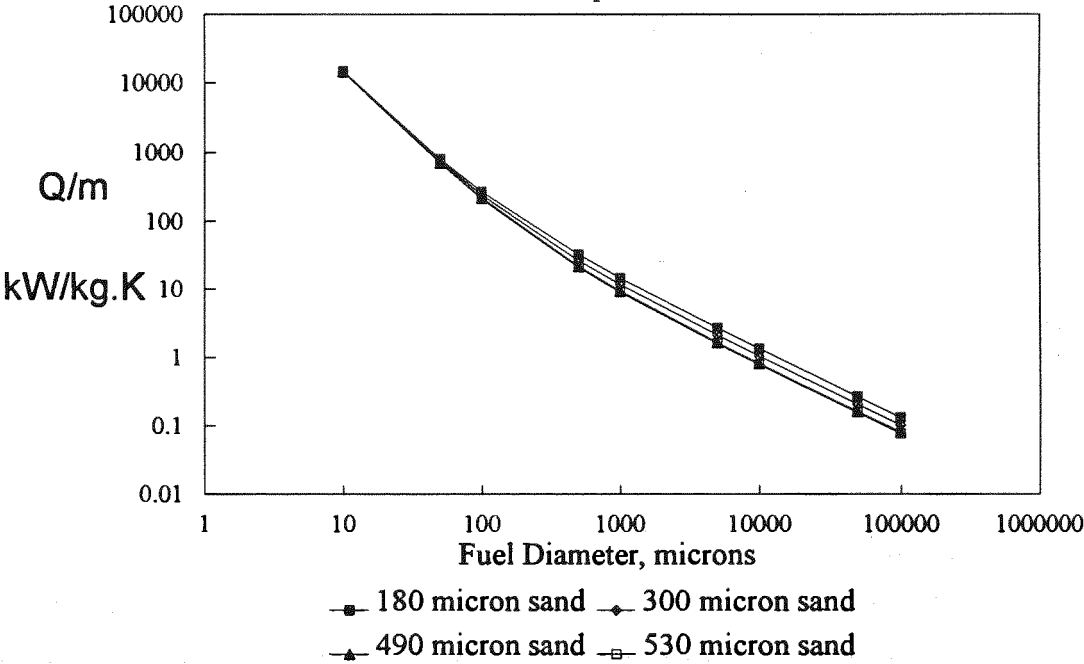


Fig.E7 Particle Heat Transfer, kW/kg.K

Bed Temperature 600 C



Appendix F: Sand Properties

Table F1 Typical Properties of Bed Sand

Property		
Sand Type	River Sand	
Particle Density, kg/m^3	2300	
Bulk Density, kg/m^3	1380-1450	
Estimated Voidage	0.37-0.4	
Estimated Sphericity	0.95	
Sand Surface Mean Diameters and Specific Surface	d_p microns	a m^2/m^3
Particle Analysis Table F3	180	21050
Particle Analysis Table F4	300	12630
Particle Analysis Table F5	490	7730
Particle Analysis Table F6	530	7150

Table F2 Typical Gas-Solid Equilibrium Depths

Sand Size microns	U_{mf} @600C	U_f @ $4U_{mf}$	Re_p	Nu_p	Equil. Depth mm
300	0.032	0.129	0.40	0.009	10.5
490	0.086	0.343	1.75	0.062	11.0
530	0.100	0.401	2.22	0.085	11.1

Sand Particle Size Analysis Tables F3 to F6

Table F3 Sand 180 micron

Size Range (microns)	Size (micro)	Mass %	f/size
75	0	37.5	4
150	75	112.5	23
300	150	225	38
425	300	362.5	14
600	425	512.5	12
1180	600	890	8

Average size 181.48 microns
Rounded to 180 microns

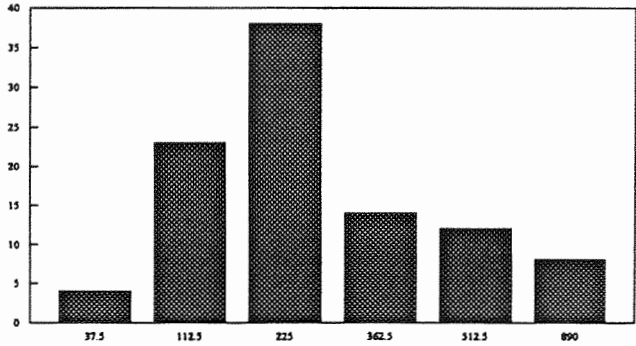


Table F4 Sand 300 micron

Size Range (microns)	Size (micro)	Mass %	f/size
75	0	37.5	0.3
150	75	112.5	12.0
300	150	225	24.2
425	300	362.5	13.9
600	425	512.5	22.8
1180	600	890	26.8

Average size 297.389 microns
Rounded to 300 microns

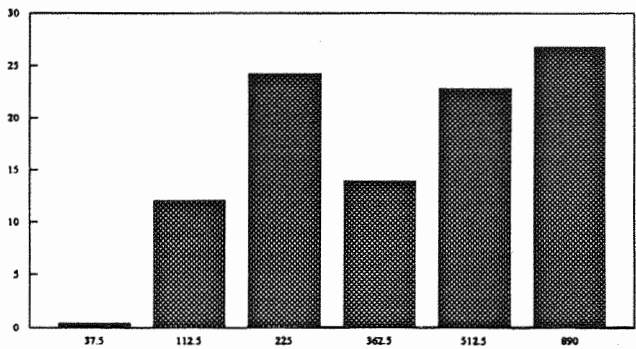


Table F5 Sand 490 micron

Size Range (microns)	Size (micro)	Mass %	f/size
75	0	37.5	0.0
150	75	112.5	1.0
300	150	225	9.0
425	300	362.5	16.0
600	425	512.5	35.0
1180	600	890	38.0

Average size 490.157 microns
Rounded to 490 microns

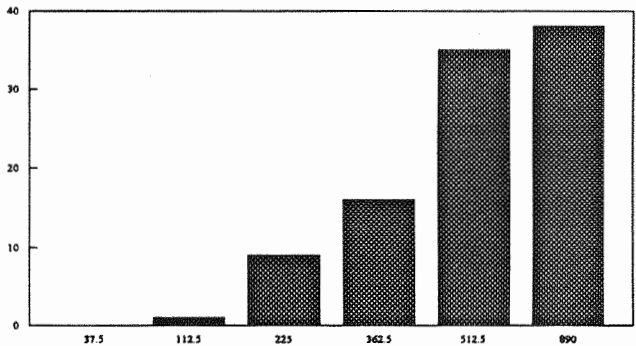


Table F6 Sand 530 micron

Size Range (microns)	Size (micro)	Mass %	f/size
75	0	37.5	0.0
150	75	112.5	0.3
300	150	225	8.2
425	300	362.5	14.1
600	425	512.5	29.7
1180	600	890	47.3

Average size 528.807 microns
Rounded to 530 microns

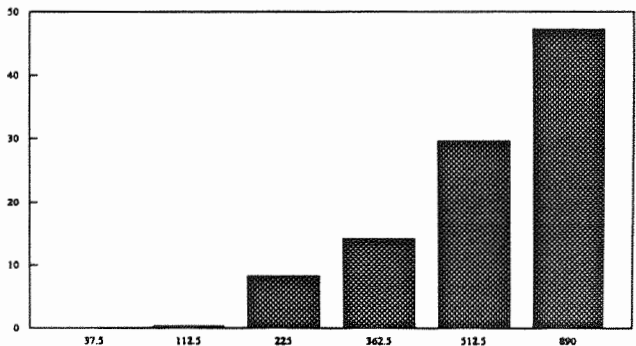


Table F7 Sand Theoretical Voidage, bubble fraction and mixing

Temp	27.00 C							
Press	101.30 kpa							
Air Dens	1.18 kg/cu.m							
Air Vis	1.85E-05 Pa.s							
Sphericity	0.90							
dp=	180.00 microns							
Voidage	Superficial		Bubble	Bubble	Solids	Emulsion	Emulsion	Solids
	Velocity		Fraction	Velocity	Turnover	Average	gas	downflow
ϵ	U	U_{mf}	δ	Eq.3.39 u_B	J	u_f	u_e	u_s
	m/sec			m/sec	kg/m2.sec	m/sec	m/sec	m/sec
	0.0240							
0.400	0.0227	0.95	0.00			0.057	0.060	
0.425	0.0284	1.18	0.04	0.14	1.95	0.067	0.058	0.001
0.450	0.0352	1.47	0.08	0.16	4.72	0.078	0.056	0.004
0.475	0.0432	1.80	0.13	0.18	7.93	0.091	0.053	0.007
0.500	0.0528	2.20	0.17	0.20	11.66	0.106	0.049	0.011
0.525	0.0641	2.67	0.21	0.22	15.99	0.122	0.044	0.016
0.550	0.0774	3.23	0.25	0.24	21.03	0.141	0.038	0.022
0.575	0.0932	3.88	0.29	0.27	26.89	0.162	0.029	0.031
0.600	0.1117	4.66	0.33	0.29	33.71	0.186	0.018	0.042
0.625	0.1335	5.56	0.37	0.32	41.65	0.214	0.003	0.057
0.650	0.1590	6.63	0.42	0.35	50.90	0.245	-0.017	0.077
0.675	0.1890	7.88	0.46	0.39	61.68	0.280	-0.045	0.105
0.700	0.2242	9.35	0.50	0.43	74.24	0.320	-0.083	0.143
0.725	0.2653	11.06	0.54	0.48	88.86	0.366	-0.139	0.199
0.750	0.3133	13.06	0.58	0.53	105.84	0.418	-0.223	0.283
0.775	0.3690	15.38	0.62	0.58	125.50	0.476	-0.356	0.416
0.800	0.4335	18.07	0.67	0.64	148.18	0.542	-0.584	0.644
0.825	0.5076	21.16	0.71	0.71	174.18	0.615	-1.042	1.102
0.850	0.5921	24.68	0.75	0.79	203.76	0.697	-2.302	2.362
0.875	0.6875	28.66	0.79	0.87	237.11	0.786	-16.435	16.495
0.900	0.7941	33.11	0.83	0.95	274.33	0.882	4.831	-4.771
0.925	0.9120	38.02	0.87	1.04	315.40	0.986	2.498	-2.438
0.950	1.0406	43.38	0.92	1.14	360.22	1.095	1.850	-1.790
0.975	1.1795	49.17	0.96	1.24	408.58	1.210	1.556	-1.496
1.000	1.3279	55.36	1.00	1.33	460.21	1.328	1.394	-1.334

Table F8 Sand Theoretical Voidage, Bubble Fraction and Mixing

Temp	27 C							
Press	101.3 kpa							
Air Dens	1.176539 kg/cu.m							
Air Vis	1.85E-05 Pa.s							
Sphericity	0.9							
dp=	300 microns							
Voidage	Superficial Velocity		Bubble Fraction	Bubble Velocity Eq.3.39	Solids Turnover Rate	Emulsion Average Velocity	Emulsion gas Velocity	Solids downflow Velocity
ϵ	U	U_{mf}	δ	u_B	J	u_f	u_e	u_s
	m/sec			m/sec	kg/m2.sec	m/sec	m/sec	m/sec
	0.0666							
0.400	0.0621	0.932	0.000			0.155	0.168	0.000
0.425	0.0772	1.159	0.042	0.337	4.85	0.182	0.163	0.004
0.450	0.0951	1.427	0.083	0.425	12.22	0.211	0.157	0.010
0.475	0.1161	1.742	0.125	0.479	20.66	0.244	0.149	0.018
0.500	0.1406	2.110	0.167	0.527	30.30	0.281	0.139	0.028
0.525	0.1689	2.535	0.208	0.574	41.27	0.322	0.126	0.040
0.550	0.2015	3.024	0.250	0.623	53.71	0.366	0.110	0.057
0.575	0.2388	3.583	0.292	0.674	67.77	0.415	0.089	0.077
0.600	0.2811	4.219	0.333	0.727	83.57	0.469	0.063	0.104
0.625	0.3288	4.935	0.375	0.783	101.24	0.526	0.028	0.138
0.650	0.3823	5.737	0.417	0.841	120.87	0.588	-0.016	0.183
0.675	0.4416	6.628	0.458	0.901	142.55	0.654	-0.075	0.242
0.700	0.5071	7.610	0.500	0.964	166.32	0.724	-0.155	0.321
0.725	0.5787	8.684	0.542	1.029	192.22	0.798	-0.265	0.431
0.750	0.6564	9.851	0.583	1.094	220.23	0.875	-0.423	0.589
0.775	0.7401	11.107	0.625	1.161	250.32	0.955	-0.663	0.829
0.800	0.8297	12.451	0.667	1.228	282.41	1.037	-1.061	1.228
0.825	0.9248	13.879	0.708	1.295	316.43	1.121	-1.835	2.001
0.850	1.0252	15.386	0.750	1.361	352.27	1.206	-3.918	4.084
0.875	1.1306	16.967	0.792	1.427	389.81	1.292	-26.951	27.118
0.900	1.2406	18.618	0.833	1.492	428.96	1.378	7.627	-7.460
0.925	1.3549	20.332	0.875	1.556	469.58	1.465	3.796	-3.630
0.950	1.4731	22.107	0.917	1.618	511.56	1.551	2.709	-2.542
0.975	1.5949	23.935	0.958	1.678	554.80	1.636	2.198	-2.031
1.000	1.7201	25.814	1.000	1.737	599.19	1.720	1.903	-1.737

Table F9. Sand Theoretical Voidage, Bubble Fraction and Mixing

Temp	27 C							
Press	101.3 kpa							
Air Dens	1.176539 kg/cu.m							
Air Vis	1.85E-05 Pa.s							
Sphericity	0.9							
dp=	490 microns							
Voidage	Superficial Velocity		Bubble Fraction	Bubble Velocity Eq.3.39	Solids Turnover Rate	Emulsion Average Velocity	Emulsion gas Velocity	Solids downflow Velocity
ϵ	U	U_{mf}	δ	u_B	J	u_f	u_e	u_s
	m/sec			m/sec	kg/m2.sec	m/sec	m/sec	m/sec
	0.1778							
0.400	0.1558	0.876	0.000			0.389	0.450	0.000
0.425	0.1908	1.073	0.042	0.535	7.69	0.449	0.439	0.006
0.450	0.2308	1.298	0.083	0.859	24.68	0.513	0.424	0.020
0.475	0.2759	1.552	0.125	1.008	43.45	0.581	0.407	0.037
0.500	0.3263	1.836	0.167	1.114	64.03	0.653	0.386	0.059
0.525	0.3820	2.149	0.208	1.203	86.44	0.728	0.360	0.085
0.550	0.4429	2.492	0.250	1.283	110.65	0.805	0.328	0.117
0.575	0.5090	2.863	0.292	1.358	136.63	0.885	0.289	0.156
0.600	0.5800	3.263	0.333	1.429	164.32	0.967	0.240	0.204
0.625	0.6557	3.689	0.375	1.497	193.64	1.049	0.180	0.264
0.650	0.7360	4.140	0.417	1.562	224.52	1.132	0.105	0.340
0.675	0.8204	4.615	0.458	1.624	256.86	1.215	0.009	0.436
0.700	0.9089	5.113	0.500	1.684	290.57	1.298	-0.117	0.561
0.725	1.0011	5.631	0.542	1.742	325.56	1.381	-0.286	0.731
0.750	1.0967	6.169	0.583	1.797	361.74	1.462	-0.523	0.968
0.775	1.1955	6.725	0.625	1.851	399.04	1.543	-0.877	1.322
0.800	1.2973	7.298	0.667	1.902	437.36	1.622	-1.457	1.902
0.825	1.4019	7.886	0.708	1.950	476.64	1.699	-2.570	3.014
0.850	1.5092	8.490	0.750	1.997	516.83	1.775	-5.548	5.992
0.875	1.6188	9.106	0.792	2.042	557.84	1.850	-38.362	38.806
0.900	1.7307	9.736	0.833	2.086	599.64	1.923	10.873	-10.429
0.925	1.8447	10.377	0.875	2.127	642.17	1.994	5.408	-4.964
0.950	1.9607	11.030	0.917	2.167	685.40	2.064	3.850	-3.406
0.975	2.0786	11.693	0.958	2.206	729.27	2.132	3.115	-2.670
1.000	2.1983	12.366	1.000	2.243	773.76	2.198	2.687	-2.243

Table F10. Sand Theoretical Voidage, Bubble Fraction and Mixing

Temp	27 C							
Press	101.3 kpa							
Air Dens	1.176539 kg/cu.m							
Air Vis	1.85E-05 Pa.s							
Sphericity	0.9							
dp=	530 microns							
Voidage	Superficial Velocity		Bubble Fraction	Bubble Velocity Eq.3.39	Solids Turnover Rate	Emulsion Average Velocity	Emulsion gas Velocity	Solids downflow Velocity
ϵ	U	$\frac{U}{U_{mf}}$	δ	u_B	J	u_f	u_e	u_s
	m/sec			m/sec	kg/m2.sec	m/sec	m/sec	m/sec
	0.2080							
0.400	0.1789	0.860	0.000			0.447	0.527	0.000
0.425	0.2182	1.049	0.042	0.504	7.25	0.513	0.514	0.006
0.450	0.2627	1.263	0.083	0.916	26.35	0.584	0.499	0.021
0.475	0.3125	1.503	0.125	1.096	47.27	0.658	0.479	0.041
0.500	0.3676	1.768	0.167	1.218	70.03	0.735	0.456	0.064
0.525	0.4280	2.058	0.208	1.316	94.60	0.815	0.427	0.093
0.550	0.4935	2.373	0.250	1.402	120.93	0.897	0.392	0.127
0.575	0.5639	2.712	0.292	1.480	148.96	0.981	0.350	0.170
0.600	0.6390	3.073	0.333	1.553	178.62	1.065	0.298	0.222
0.625	0.7186	3.455	0.375	1.622	209.80	1.150	0.234	0.286
0.650	0.8024	3.858	0.417	1.686	242.43	1.234	0.153	0.367
0.675	0.8900	4.279	0.458	1.748	276.41	1.319	0.051	0.469
0.700	0.9813	4.718	0.500	1.807	311.64	1.402	-0.082	0.602
0.725	1.0760	5.174	0.542	1.862	348.04	1.484	-0.261	0.781
0.750	1.1738	5.644	0.583	1.916	385.54	1.565	-0.512	1.032
0.775	1.2746	6.129	0.625	1.967	424.04	1.645	-0.885	1.405
0.800	1.3781	6.626	0.667	2.015	463.50	1.723	-1.495	2.015
0.825	1.4842	7.136	0.708	2.062	503.83	1.799	-2.666	3.186
0.850	1.5927	7.658	0.750	2.106	544.99	1.874	-5.799	6.319
0.875	1.7034	8.190	0.792	2.149	586.92	1.947	-40.309	40.829
0.900	1.8162	8.733	0.833	2.190	629.58	2.018	11.469	-10.949
0.925	1.9310	9.285	0.875	2.229	672.92	2.088	5.721	-5.201
0.950	2.0477	9.846	0.917	2.267	716.92	2.155	4.082	-3.562
0.975	2.1662	10.415	0.958	2.303	761.52	2.222	3.308	-2.788
1.000	2.2863	10.993	1.000	2.338	806.72	2.286	2.858	-2.338

Table F11. Sand Theoretical Voidage, Bubble Fraction and Mixing

Temp	600.00 C							
Press	101.30 kpa							
Air Dens	0.40 kg/cu.m							
Air Vis	3.83E-05 Pa.s							
Sphericity	0.90							
dp=	180.00 microns							
Voidage	Superficial Velocity		Bubble Fraction	Bubble Velocity E.3.39	Solids Turnover Rate	Emulsion Average Velocity	Emulsion gas Velocity	Solids downflow Velocity
ϵ	U	$\frac{U}{U_{mf}}$	δ	u_B	J	u_f	u_e	u_s
	m/sec			m/sec	kg/m2.sec	m/sec	m/sec	m/sec
	0.0116							
0.400	0.0110	0.95	0.00			0.027	0.029	
0.425	0.0138	1.19	0.04	0.07	0.96	0.032	0.028	0.001
0.450	0.0171	1.48	0.08	0.08	2.31	0.038	0.027	0.002
0.475	0.0210	1.82	0.13	0.09	3.89	0.044	0.026	0.003
0.500	0.0257	2.23	0.17	0.10	5.72	0.051	0.024	0.005
0.525	0.0314	2.71	0.21	0.11	7.87	0.060	0.021	0.008
0.550	0.0380	3.29	0.25	0.12	10.38	0.069	0.018	0.011
0.575	0.0460	3.98	0.29	0.13	13.34	0.080	0.014	0.015
0.600	0.0555	4.80	0.33	0.15	16.82	0.093	0.008	0.021
0.625	0.0669	5.78	0.37	0.16	20.95	0.107	0.000	0.029
0.650	0.0805	6.96	0.42	0.18	25.86	0.124	-0.010	0.039
0.675	0.0970	8.38	0.46	0.20	31.75	0.144	-0.025	0.054
0.700	0.1169	10.11	0.50	0.23	38.85	0.167	-0.046	0.075
0.725	0.1414	12.22	0.54	0.25	47.49	0.195	-0.078	0.107
0.750	0.1716	14.84	0.58	0.29	58.12	0.229	-0.127	0.155
0.775	0.2093	18.10	0.62	0.33	71.35	0.270	-0.207	0.236
0.800	0.2573	22.24	0.67	0.38	88.09	0.322	-0.354	0.383
0.825	0.3191	27.59	0.71	0.45	109.64	0.387	-0.664	0.693
0.850	0.4006	34.64	0.75	0.53	137.97	0.471	-1.571	1.600
0.875	0.5108	44.16	0.79	0.65	176.17	0.584	-12.226	12.255
0.900	0.6635	57.37	0.83	0.80	229.09	0.737	4.013	-3.984
0.925	0.8811	76.18	0.87	1.01	304.37	0.953	2.382	-2.353
0.950	1.1963	103.43	0.92	1.31	413.31	1.259	2.083	-2.054
0.975	1.6496	142.63	0.96	1.72	569.90	1.692	2.116	-2.087
1.000	2.2729	196.52	1.00	2.28	785.15	2.273	2.305	-2.276

Table F12. Sand Theoretical Voidage, Bubble Fraction and Mixing

Temp	600 C							
Press	101.3 kpa							
Air Dens	0.404309 kg/cu.m							
Air Vis	3.83E-05 Pa.s							
Sphericity	0.9							
dp=	300 microns							
Voidage	Superficial Velocity		Bubble Fraction	Bubble Velocity Eq.3.39	Solids Turnover Rate	Emulsion Average Velocity	Emulsion gas Velocity	Solids downflow Velocity
ϵ	U	$\frac{U}{U_{mf}}$	δ	u_B	J	u_f	u_e	u_s
	m/sec			m/sec	kg/m2.sec	m/sec	m/sec	m/sec
	0.0321							
0.400	0.0305	0.949	0.000		0.00	0.076	0.081	0.000
0.425	0.0381	1.187	0.042	0.184	2.65	0.090	0.078	0.002
0.450	0.0473	1.472	0.083	0.222	6.39	0.105	0.075	0.005
0.475	0.0582	1.812	0.125	0.249	10.74	0.123	0.071	0.009
0.500	0.0712	2.217	0.167	0.275	15.80	0.142	0.066	0.014
0.525	0.0867	2.698	0.208	0.302	21.71	0.165	0.059	0.021
0.550	0.1050	3.269	0.250	0.332	28.62	0.191	0.050	0.030
0.575	0.1268	3.947	0.292	0.365	36.71	0.221	0.038	0.042
0.600	0.1527	4.752	0.333	0.402	46.21	0.254	0.023	0.057
0.625	0.1834	5.709	0.375	0.444	57.39	0.293	0.002	0.078
0.650	0.2200	6.849	0.417	0.491	70.61	0.339	-0.026	0.107
0.675	0.2638	8.211	0.458	0.546	86.28	0.391	-0.066	0.146
0.700	0.3163	9.844	0.500	0.608	104.95	0.452	-0.122	0.203
0.725	0.3793	11.807	0.542	0.681	127.30	0.523	-0.205	0.286
0.750	0.4555	14.179	0.583	0.766	154.16	0.607	-0.332	0.412
0.775	0.5479	17.055	0.625	0.865	186.62	0.707	-0.538	0.618
0.800	0.6604	20.556	0.667	0.983	226.00	0.826	-0.902	0.983
0.825	0.7977	24.830	0.708	1.121	273.95	0.967	-1.652	1.732
0.850	0.9655	30.053	0.750	1.285	332.42	1.136	-3.774	3.854
0.875	1.1702	36.422	0.792	1.478	403.59	1.337	-27.996	28.076
0.900	1.4183	44.145	0.833	1.704	489.77	1.576	8.598	-8.518
0.925	1.7159	53.409	0.875	1.964	593.03	1.855	4.664	-4.584
0.950	2.0673	64.346	0.917	2.260	714.83	2.176	3.632	-3.552
0.975	2.4739	77.003	0.958	2.588	855.70	2.537	3.213	-3.133
1.000	2.9343	91.332	1.000	2.942	1015.10	2.934	3.023	-2.942

Table F13. Sand Theoretical Voidage, Bubble Fraction and Mixing

Temp	600 C							
Press	101.3 kpa							
Air Dens	0.404309 kg/cu.m							
Air Vis	3.83E-05 Pa.s							
Sphericity	0.9							
dp=	490 microns							
Voidage	Superficial Velocity		Bubble Fraction	Bubble Velocity Eq.3.39	Solids Turnover Rate	Emulsion Average Velocity	Emulsion gas Velocity	Solids downflow Velocity
ϵ	U	$\frac{U}{U_{mf}}$	δ	u_B	J	u_f	u_e	u_s
	m/sec			m/sec	kg/m2.sec	m/sec	m/sec	m/sec
	0.0857							
0.400	0.0809	0.944	0.000		0.00	0.202	0.215	0.000
0.425	0.1010	1.178	0.042	0.474	6.82	0.238	0.209	0.005
0.450	0.1250	1.458	0.083	0.579	16.64	0.278	0.201	0.013
0.475	0.1535	1.791	0.125	0.649	28.00	0.323	0.190	0.024
0.500	0.1871	2.184	0.167	0.716	41.16	0.374	0.177	0.038
0.525	0.2268	2.646	0.208	0.784	56.38	0.432	0.159	0.055
0.550	0.2734	3.190	0.250	0.858	73.99	0.497	0.136	0.078
0.575	0.3279	3.826	0.292	0.938	94.34	0.570	0.107	0.108
0.600	0.3916	4.569	0.333	1.025	117.86	0.653	0.068	0.146
0.625	0.4658	5.435	0.375	1.121	145.01	0.745	0.016	0.198
0.650	0.5520	6.441	0.417	1.226	176.28	0.849	-0.052	0.267
0.675	0.6518	7.605	0.458	1.342	212.24	0.966	-0.146	0.360
0.700	0.7668	8.947	0.500	1.469	253.47	1.095	-0.276	0.490
0.725	0.8989	10.487	0.542	1.608	300.56	1.240	-0.460	0.674
0.750	1.0496	12.246	0.583	1.760	354.10	1.399	-0.733	0.947
0.775	1.2206	14.241	0.625	1.923	414.63	1.575	-1.159	1.374
0.800	1.4131	16.487	0.667	2.098	482.59	1.766	-1.884	2.098
0.825	1.6281	18.996	0.708	2.285	558.31	1.973	-3.317	3.531
0.850	1.8662	21.773	0.750	2.481	641.98	2.195	-7.229	7.443
0.875	2.1273	24.820	0.792	2.686	733.60	2.431	-50.819	51.033
0.900	2.4110	28.130	0.833	2.897	833.03	2.679	14.702	-14.487
0.925	2.7165	31.694	0.875	3.114	939.95	2.937	7.480	-7.265
0.950	3.0425	35.497	0.917	3.333	1053.96	3.203	5.451	-5.237
0.975	3.3875	39.523	0.958	3.553	1174.55	3.474	4.515	-4.300
1.000	3.7501	43.753	1.000	3.772	1301.17	3.750	3.986	-3.772

Table F14. Sand Theoretical Voidage, Bubble Fraction and Mixing

Temp	600 C							
Press	101.3 kpa							
Air Dens	0.404309 kg/cu.m							
Air Vis	3.83E-05 Pa.s							
Sphericity	0.9							
dp=	530 microns							
Voidage	Superficial Velocity		Bubble Fraction	Bubble Velocity Eq.3.39	Solids Turnover Rate	Emulsion Average Velocity	Emulsion gas Velocity	Solids downflow Velocity
ϵ	U	$\frac{U}{U_{mf}}$	δ	u_B	J	u_f	u_e	u_s
	m/sec			m/sec	kg/m ² .sec	m/sec	m/sec	m/sec
	0.1003							
0.400	0.0944	0.942	0.000		0.00	0.236	0.252	0.000
0.425	0.1179	1.176	0.042	0.548	7.88	0.277	0.245	0.006
0.450	0.1458	1.454	0.083	0.671	19.30	0.324	0.235	0.016
0.475	0.1788	1.783	0.125	0.754	32.51	0.377	0.223	0.028
0.500	0.2178	2.172	0.167	0.831	47.76	0.436	0.207	0.044
0.525	0.2636	2.629	0.208	0.909	65.37	0.502	0.187	0.064
0.550	0.3172	3.164	0.250	0.993	85.67	0.577	0.160	0.090
0.575	0.3798	3.787	0.292	1.084	109.04	0.660	0.126	0.124
0.600	0.4525	4.512	0.333	1.182	135.92	0.754	0.082	0.169
0.625	0.5367	5.352	0.375	1.289	166.77	0.859	0.023	0.227
0.650	0.6337	6.320	0.417	1.406	202.07	0.975	-0.055	0.306
0.675	0.7452	7.432	0.458	1.533	242.33	1.104	-0.160	0.411
0.700	0.8726	8.702	0.500	1.670	288.07	1.247	-0.306	0.557
0.725	1.0172	10.145	0.542	1.818	339.78	1.403	-0.512	0.762
0.750	1.1805	11.773	0.583	1.977	397.90	1.574	-0.814	1.065
0.775	1.3634	13.596	0.625	2.146	462.80	1.759	-1.282	1.533
0.800	1.5667	15.624	0.667	2.325	534.74	1.958	-2.074	2.325
0.825	1.7908	17.859	0.708	2.512	613.85	2.171	-3.631	3.882
0.850	2.0356	20.301	0.750	2.706	700.14	2.395	-7.867	8.118
0.875	2.3009	22.947	0.792	2.905	793.47	2.630	-54.947	55.198
0.900	2.5859	25.789	0.833	3.108	893.59	2.873	15.791	-15.541
0.925	2.8896	28.817	0.875	3.313	1000.16	3.124	7.981	-7.731
0.950	3.2108	32.020	0.917	3.519	1112.76	3.380	5.780	-5.529
0.975	3.5481	35.384	0.958	3.723	1230.93	3.639	4.758	-4.507
1.000	3.9002	38.895	1.000	3.925	1354.20	3.900	4.176	-3.925

Appendix G : Combustor Operation Instructions and Charts

Operation Instructions

Preliminaries

1. Select combustor configuration and distributor type for the test program. Fit and change optional components as required.
2. Select desired bed solid size for the test program and plot a U_{mf} verses Temperature chart for use during warm up. Several U_{mf} Charts are included in this appendix, Figs G2,G4,G6,G8.
3. Check LPG main burner tubes for sand blockages.
4. Add bed solids to the Fluidised Bed to desired depth.
5. Fluidize the bed solids cold to check for adequate fluidization and mixing.
6. Check the pilot burner flame slot is free of sand particles.
7. Fit Chimney.
8. Connect instrumentation as required.
9. Begin FBC warm up procedure using LPG.

FBC Warm Up Procedure

1. Ensure both stop cocks are off and both regulators are off.
2. Open LPG cylinder cock.
3. Set main regulator to 20 kpa.
4. Open pilot burner stop cock.
5. Using a long nose gas lighter position lighter to ignite the pilot burner flame.
6. Press and hold down the flame failure valve button connected to the pilot burner.
7. The pilot burner should ignite. If ignition does not occur release the button , turn off the stop cock and inspect for problems.
8. Hold down the flame failure valve button for approximately one minute.
9. Release flame failure button and pilot flame should remain sure.

10. Inspect pilot flame extends full length of the tube and if necessary adjust pilot flame regulator to ensure a good flame.
11. Start air flow in the fluidized bed and bring to approximately $2U_{mf}$. Utilise the inverter control to gradually increase air flow to prevent pilot flame loss.
12. Inspect pilot flame again and adjust pilot flame regulator if necessary.
13. When bed fluidization is acceptable and pilot flame stable and sure, open main burner cock. Main LPG burner gas will ignite and burn above the bed.
14. Observe combustion behaviour and adjust main regulator and or air/flow to achieve stable combustion. Problems to note are:
 Frequent flame loss if mixture is too lean.
 Flame loss due to bubble burst shock waves.
15. Progressively reduce air flow and LPG pressure as the bed temperature as the bed heats up. Operation at approximately 2 to 4 U_{mf} was found to give best results. (See Operation Charts Figs. G1 to G9)

FBC Cooldown Procedure

The cooldown procedure is only necessary to prevent sand fusion at high temperatures and achieve faster cooling to allow FBC storage. It was also used to determine convective and forced air flow heat losses. The procedure is:

1. Stop fuel feed operations
2. Allow air flow to continue.
3. Observe thermocouple temperatures. If large differences immerge during cooldown this indicates a failure of the bed to mix properly. In such cases increase air flow progressively to maintain bed mixing uniformity.

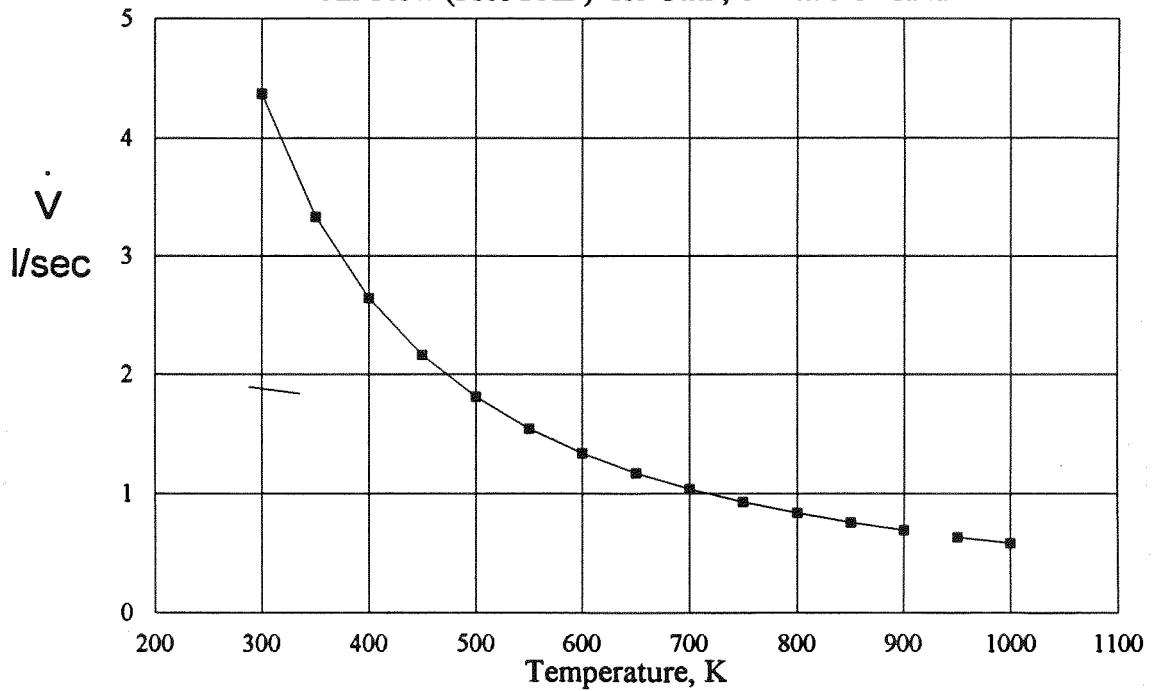
Safety Precautions.

Protective Clothing : Face Sheild., Overalls

Safe Practice : Stand Clear of all Combustor openings, including pilot burner tube, feed chutes and observation ports at ignition times, particularly the ignition of the main burners which usually results in a flame surge.

Combustor Purging. : If at any stage flame is lost or the main ignition fails to take place in 2 seconds the following procedure should be used.

1. Air purge the combustor for 1 minute.
2. Repeat the above start up proceedure. Note: The combustor air flow can be shut off at high bed temperatures up to 700 C without any permanent fusing of sand.

Fig.G1 Combustor Operation ChartAir Flow (l/sec FAD) for U_{mf} , 180 micron sand**Fig.G2 Minimum Fluidization Velocity**

180 micron sand

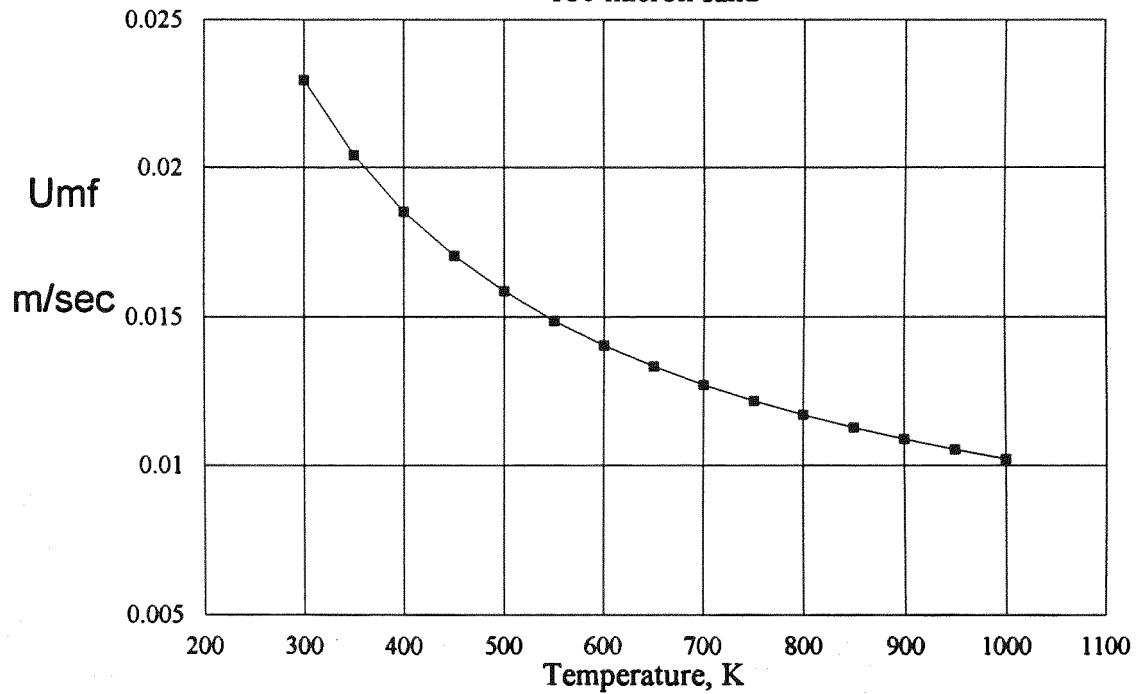


Fig. G3 Combustor Operation Chart

Air Flow (l/sec FAD) for U_{mf} , 300 micron sand

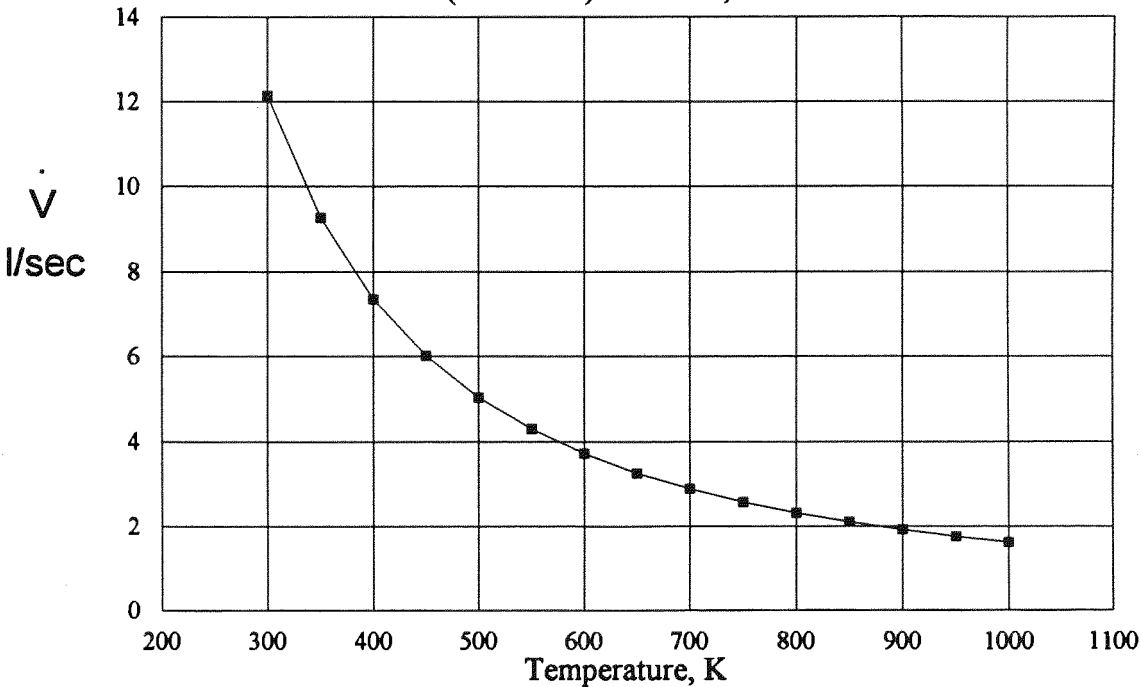


Fig. G4 Minimum Fluidization Velocity

300 micron sand

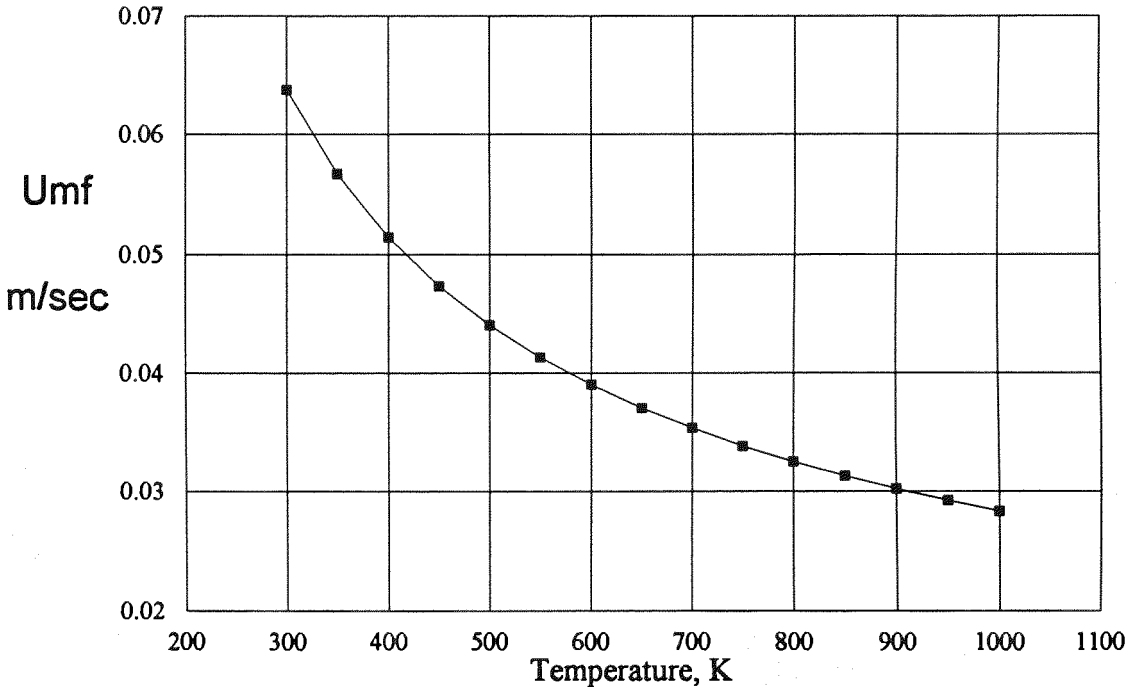


Fig. G5 Combustor Operation Chart

Air Flow (l/sec FAD) for U_{mf} , 490 micron sand

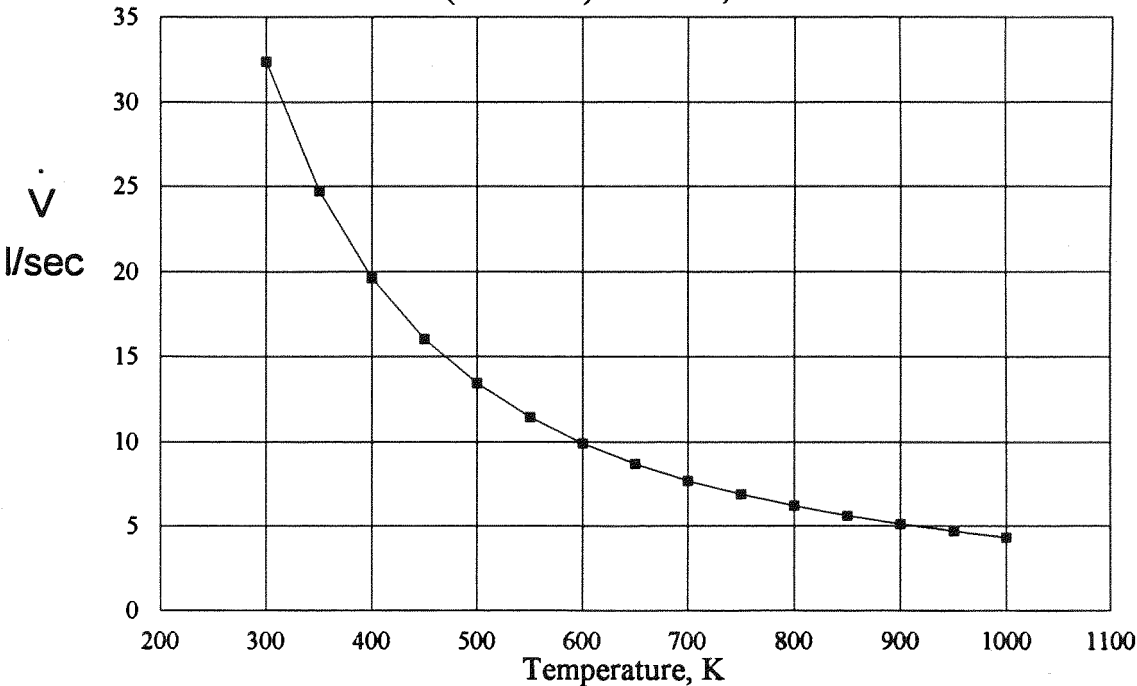


Fig.G6 Minimum Fluidization Velocity

490 micron sand

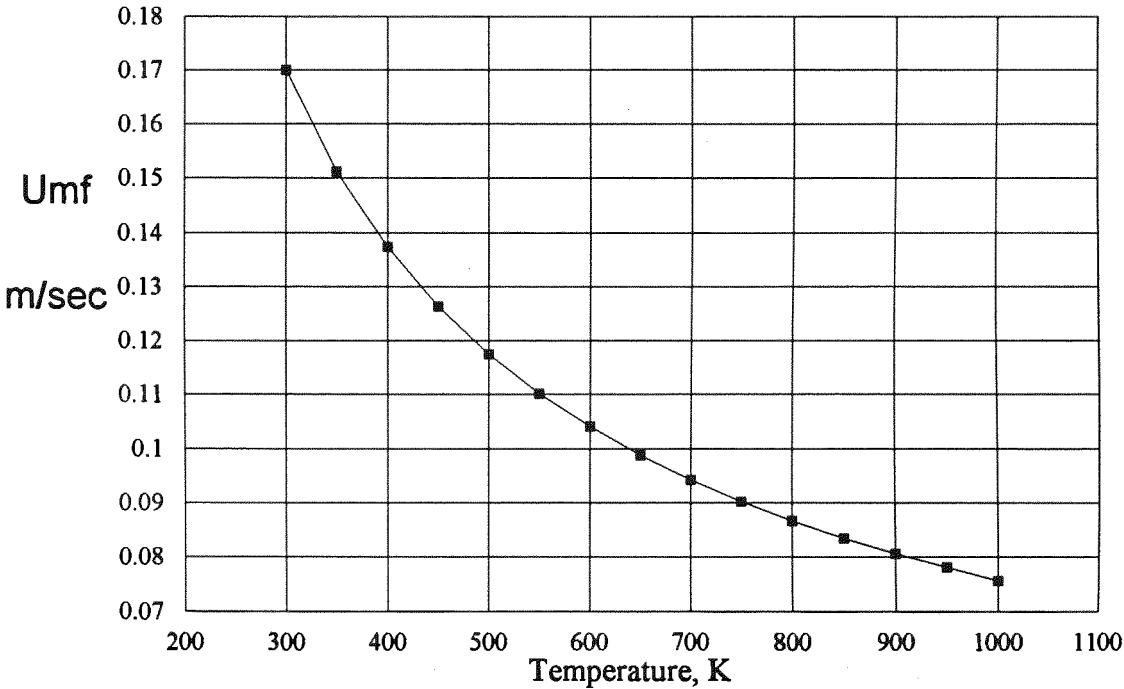


Fig. G7 Combustor Operation Chart

Air Flow (l/sec FAD) for U_{mf} , 530 micron sand

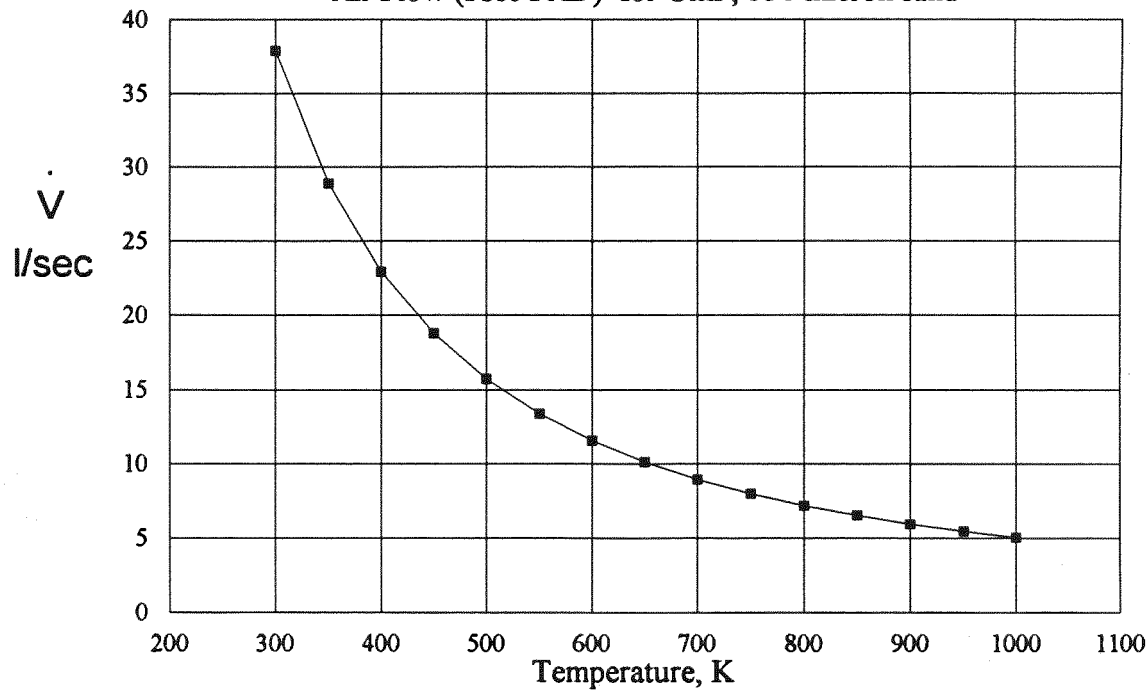


Fig. G8 Minimum Fluidization Velocity

530 micron sand

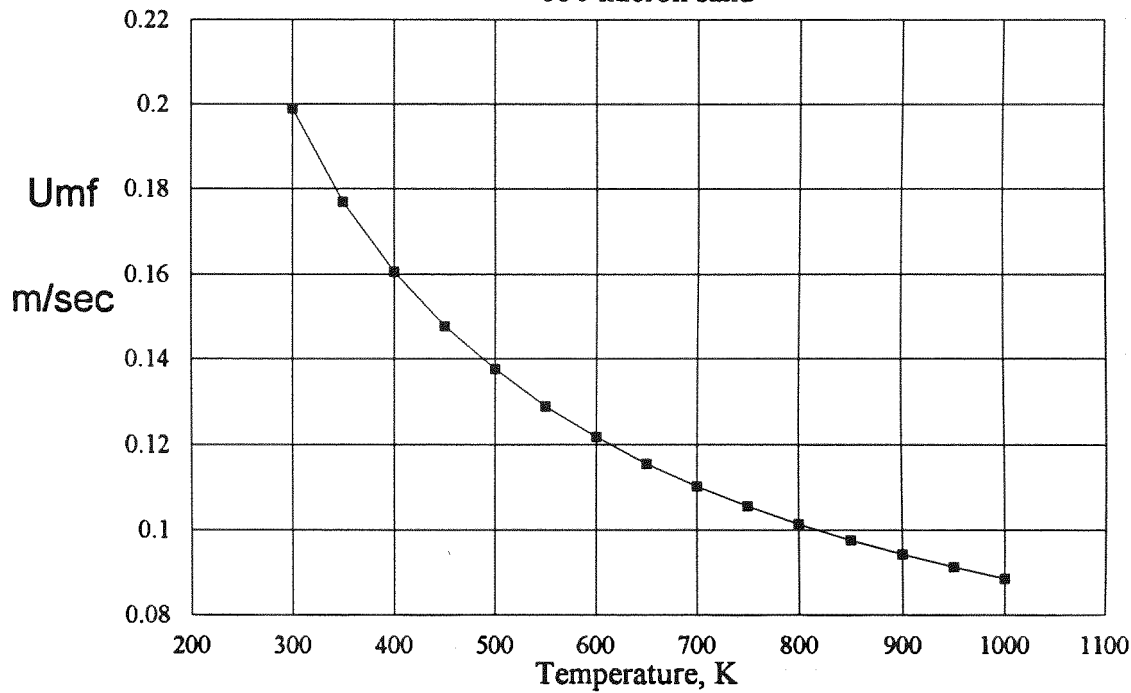
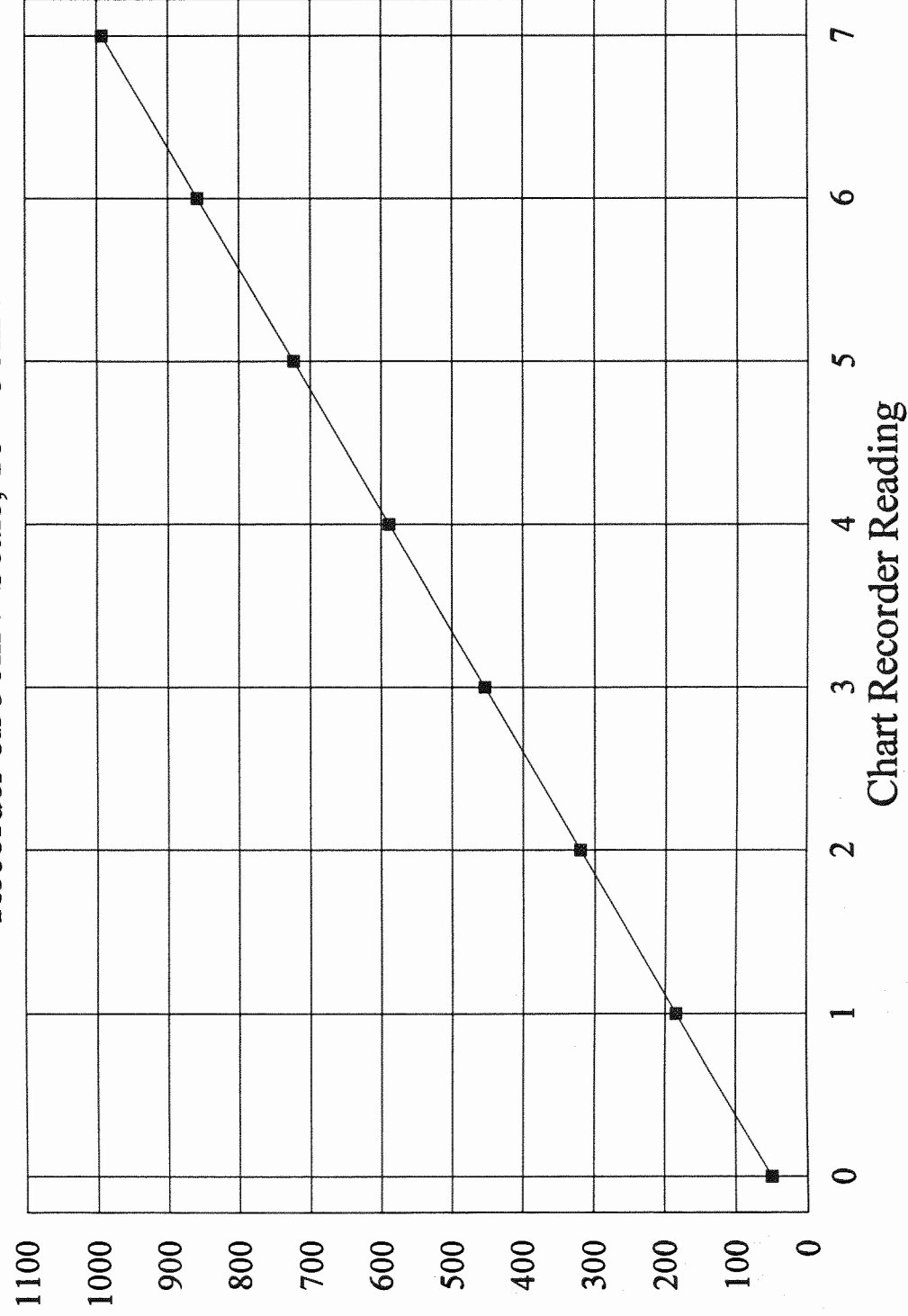


Fig.G9 Temperature vs Chart Recorder Reading
Recorder on 50mV Scale; 10 = 50mV



Appendix H: Equipment Design Calculations

Flow Visualisation Equipment Design

1. Pressure Requirement

Estimated maximum depth	1.5 m
Estimated Bed Pressure Drop	21 kPa
Estimated Distributor Drop@15%	3 kPa

Estimated Total Delivery Pressure 24 kPa

2. Roots Blower Delivery is 90 l/sec

3. Selecting perspex tube size of 190mm gives a Superficial Velocity of 3.2 m/sec

For Sand sizes 180 and 490 microns gives:

Sand Size (microns)	U_{mf} (m/sec)	Maximum U_f
180	0.024	$147U_{mf}$
490	0.178	$20U_{mf}$

Which allows adequate range for testing.

4. Roots Blower Delivery Temperatures.

Assuming a constant volume process the calculated temperatures are:

Bed Depth	Pressure Drop	Exit Temp.
300mm	$P = 1.15 \times 1450 \times 9.81 \times 0.3$ =4.91 kPa	$T_2 = (106.2/101.3) 300$ =314 K (42 C)
1500mm	$P = 1.15 \times 1450 \times 9.81 \times 1.5$ =24.5 kPa	$T_2 = (125.8/101.3) 300$ =372 K (100 C)

Since the extent of and depth of deep bed testing was not known an air cooler was added so that the perspex tube would not soften during testing.

Combustor Design

1 Pressure Requirement.

Estimated maximum depth	0.5 m
Estimated Bed Pressure Drop	7 kPa
Estimated Distributor Drop@15%	1 kPa

Estimated Total Delivery Pressure 8 kPa

2. Roots Blower Delivery is then 110 l/sec

3. Selecting 489mm internal diameter steel tube gives

0.586 m/sec at 27 C.

4. Range of Operation.

Start up (cold) velocity must exceed $2U_{mf}$ for adequate mixing of bed solids. Therefore:

$$\frac{0.586}{2} = \frac{d_p^2 (2300 - 1.2) 9.81}{1650 (1.85/10^5)}$$

Solving the equation gives maximum $d_p = 630$ microns.

As temperature increases less air mass flow is required to maintain fluidization conditions. Calculations for operating maximums with the expected sand grades using theoretical values from Appendix F give:

Sand Size (microns)	$U_{f,max@27\text{ C}}$	$U_{f,max@600\text{ C}}$
180	$24U_{mf}$	$152U_{mf}$
300	$8.8U_{mf}$	$55U_{mf}$
490	$3.3U_{mf}$	$21U_{mf}$
530	$2.8U_{mf}$	$18U_{mf}$
630	$2U_{mf}$	$12U_{mf}$

5. Distributor Plate Pressure Drop.

Based on the experience from the flow visualisation experiments it was decided to limit the number of bubble caps to 21 to increase pressure drop and improve velocity profiles. Selecting sand of mean size of 490 microns, Flowrate of air required cold is :

Air Flowrate is = $0.1878 \times 0.1778 = 0.0318$ cu.m/sec

Air Velocity in bubble cap tubes is = $0.0318 / (21 \times \pi \times 0.009^2 / 4)$
= 23.8 m/sec

Predicted Distributor Pressure Drop = 1.5 kPa. From bubble cap tests.

Pressure drop is 1.5/7.1 which is 20% which should be okay. Variations will however require reconsideration as the project proceeds. As Pressure drops in bubble caps were found to be dependent also on bed depth (or exit air density) so it was found the most reliable way of verifying sufficient pressure drop was by checking fluidization visually with a shallow bed.

For the inserts of 4mm and 2.5 mm , an estimate was made from calculations and results verified by inspection.

6. Flow Straightener Pressure Drop

Based on the aggregate flow straightener used successfully with the flow visualisation equipment a 200mm diameter, 100 mm packed bed aggregate straightener is proposed. Aggregate size 4mm.

Pressure drop is given by Erguns Equation.

$$\frac{\Delta P_b}{L} = 150 \frac{(1-\epsilon)^2}{\epsilon^3} \frac{\mu_g U_f}{(\phi d_p)^2} + 1.75 \frac{(1-\epsilon)}{\epsilon^3} \frac{\rho_g U_f^2}{\phi d_p}$$

Assuming voidage of 0.5 and sphericity of 0.9, and given maximum velocity of 3.4 m/sec. Pressure drop per m is :

$$\frac{\Delta P_b}{L} = 1498.8 + 28583 = 30 \text{ kPa/m}$$

Which for $L=100\text{mm}$ $\Delta P_b=3\text{kPa}$

7. Combustor Tube Stresses.

Pressure Stresses are minimal eg

$$\sigma = 8000 * .489 / (2 * 0.01) = 0.2 \text{ MPa}$$

Of more concern is the strength of the mild steel at elevated temperatures. Applications for mild steel are not recommended above 600 C but dimension stability is retained to much higher temperatures. It was reasoned that with stresses so low that short duration testing in the 600 to 800 C range would not present a problem. From what data could be obtained the Ultimate Tensile Strength of mild steel at 600 C is 120 MPa and approximately 50 MPa at 800 C. (Emmert.H.D and Matters.R. High Temperature Considerations in Design.)

8. Gas Explosion Stresses.

The pressure wave associated with an LPG explosion was quoted as 7 tonnes/m² by the local gas examiner. The most likely situation for such an occurrence would be during warm up. The hoop stress induced in the tube would be:

$$\sigma = 69000 * .489 / (2 * 0.01) = 4 \text{ MPa.}$$

In any case such stresses are unlikely as the combustor is an open -to -atmosphere type making it very difficult to produce conditions that would lead to any more than a gas flame surge.

9. Fluidized Bed Combustor Wall Insulation

Design Heat Wall Loss limit. 1 KW

Typical Operating Conditions:	Bed Temp	800 C
	Skin Temp	60 C

Assuming minimal temperature drop in th 10mm of mild steel and that the natural convection losses are small the heat transfer is :

$$Q_{lw} = UA(T_B - T_o) = U 1.2 \pi 0.6 (800 - 25) = 1753 U$$

Taking insulation as 100 mm of Durablanket @ 160 kg/cu.m and at the given conductivity of 0.098 W/mC gives:

$$Q_{lw} = \frac{0.098}{0.1} 1753 = 1560 \text{ Watts}$$

Note: This is the total wall loss estimate. Actual wall heat transfer from bed solids is calculated for specific bed depths for use in combustion Efficiency Calculations.

10. Gas System Requirements.

Maximum air flow : 110 l/sec which is 0.132 kg/sec.

At Stoichiometric mixture @ 15 :1,

Gas flow is : 8.8 grams/sec

Taking CV = 50 MJ/kg, The Firing rate is:

Firing Rate : 440 kW.

For most operations maximum air flow at 35% hence requiring:

Firing Rate :132 kW. or 475 MJ/hr.

11. Ingestor Mixing Design.

Require downward flow of solids greater than emulsion gas velocity.

Tube Diameter is 200mm giving an area of :	0.0314 m ²
Combustor Diameter is 489mm giving an area of :	0.1878 m ²
Annulus Area is then :	0.1564 m ²

Selecting Air Flow Distribution of 28 caps outside the tube and six caps at the edge of the tube with these bushed to 2.5 mm the flow distribution is by cap tube area.

Annulus Flow Area in Caps : 28 caps @ 9mm diameter 0.00178 m²
 3 caps @ 2.5mm diameter 1.47*10⁻⁵ m²
 Total area is 0.00179 m²

Total flow area is		0.00181 m ²
Flow Distribution is therefore	Annulus	: 99%
	Tube	: 1%

Selecting Minimum operating condition as $10 U_{mf}$ @600 C

Predicted Flowrates are:

Annulus	:	$9.9U_{mf}$
Tube	:	$0.1U_{mf}$

Solids Turnover Rate 530 sand
@9.9 U_{mf} is : $J = 105 \text{ kg/m}^2 \text{ sec.}$
Appendix F

Solid turnover @ area 0.1564 16 kg/sec

Distributing flow over entire bed area gives downward velocity of emulsion solids of:

0.06 m/sec or 60mm/sec.

Therefore assuming solids crossflow at the top of the bed the solids velocity in the ingestor tube will be at least 60mm/sec at $10 U_{mf}$.

Airflow at 10 U_{mf} @600 C is = $0.1878 \times 0.3163 \times 0.4 = 0.024$ kg/sec
Requires maximum of 4.7 grams/sec cellulose fuel

Operation Rate is 92 kW. Bagasse content in Tube is then 0.2% by mass.

A operation point of 20 U_{mf} would give $J = 226 \text{ kg/m}^2 \text{ sec.}$ or 35 kg/sec bringing tube solids downflow to 120 mm/sec.

12. Minimum Operation Point For Spouted Bed.

Terminal Velocity is given by:

$$U_t = \left[\frac{4}{225} \frac{(\rho_p - \rho_g)^2 g^2}{\rho_g \mu_g} \right]^{1/3} d_p$$

$$= \left[\frac{4}{225} \frac{(2300 - 1.2)^2 9.81^2}{(1.2) (1.85/10^{-5})} \right]^{1/3} \frac{1.18}{1000} = 8.8 \text{ m/sec}$$

Minimum operating flowrate is then at:

$$\pi * 0.05^2 / 4 * 8.8 = 17.2 \text{ l/sec FAD}$$

Table .H1.Fluidised Bed Combustor : Materials Costs

Item No.	Description	Quantity	Cost \$
1	Bubble caps, 316 Stainless Steel	21	264.00
2	Perspex Tube,Dia 190mm	3m	600.00
3	Bend, Dia.200mm, Steel	1	72.40
4	Reducer, Dia. 200mm/100mm Steel	1	34.00
5	Flexible Hose Dia. 100 mm	1.5m	113.00
6	Tube Dia 200mm. Steel	0.6m	100.00
7	PVC fittings		50.00
8	Plastic tube. Dia 6mm	5m	20.00
9	Copper tube, 10mm	13m	55.00
10	Tube Dia 489mm/10mm Steel	1.6m	400.00
11	160kg/cu.m, Durablanket,600mm	20m	746.00
12	2.4,1.2,0.01, Mild Steel Sheet	1	250.00
13	75,5mm, Square Hollow Section	8m	117.00
14	Thermocouple tube, Dia 6mm	1.2m	55.00
15	Brass Pipe fittings for thermocuoples		102.00
16	Gasket material		15.00
17	XJ1, Sealer.	450g	13.00
18	Spouted Bed Cone	1	336.00
19	Boiler bolts		20.00
20	Flanged Feeder Section, Dia 190mm	1	125.40
21	Pipe Fittings, LPG		110.45
22	Flame failure valves, 1/4 BSP	2	78.00
23	Unversal Thermocouple, 900mm	2	59.00
24	Red Devil Regulators, 140kPa	2	110.00
25	Gas Cock	2	19.50
26	Flexible LPG Hose Dia 8mm	2m	20.00
27	Check valve	1	40.00
28	Miscellaneous Pipe Fittings Dia 50mm		10.00
29	Flexible Flat Hose,,2.6 Mpa. Dia 62.5 m	1.5m	20.00
30	Tube Stainless Steel Dia 12mm	0.6 m	20.00
31	2.4,1.2,Galv Sheet		33.30
32	Thick walled Tube, 32/15 mm	1.2m	30.00
33	Bubble Caps (mild steel)	21	200.00
Total Materials Cost ***			4038.05

*****Costing does not include the following:**

Cost of UCQ scarp used
Costs for UCQ Equipment provided
 Motor Inverter Control
 Roots Blower
 Chart Plotter
 Rotameter
 Pressure Gauges
 Temperature Gauges
Cost of labour of UCQ Technical Staff

Appendix I : Commissioning Notes

(a) Flow Visualisation Equipment

The difficulties in commissioning the flow visualisation bed were compounded by inexperience in what was to be expected from typical fluidization phenomena. Considerable effort was first directed to reducing bubble size, hence the introduction of the 100 mesh distributor. The 21 cap bubble plate was never actually used in the reported tests. (It was used with centre and annulus flow patterns.) The mesh distributor gave a very small pressure drop which gave unsatisfactory flow distribution. The flow distribution problem was finally solved by levelling the mesh plate and adding a flow straightening chamber of aggregate in the range $2.36 < d_p < 4.75 \text{ mm}$.

Other problems simply relate to instruments. The measurement of air flows in the order of 1 l/sec in the perspex tube were well below the measurement range of the 74.95mm British Standard Nozzle. Initially an orifice plate was calibrated and used to measure bleed off air but the uncertainties in this technique were larger than the quantities being measured. The second method adopted was successful which involved accelerating the air to a high velocity by reducing the pipe diameter. The high velocity air was approximately 81 times that in the bed tube and could be read using a pitot-static tube. There were difficulties with the pitot tube due to fouling with fines from the bed when testing fine grade sands. The problem was solved by regular cleaning. There were no problems testing the coarser 490 micron sand.

(b) Combustor

Commissioning problems were experienced in the following areas:

1. Positioning of the LPG Pilot Flame thermocouple position.
2. Operation time of main bed burner thermocouple.
3. The original main burner holes were too large
4. Air Flow distribution
5. Spouted Bed Rupture Pressure

The positioning of the LPG pilot flame thermocouple was critical as it controlled the entire gas supply via a flame failure valve. Several movements of the thermocouple were necessary to eliminate nuisance shut-downs.

The main bed burner thermocouple proved of little use as the firing rates calculated could not be achieved without icing the LPG cylinder. Bed warm up times were therefore slow, taking between one and three hours depending on depth. The flame failure valve was therefore clipped open by adding a clip to keep the over-ride button pressed. Main burner control was reduced to an on-off control using the stop cock.

The main burners were originally drilled with eight holes each of 2mm diameter. This allowed for gas flows which could not be successfully supplied from the cylinder. For smaller flows, the LPG did not distribute along the full length of the burner. Further, sand in considerable quantities entered the tubes after warm up was complete and the burner tubes would become blocked. The burner tubes were removed, the 2mm holes covered with weld and five only 1.5mm holes drilled in each

tube. The system was workable but the tubes still required regular cleaning. In retrospect the best warm up system for experimental purposes would be an LPG combustion chamber fitted beneath the bed. With such a system gas entering the bed would be hot and rapid warm up times would be achieved. This would be a big improvement on direct introduction system which was used in which the fuel burns on the top until auto-ignition temperature is reached and heat transfer is quite slow. There would also be no sand fouling problems in the burners.

Sand also caused problems by fouling the pilot flame slot. Sand particles jammed in the slot would prevent the flame running to the end of the pilot flame tube. It was therefore required to clean the slot before each start up.

Achieving even air flow distribution through the distributor presented problems at various stages in the testing program. While the first problems just illustrated the hazards of scaling up from smaller models; ie Distributor Plate Pattern No.1 was never used in combustion tests because it was modified to Plate Pattern No.2 after unsuccessful cold trials. Problems became evident using Plate Pattern No.3 where it was desired to produce even annulus flow. There was at least $2U_{mf}$ between operating points where the first and last regions fluidized. The problem was solved by bushing the 9mm bubble cap tubes with 4mm loose bushes. The bush and bubble cap were retained by the same wire clip. The increased pressure drop gave satisfactory results. Even smaller bushes were used (2.5mm) when the number of bubble caps were increased to 42 with satisfactory results even with shallow bed depths.

The final problem encountered was that of achieving peak rupture pressure for the spouted bed with a feed pipe and baffle. Pressures above the capability of the roots blower were required to lift the sand in the tube and establish a bed spout. The reason for this was that the sand in the feed pipe would remain packed until spouting was established which would coincide with terminal velocities being reached in the feed pipe. The pressure generated just prior to rupture is quite large corresponding to the pressure drop through a sand bed at packed bed voidage and near terminal velocities. Having encountered this problem it was envisaged that another problem may be introduced by the spout baffle which would prevent a spout from rupturing in the centre of the bed in the usual way. Satisfactory start up operation was achieved by placing a bubble cap plate in the spout cone. The plate had the effect of increasing the initial spout area reducing the pressure peak. The plate was hinged and controlled from outside the combustor which allowed it to be opened during fuel feeding but closed for start-up. Using the controllable hinged plate the feed pipe could be kept free of bed solids as long as the velocity in that pipe was not reduced below the terminal velocity of the largest particles when the plate was opened. Obviously, the sequence of opening and closing has to be carefully controlled and the system, being manually operated, is certainly not foolproof.